DISSECTING PROTEIN STRATIFICATION AND REGULATION IN UROPATHOGENIC *ESCHERICHIA COLI* BIOFILMS

By

Kyle Anthony Floyd

Dissertation
Submitted to the Faculty of the
Graduate School of Vanderbilt University
in partial fulfillment of the requirements
for the degree of

DOCTOR OF PHILOSOPHY
in

Microbiology and Immunology
May, 2017
Nashville, Tennessee

Approved:	Date:
D. Borden Lacy	2/3/2017
D. Borden Lacy, Ph.D. - Chair	
Timothy L. Cover	2/3/2017
Timothy L. Cover, M.D.	
Andries Zijlstra	2/3/2017
Andries Zijlstra, Ph.D.	
Kevin Schey	2/3/2017
Kevin L. Schey, Ph.D.	
Richard Caprioli	2/3/2017
Richard M. Caprioli, Ph.D.	
Maria Hadjifrangiskou	2/3/2017
Maria Hadjifrangiskou, Ph.D.	

For my Maw Maw, Ruby Lee Cosby,

who couldn't wait to have her very own doctor in the family.

With all my love.

ACKNOWLEDGEMENTS

There is an African proverb, which says “It takes a village to raise a child”. These words are certainly true when that “child” is a graduate student seeking their Ph.D. There are many people who have contributed to the work presented here, as well as to my training over the course of my study, and without their help these words could not have manifested. I would like to begin by thanking Jessica Moore from the laboratories of Dr. Richard Caprioli and Dr. Eric Skaar, for all of her help and counsel with the adaptation of MALDI-TOF IMS for the analysis of bacterial biofilms. Without her support, truly none of this work would have ever been possible. Jessica contributed significantly to helping me lay the foundation for this project, and for that I will be ever thankful.

I want to also start by acknowledging and thanking all of the members of my lab family here at Vanderbilt. First and foremost, to the “original Hadjis” Dr. Carrie Shaffer (I would be amiss if I didn’t spell it “correctly” as Schaffer), Kirsten Guckes, Erin Breland, and Elissa Zhang; I owe a great deal of thanks for helping me to learn the ways of microbiology as well as for helping to keep me sane day in and day out. I also want to thank the newer members of the lab, Allison Eberly, Dr. John Brannon, Spencer Colling, Bradley Steiner, Madison Fitzgerald, Taryn Dunigan, and Becca Abbot for all of their help and support. Specifically, I want to thank my scientific wife, Allison Eberly, for her contributions to these studies and for being a sounding board to help me come up with new ideas and hypotheses.

To my mentor, Dr. Maria Hadjifrangiskou, I owe a great deal of thanks for taking me into her lab and under her wing. Maria gave me the freedom to explore and fall in love with my project, very seldom told me no to a proposed experiment (but often told me no to purchasing my

very own mass spectrometer), and allowed my curiosity and interests to roam free. It is with her mentorship and guidance that I have developed into the scientist I am today, and for this I am extremely grateful. I also want to thank my co-mentor, Dr. Richard Caprioli, for his invaluable advice on the development of IMS methodologies for biofilm analysis. Richard's expertise in the IMS field is unparalleled, and I am very thankful for his guidance of my education in the field. Along with Maria and Richard's mentorship, I also owe a great deal of thanks to the other members of my thesis committee for their guidance and support. To Drs. Borden Lacy, Tim Cover, Andries Zijlstra, and Kevin Schey, thank you for all of your ideas and suggestions that have helped to shape the direction of my research. Thank you for reeling me in from time to time, and keeping me focused on my long-term goals. It is a direct result of your support that I feel I am fully prepared for the next level of my professional development, and for that I cannot begin to thank you enough.

The collaborative environment of Vanderbilt University has also greatly helped to foster my research. I would like to thank the laboratory of Dr. Eric Skaar (specifically Dr. Matthew Surdel and Jacob Choby) for the use of their anaerobic chamber, without which my regulatory studies could not have happened. I want to thank Rhonda Caston from the Cover Lab, as well as Esha Dalvie, who contributed to this work during their rotations within the Hadjifrangiskou lab. I also would like to thank Theresa Barke, for all of those meaningful lunchtime discussions and the ideas and suggestions that came from them. Your friendship since our first few months here has helped me to make it through this process, and I am eternally grateful for it. The establishment of several unique collaborative opportunities has also significantly enhanced my work. I would like to thank our collaborators at the Center for Biofilm Engineering at Montana State University; Drs. Phil Stewart, Garth James, and Ellen Lauchnor

for their expertise and assistance in the development of the *in vitro* catheter-associated biofilm model. I would also like to thank our collaborators in the Vanderbilt University Medical Center Working Group for the Prevention and Treatment of CAUTI; Drs. Charles Stratton, Jonathan Schmitz, Douglas Clayton, Simon Mallal, George Nelson, and Joesph Conrad for their introduction to the clinical world of UTI. In particular I want to thank Drs. Jonathan Schmitz and Charles Stratton for their assistance in establishing our library of clinical urinary *E. coli* isolates.

This work was supported through a variety of very generous funding sources, including; Vanderbilt University Academic Development Funds to Maria Hadjifrangiskou (APS-1-04-520-9211), the Swedish Research Council (621-2010-4730), the Knut and Alice Wallenberg and the Goran Gustafasson Foundations (award to Fredrik Almqvist), the Burroughs Wellcome Fund Investigators in the Pathogenesis of Infectious Diseases Award (to Eric Skaar), grant NIH/NIAID R01AI101171 (to Eric Skaar), grant NIH/NIGMS 5P41 GM103391-03 (formerly 8P41 RR031461-02, to Richard Caprioli), grant NIH/NIAID R01 AI02954921 (to Scott Hultgren), grant NIH/NIDDK F32 DK101171-02 (to Matthew Conover), NIH/NIDDK P50 DK64540-010 (to Scott Hultgren), US DOD NDSEG Fellowship 32 CFR 168a (to Courtney Mitchell), US DOE GAANN Fellowship P200A090323 (to Courtney Mitchell), and National Gem Consortium Fellowship (to Courtney Mitchell). I would also like to thank the Vanderbilt University Graduate School for the award of a 2015 Dissertation Enhancement Grant, which supported my collaboration with the CBE at MSU.

Finally and most importantly, I want to thank my family and loved ones for their unyielding love and support. To my parents, Tim and Sylvia Floyd, I want to thank you for always being there and supporting me throughout my entire life and not only my doctoral study. You have always strove to set a strong example for the type of person I should be, and I can only

hope to one day be half the person that each of you are. It is with your love that I was brought into this world, and that love is what always keeps me going. I owe you so much for helping me to get to this point in life, and I cannot ever put into words the depth of my gratitude to you. It is with all of my heart that I say, thank you! To my sister and brother-in-law, Heather and Jonathan Andrews, I owe a great deal of thanks for truly helping to me to maintain some semblance of sanity. Thank you for all of those trips up to Nashville to brighten my spirits when I needed it the most. I love you two so very much, and this journey would have been a million times harder without your support.

To my all of my grandparents and great-grandparents (specifically my Maw Maw, Paw Paw, Nanny, Ma Floyd, and Mama Barkley) who instilled within me a curiosity for the world around me, and always told me that I could be anything I wanted in life, I owe an immense amount of gratitude and love. To all of my other family members; aunts, uncles, cousins (that means you Meggie Weggie and Bossy Lexi), thank you for all of your encouragement, support, and the occasional bouts of hysteric laughter. And as trivial as it may seem, I owe a great deal of thanks to Mr. John Bartholomew Aloicious Bates, for just being a fluffy little ball of kitten love. And last, but certainly not least, to Justin Lawson. Where do I begin? You came into my life halfway through this journey, but there is not a doubt in my mind that without you I would have never made it to this point. Thank you for dealing with my crazy, day in and day out. Thank you for putting up with Leonard, occasionally Sheldon, and for letting me be the true science nerd that I am. I love you more than the words on this paper can ever express, and I look forward to seeing what our future has in store.

TABLE OF CONTENTS

LIST OF TABLES

LIST OF FIGURES

LIST OF ABBREVIATIONS

ACN	Acetonitrile
AcOH	Acetic acid
ASB	Asymptomatic bacteriuria
ATEA	Alternative terminal electron acceptor
BSA	Bovine serum albumin
c-di-GMP	Bis-(3′-5′)-cyclic dimeric guanosine monophosphate
CA	Catheter-associated
CA-ASB	Catheter-associated asymptomatic bacteriuria
CAUTI	Catheter-associated urinary tract infection
CDC	Centers for Disease Control and Prevention
CFUs	Colony forming units
CHCA	α-Cyano-4-hydroxycinnamic acid
CUP	Chaperone-usher pathway
DHB	2,5-Dihydroxybenzoic acid
DMSO	Dimethylsulfoxide
Ebp	Endocarditis and biofilm-associated pili
ECM	Extracellular matrix
eDNA	Extracellular DNA
EMSA	Electrophoretic mobility shift assay
Fe-S	Iron-sulfur
*fim*OFF	*fimS* in transcription-incompetent state
*fim*ON	*fimS* in transcription-competent state
fimS	*fim* operon promoter element
FISH	Fluorescent *in situ* hybridization

FNR	Fumarate and nitrate reductase regulator
H_2O_2	Hydrogen peroxide
HPLC	High-performance liquid chromatography
IBCs	Intracellular bacterial communities
IMS	Imaging mass spectrometry
ITO	Indium tin oxide
LB	Lysogeny broth
LC-MS/MS	Liquid chromatography tandem mass spectrometry
MALDI	Matrix-assisted laser desorption/ionization
MS	Mass Spectrometry
MS/MS	Tandem mass spectrometry
$NaNO_3$	Sodium nitrate
PBS	Phosphate-buffered saline
PCR	Polymerase chain reaction
PMF	Proton motive force
qPCR	Quantitative PCR
RNS	Reactive nitrogen species
ROS	Reactive oxygen species
RP	Reversed-phase
SEM	Scanning electron microscopy
ST131	Sequence type 131
TBS-T	Tris-buffered saline with Tween-20
TCS	Two-component system
TEM	Transmission electron microscopy
TFA	Trifluroacetic acid
TMAO	Trimethylamine N-oxide

TOF	Time-of-flight
UTIs	Urinary tract infections
VUMC	Vanderbilt University Medical Center
VUTI	Vanderbilt Urinary Tract Isolate
YESCA	Yeast extract cas-amino acids

CHAPTER I

INTRODUCTION

Urinary Tract Infection

[1]Infections caused by bacterial pathogens are a significant source of human morbidity, resulting in the administration of ~260 million courses of antibiotics annually (Hicks *et al.*, 2015). Of these, urinary tract infections (UTIs) are among the most common, afflicting ~150 million individuals worldwide (Flores-Mireles *et al.*, 2015). The high morbidity associated with UTI results in ~13,000 infection-related deaths annually within the United States (Klevens *et al.*, 2007).

Bacterial colonization of the urinary tract can range from asymptomatic bacteriuria (ASB) with little to no presentable symptoms and should not be treated (Nicolle, 2014a), to symptomatic infection with acute and/or chronic outcomes that often requires treatment (Wagenlehner *et al.*, 2011b). Infection of the lower urinary tract (known as cystitis) is associated with increased lower abdominal pain, increased urgency and frequency of urination, painful urination, the inability to completely void the bladder, and increased risk of symptomatic upper urinary tract (kidney) infection (known as pyelonephritis) (Stamm and Hooton, 1993).

---

[1] Portions of this chapter adapted from and published in:

Floyd *et al.* The yin-yang driving urinary tract infection and how proteomics can enhance research, diagnostics and treatment. *Proteomics Clin. Appl*. 2015 Dec; 9 (11-12). (PMID: 26255866, PMCID: PMC5019064)

Floyd *et al.* Chapter 3. Adhesion of Bacteria to Surfaces and Biofilm Formation on Medical Devices. *Biofilms and implantable medical devices: infection and control (Textbook)*. Woodhead Publishing Series in Biomaterials. 2016.

Development of pyelonephritis can lead to a breakdown of the kidney-blood barrier, allowing for bacterial entry to the bloodstream, and the potential for the development of secondary site infection and/or life-threatening systemic infection or septicemia (Wagenlehner *et al.*, 2011b). Notably, of all cases of septicemia, ~20-30% stem from an initial UTI (Wagenlehner *et al.*, 2011b).

Risk of developing UTI significantly increases with advancing age (Arinzon *et al.*, 2012), and with the addition of confounding medical conditions such as diabetes (Patterson and Andriole, 1995). Community-acquired UTIs disproportionally affect women with approximately 1 in every 2 women experiencing at least one UTI over the course of their lifetime (Barber *et al.*, 2013). This gender bias is largely attributed to the spatial proximity of the urethral opening to the anus and vagina, as well as the overall shorter urethral length in females compared to males. Between 2006 and 2010, community-acquired UTIs were estimated to account for approximately 40 million ambulatory medical visits, equating to ~8 million visits each year (May *et al.*, 2014). In addition, UTIs have a significantly higher rate of recurrence after an initial episode (Hooton, 2001). Of those afflicted with a UTI, 30–50% of women and 12% of men will experience at least one recurrence within three months of the initial infection (Foxman, 2010). The incidence of a recurrent UTI within this time frame increases the risk for multiple recurrent episodes. Along with significantly decreasing the quality of life for the afflicted individual, recurrent UTIs have recently been linked to an elevated risk for the development of bladder cancer (Vermeulen *et al.*, 2015).

Community-acquired UTIs in immuno-competent females with no other confounding medical conditions are termed uncomplicated UTIs, while infection in males is almost always considered complicated regardless of immune status (Wagenlehner *et al.*, 2011a, Lipsky, 1989).

In addition, UTIs in individuals with a complicating factor such as bladder/kidney tissue abnormalities, confounding medical conditions (e.g. diabetes), physical obstruction of the urinary tract (e.g. bladder or kidney stones), pregnancy, or instillation of medical instrumentation such as indwelling urinary catheters are also considered to be complicated UTIs (Lipsky, 1989, Patterson and Andriole, 1995, Neal, 2008, Dielubanza *et al.*, 2014).

Catheter-associated Urinary Tract Infections

Within healthcare facilities such as hospitals, hospices, and long-term care nursing homes, urinary catheters are the most common indwelling medical device, with recent prevalence surveys reporting 18–24% of inpatients being catheterized (Zarb *et al.*, 2012, Magill *et al.*, 2014). Approximately 80% of the 1 million annual cases of hospital-acquired UTIs, correlate with the use of an indwelling urinary catheter, classifying them as complicated UTIs (Foxman, 2010, Daniels *et al.*, 2014, Nicolle, 2014b). In hospital and long-term healthcare facilities, each day 3-7% patients with an indwelling urinary catheter develop bacteriuria (Hooton *et al.*, 2010). Given that urinary catheterization increases the chances of bacterial introduction to the urinary tract, the gender bias observed with community-acquired UTIs is negated in hospital-acquired UTI, and males are impacted as equally as females (Foxman, 2010, Klevens *et al.*, 2007). Urinary catheter-associated (CA) conditions include asymptomatic colonization of the urinary tract or ASB (CA-ASB), as well as symptomatic catheter-associated UTI (CAUTI) (Hooton *et al.*, 2010, Nicolle, 2014b). CA-ASB is the most frequent hospital-acquired infection worldwide and accounts for up to 40% of all hospital-acquired infections in the United States annually (System, 2004, Haley *et al.*, 1981). CA-ASB can eventually lead to symptomatic UTI, though direct correlation between CA-ASB and eventual CAUTI has yet to be

thoroughly investigated (Platt *et al.*, 1982, Wagenlehner *et al.*, 2011b).

Causative agents of UTI and CAUTI

Typically, introduction of bacteria to the catheter lumen occurs upon catheter insertion into the urinary tract (Nicolle, 2014b). The majority of complicated UTIs and CAUTIs are attributed to a select group of Gram-negative and Gram-positive bacterial species, the most predominant of which include uropathogenic strains of *Escherichia coli* (UPEC) (~65%), *Enterococcus faecalis* (~11%), and *Klebsiella pneumoniae* (~8%) (**Figure 1**, (Flores-Mireles *et al.*, 2015)). These same bacterial species also contribute to the majority of uncomplicated UTIs, with a higher proportion coming from UPEC (~75%), and less from *K. pneumoniae* (~6%) and *E. faecalis* (~5%) (**Figure 1**, (Flores-Mireles *et al.*, 2015)). Interestingly the Gram-positive species *Staphylococcus saprophyticus* accounts for approximately 6% of uncomplicated UTIs, but does not generally contribute to complicated UTI (**Figure 1**, (Flores-Mireles *et al.*, 2015)). Less prevalent bacterial uropathogens include the Gram-positive pathogens, Group B *Streptococcus* spp. and *Staphylococcus aureus*, as well as the Gram-negative pathogens *Proteus mirabilis* and *Pseudomonas aeruginosa* (**Figure 1**, (Flores-Mireles *et al.*, 2015)). Finally, in addition to bacterial pathogens, fungal pathogens account for a proportion of UTIs. *Candida spp*. specifically are isolated from ~1% of uncomplicated and ~7% of complicated UTIs (**Figure 1**, (Flores-Mireles *et al.*, 2015)).

Antibiotic resistance complicates UTI and CAUTI treatment

In some cases UTIs can independently resolve without treatment (Foxman, 2010). However, in many cases short-term administration of the antimicrobial cotrimoxazole (5:1 ratio

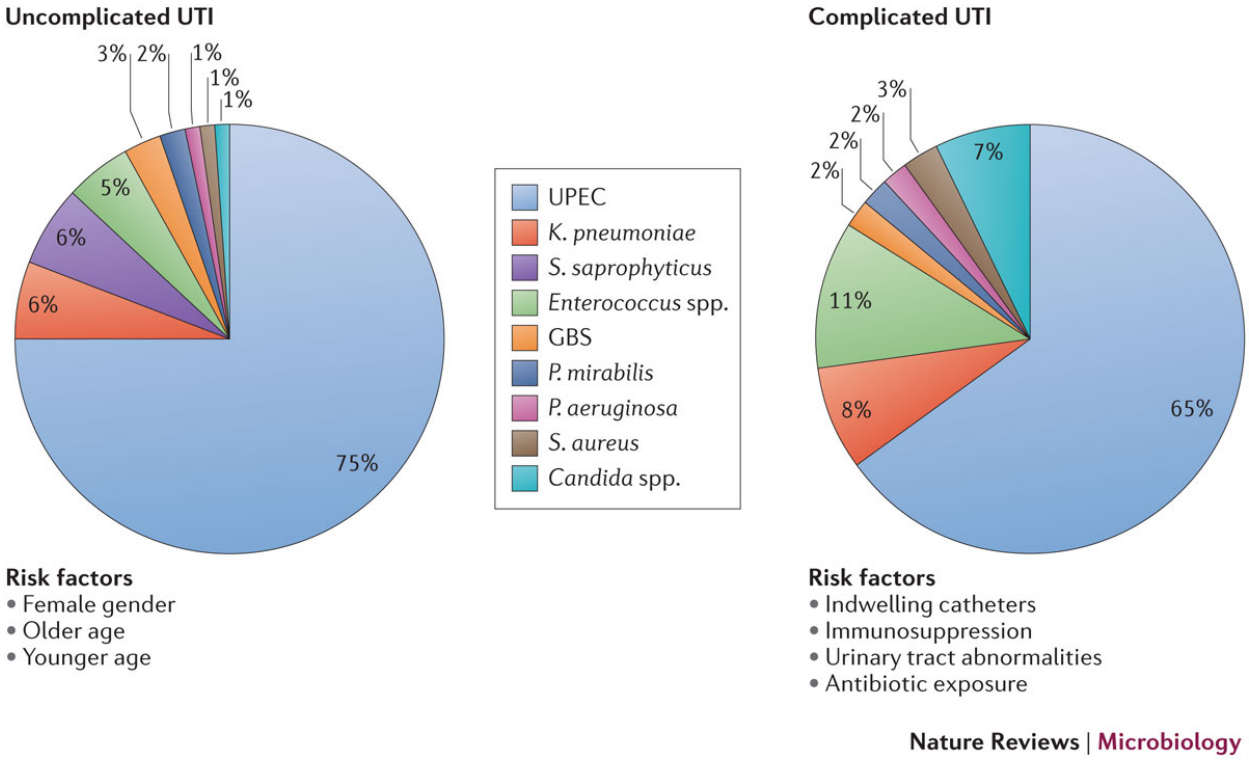

Figure 1. Epidemiology of urinary tract infections. Urinary tract infections (UTIs) are caused by a wide range of pathogens, including Gram-negative and Gram-positive bacteria, as well as fungi. Uncomplicated UTIs typically affect women, children and elderly patients who are otherwise healthy. Complicated UTIs are usually associated with indwelling catheters, urinary tract abnormalities, immunosuppression or exposure to antibiotics. The most common causative agent for both uncomplicated and complicated UTIs is uropathogenic *Escherichia coli* (UPEC). For uncomplicated UTIs, other causative agents are (in order of prevalence) *Klebsiella pneumoniae*, *Staphylococcus saprophyticus*, *Enterococcus faecalis*, group B *Streptococcus* (GBS), *Proteus mirabilis*, *Pseudomonas aeruginosa*, *Staphylococcus aureus* and *Candida* spp. For complicated UTIs, the other causative agents are (in order of prevalence) *Enterococcus* spp., *K. pneumoniae*, *Candida* spp., *S. aureus, P. mirabilis*, *P. aeruginosa* and GBS. Reprinted from (Flores-Mireles *et al.*, 2015) with all rights and permissions.

of the sulfonamide sulfamethoxazole and the dihydrofolate reductase inhibitor trimethoprim) or the fluoroquinolone ciprofloxacin is required for clearance of infection (Gonzalez and Schaeffer, 1999, Nicolle, 2008). These treatment strategies have become less effective in recent years, given the rise in antibiotic-resistant bacteria (Barber *et al.*, 2013, Shariff V A *et al.*, 2013, Foxman, 2014, Foxman and Buxton, 2013). The Centers for Disease Control and Prevention (CDC) estimate that each year in the United States approximately 2 million individuals are infected with antibiotic-resistant bacteria, and approximately 23,000 individuals succumb to infection (Prevention, 2013).

A 2005 study by the North American UTI Collaborative Alliance, examined 1990 bacterial isolates obtained from patients with UTIs, and found that 20% of isolates were resistant to co-trimoxazole (Zhanel *et al.*, 2005). More recently, multidrug resistant *E. coli* strains of the sequence type 131 (ST131) have been disseminating globaly (Petty *et al.*, 2014). Strains of *E. coli* ST131 have been observed to carry extended spectrum β-lactamase resistance, resistance to aminoglycosides, cotrimoxazole, fluoroquinolones, and even carbapenems (Coque *et al.*, 2008, Lau *et al.*, 2008a, Lau *et al.*, 2008b, Johnson *et al.*, 2012, Johnson *et al.*, 2010, Uchida *et al.*, 2010, Peirano *et al.*, 2011, Morris *et al.*, 2012). Along with high levels of antibiotic resistance, many ST131 strains carry a mutation in the *fimB* recombinase gene that increases expression of type 1 pili and their infectivity in the urinary tract (Paul *et al.*, 2013).

The last line of antibiotic defense for treatment against multidrug resistant bacteria is the antimicrobial polypeptide colistin. In 2016, a strain of *E. coli* harboring the gene *mcr-1* on a transmissible plasmid was isolated from a 49-year-old female UTI patient (McGann *et al.*, 2016). The *mcr-1* gene codes for colisitn resistance, and this was the first identification of a bacterial strain carrying the *mcr-1* gene in the United States (McGann *et al.*, 2016). Transmission of the

plasmid carrying the *mcr-1* gene to uropathogenic bacteria (as well as other bacterial pathogens) already resistant to multiple antibiotics would present an extreme public health challenge.

Biofilm formation further compounds UTI treatment

Even without antibiotic resistance, bacterial pathogens have developed strategies to tolerate antibiotic stressors as well as the host immune response. UPEC are consistently observed to be the primary causative agent of both complicated and uncomplicated UTIs (Foxman, 2010, Flores-Mireles *et al.*, 2015). UPEC are an extra-intestinal *E. coli* pathotype, which can colonize but does not establish symptomatic infection within the gastro-intestinal tract. UPEC express a number of virulence factors that facilitate colonization and persistence within the urinary tract including adhesive fibers, toxins, metal acquisition and sequestration systems, etc. (Floyd *et al.*, 2015a). Using different types of adhesive appendages, UPEC strains can attach to indwelling catheter material, as well as epithelial surfaces within the urinary tract. Much like UPEC, pathogenesis of the other leading urinary pathogens is also linked to the ability to attach and adhere to catheters and niches within the urinary tract (Flores-Mireles *et al.*, 2015, Khandelwal *et al.*, 2009, Jacobsen and Shirtliff, 2011, Niveditha *et al.*, 2012).

Attachment and adherence to the catheter material and to the host bladder and kidney epithelium, can lead to the formation of multicellular bacterial communities, known as biofilms (López *et al.*, 2010). Biofilms have characteristics that afford resident bacteria protection from antibiotic treatment and removal by urinary shear flow. The biofilm environment also provides the opportunity for horizontal gene transfer, which allows for intra- and inter-species exchange of antibiotic-resistance markers and other genetic information that may enhance bacterial fitness. Furthermore, in the case of UTI, bacteria dispersing from the catheter-associated biofilm serve as

a perpetual reservoir for infection within the lower and upper urinary tracts (**Figure 2A**). Once bacteria originating from an indwelling catheter have established infection within the urinary tract, removal of the contaminated catheter will not rid the patient of the colonizing bacteria. Upon insertion of a clean catheter, bacteria can descend from the bladder lumen, and adhere to the new catheter resulting in contamination of the sterile catheter and perpetuation of the infection cycle (**Figure 2B**).

Therefore, not surprisingly, despite development of catheters impregnated or coated with antimicrobial agents, studies indicate that the type of catheter used (treated vs. non-treated) does not reduce the probability of infection (Foxman, 2010). In fact, the CDC reports that between 2009-2013 the incidence rate of CAUTI increased by 6% (Prevention, Published January 14, 2015.). The same report indicates that while CAUTI rates increased, the rates of all other hospital-acquired infections (including methicillin-resistant *Staphylococcus aureus*, MRSA, bacteremia) decreased over the same time period (Prevention, Published January 14, 2015.). Therefore, biofilm formation on indwelling urinary catheters serves as a major reservoir for continued colonization and persistence of infection within the urinary tract. In order to develop new methods to target and treat biofilm- associated infections, such as CAUTI, it is imperative to first have a clear understanding of the underlying mechanisms that govern the complex process of biofilm formation onto catheters and within the urinary tract.

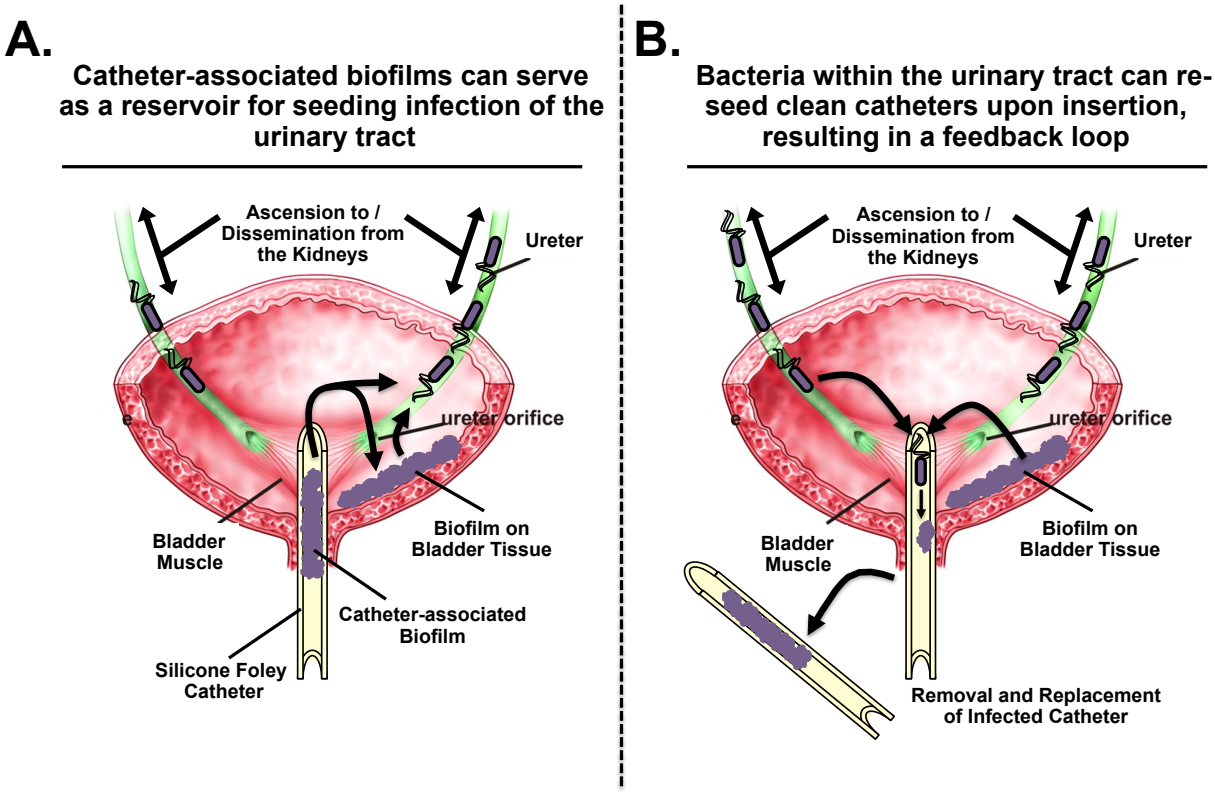

Figure 2. Multicellular biofilms enhance catheter-associated UTI and serve as a reservoir for persistence of infection. (A) Biofilm formation on the indwelling urinary catheter allows for assentation of bacteria into the urinary tract. Entry to the urinary tract allows for the colonization and establishment of infection within the bladder and/or kidneys. **(B)** Upon identification of CAUTI infection and removal of the contaminated catheter, bacteria that have preciously ascended and colonized the urinary tract can descend and reestablish biofilm on the newly introduced sterile indwelling catheter. Therefore, catheter-associated biofilm communities serve as a major reservoir for creating a continued cycle of infection within the urinary tract. Bladder schematic adapted from (Viana *et al.*, 2007), reprinted with permissions.

Stages of Biofilm Formation

Biofilm formation is considered a developmental process, which comprises four stages that are highly conserved among bacteria (**Figure 3**): reversible/irreversible attachment, (**Figure 3A-C**), micro-colony formation (**Figure 3D**), maturation (**Figure 3E**), and dispersal (**Figure 3F**). While these biofilm stages are conserved, the bacterial factors associated with each stage vary significantly from species to species and even from strain to strain, making the elucidation of biomarkers or potential therapeutic drug targets highly difficult. Following, are some examples highlighting the diversity of biofilm factors expressed at different stages in biofilm development, by different uropathogenic bacterial species.

Reversible/irreversible Attachment

Bacterial attachment to a surface (**Figure 3A-C**) is dictated by both the surface, and the types of adhesive components expressed by the bacterial cells. Bacterial adhesive components include; protein adhesins, macromolecular proteinaceous structures, and non-proteinaceous components such as extracellular DNA (eDNA), lipids, and polysaccharides. Typically, the initial interaction of the bacteria with the surface may be transient and reversible (**Figure 3A-B**). This can be due to weak interactions of bacteria with the surface that result from the hydrodynamics of the surrounding environment, the presence of a strong chemotactic signal away from the surface, or simply the lack of adhesive components that are compatible with the surface (Petrova and Sauer, 2012). However, the act of adhering to a surface, if it persists long enough, can signal for contact-dependent alterations in gene expression that will pivot the cellular processes towards irreversible attachment to the surface and subsequent biofilm formation.

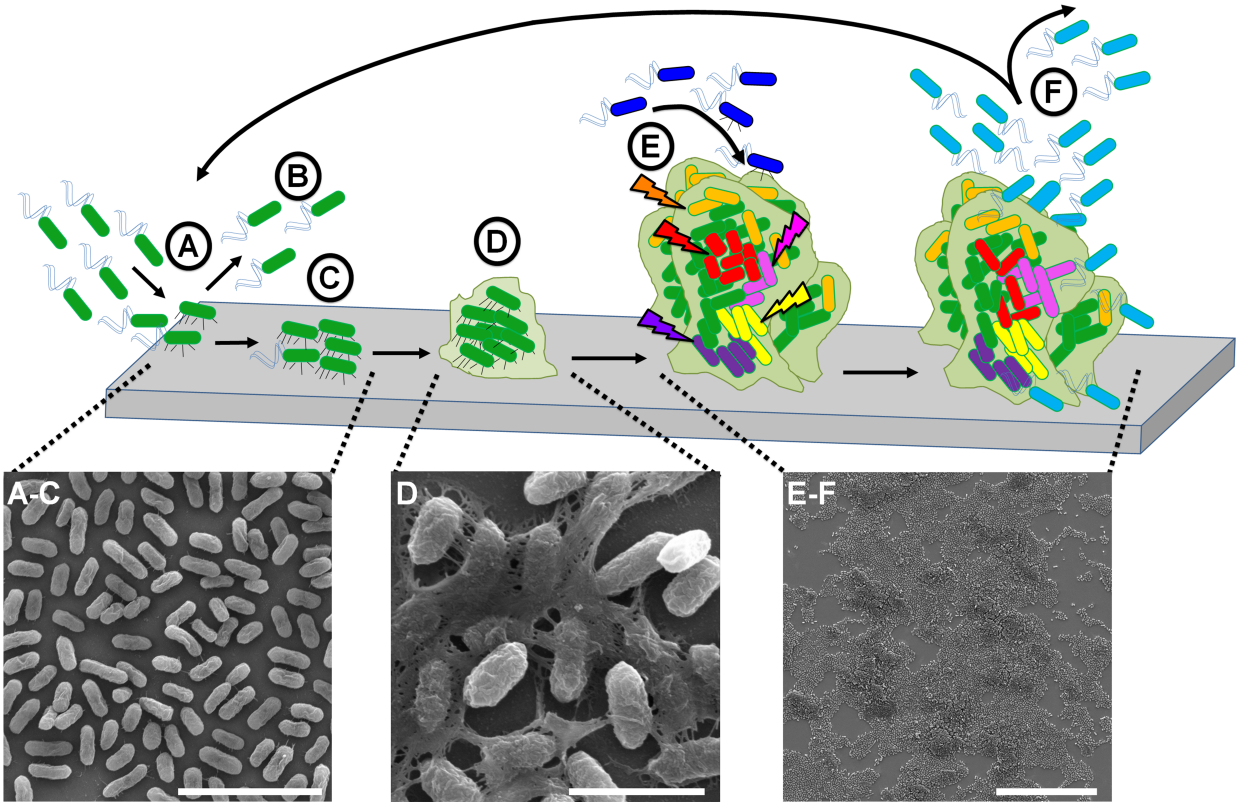

Figure 3. Schematic of the canonical biofilm formation pathway presented from the standpoint of Gram-negative bacteria. This schematic depicts the four main stages of bacterial biofilm formation. Though it is presented from the viewpoint of Gram-negative bacteria, the overall pathway and stages of development apply to Gram-positive bacteria. Surface schematic (gray rectangle) represents a biotic or abiotic surface, which serves as the substratum for bacterial attachment. The stages presented are; **(A-C) Reversible/irreversible attachment** with the scanning electron micrograph below depicting uropathogenic *Escherichia coli* (UPEC) strain UTI89 irreversibly attached to a charged glass surface (Scale bar = 5μm), **(D) Micro-colony formation** with the micrograph below depicting UPEC strain UTI89 that has begun to secrete the encapsulating extracellular matrix on a charged glass surface (Scale bar = 2μm), **(E) Maturation of the biofilm** with the micrograph below depicting a bird's eye view of a mature surface-associated biofilm formed on a charged glass surface by UPEC strain UTI89 (Scale bar = 50μm), and **(F) Dispersal from the biofilm**.

Many species of Gram-negative bacteria encode an array of different individual protein adhesins that allow for the sampling of a multitude of surfaces. One such example is the family of autotransporter proteins, which mediate their own translocation to the bacterial cell surface and facilitate attachment. UPEC protein Antigen 43 is an auto-transporter adhesin that is critical for long-term persistence of bacteria in the urinary tract (Ulett *et al.*, 2007). In addition to adhesins, both Gram-negative and Gram-positive bacteria can elaborate adhesive macromolecular structures, called pili or fimbriae, to make contact with the surface (**Figure 4**). Gram-positive bacteria typically assemble pili via a sortase-dependent pathway (**Figure 4A**). One example of Gram-positive pili assembled in this manner is the endocarditis-and biofilm-associated pili (Ebp) in *Enterococcus faecalis* that are critical for adherence and biofilm formation contributing to CAUTI (Singh *et al.*, 2007, Nielsen *et al.*, 2013). Type IV pili (**Figure 4C**) can be elaborated by both Gram-positive and Gram-negative bacterial species, and are typically assembled via a type 2 secretion system pathway among uropathogens (Merz *et al.*, 2000). *P. aeruginosa* use type IV pili to engage in a process termed "walking", or twitching motility, that is crucial for reversible to irreversible attachment (van Schaik *et al.*, 2005, Qi *et al.*, 2012, Barken *et al.*, 2008, Klausen *et al.*, 2003).

Another class of pili, assembled by the chaperone-usher pathway (CUP) pili is unique to Gram-negative bacteria including *E. coli, Pseudomonas, and Klebsiella* species (Busch and Waksman, 2012, Fronzes *et al.*, 2008, Chen *et al.*, 2009, Dodson *et al.*, 2001) (**Figure 4B**). CUP pili are multi-subunit pili with adhesive properties mediated by their tip adhesins (Busch and Waksman, 2012, Fronzes *et al.*, 2008, Chen *et al.*, 2009). Elaboration of CUP pili to the bacterial outer membrane, occurs via a conserved process in which incorporation of a pilus subunit through a membrane "usher" completes an immunoglobulin fold in another protein subunit.

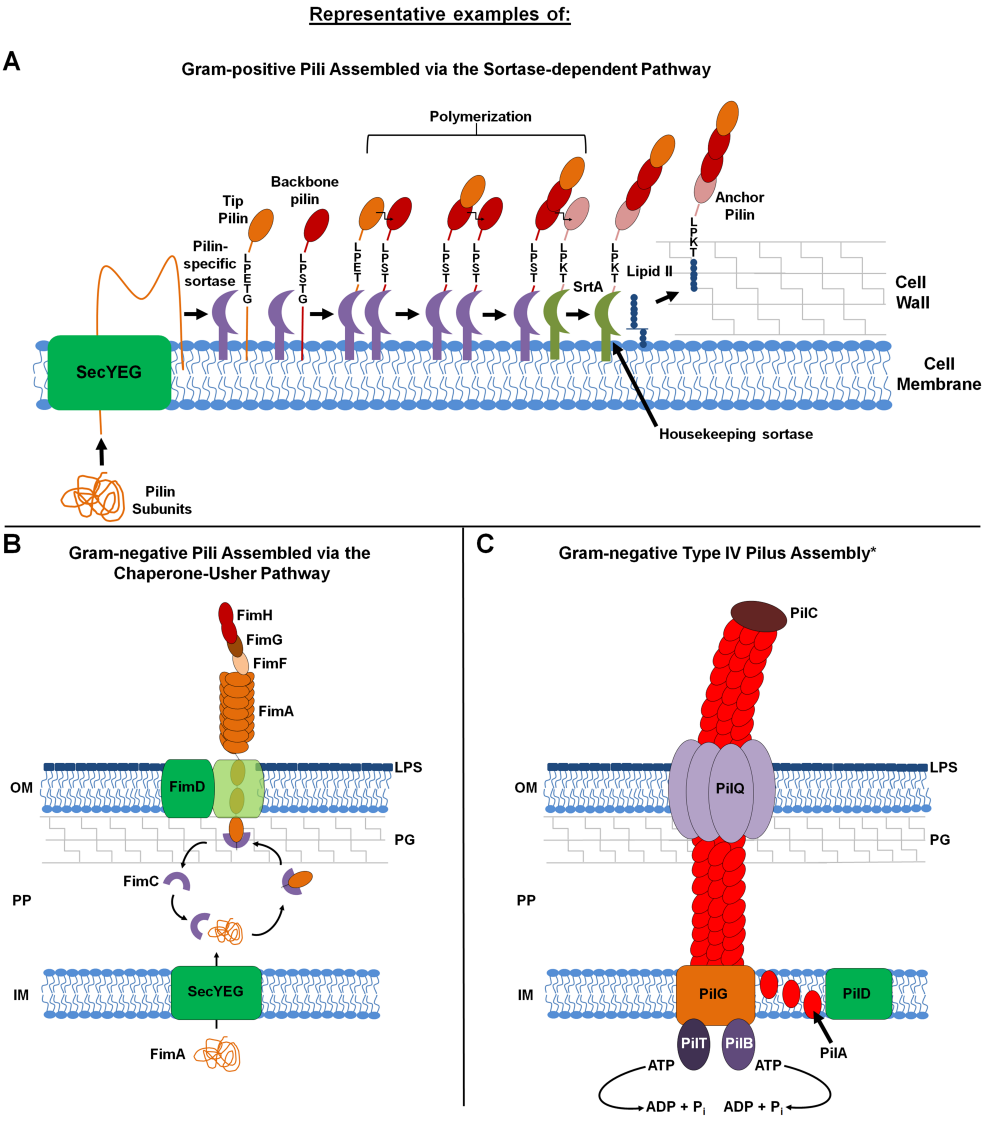

Figure 4. Macromolecular adhesive fibers can contribute to bacterial adherence and attachment to surfaces. This schematic depicts three different mechanistic pathways by which adhesive macromolecular fibers are assembled onto the surface of bacteria. **(A) Sortase-dependent pilus biogenesis in Gram-positive bacteria.** Depicted is a model for sortase-dependent pilus biogenesis as it has been defined for *Enterococcus faecalis* Ebp pili (Nielsen *et al.*, 2013). **(B) Chaperone-usher pathway (CUP) pilus biogenesis.** Depicted is a model of the assembly of the CUP type 1 pili in *Escherichia coli* (Waksman and Hultgren, 2009). **(C) Type IV pilus biogenesis.** Both Gram-positive and Gram-negative bacteria can produce type IV pili. This model depicts assembly of type IV pili within Gram-negative bacteria, specifically within *Vibrio cholerae* (Craig *et al.*, 2003). Abbreviations: IM, inner membrane; LPS, lipopolysaccharide; OM, outer membrane; PG, peptidoglycan; PP, periplasm.

Once pilus subunits are translocated across the inner membrane by the Sec translocon, they are collected by a periplasmic "chaperone" that stabilizes folding and escorts subunits to the outer membrane usher for assembly. Pilus subunits are characterized by an incomplete immunoglobulin-like fold, which lacks the C-terminal beta-strand (Waksman and Hultgren, 2009). This incomplete fold is stabilized by the interaction of one of the chaperone strands, called the G1 strand that is "donated" by the chaperone during chaperone-subunit interaction (Waksman and Hultgren, 2009), in a process termed "donor strand complementation" (Waksman and Hultgren, 2009, Geibel and Waksman, 2014). The same process drives subunit interactions between pilin subunits, facilitated by the chaperone and the usher, to allow for pilus elaboration and extrusion to the cell surface.

Pilus-mediated adherence is primarily achieved via a tip adhesin, which has stereochemical specificity for specific moieties. For example the FimH adhesin found on the tip of type 1 pili in UPEC and *K. pneumoniae*, mediates adherence to mannosylated uroplakin receptors on the bladder epithelial surface (Eto *et al.*, 2007, Bouckaert *et al.*, 2005, Hung *et al.*, 2002, Martinez *et al.*, 2000, Thankavel *et al.*, 1997, Zhou *et al.*, 2001, Thumbikat *et al.*, 2009, Struve *et al.*, 2009, Struve *et al.*, 2008). The PapG adhesin found at the tip of P pili of UPEC, facilitates binding to digalactoside receptors found on renal epithelial cells to facilitate colonization of the kidney (Kuehn *et al.*, 1992, Hultgren *et al.*, 1989). The recent increase in sequenced *E. coli* genomes has revealed the presence of numerous additional, uncharacterized CUP pili in each of the UPEC chromosomes, suggesting an expanded repertoire of surfaces that UPEC can adhere to (Chen *et al.*, 2006, Welch *et al.*, 2002). *K. pneumoniae* can also express another class of CUP pili, known as type 3 pili, which have been shown to contribute to bacterial

adherence in the host and during biofilm formation on silicone catheters (Di Martino *et al.*, 2003, Murphy *et al.*, 2013).

Other proteinaceous macromolecular complexes mediating attachment that are encoded by both Gram-positive and Gram-negative bacteria, include amyloid fibers, homologous in structure to the amyloids that are associated with Parkinson's and Alzheimer's diseases in humans (Collinson *et al.*, 1993, Evans and Chapman, 2014). Functional bacterial amyloids have been characterized in UPEC, and have been shown to specifically contribute to adhesion on abiotic surfaces, to be a component of the biofilm extracellular matrix, as well as to be a host immunogen (Evans *et al.*, 2015, Gallo *et al.*, 2015, Rapsinski *et al.*, 2013, Tükel *et al.*, 2009, Barnhart and Chapman, 2006, Kikuchi *et al.*, 2005). Bacteria can also engage a surface using non-proteinaceous components, such as their capsule that is typically made up of polysaccharides (Kasper, 1986, Cantey *et al.*, 1981, Schrager *et al.*, 1998, Huebner and Goldmann, 1999). Along with the capsule, extracellular DNA (eDNA) has been shown to alter the hydrophobicity of the bacterial cell surface, modulating bacterial interactions with surfaces of varying hydrophobicity (Okshevsky and Meyer, 2015). For example, surface attachment by *Pseudomonas* spp. has been shown to be dependent on the presence of eDNA (Whitchurch *et al.*, 2002).

Micro-colony Formation

Once bacteria "commit" to adhering productively to a surface they begin to multiply forming small bacterial communities with some three-dimensional architecture, known as micro-colonies. Critical to this stage is the simultaneous production of an encapsulating extracellular matrix (ECM) by the adherent bacteria (**Figure 3D**). The ECM is considered a hallmark feature

of biofilm formation, as it serves as a scaffold to maintain the integrity and three-dimensionality of the community as it grows (Flemming and Wingender, 2010, Branda *et al.*, 2005). Perhaps the most important function of the ECM is to serve as a protective barrier from environmental stresses (including antibiotics) and predatory microorganisms (Flemming and Wingender, 2010, Branda *et al.*, 2005, López *et al.*, 2010, Donlan, 2002, Matz and Kjelleberg, 2005, Matz *et al.*, 2005). As is true for the repertoire of adhesive components already discussed, the composition of the ECM can vary significantly by bacterial species, and even among strains of the same species. ECM composition also varies in response to environmental conditions, including but not limited to temperature, nutrient resources, and oxygen concentration. Typically the ECM comprises a combination of lipids, polysaccharides, eDNA, and proteins (Steinberg and Kolodkin-Gal, 2015, Thomas *et al.*, 2009, Vilain *et al.*, 2009, Izano *et al.*, 2008, Andes *et al.*, 2004, Friedman and Kolter, 2004, Sutherland, 2001, Zogaj *et al.*, 2001, Koo *et al.*, 2010, Tetz *et al.*, 2009). Almost all adhesive components previously discussed in this chapter can also be found as part of the bacterial ECM under the appropriate growth conditions.

Biofilm Maturation

Growth of the ECM-encapsulated micro-colony via cell division, and/or by incoming planktonic cells to the biofilm community (**Figure 3E**), leads to spatial expansion of the biofilm within the physical constraints of the surrounding environment. As the biofilm expands in size, the three-dimensional architecture of the community increases in complexity. Biofilm bacteria expand radially, as well as vertically, from the point of initial attachment in an effort to increase access to electron acceptors and nutrients needed to maintain the health of the community (Stoodley *et al.*, 2002). Formation of water or nutrient channels in the expanding population can

funnel required nutrients throughout the growing biofilm community (Hall-Stoodley and Stoodley, 2002, de Beer *et al.*, 1994, Stewart, 2003).

However, given the increasing surface area and volume of the biofilm, bacteria within the community begin to be surrounded by varying environmental gradients; such as nutritional availability, oxygen concentration, and population density. The presence of gradients along and around the biofilm influences local gene expression within the community, and gives rise to population heterogeneity among the residents. These "subpopulations" encode different factors that can contribute to "common goods" used by all bacteria in the biofilm, or they can exhibit unique characteristics (such as antibiotic tolerance or hyper-infectivity) that can enhance bacterial fitness (Savage *et al.*, 2013, Rani *et al.*, 2007). Phenotypic heterogeneity is schematically depicted in **Figure 3E**, where signals from the surrounding environment (colored lightning bolts) lead to altered gene expression and the development of distinct subpopulations (of corresponding color).

An example of one subpopulation that develops within many bacterial biofilms, are metabolically inactive cells that tolerate high doses of antimicrobial treatment These subpopulations, termed persister cells, can regain metabolic activity to re-establish infection upon cessation of the initial antibiotic treatment that abolished their metabolically active brethren (Lewis, 2010, Hung *et al.*, 2013b, Lewis, 2007). Persisters and "persister-like" bacterial subpopulations have been identified for pathogenic *E. coli* (Balaban *et al.*, 2004, Keren *et al.*, 2004), *P. aeruginosa* (Möker *et al.*, 2010, Harrison *et al.*, 2005, Mulcahy *et al.*, 2010), and *S. aureus* (Singh *et al.*, 2009, Hammer *et al.*, 2014). The presence of persister cell populations significantly dampens treatment and increases the risk of persistence of these infections within the host, demonstrating how phenotypic diversification within the biofilm enhance bacterial

survival and persistence. A great hurdle in identifying persisters and other types of subpopulations within maturing biofilms is the lack of knowledge with regards to subpopulation-specific gene expression signatures, as well as the precise location of these cells within the biofilm community.

Dispersal from the Biofilm

A mature biofilm community can persist for extended periods of time, owing to the ECM and the subpopulations that arise and contribute to resilience. However, bacteria can disperse from the biofilm and regain a planktonic lifestyle, if they intercept an environment cue that allows for their mobilization from the ECM (**Figure 3F**). The mechanisms that drive dispersal are perhaps the least well understood (Hall-Stoodley and Stoodley, 2005, Kaplan, 2010, Kostakioti *et al.*, 2013). Cues like increased cell density (Parsek and Greenberg, 2005), nutrient availability (Sauer *et al.*, 2004), and atmospheric cues can also lead to dissemination from the biofilm. In *P. aeruginosa* biofilms, dispersal can be signaled through nitric oxide (NO) that enhances the phosphodiesterase activity of certain enzymes leading to the degradation of the biofilm-promoting molecule Bis-(3′-5′)-cyclic dimeric guanosine monophosphate (c-di-GMP) (Barraud *et al.*, 2006, Barraud *et al.*, 2015, Plate and Marletta, 2012). In situations where dispersing bacteria originate from a catheter surface, these bacteria can lead to ascending UTI and possible bacteremia and sepsis. Therefore, dispersing bacteria that are responsible for the establishment of secondary-site infection can also be thought of as a biofilm subpopulation. Subpopulations that contribute to the resilience and persistence of bacterial biofilms on urinary catheters, and biotic surfaces of the urinary tract, present possible targets for novel anti-biofilm strategies that could attenuate biofilm-associated pathogenesis.

Research Objectives and Significance

This thesis dissertation describes studies aimed at identifying UPEC biofilm subpopulations; with the ultimate goal of better understanding UPEC biofilm architecture, conservation of spatial localization of subpopulations between different UPEC strains, and the identification of potential pathogen specific drug targets. Prior to the initiation of these studies little was known about the types of subpopulations that existed, or the genes that were expressed by UPEC biofilm subpopulations. By adapting MALDI-TOF Imaging Mass Spectrometry methodologies for the analysis of protein stratification within UPEC biofilms, we were able to identify distinct UPEC subpopulations that express unique protein species (**Chapter II**). Identification of the proteins expressed within these subpopulations, revealed environmental-induced segregation of adhesive fibers within the biofilm. Further studies revealed that environmental oxygen concentration influences the expression of type 1 pili through multiple mechanisms (**Chapter II and III**). Specifically, decreased oxygen concentrations influences the orientation of the phase-variable *fimS* promoter (**Chapter III**), which is mediated by the regulators FimE (**Chapter III**) and FNR (**Chapter IV**). These findings prompted investigations that revealed the murine bladder contains enough oxygen to force aerobic respiration by UPEC (**Chapter V**). Preliminary data also suggest the presence of an additional mechanism, which acts post-translationally to prevent the elaboration of type 1 pili in the absence of oxygen (**Chapter IV**). Together, these studies highlight the power of MALDI-TOF IMS for the identification and characterization of UPEC biofilm subpopulations, and provide insights into environmental regulation of type 1 pili that help explain the preference of UPEC for the bladder as an infectious niche.

Future studies (**Chapter VI**) will examine the application of high-resolution MALDI-TOF IMS for the analysis of protein stratification directly within biofilms obtained directly from CAUTI patients. Along with enhancement of IMS methodologies, future studies will continue to dissect the mechanisms underlying the oxygen-dependent regulation of type 1 pili within UPEC. The precise mechanism(s) by which the regulatory protein FNR transcriptionally suppresses type 1 pili expression under atmospheric and anoxic conditions will be determined, along with the mechanism(s) underlying potential secondary post-translational suppression of type 1 pili elaboration under anoxic conditions.

CHAPTER II

EXPANDING THE TOOLKIT: APPLICATION OF MALDI-TOF IMAGING MASS SPECTROMETRY METHODOLOGIES FOR THE ANALYSIS OF PROTEIN STRATIFICATION WITHIN INTACT BACTERIAL BIOFILMS

Introduction

[2]The development of bacterial subpopulations contributes to biofilm resilience and persistence (**Figure 3E**). Fluorescent *in-situ* hybridization (FISH) using probes specific for distinct regions of 16S ribosomal RNA, has been previously used to decipher bacterial species present within multi-species biofilms (Valm *et al.*, 2011). While FISH is excellent for species identification, the detection of bacterial subpopulations arising within single-species biofilms is impossible with this methodology. In single-species biofilms all members of the community harbor the same genes but express them differently. Traditional techniques for the analysis and characterization of subpopulations within a single-species biofilm have been requisite upon known protein targets for either detection by immuno-fluorescence (Rani *et al.*, 2007) or labeling via genetic fusion with a fluorescent protein (Vlamakis *et al.*, 2008, Williamson *et al.*, 2012). Both techniques are also generally limited in the number of proteins that they can detect within a single-analysis. The presence of subpopulations in UPEC biofilms is largely hypothesized based upon observations of phenotypic differences within varying regions of biofilms (Hung *et al.*,

[2] Portions of this chapter adapted from and published in:

Floyd *et al.* Adhesive Fiber Stratification in Uropathogenic *Escherichia coli* Biofilms Unveils Oxygen-Mediated Control of Type 1 Pili. *PLoS Pathog.* 2015 Mar 4;11(3):e1004697. (PMID: 25738819)

2013a), and from studies that have identified the presence of persister cells in K12 *E. coli* biofilms (Lewis, 2005). Therefore, there is the need for methods that can help visualize multiple protein profiles within intact bacterial biofilms without *a priori* knowledge of protein targets. Such approaches would also open avenues for identifying potentially new subpopulations, based upon common patterns of spatial localization and relative abundance of different protein species.

Matrix-assisted laser desorption/ionization (MALDI) time-of-flight (TOF) imaging mass spectrometry (IMS) is a fairly unbiased surface-sampling approach for the detection and spatial localization of analytes within intact biological samples (Caprioli *et al.*, 1997). Depending upon the exact methods used for MALDI-TOF IMS, analytes can include small molecules, lipids, peptides, and small or large molecular weight proteins (Norris and Caprioli, 2013). A general schematic for MALDI-TOF mass spectrometry (MS) and imaging mass spectrometry (IMS) is shown in **Figure 5**. For MALDI-TOF MS and IMS analyses, samples are treated with a matrix that absorbs energy from an ultra-violet (UV) laser source to ionize analytes of interest that have co-crystallized with the UV-absorbing matrix (**Figure 5**). The sample preparation used methods prior to matrix application, as well as the matrix chosen for the analysis, will dictate the type of analytes observed. Therefore, selection of these parameters will bias the analytes observed based upon biochemical properties, size, or charge (Seeley *et al.*, 2008). Upon laser excitation, the generated ions are accelerated along a TOF mass analyzer for separation and detection (Pól *et al.*, 2010). For IMS, MALDI-TOF mass spectra are collected in a defined spatial array (in x and y dimensions) across the sample. Each point within the spatial array can be considered a “pixel”, and at each pixel the peak intensity in the spectra is extrapolated and compared to the intensity of all other pixels in the sample to generate an ion intensity map across the entire imaged area. This ion intensity map will show areas or pixels where a selected analyte is found, and compare its

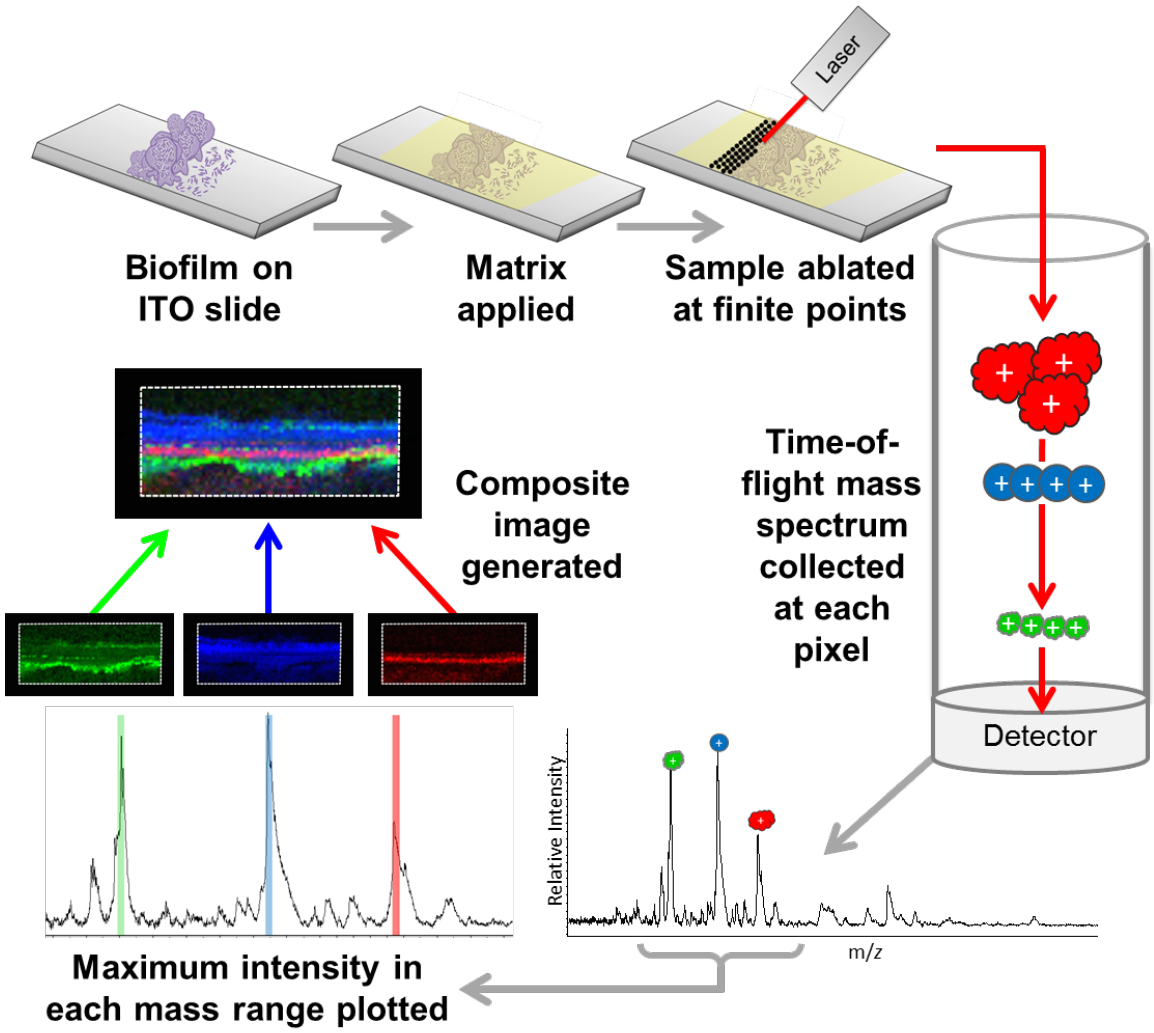

Figure 5. MALDI-TOF IMS is an unbiased surface-sampling approach for the analysis of analyte localization and distribution within intact biological samples. Schematic depicts the MALDI-TOF IMS pipeline as applied to the analysis of bacterial biofilms. Surface-associated biofilms were given an organic solvent wash to decrease lipids and salts from within the sample that interfere with protein ionization. The biofilm was then overlaid with an UV-absorbing matrix, and analyzed by MALDI-TOF IMS. The UV-absorbing matrix takes energy coming from a laser, and generates ions into the gas phase from analytes that have crystallized with the matrix. The type of analytes visualized can vary with the type of matrix selected for the analysis. Ions are collected at the base of a time-of-flight (TOF) mass analyzer. All ions are given the same accelerating pulse, allowing them to travel down the TOF mass analyzer to the detector. In this method the speed at which the ions travel is dependent upon the size and charge of the ion. The resulting mass spectrum is a total of the mass-to-charge (*m/z*) ratios obtained from the analysis. For the IMS analysis, MALDI-TOF methods are applied in a spatial array across a biological sample of interest.

relative intensity with the other pixels across the imaged area, and can be represented as a two-dimensional heat map based upon the analyte's distribution and relative abundance at each pixel within the imaged array (Cornett *et al.*, 2007). This label-free technology does not require prior knowledge of sample composition or analyte distribution and provides an unbiased approach for the simultaneous visualization and relative quantification of multiple analytes within a single intact biological sample. Previous MALDI-TOF IMS analysis of bacterial biofilms has focused largely on small molecule and metabolite signaling interactions between two microbial communities on a macro-scale (Traxler *et al.*, 2013, Watrous *et al.*, 2013b, Watrous *et al.*, 2013a, Watrous *et al.*, 2012). To date, only one other study has utilized MALDI IMS for the direct analysis of protein species within a bacterial biofilm community (M T *et al.*, 2012). M.T. *et al.* used MALDI IMS for the analysis of peptides and proteins found at the site of interaction between *E. coli* and *Enterococcus faecalis* biofilms co-cultured on an agar surface, as well as within each individual biofilm (M T *et al.*, 2012). In this work, we sought to adapt MALDI-TOF IMS methodologies for the localization and identification of spatially segregated protein species within single-species surface-associated bacterial biofilms. The results of these studies are discussed extensively below.

Methods

Bacterial strains

All bacterial strains used in these studies, are listed in **Table 1** of **Appendix A**. UTI89Δ*hupA* and UTI89Δ*yahO* were created using the previously established λ Red

recombinase methods (Murphy and Campellone, 2003) and the primers listed in **Table 2** of **Appendix B** (Integrated DNA Technologies).

Surface-associated biofilm growth conditions

UPEC and *K. pneumoniae* strains were grown overnight in Lysogeny broth (LB) (Fisher), pH 7.4, at 37 °C with shaking, unless otherwise specified. UPEC overnight cultures were then sub-cultured in fresh 1.2x Yeast-Extract/Casamino Acids (YESCA) broth (Hadjifrangiskou *et al.*, 2012) to an OD_{600} of 0.06. *K. pneumoniae* was sub-cultured into fresh LB to and OD_{600} of 0.06. Bacterial suspensions at an OD_{600} of 0.06 were then dispensed into 50 mL conical tubes, containing indium tin oxide (ITO)-coated glass slides (Delta Technologies), and incubated for 48 hours at either room temperature (UPEC) or 37°C (*K. pneumoniae*). After 48 hours, slides were removed, rinsed with water to remove non-adherent bacteria and stored at -80°C until analysis.

Biofilm Quantitation

Biofilms were quantified as previously described (Hadjifrangiskou *et al.*, 2012). Crystal violet stained biofilms were removed from ITO slides using 35% acetic acid and transferred to 96-well plates for absorbance readings. Absorbance at 570 nm was determined using a BioRad Model 680 microplate reader (BioRad). Data are presented as the average absorbance from at least three independent experiments. Statistical analysis was performed using a two-tailed unpaired Student's *t*-test (GraphPad Prism 6).

Scanning electron microscopy (SEM)

Bacterial biofilms grown as described for MALDI IMS were treated for SEM as previously described (Gaddy *et al.*, 2009). Samples were dried at the critical point, mounted onto aluminum sample stubs and sputter coated with gold-palladium. A small strip of silver paint was applied to the sample edge, and biofilms were imaged with an FEI Quanta 250 Field-emission gun scanning electron microscope (FEI). At least two biological replicates were imaged for each sample preparation and representative images were collected.

Immuno-fluorescence by Super-resolution Structured Illumination Microscopy (SIM)

The α-CsgA antibody was provided by Dr. Matthew Chapman at the University of Michigan – Ann Arbor. UPEC biofilms grown for 48 hours as described above, were fixed in 4% paraformaldehyde in phosphate-buffered saline (PBS) for 30 minutes at room temperature and blocked in 5% bovine serum albumin (BSA) overnight at 4°C. Biofilms were immuno-stained with α-CsgA (1:1000) for 1 hour at room temperature, followed by 3 washes in PBS and secondary detection with Alexa Fluor-555 goat anti-rabbit (1:1000) (Life Technologies) for 1 hour at room temperature. Samples were washed 3 times in PBS and mounted under a 1.5 size coverslip (Fisher Scientific) using ProLong Gold antifade reagent containing DAPI for DNA counterstain (Life Technologies). Cells were imaged using a GE/Applied Precision DeltaVision OMX in SIM mode with 1.516 immersion oil at 63X magnification. Post-data acquisition processing was performed using SoftWorx for OMX. Images were processed for contrast enhancement and cropping in Photoshop. With the exception of x-y sections (z stacks), images are shown as maximum intensity projections through the entire imaged area (ranging from 3-6

μm in z, 40 μm in x-y). Videos depicting three-dimensional reconstruction of biofilms were generated using the Volume Viewer in Progressive mode in SoftWorx for OMX.

MALDI- TOF Imaging Mass Spectrometry

Biofilms grown on ITO-coated glass slides were washed to remove interfering salts and lipids in sequential 30-second washes of 70, 90, and 95% HPLC-grade ethanol (Fisher Scientific). A matrix of recrystallized 15 mg/mL 2,5-Dihydroxybenzoic acid (DHB) (Fisher Scientific) and 5 mg/mL α-Cyano-4-hydroxycinnamic acid (CHCA) (Sigma Alderich Chemical Company) was prepared in 90% HPLC-grade acetonitrile (ACN) (Fisher Scientific) with 0.2% trifluoroacetic acid (TFA) (Sigma-Alderich). Matrix was applied to dry films using a TM-Sprayer (HTX Imaging). Matrix was applied with 8 passes of the TM-Sprayer in an offset/overlay pattern with 2 mm spacing at 1200 mm/min, using a solvent of 90% ACN flowed at 0.2 mL/min at a nozzle temperature of 100°C, utilizing nitrogen as an inert nebulizing gas. Spray passes were offset and rotated to ensure homogenous sample coverage. Samples were rehydrated in an oven at 85°C to facilitate analyte crystallization with matrix. Samples were warmed for 2 minutes in the oven, and then sealed in a rehydration chamber with 1 mL of 10% acetic acid (AcOH) for 2.5 minutes. Samples were analyzed using a Bruker Autoflex Speed mass spectrometer (Bruker Daltonics) equipped with a Nd:YAG (355 nm) Smartbeam laser operated in linear positive-ion mode. Images were obtained at 150 micron (μm) lateral resolution. Laser repetition rate was 1 KHz. Two hundred laser shots were collected at each pixel in 50 shot increments in a random walk pattern. Ion extraction voltage was 19.17 kV and ion acceleration voltage was 17.90 kV. Ions were collected with a delayed extraction time of 350 ns and a lens voltage of 6.30 kV. Ions under *m/z* 2000 were suppressed. A mass range of *m/z* 2,000- 25,000

was collected. The detector gain was 3,400 volts. Data were analyzed using FlexImaging 3.0 Build 42 (Bruker Daltonics). Datasets were normalized to total ion current unless otherwise indicated. Ion intensity maps were extracted for each range of interest and were plotted using the maximum intensity within the range.

Protein Fractionation and Identification

To identify 48-hour UPEC biofilm *m/z* ion species observed by IMS, multiple slide-associated biofilms were lysed and pooled together. UPEC biofilms were lysed under one of the following conditions; 88% formic acid (FA), 35% AcOH, 50% ACN / 0.2% TFA, or 0.5 µg/mL lysozyme in tris-EDTA Buffer (pH 8.0). Lysates obtained under the same lysis condition were pooled together and sonicated for 15 minutes in a room-temperature water bath, and then centrifuged at 14,000 x g and 4°C for 15 minutes. The supernatant was then transferred to a new 1.5 mL microfuge tube, and dried under vacuum centrifugation using a SpeedVac Vacuum Concentrator (Thermo Scientific). Extracts were fractionated using reversed-phase (RP) high performance liquid chromatography (HPLC). RP-HPLC fractionation was performed using a Waters 2690 (Alliance) HPLC (Milford, MA) with a 2478 Dual Wavelength Absorbance Detector (Waters Corporation), and a Gilson FC 203B 96-well plate fraction collector. UPEC lysates were fractionated on either a Vydac 208TP series 208TP5315, 150 x 3.2mm 5µ C8 column fitted with a Vydac 208TP C8 7.1x4.6mm guard column (Grace Vydac), or an Aeris Widepore 150 x 2.1 mm 3.6µ C18 column fitted with a SecurityGuard ULTRA UHPLC Widepore C18 guard cartridge (Phenomenex. Solvent A was 100% H_2O with 0.1% TFA, and Solvent B was 100% ACN with 0.1% TFA. Fractionation was performed at a flow-rate of 0.5mL/min, with fractions collected in 1-minute intervals into a 96-well plate, and elution off of

the column was monitored at 214 and 280nm. The column was equilibrated with 5% Solvent B, and 200µL of the lysate was loaded onto the column and washed with 5% Solvent B for 10 minutes. The elution was performed with a gradient of 5-25% Solvent B from 10-15 minutes, 25-60% Solvent B from 15-65 minutes, and then 60-95% Solvent B from 65-75 minutes. The column was then washed with 95% Solvent B, and re-equilibrated back to 5% Solvent B. After fractionation, 96-well plates were dried using the Speedvac vacuum concentrator, and dried samples were stored at 4ºC until MALDI-TOF MS analysis. Fractions were reconstituted in a minimal volume of 60% ACN / 0.2% TFA, and a MALDI spectrum was acquired from each fraction. Fractions containing *m/z* species of interest were selected for in-solution tryptic digestion for protein identification. Fractions were extracted from the 96-well plate and dried. Samples were resuspended in 100 mM Tris-HCl (pH 7.8) / 8 M urea, and disulfide bonds were then reduced with 10 mM dithiothreitol (DTT) (Sigma-Aldrich, St. Louis, MO) for 1 hour at 37°C. After reduction, samples were alkylated with 55 mM iodoacetamide (IA) for 30 minutes at room temperature in the dark. The concentration of urea was the reduced to 2 mM with the addition of 100 mM Tris-HCl (pH 7.8), and 500 ng of trypsin (Promega or Sigma-Aldrich) was added to each sample and incubated overnight at 37°C. After overnight digestion, the reaction was stopped with the addition of 1 µL of 100% AcOH. Digested fractions were submitted to the Vanderbilt University Mass Spectrometry Research Center Proteomics Core for LC-MS/MS identification. Resulting peptides were analyzed by a 70-minute data dependent LC-MS/MS analysis. Briefly, peptides were auto-sampled onto a 200 mm by 0.1 mm (Jupiter 3 micron, 300A), self-packed analytical column coupled directly to an LTQ (ThermoFisher) using a nanoelectrospray source and resolved using an aqueous to organic gradient. A series of a full scan mass spectrum followed by 5 data-dependent tandem mass spectra (MS/MS) was collected

throughout the run and dynamic exclusion was enabled to minimize acquisition of redundant spectra. MS/MS spectra were searched via SEQUEST against the *E. coli* strain UTI89 (taxon identifier 364106) database that also contained reversed version for each of the entries. (http://www.ncbi.nlm.nih.gov/pubmed/7741214). Identifications were filtered and collated at the protein level using Scaffold (Proteome Software).

Results

Development of surface-associated UPEC biofilms for MALDI-TOF IMS analysis

In order to assess the utility of MALDI-TOF IMS for evaluating protein localization within intact bacterial biofilms, we adapted a simple surface-associated biofilm setup that enabled the sampling of single-species bacterial biofilms. Given that MALDI-TOF IMS must be performed directly from an electrically conductive surface for high voltage analyses (Seeley *et al.*, 2008), growth conditions were optimized to facilitate surface-associated biofilm formation directly ITO-coated glass slides. In these studies, mature 48-hour biofilms were analyzed from two species of uropathogens. This setup created an environmental gradient of oxygen and nutrients that induced biofilm formation at the air-liquid interface. Under the experimental conditions used, the relative abundance and localization of up to 60 different protein species could be reproducibly obtained for UPEC biofilms, and analysis of *K. pneumoniae* biofilms revealed up to 45 reproducible protein species. Sterile slides were placed vertically into culture media seeded with bacteria, such that only half of the slide was submerged within the media. A schematic depiction of this culture setup, and representative scanning electron micrographs of different regions of resulting UPEC biofilms are shown in **Figure 6**.

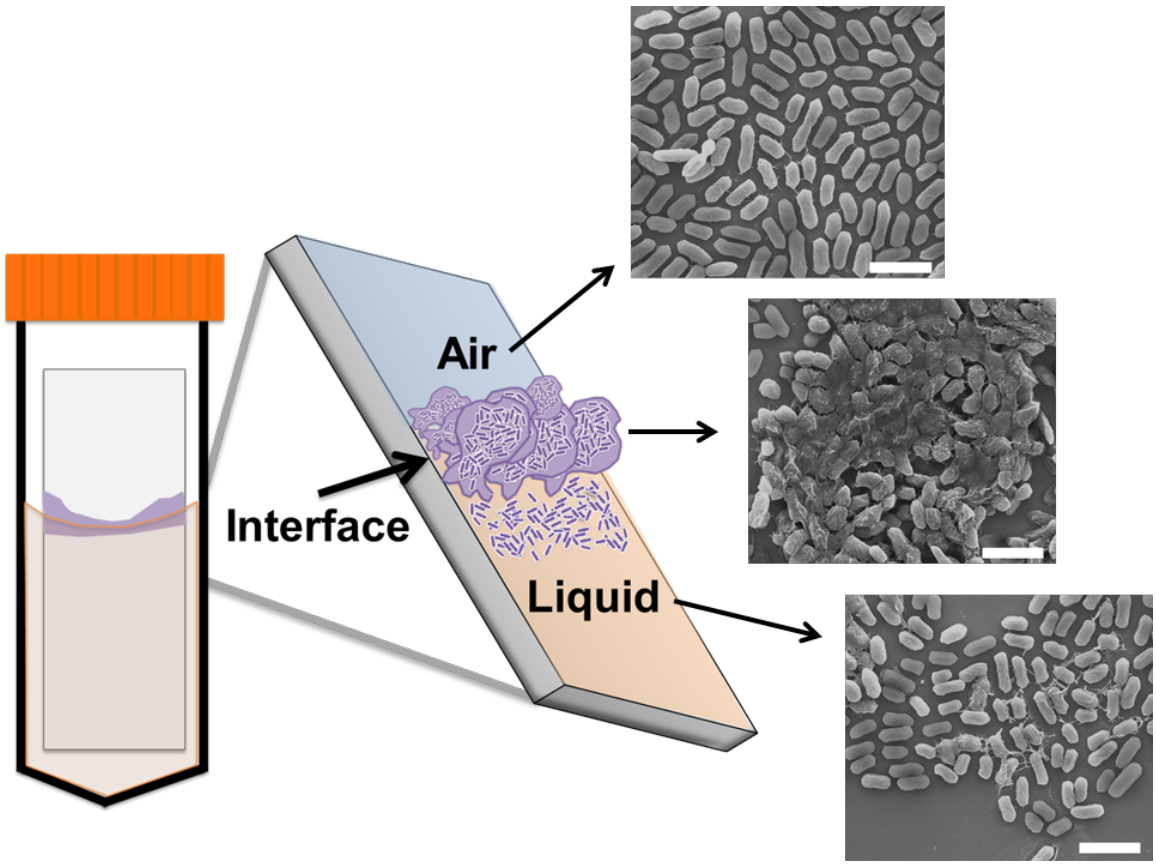

Figure 6. Development of surface-associated bacterial biofilms for analysis by MALDI-TOF IMS. Schematic depicting the culture method for single species surface-associated biofilms. Sterile ITO-coated borosilicate glass slides were placed into a 50 mL conical containing media seeded with bacteria, such that the air-liquid interface would constitute the center of the slide, and biofilms were cultured for 48 hours. The biofilms form at the air-liquid interface in response to the induced environmental and nutrient gradients created by the culture conditions, as indicated in the schematic of the resulting surface-associated biofilm and depicted by representative SEM micrographs of each region. Micrographs were obtained from a 48-hour ethanol-washed UPEC surface associated biofilm. Scale bar = 2.5 μm.

IMS sample preparation methods do not impact UPEC biofilm levels or architecture

MALDI-TOF IMS requires the application of a UV-absorbing matrix for analyte ionization (Seeley *et al.*, 2008) (**Figure 5**). Typical sample preparation methods for the analysis of proteins by MALDI-TOF IMS, begin with solvent washes that serve to decrease ion suppression from lipids and salts, enhancing protein ionization (Seeley *et al.*, 2008). Here, a sequential washing procedure of 70%, 90%, and 95% ice-cold ethanol was performed for 30 seconds each. Following washes, we evaluated biofilm integrity using crystal violet staining for total biomass levels and scanning electron microscopy (SEM) for the examination of biofilm architecture. Ethanol-washed biofilms were compared to non-washed biofilms, to ensure that IMS sample preparation methods did not alter the bacterial biofilm. Crystal violet staining (O'Toole *et al.*, 1999) and subsequent quantitation showed that the preparative ethanol washes did not significantly alter biomass levels between washed and unwashed biofilms (**Figure 7**). SEM analysis of the air-exposed, the air-liquid interface, and liquid-exposed regions of washed and unwashed biofilms indicated that the tertiary structure, along with cell shape and surface features, were preserved post-washing (**Figure 7**). Combined, these approaches indicated that the sample preparation methods for MALDI IMS did not significantly perturb biofilm integrity.

IMS reveals differential protein stratification within surface-associated UPEC biofilms

A schematic for the MALDI-TOF IMS analysis of UPEC biofilms is shown in **Figure 5**. The MALDI methods and matrix selected for these studies were optimized for lower molecular weight protein species; therefore, all analyses were carried out over an ion range of mass-to-charge ratio (*m/z*) 2,000 – 25,000. IMS analyses were performed at 150μm spatial resolution (in both the x and y directions) across the biofilm encompassing region. The extent of the biofilm

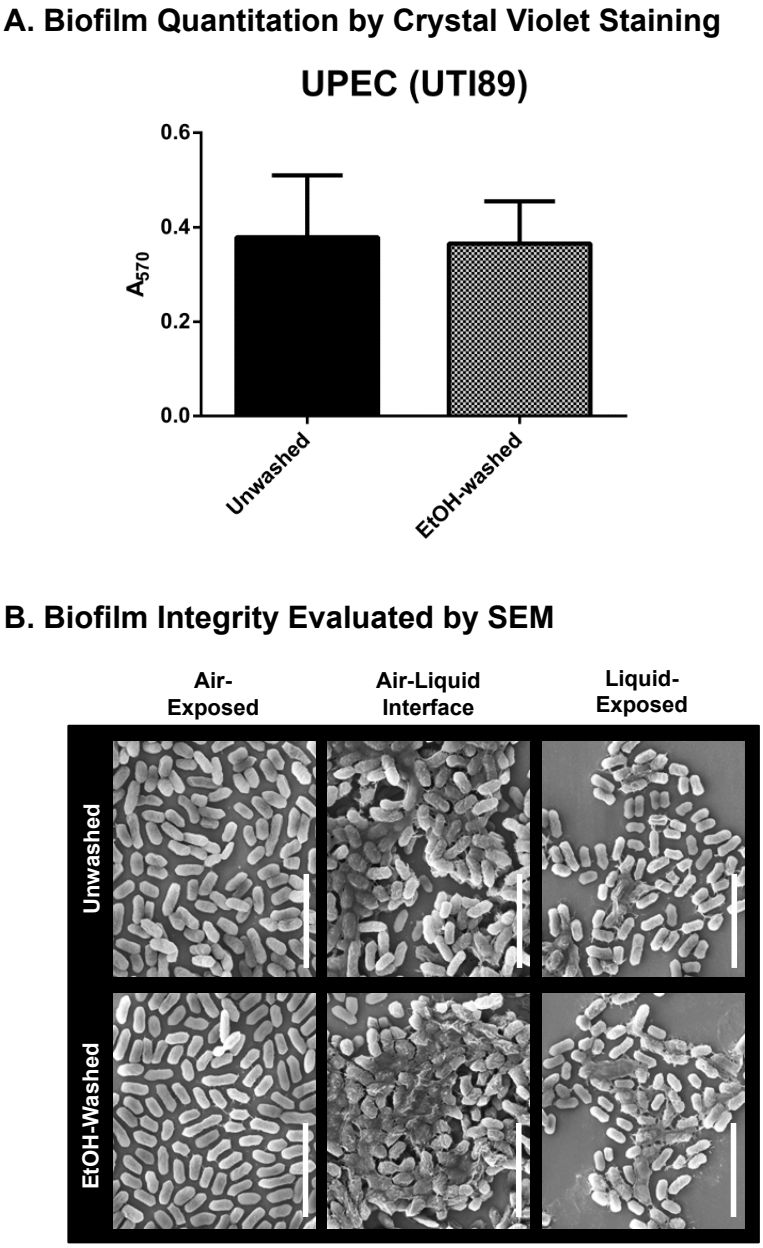

Figure 7. IMS sample preparation methods do not alter UPEC biofilm architecture. (A) Biofilm quantitation by crystal violet staining. Graph depicts quantified biofilm of ethanol-washed and unwashed biofilms measured at 48 hours post-seeding. Data are presented as the mean with the standard deviation. EtOH, ethanol; *Statistical analysis was performed using two-tailed unpaired Student's *t*-test (n=9, p = 0.7864). **(B)** Representative SEM micrographs of unwashed and ethanol-washed UPEC biofilms. Representative micrographs from at least two biological replicates are shown. Magnification shown, 10,000x; scale bar = 5 μm.

was determined by MALDI analysis, until the loss of signal was observed in both directions of the air- and liquid-exposed regions of the slide. At this spatial resolution and within this *m/z* range, 60 UPEC protein ion species were reproducibly detected (in at least 5 biological replicates). The complete list of all reproducible ion species, and their localizations within the biofilm, are given in **Table 3** in **Appendix C**.

The relative abundance and localization patterns for representative ion species from a single UPEC biofilm analysis are shown in **Figure 8.** Each panel depicts a heat-map intensity plot for a unique ion species within the biofilm, where red/white indicates the highest levels of relative abundance, and black/blue the lowest levels (**Figure 8**). All of the observed ion species displayed one of the following localization/distribution patterns within the biofilm: diffuse distribution throughout the biofilm, localization specific to the air-exposed or liquid-exposed region, or localization to the air-liquid interface (**Figure 8)**. Ion image overlay analysis demonstrated that there were protein species localized within each of these regions, independent from the other regions of the biofilm. Overlay of two ion species that localized specifically to the air-liquid interface of the biofilm, *m/z* 5,596 (**Figure 8** - red) and *m/z* 13,036 (**Figure 8** - yellow), demonstrated that differential localization of distinct protein species can be observed within the same sub-region of the biofilm. Together, these data demonstrate that MALDI-TOF IMS can be used for the localization of small molecular weight protein species within intact surface-associated biofilms formed by UPEC.

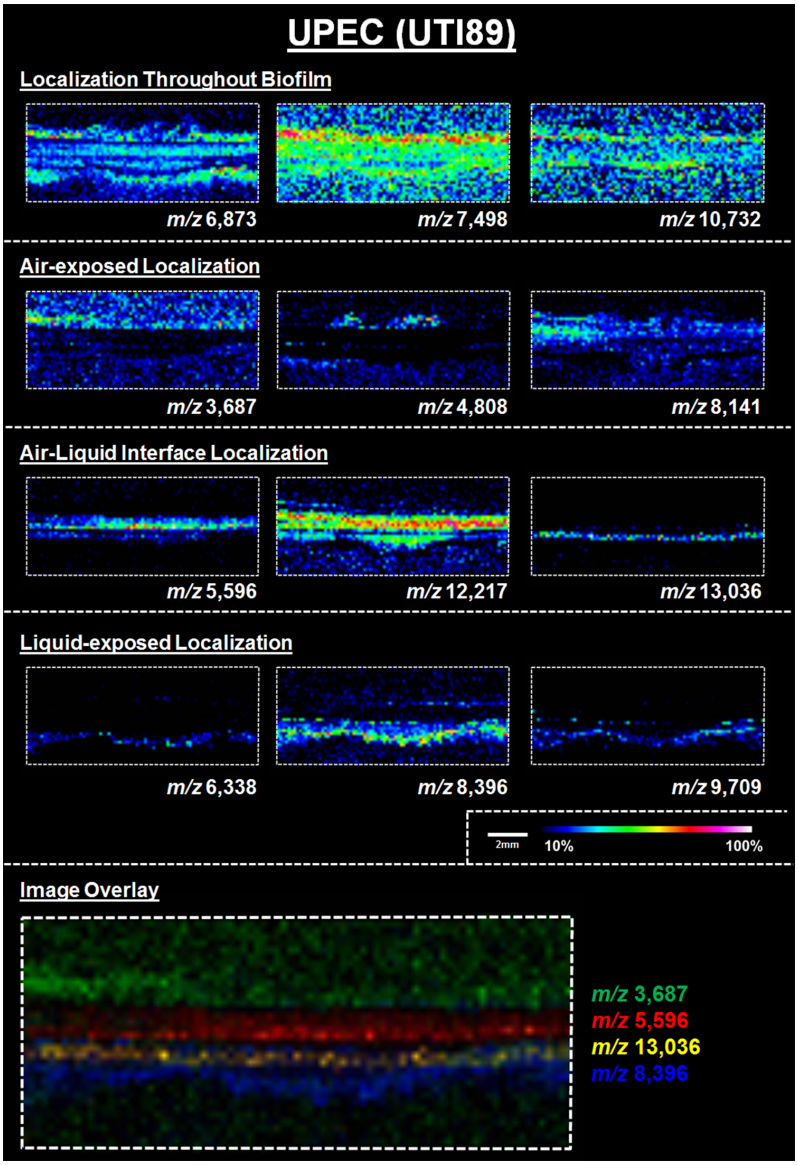

Figure 8. MALDI IMS reveals distinct protein localizations within UPEC biofilms. Representative ion images depicting distinct protein localization patterns observed in UPEC biofilms after 48 hours of growth. Images shown are from the same IMS analysis. Protein localizations for UPEC were validated in 16 biological replicates. The depicted mass-to-charge (m/z) ratio of each selected ion was determined after internal calibration of the total ion current-normalized average spectrum using mMass software (Strohalm *et al.*, 2008). Internal calibration used the theoretical mass, minus the signal peptide for proteins identified in the LC-MS/MS analyses to obtain the best mass accuracy for the data (as previously described (Anderson *et al.*, 2013)). Images are depicted ± 5 Da for each m/z species and data are presented as a heat map intensity of relative abundance from 10 (blue) – 100% (Red/White). Overlay images are presented using the same criteria, with single color distribution instead of a heat map from 10 - 100% intensity. Scale bar = 2 mm.

IMS analysis of uropathogenic K. pneumoniae surface-associated biofilms reveals protein stratification patterns similar to UPEC

To determine whether this approach would decipher similar distinct protein localizations in other bacterial biofilms, we performed similar analyses on biofilms formed by uropathogenic *K. pneumoniae* (TOP52) (Rosen *et al.*, 2008). *K. pneumoniae* biofilms were cultured as described for UPEC (**Figure 6**), with optimal growth conditions determined to be static culture at 37°C for 48-hours in LB media. IMS samplepreparation methods had no impact on *K. pneumoniae* biomass levels or biofilm architecture (**Figure 9**). Biofilms were analyzed by IMS using the same matrix and MALDI parameters as outlined for UPEC biofilms. IMS analysis of *K. pneumoniae* biofilms revealed the same four distinct protein localization patterns as observed for UPEC (**Figure 10**), for a total of 45 individual protein ion species detected reproducibly in at least 5 biological replicates (full list of ions and their localization within the biofilm can be found in **Table 4** in **Appendix D**). These data demonstrated that MALDI-TOF IMS has broad application for the analysis of small molecular weight protein localization within biofilms formed by different bacterial pathogens.

Identification of UPEC protein signals observed by IMS

The output of MALDI-TOF IMS results in a list of *m/z*'s, of which the relative abundance and localization within the biofilm can be mapped using the imaging software. Based on the sample preparation methods, matrices, and MALDI methods selected for these experiments, we hypothesized that these *m/z* ion species correspond to proteins unique to the different regions of the biofilm. However, further identification is required to determine the identity of the individual proteins observed by IMS within each region. To this end, biofilm lysates were fractionated by

A. Biofilm Quantitation by Crystal Violet Staining

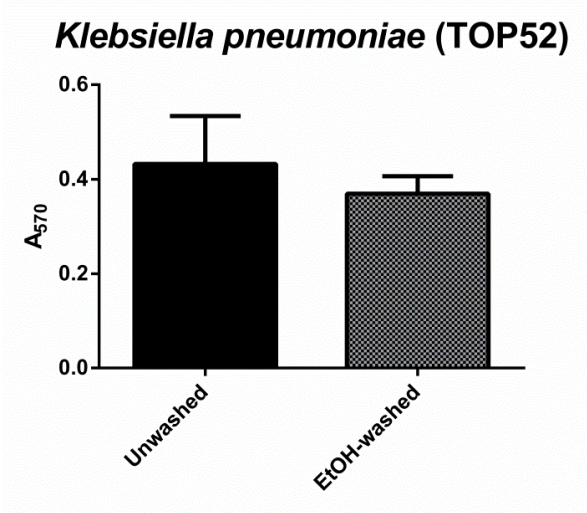

B. Biofilm Integrity Evaluated by SEM

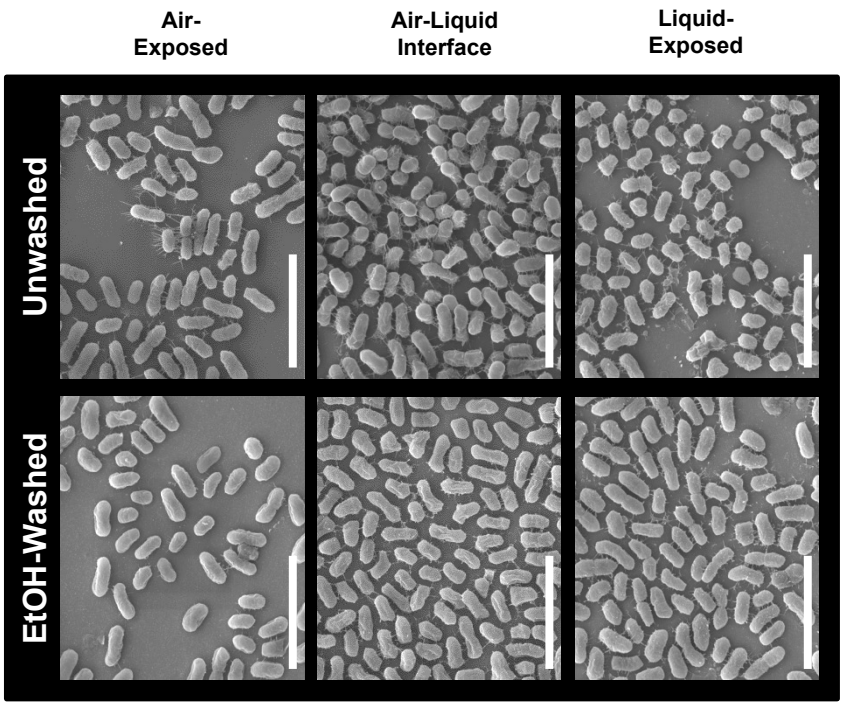

Figure 9. IMS sample preparation methods do not alter *K. pneumoniae* biomass architecture. (A) Representative SEM micrographs of unwashed and ethanol-washed biofilms from *K. pneumoniae.* Representative micrographs from at least two biological replicates are shown. Magnification shown, 10,000x; scale bar, 5 μm. **(B)** Biomass quantitation by crystal violet staining. Graphs depicting quantified biomass of ethanol-washed and unwashed biofilms measured at 48 hours post-seeding. Data are presented as the mean with the standard deviation. EtOH, ethanol; *Statistical analysis was performed using two-tailed unpaired Student's *t*-test, n=8, $p = 0.1193$.

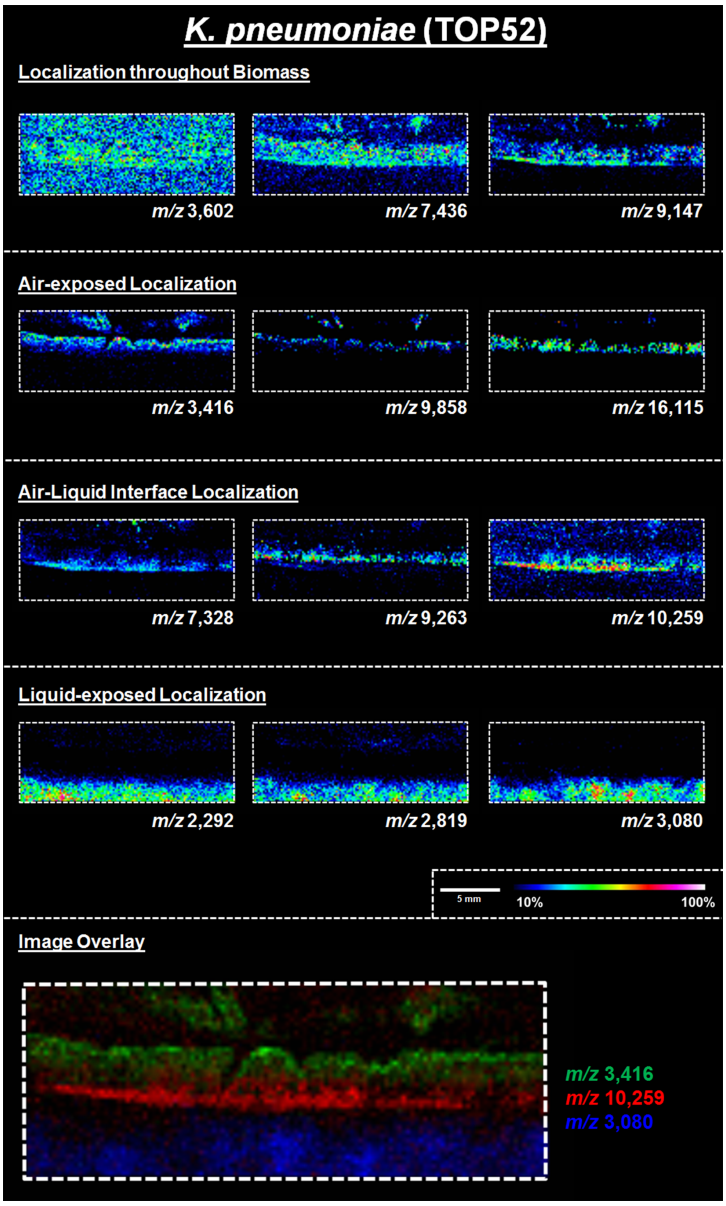

Figure 10. MALDI-TOF IMS reveals distinct protein localizations within *Klebsiella pneumoniae* biofilms. Representative ion images depicting protein localization patterns observed in *K. pneumoniae* biofilms after 48 hours. Images used were from the same IMS analysis. Protein localizations were validated in at least 5 biological replicates. The average spectrum was normalized to the total ion current of the analysis, and the mass-to-charge (*m/z*) ratio of each selected ion is given. Images are shown as ± 5 Da for each *m/z* species. Data are presented as a heat map intensity of relative abundance from 10 (blue) – 100% (Red/White). Overlay images are presented using the same criteria, with single color distribution instead of a heat map from 10 - 100% intensity. Scale bar, 5 mm. Data processed and presented as outlined in Figure 8.

RP-HPLC, and fractions were examined for *m/z* species corresponding to those observed by IMS. Fractions with m/z species of interest were enzymatically digested, and analyzed by tandem mass spectrometry analysis or protein identification. Using this workflow, identification was established for 6 of the 60 observed protein ion species (**Table 5** in **Appendix E**).

These proteins included, the histone-like global transcriptional regulators HU-α (UniProt KB Q1R5W6, *m/z* 9,535) and HU-β (UniProt KB Q1RF95, *m/z* 9,226), which co-localized throughout the biofilm and were most abundant in the air-exposed region (**Figure 11**); the acid stress-response chaperone protein, HdeB (UniProt KB Q1R595, *m/z* 9,064), and the uncharacterized protein YahO (UniProt KB Q1RFK1, *m/z* 7,718). HdeB localized to the air-liquid interface and was most abundant towards the liquid-exposed surface (similar to the unidentified ion species m/z 8,396, **Figures 8 and 11**), while YahO localized throughout the biofilm (**Figure 11**). Finally, two of the IMS signals identified by proteomics corresponded to major subunits of two UPEC adhesive organelles (**Table 2**): The major curli subunit CsgA (UniProt KB Q1RDB7, *m/z* 13,036), an essential determinant for UPEC biofilm formation under the culture conditions used for these studies (McCrate *et al.*, 2013), and; the major subunit of type 1 pili, FimA (UniProt KB Q1R2K0, *m/z* 16,269).

Based on MALDI IMS, CsgA predominantly localized to the air-liquid interface of the biofilm (**Figures 11 and 12**). However, FimA localized unique to the air-exposed region of the biofilm (**Figures 11 and 12**). Under the biofilm growth conditions used for these studies, type 1 pili have been shown to play an accessory role to biofilm infrastructure, and loss of type 1 pili impairs integrity but does not abolish biofilm formation (Hung *et al.*, 2013a). Thus, we took advantage of a *fim* deletion mutant (UTI89Δ*fimA-H*) to validate the identification of the *m/z* 16,269 ion as FimA. MALDI IMS analysis of UTI89Δ*fimA-H* biofilms showed a loss of the ion

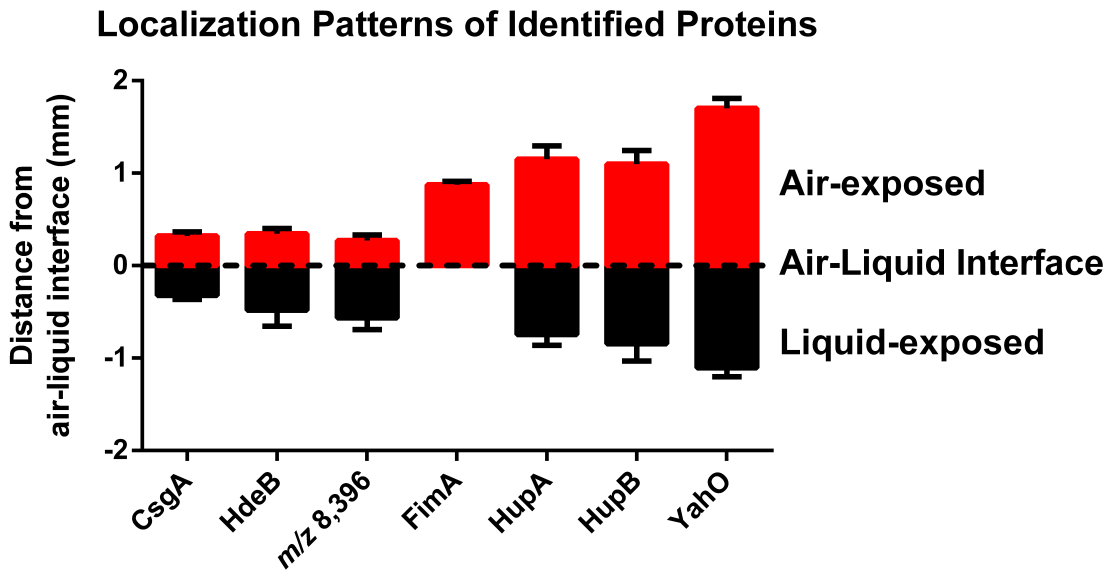

Figure 11. IMS analysis reveals stratification of identified UPEC proteins. Graphical representation of the localization of each protein identified in Table 2, along with the unidentified ion m/z 8,396. The localization of the major curli subunit, CsgA, was used to demarcate the air-liquid interface. Localization of ions were measured as the distance (mm) from the middle of CsgA localization to the middle of the localization of each individual ion using Fiji Image J software (Schneider *et al.*, 2012). Localizations were plotted using GraphPad Prism version 6. The localization of the unidentified ion species *m/z* 8,396 demonstrates a signal localizing more to the liquid-exposed region of the biofilm. To date, none of the liquid-exposed proteins have been identified by LC-MS/MS analysis.

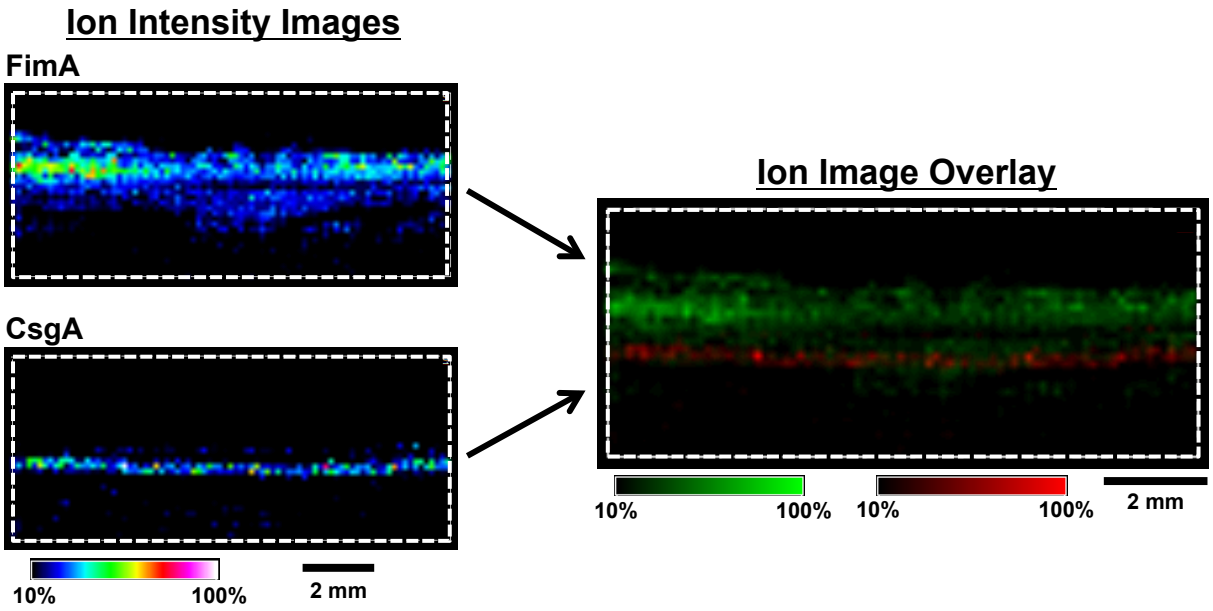

Figure 12. IMS analysis reveals distinct localization of FimA and CsgA within the biofilm. IMS ion images of FimA and CsgA localization. Images are depicted ± 5 Da for each ion, and data are presented as a heat map intensity of relative abundance from 10 (blue) – 100% (Red/White). FimA (green) and CsgA (red) ion overlay image presented using the same criteria, with single color distribution instead of a heat map from 10 - 100% intensity. Scale bar = 2 mm.

at *m/z* 16,269 (**Figure 13**), confirming the ion *m/z* 16,269 as FimA. Similarly, the ions *m/z* 9,535 and *m/z* 7,718 were validated as HupA and YahO respectively, through MALDI MS analysis of UTI89 mutants lacking the respective gene (UTI89Δ*hupA* and UTI89Δ*yahO*) (**Figure 13**).

Immunofluorescence microscopy validates IMS localization of CsgA

Following identification of some of the protein species observed by IMS, we utilized more traditional immuno-fluorescence approaches with an available anti-CsgA antibody to visualize curli-expressing bacteria within the biofilm. Immunohistochemistry, combined with super-resolution structured illumination microscopy (SIM), revealed that consistent with the IMS localization the majority of curli-producing bacteria localized to the air-liquid interface of the biofilm (**Figure 14**).

Discussion

The work presented in this chapter demonstrates that MALDI-TOF IMS can be a strong analytical tool for analyzing the spatial proteome within intact bacterial biofilms. Previous studies have used various mass spectrometric techniques for the study of microbial systems (Watrous and Dorrestein, 2011). Examples include the use of laser desorption post-ionization mass spectrometry to analyze peptides involved in sporulation and bacterial competence (Edirisinghe *et al.*, 2007), and the use of secondary ion mass spectrometry (SIMS) for the analysis of peptides involved in bacterial swarming (Debois *et al.*, 2008). In the context of biofilms, MALDI IMS has been used previously used for the analysis of small molecules and metabolites secreted by bacterial communities forced to grow in close proximity to one another

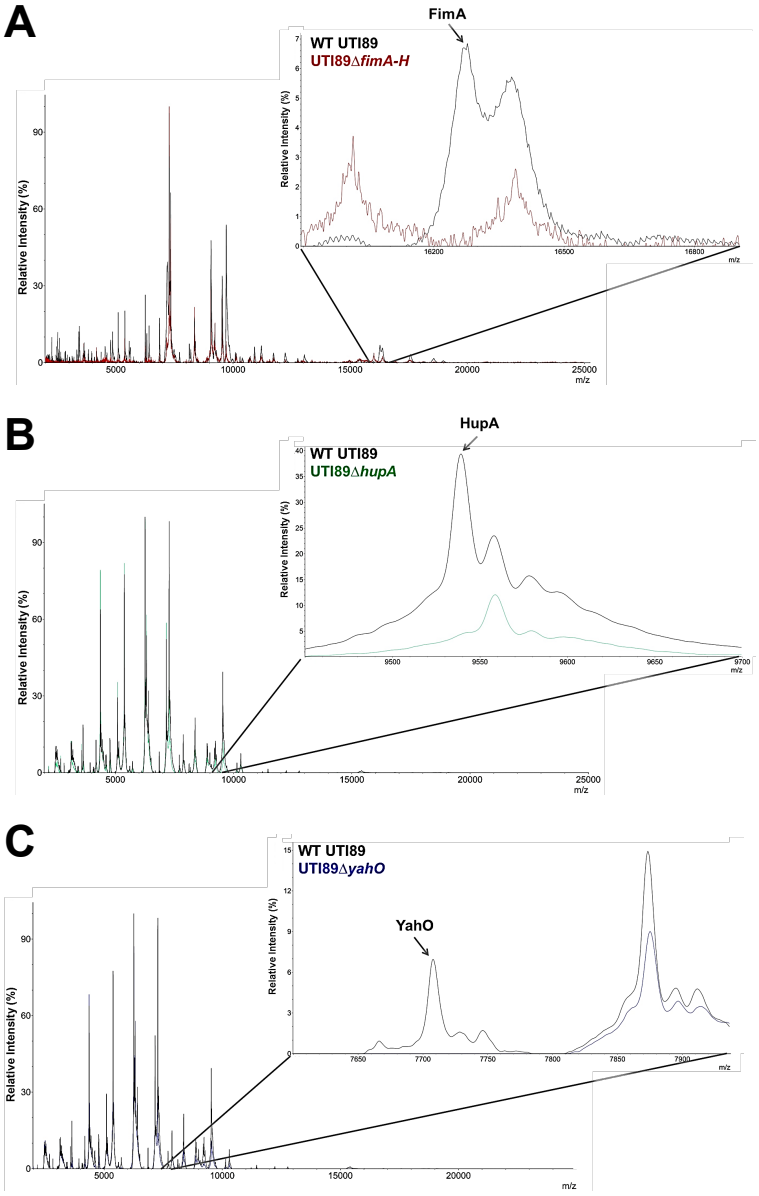

Figure 13. Mass spectrometry analysis of gene deletion mutants validates IMS ion identifications for FimA, HupA, and YahO. (A) IMS analysis of UTI89ΔfimA-H reveals loss of ion at m/z 16,269, corresponding to FimA. A representative single spectrum for the UTI89ΔfimA-H mutant (red) is shown, compared to an average spectrum taken from two biological replicates of wild-type (WT) UTI89 (black) after 48 hours of growth. **(B - C)** MALDI mass spectrometry analysis of lysed UTI89ΔhupA (B) and UTI89ΔyahO (C) bacteria pellets. **(B)** Traditional proteomics had identified the ion at m/z 9,535 as the transcriptional regulator, HupA (Table 1). Analysis of the UTI89ΔhupA mutant (green) indicates a loss of this ion peak. **(C)** Traditional proteomics had identified the ion at m/z 7,718 as the uncharacterized protein factor, YahO (Table 1). Analysis of the UTI89ΔyahO mutant (blue) indicates a loss of this ion peak. All spectra were imported to the mMass software, baseline subtracted, smoothed, and normalized to the most abundant ion in the spectra.

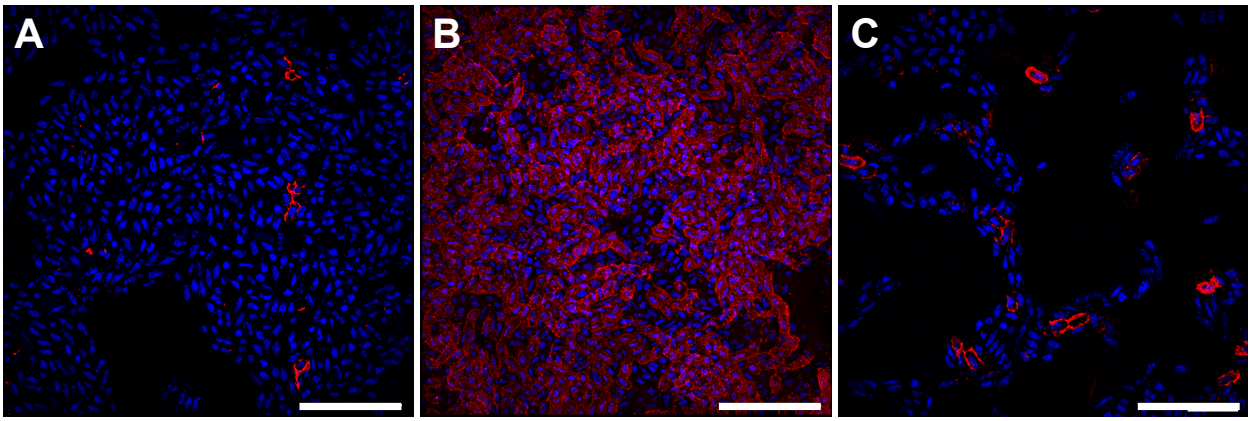

Figure 14. Bacteria expressing curli amyloid fibers localize primarily to the air-liquid interface of a 48-hour surface-associated biofilm. Representative immuno-fluorescence images obtained with super-resolution SIM microscopy from the **(A)** air-exposed region, **(B)** air-liquid interface, and **(C)** liquid-exposed region of the biofilm. Immuno-fluorescence was performed with DAPI staining for nucleic acid (Blue) and Alexa Fluor-555 conjugated secondary antibody detection of α-CsgA antibody (Red). Images shown are from a single biological replicate and are representative of two biological replicates total. Scale bar, 10 μm.

(Nguyen *et al.*, 2013, Traxler *et al.*, 2013, Watrous *et al.*, 2013b, Yang *et al.*, 2012). To date, only one other study has utilized MALDI IMS for the direct analysis of protein species within a bacterial community. M.T. *et al.* used MALDI IMS to analyze peptides and proteins found at the site of interaction between *E. coli* and *Enterococcus faecalis* biofilms co-cultured on an agar surface, as well as within each individual biofilm (M T *et al.*, 2012). Other than this initial study, little has been done to define the spatial localization of proteins within intact biofilms by IMS, nor had the technology been used to determine differential protein localization could be an indicator of biofilm subpopulations. Therefore, the application of MALDI IMS for the analysis of the intact spatial proteome of a single-species bacterial community represents an emerging approach that has the potential to offer new insights into the role and regulation of protein stratification within bacterial biofilms.

Notably, among the proteins observed in the IMS analyses presented here, were both cytoplasmic (HdeB, HupA, HupB, and YahO) and extracellular (FimA and CsgA) protein species. The detection of both cytoplasmic ad surface-associated proteins indicates the capability of the IMS methodologies used to detect proteins that are localized within and outside of the bacteria. Traditional immunofluorescence methodologies can be limited in their ability to detect bacterial cytoplasmic proteins, especially within multicellular communities, due to possible penetrance issues with the antibody against the cytoplasmic target of interest. Thus demonstrating another way in which MALDI-TOF IMS methodologies can present significant advantages over more traditional techniques for protein localization.

One caveat to MALDI-TOF IMS analyses of intact protein localization is that the species observed are typically limited to those most abundant within the sample, or those that crystallize

and ionize best with the MALDI matrix selected (Seeley *et al.*, 2008, Seeley and Caprioli, 2008, Norris and Caprioli, 2013). This limitation can restrict the sensitivity and dynamic range of the analytes observed by IMS. In turn, large molecular weight proteins or large polymeric protein complexes vital to biofilm formation, which are harder to ionize by MALDI and detect by time-of-flight mass analysis could be intrinsically excluded from the data. Thus, orthologous approaches (such as immunofluorescence, used here to validate CsgA localization (**Figure 14**)) are still critical for validating MALDI IMS findings.

The detection of up to 60 reproducible protein species under the conditions tested clearly does not represent the entire proteome of UPEC. However, the number of proteins observed within a single analysis represents a significant advancement compared to more traditional antibody- or fluorescent tag-based approaches, which are largely limited in the number of protein species visualized per analysis. The profile of protein species observed can be expanded by varying the UV-absorbing matrix used for the analysis and by extending the overall *m/z* ion range analyzed (e.g. from 2,000 - 25,000 *m/z* to 2,000 - 40,000 *m/z*, and so on) (Schwartz *et al.*, 2003). The sensitivity of MALDI IMS can also be refined further by increasing the spatial resolution at which the biofilm is imaged from the current resolution of 150 μm to as low as 20 μm in order to better define stratification of subpopulations. We have already begun working towards this goal, by increasing the imaging resolution to 50 μm and obtaining IMS data from *K. pneumoniae* biofilms (see **Chapter VI – Future Directions**). Another limitation of the technology is the actual identification of the protein ion species observed by IMS. Although straightforward, the process can be time-consuming and costly, restricting the identification of all ion species observed by IMS in many cases.

From the proteins identified in our analyses, we were able to discern subpopulations expressing distinct adhesive fibers within the 48-hour UPEC surface-associated biofilm (**Figure 8**). In addition, the IMS localization of proteins such as FimA and CsgA, which have been shown to play a crucial role in UPEC biofilm formation and pathogenesis but cannot be epitope-tagged due to their incorporation in macromolecular structures, also highlights the strength of this application. MALDI-TOF IMS analyses revealed that type 1 pili-producing bacteria stratify above curli fiber-producing bacteria within the UPEC surface-associated biofilms cultured in YESCA media on ITO-coated glass slides (**Figure 12**). UPEC biofilms cultured under similar conditions have been previously shown to consist of an extracellular matrix comprised of only curli (85%) and cellulose (15%) (Hung *et al.*, 2013a, McCrate *et al.*, 2013), with type 1 pili playing an accessory role in biofilm tensile strength (Hung *et al.*, 2013a). The study by Hung *et al.*, revealed that the bacteria on the air-exposed layer of a floating pellicle biofilm (formed during growth in the same media used in our studies), are morphologically distinct from those at the liquid interface (Hung *et al.*, 2013a). In the same study, Hung *et al.* also reported that disruption of *fim*-mediated adhesion did not ablate biofilm formation, but rather impaired biofilm integrity through the formation of large holes on the air-exposed side of the biomass (Hung *et al.*, 2013a).

Here, MALDI-TOF IMS demonstrated that type 1 pili are produced by the bacteria forming the topmost air-exposed layer of the biofilm. In our studies, we observed that a pellicle biofilm typically surrounded the UPEC slides cultured for IMS analysis within 72-96 hours of starting the culture. If the slide-associated biofilm analyzed by MALDI IMS, is representative of a cross-section of the growing pellicle biomass biofilm, stratification of type 1 pili observed in surface-associated biofilms by IMS could help to explain the loss in tensile strength upon

disruption of *fim*-mediated adhesion observed by Hung *et al.* (Hung *et al.*, 2013a). However, it is important to note that the type of surface to which the bacteria adhere and the nutrient or surrounding environmental conditions can alter the genetic expression profiles within the biofilm community. Therefore, we recognize that the conclusions drawn here are representative of biofilms formed on a glass surface in a laboratory setting and may bear differences from cross-sections obtained from floating pellicles.

As mentioned earlier, bacterial biofilms constitute a serious problem in the healthcare setting. The unique heterogeneous architecture of the biofilm, combined with the composition of a self-secreted extracellular matrix, greatly hampers the penetrance and efficacy of bactericidal drugs and limits treatment options against biofilm-related infection (Foxman, 2010). It is thus imperative to identify new strategies to combat or re-program how bacteria form these multicellular structures. Numerous studies identified the presence of bacterial subpopulations within bacterial biofilms and have identified that these subpopulations execute unique "tasks" (Lewis, 2007, Lopez *et al.*, 2010). For example, in the benign *Bacillus subtilis* biofilms, specific subpopulations produce extracellular matrix while others undergo sporulation (Lopez *et al.*, 2010, Hobley *et al.*, 2013). Further studies indicated that *Bacillus subtilis* biofilms are coated with a hydrophobin that renders the biofilm colony impervious to penetration (Hobley *et al.*, 2013). In *E. coli* and other biofilm-forming pathogens, metabolically inactive "persister" cells within the biofilm re-seed the infection upon cessation of antibiotic treatment (Lewis, 2008, Lewis, 2007, Lewis, 2005). Identifying the spatial proteome of biofilms may uncover markers for distinct subpopulations, thereby aiding in the development of new strategies for thwarting biofilm formation. Beyond the identification of the types of subpopulations that exist within biofilm, the key to developing subpopulation-targeting novel anti-biofilm strategies lies in the

understanding of how these subpopulations are regulated, how they arise, how they change temporally, and how they contribute to biofilm resilience. **Chapter III** will begin to elucidate some of the mechanisms that drive differential regulation of type 1 pili to distinct subpopulations within the UPEC biofilm.

CHAPTER III

WHEN THE AIR GETS THIN: OXYGEN-DEPENDENT REGULATION OF TYPE 1 PILI EXPRESSION WITHIN UROPATHOGENIC *E. COLI*

Introduction

[3]MALDI-TOF IMS analysis of 48-hour surface-associated UPEC biofilms revealed that expression of type 1 pili (*fim*) was unique to bacterial subpopulations comprising the air-exposed region of the biofilm, while curli amyloid fibers localized specifically to the air-liquid interface (**Figure 12**). These data suggested that UPEC respond to environmental gradients to direct the expression of adhesive fibers. Type 1 pili (*fim*) (**Figure 4B**) are assembled by the chaperone-usher pathway (Geibel and Waksman, 2014), as outlined in **Chapter I**. The FimH tip adhesin binds to mannosylated uroplakin proteins on the surface of bladder epithelial cells, facilitating UPEC adherence to the urothelium (Mulvey *et al.*, 1998). Type 1 pili are vital for the establishment of bladder infection, and strains lacking functional type 1 pili are severely attenuated for pathogenesis (Wright *et al.*, 2007). In addition to mediating the initiation of infection, type 1 pili are also vital to the maintenance of extracellular biofilm integrity. Comparison of pellicle biofilms formed by *fim*-competent and *fim*-deficient UPEC strains, revealed that *fim*-deficient UPEC formed biofilms with large holes and significantly lower tensile strength (Hung *et al.*, 2013a). Finally, type 1 pili have been shown to play a role in the

[3] Portions of this chapter adapted from and published in:

Floyd *et al.* Adhesive Fiber Stratification in Uropathogenic *Escherichia coli* Biofilms Unveils Oxygen-Mediated Control of Type 1 Pili. *PLoS Pathog.* 2015 Mar 4;11(3):e1004697. (PMID: 25738819)

attachment of bacteria to indwelling urinary catheters and other abiotic surfaces (Reisner *et al.*, 2003, Schilling *et al.*, 2001, Connell *et al.*, 1996, Hultgren *et al.*, 1986).

In *E. coli*, type 1 pili expression is under the control of a phase-variable promoter region, termed *fimS*, the orientation of which is dictated by site-specific recombinase proteins showing significant homology to the lambda integrase recombinase family (Gally *et al.*, 1996, Abraham *et al.*, 1985, Schwan, 2011, Hultgren *et al.*, 1986). Recombinases FimB and FimE are conserved among all *fim*-expressing *E. coli* strains, and transcribed upstream of the *fim* operon (**Figure 15**) (Holden *et al.*, 2007, Schwan, 2011). Beyond the conserved recombinases, UPEC strains can also encode accessory recombinase enzymes such as FimX in UPEC strain UTI89, and IpuA, IpuB, and IpbA in UPEC strain CFT073 (Bateman *et al.*, 2013, Bryan *et al.*, 2006). The *fimS* promoter region is flanked on either side by invertible repeats that are recognized by the Fim recombinase enzymes (**Figure 15**). Previous studies suggest that DNA relaxation proteins, such as H-NS, IHF, and LRP facilitate recombination by bringing the invertible repeats in close proximity to each other for the recombinase enzymes to function (Corcoran and Dorman, 2009).

Of the conserved recombinases, FimB preferentially binds to invertible repeat sequences when the promoter is inverted in the transcription-incompetent (*fim*OFF) orientation, to facilitate promoter recombination to a transcription-competent (*fim*ON) orientation (Holden *et al.*, 2007, Burns *et al.*, 2000). The FimB recombinase can facilitate the reverse reaction, however it has a much lower binding affinity for invertible repeats that are found *fim*ON position and therefore performs the *fim*ON to *fim*OFF switch less frequently (Holden *et al.*, 2007, Burns *et al.*, 2000). In most UPEC strains studied to date, the FimE recombinase only recognizes the invertible repeats in the *fim*ON position to facilitate inversion to the *fim*OFF orientation (Holden *et al.*, 2007). In UTI89, the accessory recombinase FimX can only facilitate *fim*OFF to *fim*ON recombination

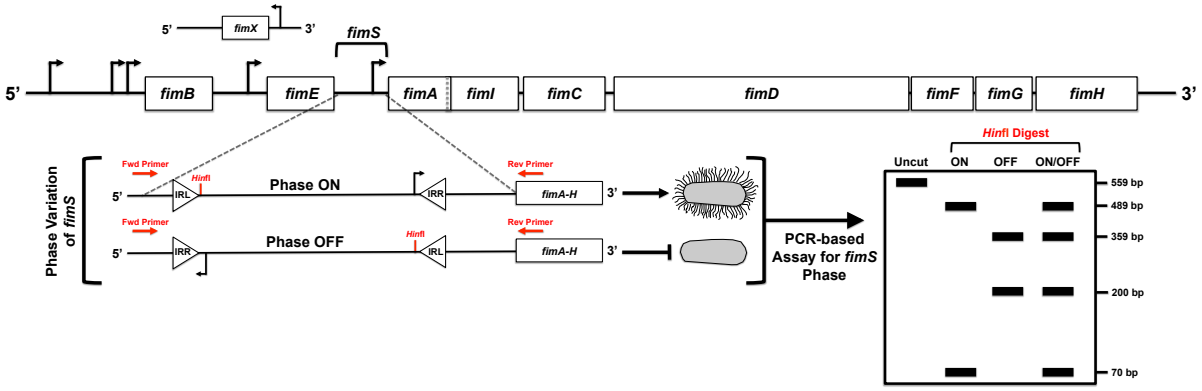

Figure 15. Schematic depiction of the *fim* operon in UPEC strain UTI89, and description of *fimS* phase assay. The *fim* operon is a 6,600bp element of the UTI89 chromosome, the transcription of which is controlled by the phase-variable promoter region *fimS*. The recombinases FimB and FimE are encoded up-stream of *fimS*, each with their own promoter(s). The accessory recombinase FimX is encoded elsewhere on the UTI89 chromosome. The blown out inset depicts the *fimS* region with the invertible repeats, in the *fim*ON and *fim*OFF orientations. Phase of the *fimS* promoter region is determined by a PCR-based assay, which after amplification takes advantage of an inherent *Hinf*I restriction enzyme site for enzymatic digestion and analysis of digested-product size by agarose gel electrophoresis. The size product observed demonstrates whether the promoter is in the *fim*ON or *fim*OFF orientations. As is most often is the case, the population is a heterogeneous mixture of both *fim*ON and *fim*OFF bacteria. Therefore the ratio between the *fim*ON and *fim*OFF bands determines whether the overall population is more in the *fim*ON or *fim*OFF states.

(Bateman *et al.*, 2013). The abundance and activity of the recombinase enzymes in each UPEC cell influences the orientation of the *fimS* promoter, leading to heterogeneous populations with varying expression levels of *fim* expression. An additional variable adding to the heterogeneity in piliation is the fact that *fim* promoter regions oriented in the *fim*ON state are not always quarantined to drive transcription of the operon. Several regulators have been shown to control *fim* operon transcription in response to a variety of environmental signals, such as pH, osmolality, and nutrient availability (Rentschler *et al.*, 2013, Greene *et al.*, 2015). Given the robustly reproducible localization of *fim*-expressing bacterial to the air-exposed region of the biofilms analyzed by IMS, we hypothesized that the environmental oxygen concentration is another regulator of type 1 pili expression. The work described in this chapter interrogates the effects of oxygen on *fimS* promoter orientation via the action of the Fim recombinase enzymes.

Methods

Bacterial Strains

All strains used in these studies are listed in **Table 1** in **Appendix A**. UTI89Δ*fimE* was created using the previously established λ Red recombinase methods (Murphy and Campellone, 2003) and the primers listed in **Table 2** in **Appendix B** (Integrated DNA Technologies). The complementation construct pFimE was created by cloning the *fimE* gene into the XbaI-HindIII restriction sites of vector pBAD33 (Kostakioti *et al.*, 2009), using the primers listed in **Table 2** in **Appendix B**. The resulting construct was verified by sequencing.

Bacterial Growth Conditions

Bacteria were grown at 37°C overnight either with 225rpm shaking (known to induce a "*fim*OFF" state) or statically (known to induce a "*fim*ON" state). These cultures were used to inoculate fresh cultures for incubation in oxygen-replete or oxygen-deplete conditions. Oxygen-deplete cultures were incubated in an anaerobic chamber maintained at 0% oxygen with ~2-3% hydrogen (chamber courtesy of Dr. Eric Skaar). All cultures were incubated for 48 hours to mimic biofilm growth conditions used in IMS analyses, in either LB or 1.2x YESCA media as specified in the relevant results sections. After 48 hours, cultures were normalized to an OD_{600} of 1.0 in sterile PBS for subsequent analyses.

Phase Assays

Phase assays (**Figure 15**) were performed as previously described (Struve and Krogfelt, 1999) using 100 ng of genomic DNA, or an aliquot of normalized cells (OD_{600} 1.0) and with the following modifications: Primers in **Table 2** in **Appendix B** were used and the PCR was performed using the following parameters: 95 °C – 5min, 30 cycles (95 °C – 45sec, 50 °C – 20sec, 72 °C – 45sec), 72 °C – 5min. To determine the proportion of the population *fim*ON vs. *fim*OFF, mean pixel intensity of the bands at 489 bp (*fim*ON) and 359 bp (*fim*OFF) was determined within each sample using Adobe Photoshop CS6 (Adobe Systems). Background taken from a blank area of the gel at a position equivalent to each band, was subtracted. The mean intensity of the *fim*ON and *fim*OFF band for each sample was then summed, and the percentage ON vs. OFF was then determined for each sample. The percentage of each sample *fim*OFF was plotted in GraphPad Prism 6 (GraphPad Software Inc.), and statistical analysis was performed using a one-way ANOVA with Bonferroni's multiple comparisons test.

FimA Immunoblot Analysis

Immunoblots probing for FimA were performed as previously described (Hadjifrangiskou *et al.*, 2012). Briefly, cultures were normalized to an OD_{600} = 1.0 and 1 ml of normalized cultures was pelleted by centrifugation. Cell pellets were resuspended in 1x Laemmli sample buffer (BioRad) containing 5% 2-mercaptoetahnol (Sigma-Aldrich). Samples were acidified with 1M hydrochloric acid (HCl), denatured at 100°C for 10 minutes, and then neutralized with 1N sodium hydroxide (NaOH). 5 µL of each sample was loaded and resolved on a 16% SDS-PAGE gel. Following SDS-PAGE, proteins were transferred to nitrocellulose using the Trans-Blot Turbo Transfer System (BioRad), (7 minute transfer at 1.3A and 25V). Transfer efficiency was verified with Ponceau S stain (Sigma-Aldrich), and equal loading of the gel was verified with coomassie staining post-transfer. Following transfer, membranes were blocked with 5% non-fat milk in 1x tris-buffered saline with tween-20 (TBS-T) overnight at 4°C. After blocking, membranes were washed twice with 1x TBST and incubated with anti-FimA antibody [1:5,000] (Hadjifrangiskou *et al.*, 2012) for 1 hour at room temperature, washed twice with 1x TBST, and incubated with HRP-conjugated goat – anti-rabbit antibody (Promega) for 30 minutes at room temperature. Membranes were washed three times for 5 minutes each with 1x TBST, developed with SuperSignal West Pico Chemiluminescent Substrate (Thermo Scientific), and exposed on x-ray film (MidSci).

Hemagglutination Assays

Hemagglutination assays were performed as described previously (Hadjifrangiskou *et al.*, 2012). Guinea pig erythrocytes were obtained from the Colorado Serum Company. Erythrocyte

de-sialylation was performed using *Clostridium perfringens* neuraminidase (New England BioLabs) for 2 hours at 37 °C with gentle agitation.

Transmission Electron Microscopy (TEM)

TEM analyses were performed as outlined previously (Kostakioti *et al.*, 2009). Briefly, 100 µL of normalized bacterial cultures (OD_{600} = 1.0) from each condition were centrifuged at 4,000 rpm for 10 minutes and resuspended in 100 µL of 1% glutaraldehyde in 1xPBS. Samples were then submitted to the Imaging Facility of the Department of Molecular Microbiology at the Washington University School of Medicine in St. Louis for analysis. Two biological replicates of each strain and condition were submitted for analysis.

qPCR Analysis

To obtain samples for qPCR analysis, cultures were grown as previously described with the exception that the starting OD_{600} was set to 1.0 instead of 0.06. RNA extraction, reverse transcription, and real-time quantitative PCR were performed as previously described (Guckes *et al.*, 2013). qPCR was performed using two concentrations of cDNA (50 ng and 25 ng) in duplicate for each sample, and internal 16s rRNA (*rrsH*) levels were used for normalization. The primers (Integrated DNA Technologies) and probes (Applied Biosystems) listed in **Table 2** in **Appendix B** were used for amplification and quantitation respectively.

Results

Anoxic growth conditions reduce UPEC FimA protein levels and surface pili expression formation

To evaluate whether fim expression is subject to oxygen-mediated regulation, we first assessed how total FimA protein levels change in cells grown under atmospheric (~21% oxygen) or anoxic (0% oxygen) conditions. To account for potential differences in bacterial growth rate due to fermentation under anoxic conditions, bacterial cultures at the end of the 48-hour incubation period were normalized to an OD_{600} of 1.0. Coomassie and Ponceau S staining were used to verify that total protein loaded per condition was not inherently different among samples evaluated by immunoblot. Immunoblot analysis revealed high abundance of FimA protein in total cell lysates of aerobically grown cells (**Figure 16A-B**). However, very low levels of FimA were detected in cultures grown under anoxic conditions (**Figure 16A-B**).

Studies in UPEC have revealed that incubation of UPEC strains with agitation, either at 37°C or room temperature, induces a "*fim*OFF" state in which the majority of bacteria have the *fimS* promoter inverted in the transcription-incompetent orientation (Greene *et al.*, 2015, Greene *et al.*, 2014). Conversely, static incubation promotes inversion of the *fimS* promoter to a transcription-competent "*fim*ON" state (Greene *et al.*, 2015, Greene *et al.*, 2014). The initial starter cultures used to seed the cultures presented in **Figure 16A**, were incubated at 37°C with 225rpm shaking. Subsequent FimA immunoblot analysis of normalized overnight culture showed initial low FimA levels. These data suggested that upon initial seeding, both atmospheric and anoxic cultures had comparable levels of bacteria in which the *fimS* promoter was in the *fim*OFF state. These cultures demonstrated increased total FimA protein levels during growth under atmospheric, but not anoxic conditions (**Figure 16A**). We then performed an additional

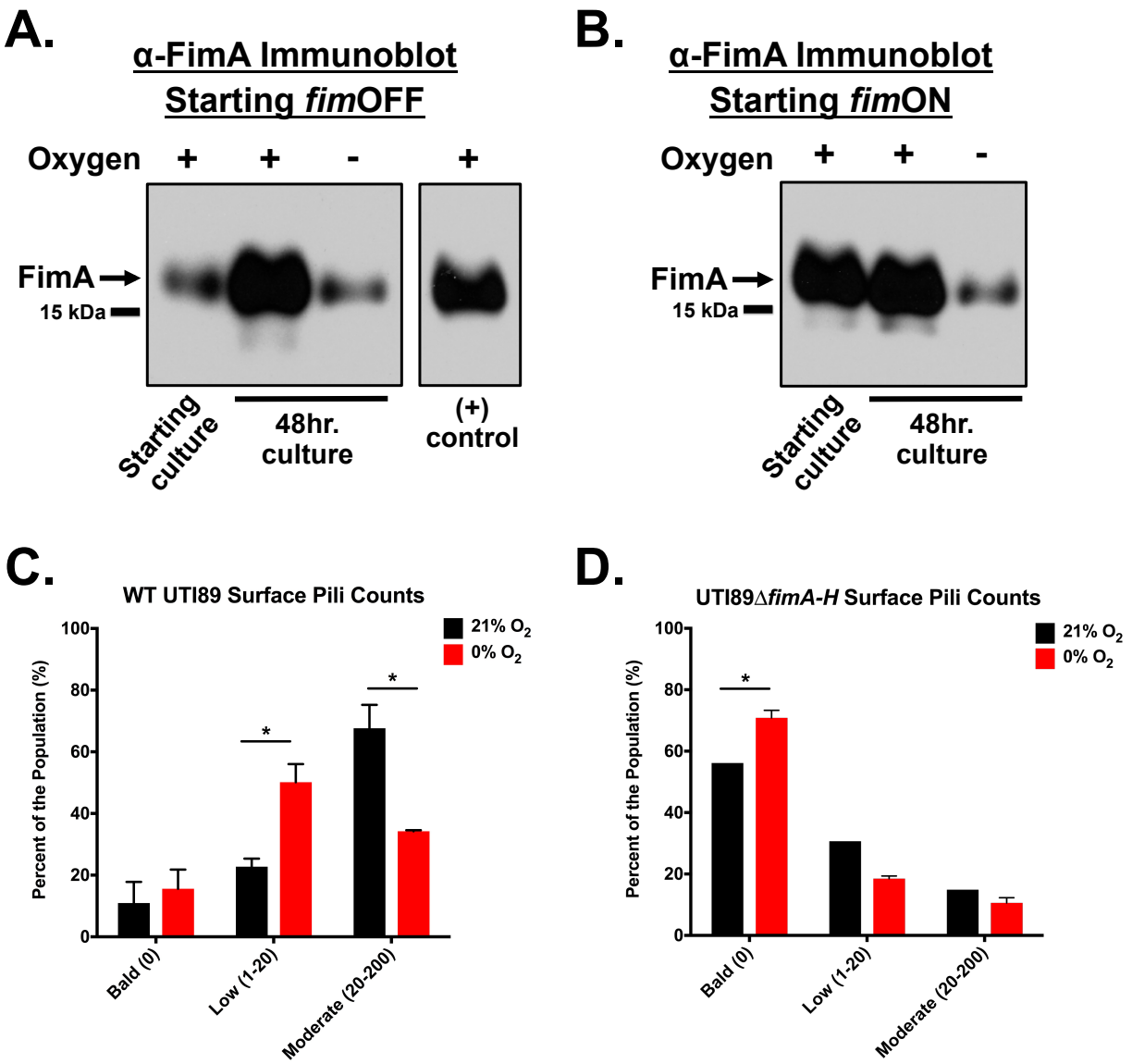

Figure 16. Anoxic conditions decrease FimA protein levels and total surface pili levels. (A-B) For immunoblot, cultures were grown statically in LB media for 48 hours in either the presence or absence of oxygen at 37°C. Cultures were started from both initial populations with **(A)** low levels of type 1 pili expression (starting *fim*OFF) and **(B)** with high levels of type 1pili expression (starting *fim*ON). **(C)** WT UTI89 pili were enumerated from 48 hour static cultures grown in LB media in either the presence or absence of oxygen at 37°C, from starting cultures with high levels of type 1 pili expression. A total of 229 bacteria at 21%, and 227 bacteria at 0% from two independent biological replicates (~110 from each) were enumerated from TEM micrographs by a blinded reviewer. **(D)** UTI89Δ*fimA-H* pili were enumerated from 48 hour static cultures grown in LB media in either the presence or absence of oxygen at 37°C, from starting cultures with high levels of type 1 pili expression. A total of 114 bacteria at 21% from one biological replicate, and 231 bacteria at 0% from two independent biological replicates (~110 from each) were enumerated from TEM micrographs by a blinded reviewer. Statistical analysis for **C-D**, performed by two-way ANOVA with Tukey correction for multiple comparisons ($p < 0.05$) using GraphPad Prism 7.

experiment, in which both atmospheric and anoxic cultures were seeded from overnight cultures grown statically. Immunoblot analysis demonstrated that these overnight starting populations were largely *fim*ON, having high levels of FimA expression (**Figure 16B**). Sub-culturing these populations into fresh media and culturing for 48 hours under atmospheric oxygen concentrations resulted in continued high-level expression of FimA, while growth under anoxic conditions led to a significant reduction in total FimA protein levels (**Figure 16B**). These data show that FimA protein expression can be actively induced under atmospheric conditions, and actively repressed under anoxic conditions.

Next, we determined whether decreased total FimA protein levels under anoxic conditions resulted in lower numbers of pili on the surface of bacterial cells using transmission electron microscopy (TEM). Bacteria were grown under the same conditions used for immunoblot analyses in the presence or absence of oxygen from starting cultures with initial high levels of FimA expression (**Figure 16A**, starting *fim*ON). Bacteria were binned into one of four categories (as previously described (Greene *et al.*, 2015, Pinkner *et al.*, 2006)), based on the total number of pili expressed on the surface of each cell; bald (no pili), low (1-20 pili), moderate (20-200 pili), or high (200+ pili). On average ~15% of the UTI89 population was bald, and this population did not have a significant shift between atmospheric and anoxic conditions (**Figure 16C**). During growth at atmospheric oxygen levels, ~65% of the population fell into the moderately piliated category elaborating 20-200 pili per cell, while the remaining ~20% were binned as sparsely piliated (1-20 pili per cell) (**Figure 16C**). However, in anoxically grown cultures a drastic shift was observed, in which the majority of the population (~55%) was sparsely piliated (1-20 pili per cell) and only ~35% of the population fell into the moderately piliated category (**Figure 16C**). These data indicated that the majority of bacteria grown under

anoxic conditions have lower levels of pili on their surface compared to those grown under atmospheric conditions. One caveat of TEM as performed, is that it does not distinguish between the different classes of CUP pili encoded by *E. coli*. Given that UPEC strain UTI89 harbors at least ten CUP pili systems, it is possible that other types of pili are also affected despite the analyzed cells being grown under *fim*-inducing conditions (static incubation). To partially address this issue an UTI89Δ*fimA-H* strain, lacking the entire biosynthetic *fim* operon, was subjected to TEM analysis after culture under both oxygen conditions. Analysis of UTI89Δ*fimA-H* demonstrated that in both oxygen conditions approximately 60-70% of the population was bald, with the remaining populations being low to moderately piliated (**Figure 16D**). These results indicated that in the absence of oxygen, another class (or classes) of pili makes up the piliated population.

Previous studies indicated that reduction in the expression of type 1 pili induces the expression of another CUP system, S pili, under type 1 pili-inducing conditions (Greene *et al.*, 2014, Kostakioti *et al.*, 2012, Hadjifrangiskou *et al.*, 2011). Due to structural homology among the major subunits of CUP pili, the anti-FimA antibody used in these studies cannot be used for immuno-gold labeling by TEM to differentiate type 1 pili on the cell surface. However, differences in binding specificity of the CUP pilus tip adhesins allow for their differentiation by other ligand-specific methodologies. Type 1 pili are characterized by their ability to bind mannosylated proteins (Hultgren *et al.*, 1986). An assay to quantify type 1 pili in a UPEC population involves the agglutination of guinea pig red blood cells in the presence and absence of mannose. In bacteria that solely express type 1 pili, hemagglutination (HA) can be abolished by the addition of free mannose to the agglutination reaction (Hultgren *et al.*, 1986). Given the differential specificity of their tip adhesin, S pili bind to sialic acid residues (Korhonen *et al.*,

1984). Therefore, desialylation of red blood cells using neuraminidase prior to the agglutination assay will abrogate S pili-dependent HA (Hadjifrangiskou *et al.*, 2012). Combined these two approaches can be used to distinguish HA attributed to type 1 pili, compared to HA attributed to S pili. To evaluate if S pili were found on the surface of UPEC under anoxic conditions, HA assays were performed on normalized cells grown under either atmospheric or anoxic conditions.

As expected, when UTI89 was grown statically under atmospheric oxygen conditions, HA was abolished in the presence of free mannose and was unaffected by neuraminidase treatment (**Figure 17A**), suggesting high numbers of type 1 pili on the bacterial surface. However, UTI89 grown under anoxic conditions exhibited lower HA titers that were inhibited by both mannose and by neuraminidase treatment (**Figure 17B**), indicating that the observed agglutination was mediated by both type 1 and S pili. Given the inverse relationship between these two CUP pili systems, the observable increase in S pili-mediated agglutination under anoxic conditions further demonstrated that type 1 pili are down-regulated in response to the lack of oxygen, as previously described (Greene *et al.*, 2014, Kostakioti *et al.*, 2012, Hadjifrangiskou *et al.*, 2011). Control experiments with UTI89Δ*fimA-H* revealed that as expected HA was significantly reduced compared to WT UTI89 under both atmospheric and anoxic conditions, consistent with the absence of type 1 pili (**Figure 17**). However, under both conditions the low HA observed was unaffected by mannose addition and abolished upon pre-treatment of cells with neuraminidase, confirming that UTI89Δ*fimA-H* predominantly expresses S pili, and that the levels of S pili are relatively unaffected by variations in oxygen concentration (**Figure 17**). Therefore, these data indicated that depletion of oxygen does not repress expression of all CUP pili systems within UTI89.

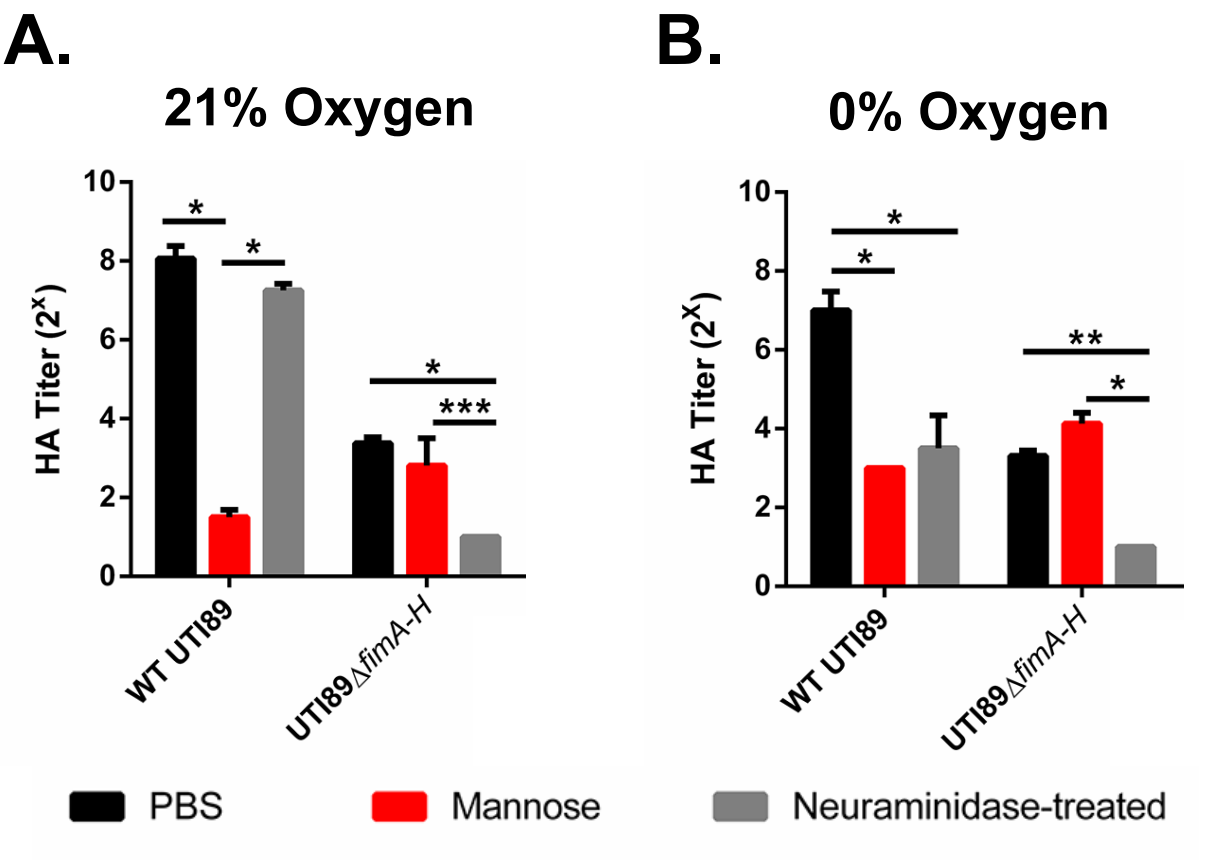

Figure 17. S pili are unaffected by varying oxygen conditions. Hemagglutination assay measuring type 1 (mannose-dependent) and S pili (sialic acid dependent) mediated agglutination under **(A)** atmospheric (~21%) oxygen and **(B)** anoxic (0%) growth conditions from cultures started from a population primarily *fim*ON. Data presented as mean with SEM, obtained from two technical replicates of two biological replicates. Statistical analysis performed as a two-way ANOVA with Bonferroni's multiple comparisons test using GraphPad ($^{\#}p$ = <0.05, ***p = <0.01, *p = <0.001, *p = <0.0001).

Anoxic conditions actively promoter inversion the fimS promoter to a fimOFF orientation

From the observation that anoxic conditions decrease total FimA protein levels, as well as surface pili numbers, we next sought to determine how this reduction occurs. The TEM results of WT UTI89 suggested that the numbers of bald bacteria do not change between atmospheric and anoxic conditions, indicating that anoxic conditions do not lead to a complete repression of the *fim* operon. However, a significant shift to low piliated populations was observed, suggesting possible increase in the frequency of *fimS* promoter inversion and/or possible transcriptional and post-transcriptional effects. To determine how anoxia influence *fimS* promoter orientation, we used a previously developed PCR-based "phase assay" (Struve and Krogfelt, 1999) that can distinguish between transcription-competent (*fim*ON) and transcription-incompetent (*fim*OFF) orientations of the *fimS* promoter (**Figure 15**). When starting these experiments from cultures in which the *fimS* promoter is primarily *fim*OFF (grown with 225rpm shaking at 37°C), we observed that sub-culturing statically in the presence of oxygen induced a switch of *fimS* to the *fim*ON orientation (**Figure 18A**). This switch correlated with an increase in FimA protein levels within the same culture (**Figure 16A**). However, the *fimS* promoter remained in the *fim*OFF orientation when bacteria were cultured under anoxic conditions (**Figure 18A**).

When starting from cultures in which the *fimS* promoter is primarily *fim*ON (grown statically at 37°C), we observed that sub-culturing statically in the presence of oxygen maintained *fimS* in the *fim*ON orientation (**Figure 18B**). Culturing *fim*ON populations under anoxic conditions for 48 hours induced an inversion of *fimS* to the *fim*OFF orientation (**Figure 18B**). Consistent with a greater proportion of cells with the *fimS* promoter in the *fim*OFF orientation, qPCR analysis probing for *fim* operon steady-state transcript levels revealed an overall two-fold reduction in *fimI* transcript during growth under anoxic conditions (**Figure 19**).

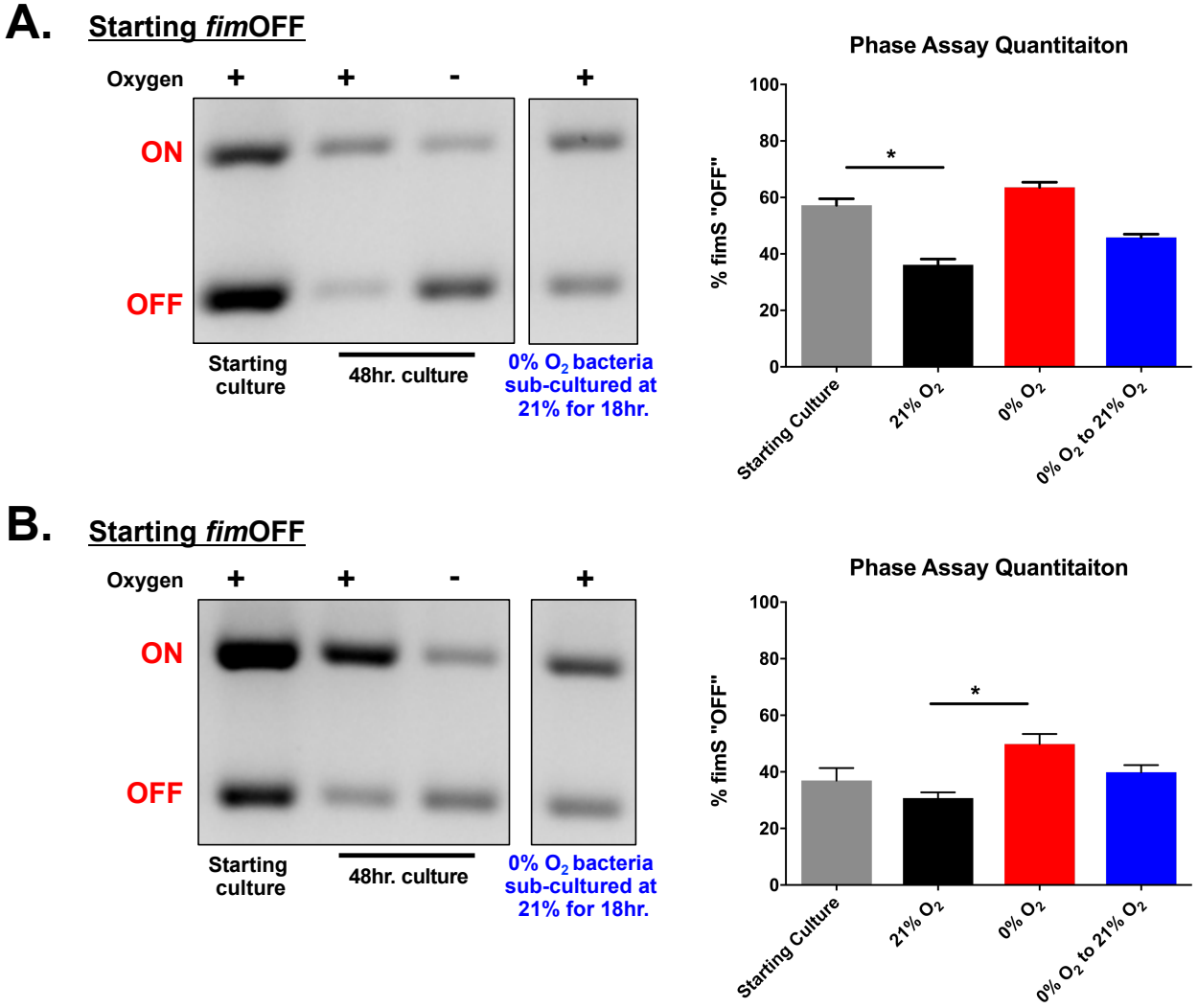

Figure 18. Anoxic type 1 pili repression is mediated by inversion of the *fimS* promoter to a *fim*OFF orientation. (A) Analysis with cultures starting primarily *fim*OFF cultured for 48 hours under atmospheric (21%) and anoxic (0%) conditions. The gel depicts a representative phase assay gel. The percentage *fim*OFF for each sample from multiple biological replicates is graphed as mean with SEM using GraphPad Prism 7 for each sample (starting culture/anoxic sub-culture, n = 2; atmospheric/anoxic, n = 9). Statistical difference from atmospheric culture shown and determined by one-way ANOVA with Bonferroni's multiple comparisons test using GraphPad (*p = 0.0019, ** and ***p = <0.0001). Statistically significant differences were also noted (but not indicated on the graph) between anoxic/anoxic sub-cultured [p = 0.0123]. Representative anti-FimA immunoblots for samples grown under these conditions are shown in **Figure 16**. **(B)** Analyses as shown in **A**, for cultures starting predominantly *fim*ON. Phase assay quantitation taken from biological replicates of starting culture/anoxic sub-culture, n = 2; atmospheric/anoxic, n = 6. Statistical analysis performed as in **A** (*p = 0.0004, **p = 0.0344), with representative immunoblots again in **Figure 16**.

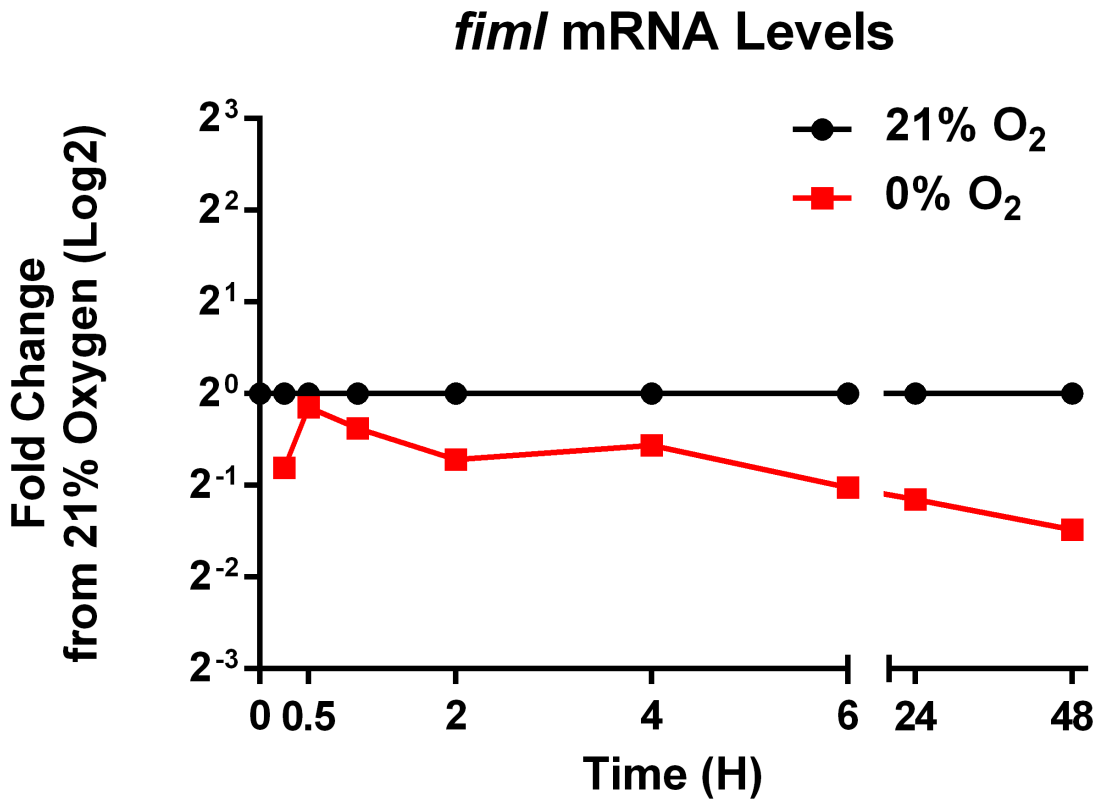

Figure 19. Anoxic conditions repress expression of the *fim* operon. Graphs depict qPCR analysis of *fimI* steady-state mRNA transcript levels at 0.25, 0.5, 1, 2, 4, 6, 24, and 48 hours from cultures grown statically at 37°C in either the presence or absence of oxygen. Cultures were seeded at an OD_{600} of 1.0 from overnight cultures grown statically in LB media at 37°C. qPCR analysis was performed using primers and probes specific to the target gene of interest with two concentrations of cDNA (50 ng and 25 ng) in duplicate for each sample, and internal 16s rRNA (*rrsH*) levels were used for normalization. *fimI* expression levels at each time point in the presence of oxygen were normalized to the starting culture. *fimI* expression levels at each time point in the absence of oxygen, are presented as fold-change from the corresponding time-point in the presence of oxygen. Data are representative of one biological replicate.

These data suggest that in the absence of oxygen the *fimS* promoter becomes inverted to the *fim*OFF orientation, resulting in reduced transcription of the *fim* operon. If this inversion and reduction occurs within already moderate to highly piliated bacteria, then following cell division the daughter cells would still harbor some of the original pili, resulting in populations with a low abundance of pili on the cell surface.

Given that static growth at 37°C in LB media under atmospheric conditions enhances expression of type 1 pili in UPEC (Kostakioti *et al.*, 2012, Chen *et al.*, 2009, Pinkner *et al.*, 2006), we sought to determine if the oxygen-dependent repression observed was affected by nutrient or temperature environments. Therefore, along with the studies at 37°C in LB media, anoxic studies were also performed in 1.2x YESCA media (same as used for original biofilm IMS studies) at both room temperature and 37°C, as well as in LB media at room temperature. Compared to LB, 1.2x YESCA media is nutrient limiting. Comparative analysis of *fimS* phase and FimA protein levels in YESCA media at room temperature and 37°C, and LB media at room temperature, yielded *fimS* phase and FimA protein expression profiles similar to those observed in LB media at 37°C under both atmospheric and anoxic oxygen conditions (**Figure 20**). These data suggest that the anoxic *fimS* switch does not result from either alteration is nutrients or surrounding environmental temperature.

Inversion of fimS is mediated by an imbalance in fimB and fimE recombinase expression under anoxic conditions

Given that inversion of the *fimS* promoter occurs via the action of conserved and species-specific Fim recombinases (Schwan, 2011, Hannan *et al.*, 2008), we next determined how anoxic conditions impact expression of the UTI89 recombinase-encoding genes *fimB*, *fimE*, and *fimX*

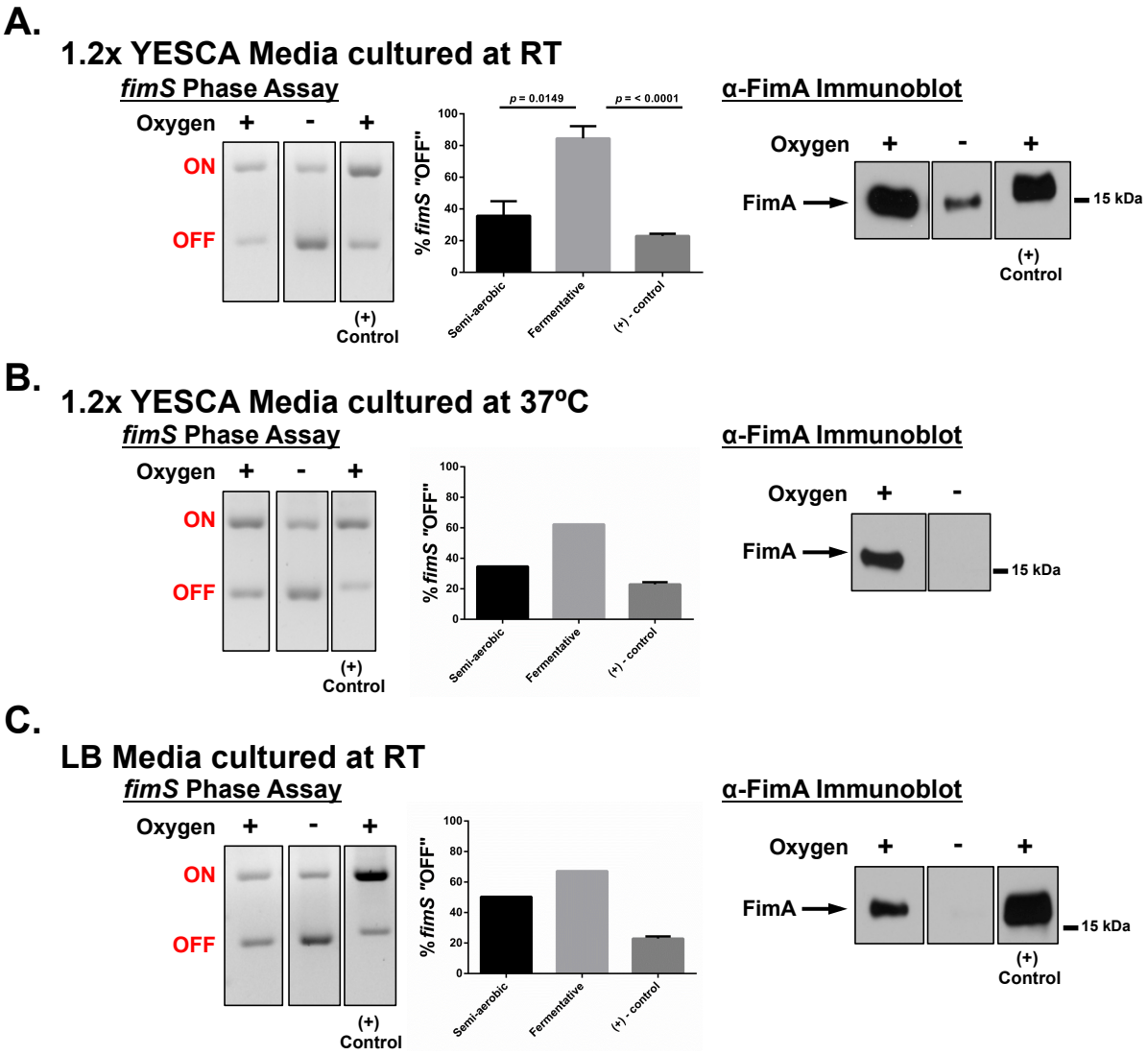

Figure 20. UPEC type 1 pili expression is repressed under oxygen-deplete growth conditions regardless of growth medium and temperature. (A) Phase assay and FimA immunoblot analysis of WT UTI89 cultured in 1.2x YESCA media at room temperature under semi-aerobic and anaerobic/fermentative growth conditions. Phase assay quantitation, n = 3. Statistical analysis performed by two-tailed unpaired Student's *t*-test in GraphPad Prism 6, with determined p-values shown. Immunoblot representative of n = 4 analyses. **(B)** Phase assay and FimA immunoblot analysis of WT UTI89 cultured in 1.2x YESCA media at 37 °C under semi-aerobic and fermentative growth conditions. Phase assay quantitation, n = 1. Immunoblot representative of n = 2 analyses. **(C)** Phase assay and FimA immunoblot analysis of WT UTI89 cultured in LB media (pH 7.4) at room temperature under semi-aerobic and fermentative growth conditions. Phase assay quantitation, n = 1. Immunoblot representative of n = 2 analyses. Statistical analysis of phase quantitation not performed for (B) and (C) due to insufficient number of biological replicates. All data presented as outlined in Figure 2. All cultures for the analyses in A-C were started from primary overnight cultures grown at 37 °C with shaking conditions therefore each population began primarily phase *fim*OFF.

(**Figure 15**). By qPCR we observed that compared to transcript levels under atmospheric oxygen concentration, under anoxic conditions *fimB* steady-state transcript levels were consistently two-fold lower, while *fimE* transcript levels did not significantly change (**Figure 21**). Together, these data suggested that expression of *fimE*, or *fimE* transcript stability, is unaffected by anoxic conditions while transcript levels of *fimB* are reduced. Given the opposing roles of FimB and FimE on fimS promoter inversion, decreased levels of *fimB* and higher levels of *fimE* may account for the increased inversion to the *fim*OFF state observed in anoxic conditions (**Figure 18**).

FimX may play a role in mediating the phase switch in extended stationary phase cultures

While the *fimB* and *fimE* genes are conserved across all *fim*-expressing *E. coli* strains, the accessory recombinase FimX (specifically *fim*ON switching) is found only in select *E. coli* strains, including UPEC strain UTI89 and several of the multi-drug resistant UPEC strains belonging to the ST131 lineage (Bateman *et al.*, 2013, Sarkar *et al.*, 2016). Monitoring *fimX* steady-state transcript levels over time by qPCR, post-inoculation into fresh media and under atmospheric culture conditions, revealed that expression of *fimX* decreased to levels approximately two- to four-fold lower than the starting culture by 2 hours (**Figure 22**). Then between 2 and 4 hours post-inoculation, *fimX* transcript levels begin increasing until levels are approximately 5-fold higher than the starting culture at 48 hours (**Figure 22**). These observations suggest that in older populations, FimX may be the primary *fim*ON-switching recombinase. We are currently investigating this hypothesis. Compared to atmospheric conditions *fimX* transcript levels were higher in young cultures grown anoxically and displayed non-significant

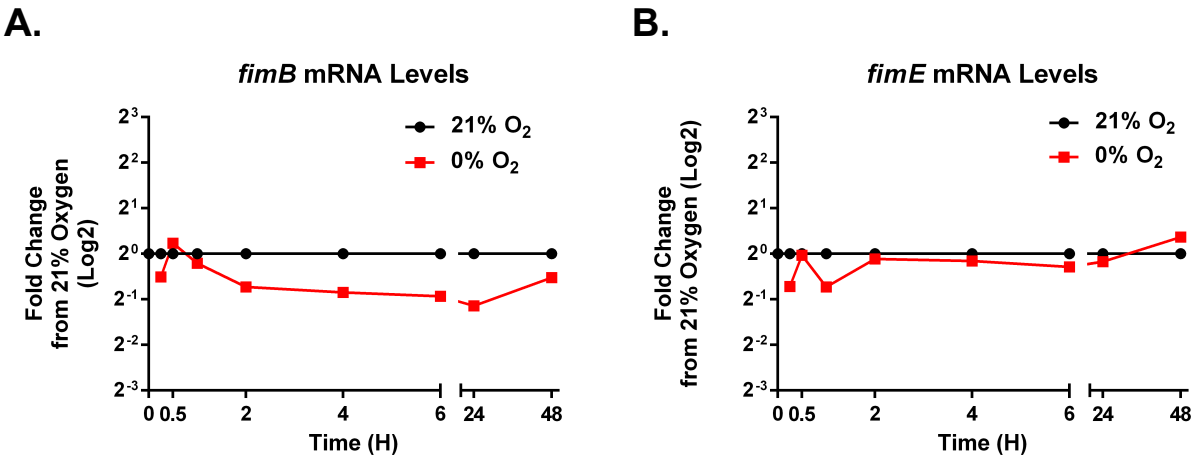

Figure 21. Anoxic growth conditions induce an imbalance in recombinase enzyme expression that favors the *fim*OFF switch. (A) *fimB* steady-state mRNA levels, and **(B)** *fimE* steady-state mRNA levels under anoxic conditions compared to atmospheric conditions. Graphs depict qPCR analysis of recombinase steady-state mRNA transcript levels at 0.25, 0.5, 1, 2, 4, 6, 24, and 48 hours from cultures grown statically at 37°C in either the presence or absence of oxygen. Cultures were seeded at an OD_{600} of 1.0 from overnight cultures grown statically in LB media at 37°C. qPCR analysis was performed using primers and probes specific to the target gene of interest with two concentrations of cDNA (50 ng and 25 ng) in duplicate for each sample, and internal 16s rRNA (*rrsH*) levels were used for normalization. Atmospheric levels at each time point were normalized to the starting culture. Anoxic transcript levels at each time point are presented as fold-change from the corresponding time-point under atmospheric conditions. Data are representative of one biological replicate.

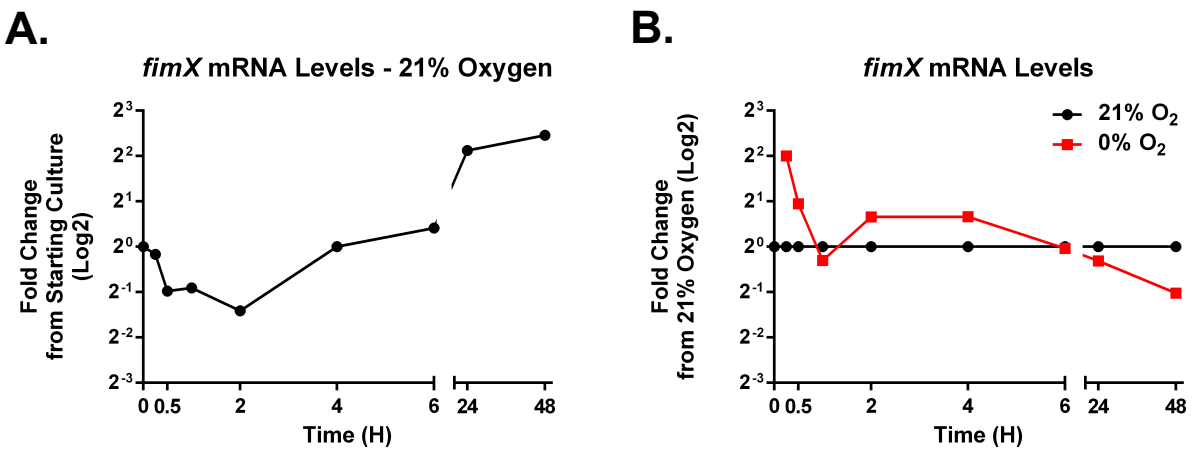

Figure 22. FimX may be the primary *fim*ON-switching recombinase in late stationary phase cultures. Graphs depict qPCR analysis of recombinase steady-state mRNA transcript levels at 0.25, 0.5, 1, 2, 4, 6, 24, and 48 hours from cultures grown statically at 37°C in either the presence **(A)** or absence of oxygen **(B)**. Cultures were seeded at an OD_{600} of 1.0 from overnight cultures grown statically in LB media at 37°C. qPCR analysis was performed using primers and probes specific to the target gene of interest with two concentrations of cDNA (50 ng and 25 ng) in duplicate for each sample, and internal 16s rRNA (*rrsH*) levels were used for normalization. **(A)** Atmospheric expression levels at each time point in the presence of oxygen, presented as the fold-change from the starting culture. **(B)** Anoxic transcript levels at each time point are presented as fold-change from the corresponding time-point under atmospheric conditions. Data are representative of one biological replicate.

fluctuations over 24 hours (**Figure 22**). Given that FimX is a strain-specific recombinase, we next sought to understand how the differences in *fimB* and *fimE* transcript levels influences piliation. We hypothesized that the imbalance in *fimB/E* transcript levels accounts for at least part of the reduced piliation of UPEC under anoxic conditions.

The FimE recombinase is primarily responsible for the anoxic fimS inversion

To investigate the *fimB/E* imbalance further, we generated a non-polar UTI89 mutant lacking the *fimE* gene (UTI89Δ*fimE*) while leaving *fimS* promoter elements intact. The resulting mutant was tested using phase assays, FimA immunoblot, and TEM analyses (**Figure 23**). After 48-hour culture under atmospheric oxygen conditions UTI89Δ*fimE* demonstrated *fimS* phase similar to WT UTI89 (**Figure 23A**), while phase from cultures under anoxic conditions demonstrated a lower proportion of the population in the *fim*OFF orientation (**Figure 23A**). These data suggest that FimB may also be contributing to anoxic inversion of *fimS* to the *fim*OFF orientation.

The observed increased *fim*ON population at 48 hours under anoxic conditions with the UTI89Δ*fimE* strain also corresponds to an increase in FimA protein levels compared to WT UTI89 (**Figure 23A**). TEM analysis of UTI89Δ*fimE* demonstrated that under growth in atmospheric oxygen conditions the numbers of bald, low- and moderately-piliated bacteria was equivalent to WT UTI89, but a higher proportion of highly-piliated (200^{+} pili per cell) bacteria were recorded (**Figure 23B**). Under anoxic conditions the UTI89Δ*fimE* strain still produced a small subpopulation of highly-piliated cells (**Figure 23B**). Expression of FimE *in trans* fully complements the anoxic inversion of *fimS* with ~80% of the population *fim*OFF, resulting in significantly reduced FimA protein levels (**Figure 23A**) and greater than 55% of the population

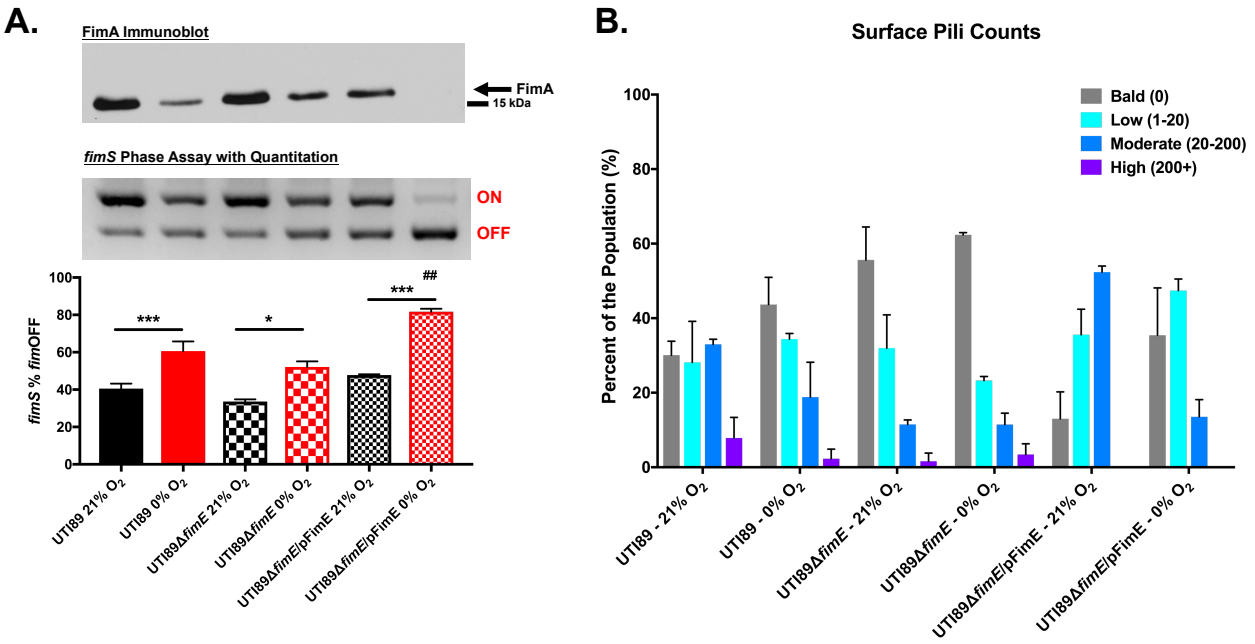

Figure 23. The FimE recombinase is primarily responsible for anoxic *fimS* inversion. (A) Phase assay analysis of *fimS* orientation demonstrates a partial restoration in anoxic *fim*ON populations in the UTI89Δ*fimE* strain, resulting in a partial restoration of anoxic FimA protein levels. Complementation of FimE *in trans* demonstrates an increase in the anoxic fimOFF population, as well as a significant decrease in FimA protein levels. These data indicate that FimE is the primary, but not only, Fim recombinase that mediates the anoxic *fimS* inversion. All strains in this analysis carried the pBAD33 vector, either without or with a copy of FimE (pFimE), and were grown in the presence of 20µg/ml chloramphenicol and either 0.05% or 0.01% arabinose for induction. Immunoblot is representative of at least n = 3. The percent *fimS* *fim*OFF was determined as previously described, and plotted using GraphPad Prism 7 as the mean with the standard error of the mean (UTI89 n=5, UTI89Δ*fimE* and UTI89Δ*fimE*/pFimE n=3). Statistical analysis performed by one-way ANOVA with Tukey correction for multiple comparisons (*p<0.05, ***p<0.0001). $^{\#\#}$ UTI89Δ*fimE*/pFimE grown at 0% oxygen is statistically significant from all other columns (p<0.005). **(B)** Surface pili were enumerated from 48 hour static cultures grown in LB media with 20µg/mL chloramphenicol and 0.05% arabinose, in either the presence or absence of oxygen at 37°C, from starting cultures with high levels of type 1 pili expression. All strains carried the either the pBAD33 or pBAD33-*fimE* plasmid. The total number of bacteria counted for each strain from two independent biological replicates, were: WT UTI89, 241 at 21% and 251 at 0%; UTI89Δ*fimE,* 315 at 21% and 228 at 0%; UTI89Δ*fimE*/pFimE, 403 at 21% and 276 at 0%. All pili were enumerated from TEM micrographs by a blinded reviewer. Statistical analysis performed by one-way ANOVA with Tukey correction for multiple comparisons (p < 0.05) using GraphPad Prism 7, comparing within each pili bin.

being devoid of surface pili (**Figure 23B**). Together, these results also indicated that promoter inversion is not the only mechanism by which regulation of pili expression occurs under anoxic conditions.

Discussion

This work demonstrates that oxygen regulates the expression of type 1 pili in UPEC strain UTI89, validating that the air-exposed specific localization of FimA observed by MALDI-TOF IMS is representative of a unique biofilm subpopulation. Based on these observations, it appears that induction of type 1 pili occurs on the topmost layer of the imaged biofilm due to the increased oxygen levels in this region. Further investigation of how oxygen influences total FimA protein levels and bacterial surface pili levels using planktonic populations, revealed that anoxic conditions lead to specific down-regulation of type 1 pili and not necessarily all CUP systems. We eliminated the possibility that this phenomenon was driven by nutrient availability and/or temperature, as anoxic studies were performed in YESCA and LB media at both room temperature and 37°. Static growth at 37°C in LB media under atmospheric conditions enhances, and has been previously reported as the optimal conditions for expression of type 1 pili in UPEC (Kostakioti *et al.*, 2012, Chen *et al.*, 2009, Pinkner *et al.*, 2006). Comparative analysis of *fimS* phase and FimA protein levels in YESCA media at room temperature and 37°C, and in LB media at room temperature, provided phase and protein expression profiles similar to those observed in LB media at 37°C under both atmospheric and anoxic oxygen conditions.

Further analysis of this anoxic down-regulation of type 1 pili revealed the presence of a transcriptional regulatory mechanism, which represses their production through inversion of the

fimS promoter to a transcription-incompetent orientation. Data also suggest the presence of a secondary regulatory mechanism that functions independent of the *fimS* promoter to repress type 1 pili under anoxic conditions. Both of these mechanisms are engaged under fermentative growth, but not conditions conducive to anaerobic respiration, strongly suggesting that loss of the ability to use the electron transport processes imposes an energetic cost to the bacteria and necessitates the down-regulation of energetically expensive structures.

In probing the basis of how oxygen could mediate *fimS* recombination, we have found that under fermentative anoxic conditions there is decreased expression of the *fim*ON-switching recombinases *fimB* and *fimX*, with no significant alterations in the *fim*OFF-switching recombinase *fimE*. Therefore the anoxic effects on the phase-state of the *fimS* promoter result from the effects of an imbalance in *fim*ON/*fim*OFF switching recombinases, and overall decreased transcription of the *fim* operon. Alterations in recombinase expression have been previously described to impact the phase-state of the *fimS* promoter (Muller *et al.*, 2009). Muller *et al.* elegantly demonstrated how the regulatory protein CRP impacts *fim* gene expression by interfering with FimB function, and repressing the expression of the DNA relaxation protein Lrp (Muller *et al.*, 2009).

Along with characterization of an imbalance in recombinase expression, this is the first time that time-course expression levels of *fimX* have been reported for UTI89 and directly compared to expression levels of the other two recombinases. Time-course analysis of the expression of the two *fim*ON switching recombinases, *fimB* and *fimX*, demonstrates some interesting possible correlations between their expression (**Figure 22**). I have shown that atmospheric oxygen conditions promote inversion of *fimS* to, or maintain *fimS* in the *fim*ON orientation. In the presence of oxygen, as *fimB* mRNA levels surge post-inoculation into fresh

media *fimX* mRNA levels coincidently decrease. The surge in *fimB* expression so early post-inoculation in fresh media and the presence of oxygen suggests a possible nutritional regulation of *fimB* expression under conditions conducive to aerobic respiration. Subsequently as *fimB* levels decrease at 24-48 hours in the presence of oxygen, *fimX* expression drastically increases. This suggests a possible cross-regulation between the expression of *fimB* and *fimX* in UTI89, where high-level expression of *fimB* represses the expression of *fimX* through an unidentified mechanism. This revelation further highlights the extensive complexity of the regulation of the *fim* operon, in that the possible cross-regulation between the expression of recombinases adds another potential regulatory level that will govern operon transcription.

Due to the lack of recombinase specific antibodies, we could not quantify FimB and FimE protein levels. However, analysis of a UTI89 mutant lacking the *fimE* gene suggested that FimE does indeed contribute to *fim* down-regulation under anoxic conditions. Interestingly, the continued presence of bald and low abundance surface pili subpopulation in the absence of *fimE*, points to the presence of additional mechanisms that operate to regulate pilus production at a level downstream of the *fimS* promoter. **Chapter IV** describes work aimed at delineating the sensory mechanisms that drive the observed FimE-mediated oxygen-dependent inversion of *fimS* to the *fim*OFF orientation under anoxic conditions, specifically examining the impacts of the fumarate and nitrate reductase regulator (FNR).

CHAPTER IV

WHO'S THE BOSS? FNR MEDIATES TRANSCRIPTIONAL REGULATION OF TYPE 1 PILI WITHIN UROPATHOGENIC *E. COLI*

Introduction

[4]There is a high level of diversity in the types of adhesive components bacteria utilize for attachment and adherence to surfaces, and most use different combinations in response to varying environmental conditions and the type of surface encountered (Absolom *et al.*, 1983, Dickson and Koohmaraie, 1989, van Loosdrecht *et al.*, 1987, Arnold and Bailey, 2000, Das *et al.*, 2011). Attachment to a surface and the initiation of biofilm formation is a commitment to the development of a multicellular lifestyle. Therefore, the timing in expression of adhesive components is crucial in ensuring that productive attachment only occurs within the desired niche and under the most favorable conditions. Production of structurally complex adhesive components, such as pili, can also be very energetically costly (Allen *et al.*, 2012). Therefore, the expression of adhesive components is often tightly controlled at multiple levels. Although not much is known regarding precisely what transduces the contact-dependent or other environmental signals to the regulatory machineries that control pili and adhesins, significant knowledge has been gained about mechanisms that control transcription and translation of adhesins and pili components.

[4] Portions of this chapter adapted from and published in:

Floyd *et al.* Adhesive Fiber Stratification in Uropathogenic *Escherichia coli* Biofilms Unveils Oxygen-Mediated Control of Type 1 Pili. *PLoS Pathog.* 2015 Mar 4;11(3):e1004697. (PMID: 25738819)

As discussed in **Chapter III**, the coordination of type 1 pili expression is under complex regulation that involves a phase-variable promoter region, and transcriptional regulators (Gally *et al.*, 1996, Abraham *et al.*, 1985, Schwan, 2011, Hultgren *et al.*, 1986). Regulators responsive to environmental signals such as pH, osmolality, and nutrient availability have been shown to alter the orientation of the promoter and thereby expression of the operon (Rentschler *et al.*, 2013, Greene *et al.*, 2015). In the work from **Chapters II and III**, we presented evidence that type 1 pili are regulated in response to oxygen. Thus far, our data indicate that depletion of oxygen leads to overall lower levels of pilus components and a shift to less piliated UPEC populations (**Figure 16**). This reduction is partially attributed to the functions of the FimB and FimE recombinases, which appear to mediate the inversion of the *fimS* promoter to a *fim*OFF orientation under anoxic conditions (**Figure 18**). However, how the expression and function of the Fim recombinases is coordinated in response to oxygen, as well as the basis of additional observed regulatory mechanisms occurring at the transcriptional or post-transcriptional levels, remains to be elucidated.

In *E. coli*, there are two primary systems that sense and mediate responses to reduction in environmental oxygen levels. First among these systems, is the ArcAB anaerobic-sensing two-component system (TCS). The ArcAB TCS is comprised of the ArcB sensor histidine kinase and the ArcA response regulator, and is one of the major *E. coli* regulators mediating the switch from aerobic to anaerobic growth (Gunsalus and Park, 1994, Alexeeva *et al.*, 2003, Alexeeva *et al.*, 2000). While not responding directly to environmental oxygen levels, the ArcB sensor responds to the presence of reduced quinones in the inner bacterial membrane that are produced under low oxygen conditions (Georgellis *et al.*, 2001). Signaling through ArcB activates the ArcA transcriptional regulator, which alters the transcription of >100 genes that facilitate bacterial

growth under low oxygen or anoxic conditions (Georgellis *et al.*, 2001, Malpica *et al.*, 2006). Transcriptional targets of the ArcAB system include genes related to metabolism, oxidative stress responses, acid stress responses, pH stress responses, and outer membrane protein transporters (Rolfe *et al.*, 2011). Regulation by ArcA has been linked to pathogenesis of other extra-intestinal *E. coli* pathotypes, such as avian pathogenic *E. coli* (Jiang *et al.*, 2015).

In addition to ArcAB, the fumarate and nitrate reductase regulator (FNR) is another protein that responds specifically to reduced oxygen environments, to facilitate the switch from aerobic to anaerobic bacterial respiration (Unden *et al.*, 1995, Spiro and Guest, 1990, Gunsalus, 1992). Contrary to the membrane-embedded ArcB sensor, FNR is a cytoplasmic regulator that responds directly to the oxygen concentration within the bacterial cytoplasm (Unden *et al.*, 2002). FNR protein levels do not significantly change between aerobic and anoxic conditions; rather, the activation state of the protein in response to oxygen will dictate its function. In its active form under anoxic conditions FNR functions as a dimer where each monomer contains an iron-sulfur [4Fe-4S] cluster. The $[4Fe\text{-}4S]^{2+}$ cluster on the FNR dimer is crucial for oxygen sensing (Lazazzera *et al.*, 1996). Under oxygen-rich conditions, oxygen acts as an oxidizing agent reducing the $[4Fe\text{-}4S]^{2+}$ cluster to $[2Fe\text{-}2S]^{2+}$ to inactivate functional FNR (Lazazzera *et al.*, 1996). Oxygen concentrations in the surrounding environment as low as 1μM will allow for sufficient accumulation of oxygen within the bacterial cytoplasm to inhibit the function of FNR within the cell (Tran *et al.*, 2000). If exposed to oxygen for an extended period of time, FNR can be further inactivated to an apo state lacking the $[2Fe\text{-}2S]^{2+}$ cluster (Lazazzera *et al.*, 1996). The inactive $[2Fe\text{-}2S]^{2+}$ FNR dimer can readily transition back to an active $[4Fe\text{-}4S]^{2+}$ FNR dimer, but this process is more complex for apoFNR, involving reduction by glutathione and the

function of cysteine disulfurase enzymes that help to reestablish the $[4Fe\text{-}4S]^{2+}$ cluster (Lazazzera *et al.*, 1996).

The regulon of genes controlled by FNR is extensive (~103 – 155 genes) and includes genes involved in nitrate metabolism, metal ion transport, stress response, etc. (Constantinidou *et al.*, 2006). We hypothesized that either one or both of these major oxygen-sensing regulatory systems could influence the transcription of type 1 pili directly, and/or influence the transcription of the Fim recombinases under anoxic conditions to control *fim* expression. In the work presented here, we sought to determine the roles of AcrAB and FNR in regulating type 1 pili expression in UPEC under anoxic conditions.

Methods

Bacterial Strains

All strains used for these studies are listed in **Table 1** in **Appendix A**. UTI89Δ*fnr*, UTI89_LONΔ*fnr*, and UTI89_LONΔ*fimE* were created using the previously established λ Red recombinase methods (Murphy and Campellone, 2003) and the primers listed in **Table 2** in **Appendix B** (Integrated DNA Technologies).

Bacterial Growth Conditions

WT UTI89 and UTI89Δ*fnr* were grown at 37°C statically overnight (known to induce a "*fim*ON" state). These cultures were used to inoculate fresh cultures for incubation in oxygen-replete or oxygen-deplete conditions. Oxygen-deplete cultures were incubated in an anaerobic chamber maintained at 0% oxygen with ~2-3% hydrogen (chamber courtesy of Dr. Eric Skaar).

All cultures were incubated for 48 hours to mimic biofilm growth conditions used in IMS analyses, in either LB or 1.2x YESCA media as specified in the relevant results sections. After 48 hours, cultures were normalized to an OD_{600} of 1.0 in sterile 1x PBS for subsequent analyses (as described in the relevant sections below). Cultures for the analysis of impacts of the alternative terminal electron acceptor nitrate ($NaNO_3$) were set up in the same way as all other cultures, simply with the addition of 40mM $NaNO_3$ and cultured for 48 hours in the anaerobic chamber.

Phase Assays

Phase assays (**Figure 15**) were performed as previously described (Struve and Krogfelt, 1999) using 100 ng of genomic DNA, or an aliquot of normalized cells (OD_{600} 1.0) and with the following modifications: Primers in **Table 2** in **Appendix B** were used and the PCR was performed using the following parameters: 95 °C – 5min, 30 cycles (95 °C – 45sec, 50 °C – 20sec, 72 °C – 45sec), 72 °C – 5min. To determine the proportion of the population *fim*ON vs. *fim*OFF, mean pixel intensity of the bands at 489 bp (*fim*ON) and 359 bp (*fim*OFF) was determined within each sample using Adobe Photoshop CS6 (Adobe Systems). Background taken from a blank area of the gel at a position equivalent to each band, was subtracted. The mean intensity of the *fim*ON and *fim*OFF band for each sample was then summed, and the percentage ON vs. OFF was then determined for each sample. The percentage of each sample *fim*OFF was plotted in GraphPad Prism 6 (GraphPad Software Inc.), and statistical analysis was performed using a one-way ANOVA with Bonferroni's multiple comparisons test.

FimA Immunoblot Analysis

Immunoblots probing for FimA were performed as previously described (Hadjifrangiskou *et al.*, 2012). Briefly, cultures were normalized to an OD_{600} = 1.0 and 1 ml of normalized cultures was pelleted by centrifugation. Cell pellets were resuspended in 1x Laemmli sample buffer (BioRad) containing 5% 2-mercaptoetahnol (Sigma-Aldrich). Samples were acidified with 1M hydrochloric acid (HCl), denatured at 100°C for 10 minutes, and then neutralized with 1N NaOH. 5 µL of each sample was loaded and resolved on a 16% SDS-PAGE gel. Following SDS-PAGE, proteins were transferred to nitrocellulose using the Trans-Blot Turbo Transfer System (BioRad), (7 minute transfer at 1.3A and 25V). Transfer efficiency was verified with Ponceau S stain (Sigma-Aldrich), and equal loading of the gel was verified with coomassie staining post-transfer. Following transfer, membranes were blocked with 5% non-fat milk in 1x TBS-T overnight at 4°C. After blocking, membranes were washed twice with 1x TBST and incubated with anti-FimA antibody [1:5,000] (Hadjifrangiskou *et al.*, 2012) for 1 hour at room temperature, washed twice with 1x TBST, and incubated with HRP-conjugated goat – anti-rabbit antibody (Promega) for 30 minutes at room temperature. Membranes were washed three times for 5 minutes each with 1x TBST, developed with SuperSignal West Pico Chemiluminescent Substrate (Thermo Scientific), and exposed on x-ray film (MidSci).

qPCR Analysis

To obtain samples for qPCR analysis, WT UTI89 and UTI89Δ*fnr* cultures were grown in the presence and absence of oxygen as previously described with the exception that the starting OD_{600} was set to 1.0 instead of 0.06. RNA extraction, reverse transcription, and real-time quantitative PCR were performed as previously described (Guckes *et al.*, 2013). qPCR was

performed using two concentrations of cDNA (50 ng and 25 ng) in duplicate for each sample, and internal 16s rRNA (*rrsH*) levels were used for normalization. The primers (Integrated DNA Technologies) and probes (Applied Biosystems) listed in **Table 2** in **Appendix B** were used for amplification and quantitation respectively.

Motility assays

Motility assays were performed as previously described (Nobelmann and Lengeler, 1996). Briefly, strains were stabbed in soft LB agar (0.25%) containing tetrazolium chloride, and incubated at 37°C for 7 h in the presence of atmospheric oxygen. Motility was recorded as the diameter (in mm) containing bacteria migrating away from the inoculation point. For the assays set up under anoxic conditions (0% O_2, 2-3% H_2), bacteria were inoculated and incubated in an anaerobic chamber for the duration of the assay.

Biofilm Assays

Analysis of biofilm levels was performed as previously described (Hadjifrangiskou *et al.*, 2012). Overnight cultures were used to seed fresh LB media to OD_{600} of 0.06, and transferred to sterile polyvinylchloride (PVC) 96-well plate (VENDOR). Plates were loosely covered and incubated at room temperature in either the presence or absence of oxygen for 48 hours. After 48 hours, media was removed and plates were washed with water to remove non-adherent bacteria. Plates were then stained with 125 µL of 0.5% crystal violet for 15 minutes, and then washed to remove residual stain. Plates were allowed to dry for 15-60 minutes. Adherent bacteria harboring the crystal violet stain were removed from the wells using 200µL of 35% AcOH. 100µL of each suspension was then transferred to a clean flat-bottom 96-well plate and the absorbance at 570nm

was obtained. Background absorbance was subtracted using wells that harbored only media. Absorbance averages for each strain and condition were obtained, and analyzed using GraphPad Prism 6 (GraphPad Software Inc.) with statistical analysis performed using Student's *t*-Test.

Transmission Electron Microscopy (TEM)

TEM analyses were performed as outlined previously (Kostakioti *et al.*, 2009). Briefly, 100 µL of normalized bacterial cultures (OD_{600} = 1.0) from each condition were centrifuged at 4,000 rpm for 10 minutes and resuspended in 100 µL of 1% glutaraldehyde in 1xPBS. Samples were then submitted to the Imaging Facility of the Department of Molecular Microbiology at the Washington University School of Medicine in St. Louis for analysis. Two biological replicates of each strain and condition were submitted for analysis.

Results

The anaerobic sensing two-component system ArcAB does not mediate anoxic fimS inversion

The ArcAB two-component sensing system is a major *E. coli* regulator mediating the switch from aerobic to anaerobic growth. ArcAB responds to the presence of reduced quinones in the inner membrane under reduced oxygen, to regulate an extensive set of genes (100+) that allows for bacterial growth under anoxic conditions (Georgellis *et al.*, 2001, Malpica *et al.*, 2006). Given this role, we sought to determine if ArcAB was responsible for anoxic repression of type 1 pili expression, by taking advantage of an existing *arcA* deletion mutant in UTI89. Comparison of the *fimS* promoter orientation and total FimA protein levels between WT UTI89 and UTI89Δ*arcA* (**Figure 24**) revealed no significant differences in *fimS* phase and total FimA

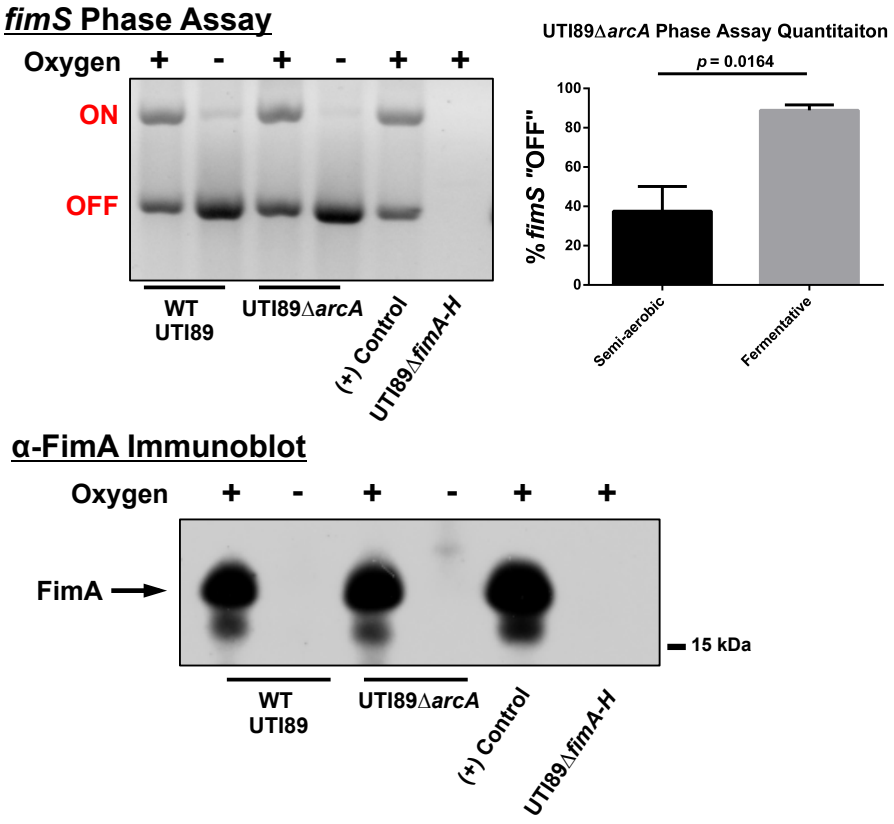

Figure 24. Oxygen-dependent regulation of *fim* expression is independent of the ArcAB two-component system. Phase assay and FimA immunoblot with UTI89Δ*arcA* indicates this oxygen-dependent regulation of *fim* expression is not governed by the ArcAB two-component system. Data shown was obtained from cultures starting from populations primarily *fim*OFF (shaking) and grown in 1.2x YESCA media at room temperature. Phase assay quantitation, n = 3. Statistical analysis performed by two-tailed unpaired Student's *t*-Test in GraphPad Prism 6, with determined *p*-values shown. Immunoblot representative of n = 5 analyses.

protein levels between the two strains regardless of oxygen concentration. These data suggest that the ArcAB system does not function upstream of the *fim* operon under anoxic conditions.

Deletion of fnr reduces fimS inversion and restores FimA protein levels

We next evaluated the role of FNR in mediating *fim* or Fim recombinase transcription in response to oxygen. FNR responds to oxygen-deplete environments and derives its name (fumarate and nitrate reductase regulator) from its role in regulating the redox state of alternative terminal electron acceptors. In the presence of oxygen, *E. coli* utilize aerobic respiration for energy generation. However, as a facultative anaerobe, in the absence of oxygen *E. coli* can utilize alternative terminal electron acceptors, such as nitrate, DMSO, TMAO, or fumarate for energy generation by anaerobic respiration (Unden and Bongaerts, 1997). In the absence of both oxygen and any alternative terminal electron acceptors *E. coli* must utilize mixed acid fermentation, and thereby produce significantly less energy than by either aerobic or anaerobic respiration (Unden and Bongaerts, 1997). Given that nitrate is the preferred alternative electron acceptor for *E. coli*, we assayed how anoxic growth in the presence of nitrate (in the form of 40 mM sodium nitrate, $NaNO_3$) would impact expression of type 1 pili. We observed that static cultures started *fim*OFF remained largely *fim*OFF during anaerobic growth in the presence of $NaNO_3$ similar to what was observed with cultures grown fermentatively (**Figure 25A**). Conversely, the addition of nitrate was able to partially maintain the *fimS* promoter in a *fim*ON orientation, and some FimA protein levels, in cultures started from *fim*ON populations (**Figure 25B**). When populations grown fermentatively or anaerobically with nitrate (from both *fim*ON and *fim*OFF starting populations) were sub-cultured into semi-aerobic conditions for 18 hours,

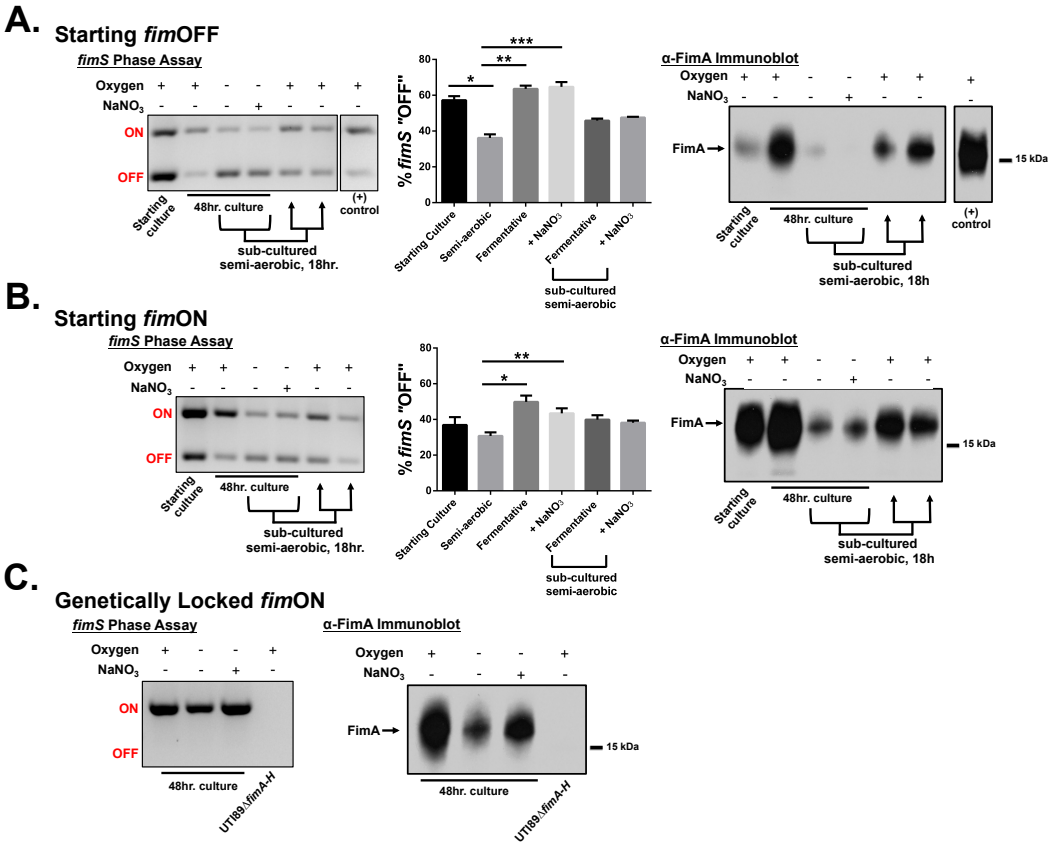

Figure 25. An alternative terminal electron acceptor only prevents anoxic *fimS* inversion in populations starting *fim*ON. (A) Analysis with cultures starting primarily *fim*OFF cultured for 48 hours under semi-aerobic (atmospheric, 21%), fermentative (anoxic, 0%), or anaerobic conditions in the presence of nitrate (anoxic, 0%, + $NaNO_3$). The gel depicts a representative phase assay gel. The percentage *fim*OFF for each sample from multiple biological replicates is graphed as mean with SEM using GraphPad Prism 6 for each sample (starting culture/fermentative sub-culture/+NaNO3 subculture, n = 2; semi-aerobic/fermentative, n = 9; +$NaNO_3$, n = 8). Statistical difference from semi-aerobic culture shown and determined by one-way ANOVA with Bonferroni's multiple comparisons test using GraphPad (*p = 0.0019, ** and ***p = <0.0001). Statistically significant differences were also noted (but not indicated on the graph) between fermentative/fermentative sub-cultured [p = 0.0123], fermentative/+NaNO3 sub-cultured [p = 0.0316], +$NaNO_3$/fermentative sub-cultured [p = 0.0072], and +$NaNO_3$/+$NaNO_3$ sub-cultured [p = 0.0185]. Corresponding anti-FimA immunoblots from the same samples used for each phase assay are shown. **(B)** Analyses as shown in A, for cultures starting predominantly *fim*ON. Phase assay quantitation taken from biological replicates of starting culture/fermentative sub-culture/+$NaNO_3$ subculture, n = 2; semi-aerobic/fermentative/+$NaNO_3$, n = 6. Statistical analysis performed as in B (*p = 0.0004, **p = 0.0344). Immunoblot is representative of five biological replicates. **(C)** Representative phase assay gel (n = 8) and anti-FimA immunoblot (n = 8) of cultures using UTI89_LON strain. Coomassie stained gels were used to verify equal loading and Ponceau S used to stain membranes to show equal transfer.

fimS predominantly returned to the *fim*ON orientation leading to increased FimA protein levels (**Figure 25A-B**). These results suggested that the phase-switch from *fim*OFF to *fim*ON is affected by the bacterial respiration state, favoring aerobic respiration.

To determine if FNR impacts the anoxic *fimS* switch, a deletion mutant lacking the *fnr* gene was generated in UTI89 (UTI89Δ*fnr*). WT UTI89 and UTI89Δ*fnr* were grown overnight under type 1 pili inducing conditions, and then inoculated into fresh LB media and grown statically for 48 hours at 37°C in either the presence or the absence of oxygen. After 48 hours cultured under anoxic conditions, UTI89Δ*fnr* demonstrated a lower percentage of the population with *fimS* in the *fim*OFF orientation (~40%) compared to WT UTI89 (~60%) (**Figure 26**). This decrease in the anoxic *fim*OFF population in UTI89Δ*fnr* corresponded with an increase in total FimA protein levels (**Figure 26**). Interestingly, when cultured under atmospheric conditions, UTI89Δ*fnr* still showed a lower percentage of the population in the *fim*OFF orientation (~25%) compared to WT UTI89 (~40%) with a slight increase in total FimA protein levels (**Figure 26**).

Static culture of UTI89 in LB media at 37°C for 24 hours, followed by 1:100 dilution of bacteria into fresh LB media and a second static incubation at 37°C for 24 hours significantly enhances the *fim*ON population in the culture (Greene *et al.*, 2015). Conversely, shaking culture of UTI89 in LB media at 25°C for 24 hours followed by 1:100 dilution into fresh LB media and a second culture for 24 hours significantly enhances the *fim*OFF population (Greene *et al.*, 2015). Using these growth conditions to force WT UTI89 and UTI89Δ*fnr* into either the *fim*ON or *fim*OFF states prior analysis in atmospheric or anoxic conditions, revealed that forcing the population *fim*ON showed a slight shift to a *fim*OFF population when cultured under atmospheric conditions, and a larger shift to a *fim*OFF population under anoxic conditions (**Figure 27A**). UTI89Δ*fnr* forced *fim*ON remained *fim*ON when cultured under both atmospheric and anoxic

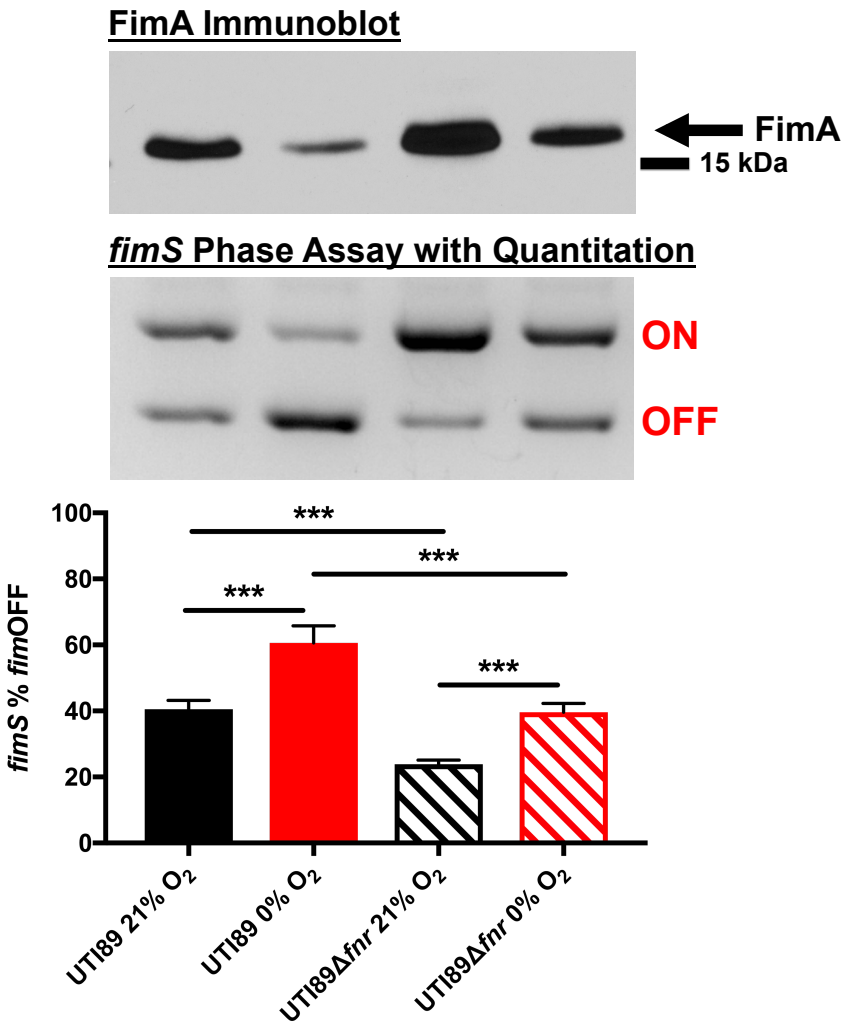

Figure 26. Deletion of *fnr* impacts atmospheric and anoxic *fimS* inversion and FimA protein expression. Phase assay analysis of *fimS* orientation demonstrates a partial restoration in anoxic *fim*ON populations in the UTI89Δ*fnr* strain, resulting in a restoration of anoxic FimA protein levels. The UTI89Δ*fnr* strain also indicates increased fimON populations under atmospheric oxygen conditions, resulting in increased FimA protein levels. All strains in this analysis carried the empty pBAD33 vector, and were grown in the presence of 20µg/ml chloramphenicol and 0.01% - 0.05% arabinose for induction. Immunoblot is representative of at least n = 3. The percent *fimS fim*OFF was determined as previously described, and plotted using GraphPad Prism 7 as the mean with the standard error of the mean (UTI89 n=5, UTI89Δ*nr* n=6). Statistical analysis performed by one-way ANOVA with Tukey correction for multiple comparisons (***$p<0.005$).

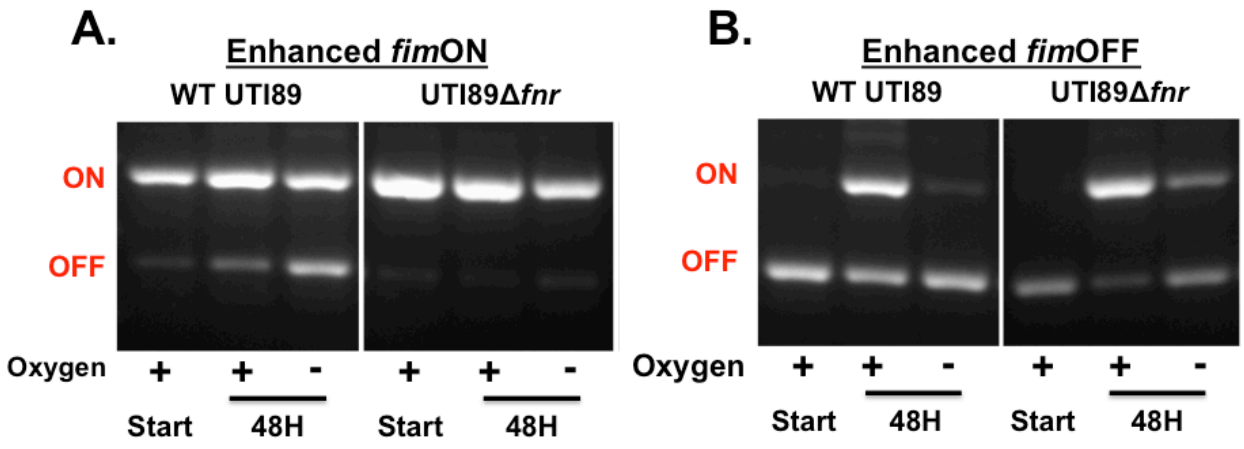

Figure 27. UTI89Δ*fnr* demonstrates increased ability to maintain or switch *fim*ON under anoxic conditions. Representative *fimS* phase assay analysis of WT UTI89 and UTI89Δ*fnr* where starting cultures were enhanced into either the *fim*ON or *fim*OFF orientations prior to static culture for 48 hours in either the presence or absence of oxygen.

conditions (**Figure 27A**). WT UTI89 populations forced *fim*OFF showed robust inversion to the *fim*ON state under atmospheric culture conditions, with significantly less inversion under anoxic conditions (**Figure 27B**). UTI89Δ*fnr* forced *fim*OFF also demonstrated robust inversion to the *fim*ON state under atmospheric culture conditions, but also demonstrated an increased ability for inversion to the *fim*ON state under anoxic conditions compared to WT UTI89 (**Figure 27B**). These data combined suggest that FNR transcriptionally regulates the *fim* operon, either directly or by regulating transcription of the Fim recombinases, under both atmospheric and anoxic oxygen conditions.

Deletion of fnr alters the expression of the fim operon and the FimB/E recombinases

To test the effects of *fnr* deletion on *fim* operon and *fimB/fimE* transcription, qPCR was employed to monitor steady-state transcript levels with time. Analysis of *fim* operon (*fimI*) steady-state mRNA transcript levels with time, demonstrated consistently higher *fimI* transcript levels under anoxic conditions in the UTI89Δ*fnr* mutant compared to WT UTI89 (**Figure 28D**). Transcript levels of the *fim* operon in the UTI89Δ*fnr* mutant also showed varied increases over WT UTI89 under atmospheric conditions (**Figure 28B**). Combined, these data suggest that FNR influences *fim* operon transcription under both oxygen environments, with slight preference for exerting influence under anoxic conditions. However, these data do not clarify whether FNR directly influences transcription of the *fim* operon or expression of the Fim recombinases.

Given that deletion of *fnr* impacts the *fimS* switch, we next quantified *fimB* and *fimE* transcript levels in the UTI89Δ*fnr* strain. Our data indicated that under anoxic conditions, UTI89Δ*fnr* had increased *fimB* transcript levels at most time points (between 2- and 6-fold) compared to WT UTI89 (**Figure 29D**). Analysis of *fimE* transcript levels

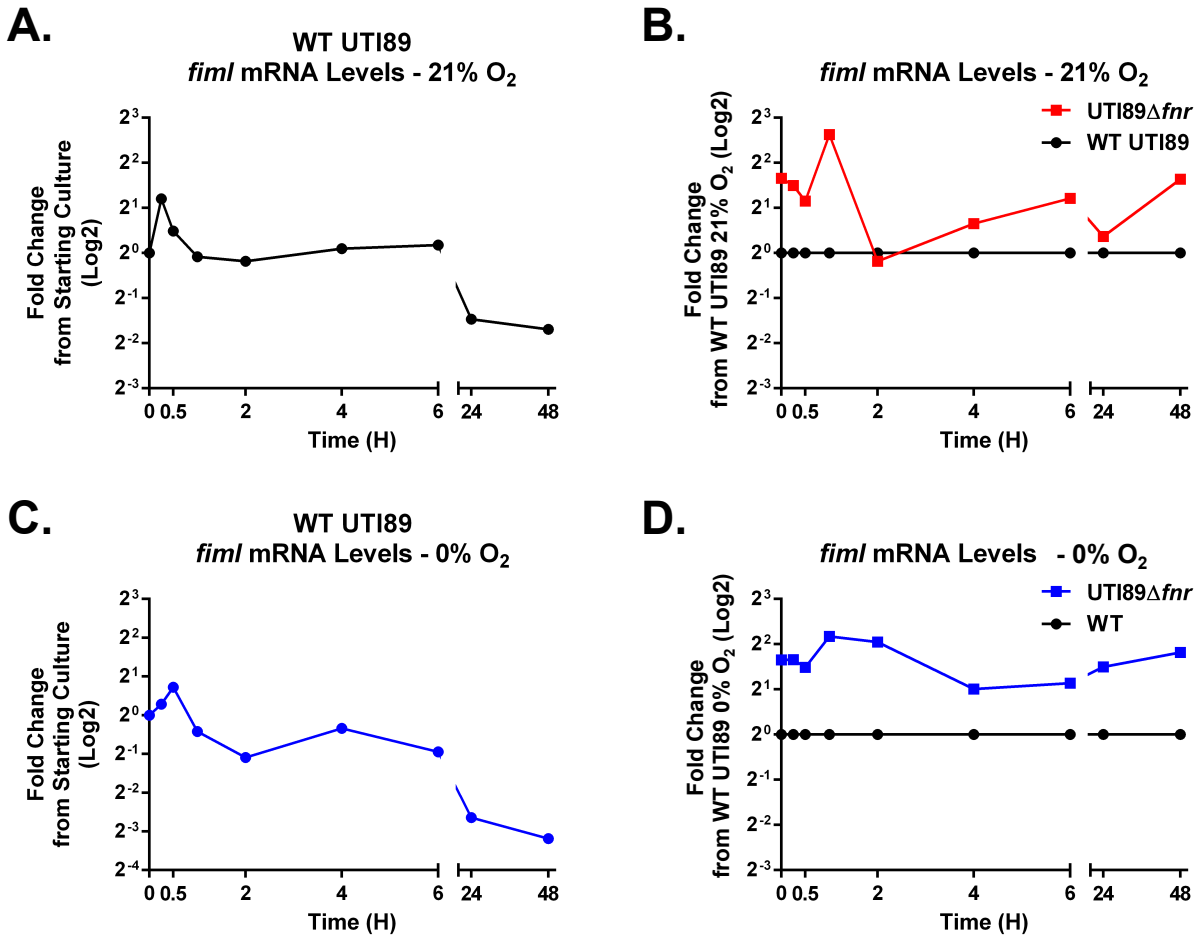

Figure 28. Deletion of *fnr* increases anoxic *fim* operon transcript levels. Graphs depict qPCR analysis of recombinase steady-state mRNA transcript levels at 0.25, 0.5, 1, 2, 4, 6, 24, and 48 hours from cultures grown statically at 37°C in either the presence or absence of oxygen. Cultures were seeded at an OD_{600} of 1.0 from overnight cultures grown statically in LB media at 37°C. qPCR analysis was performed using primers and probes specific to the target gene of interest with two concentrations of cDNA (50 ng and 25 ng) in duplicate for each sample, and internal 16s rRNA (*rrsH*) levels were used for normalization. **(A)** Represents *fimI* expression levels in WT UTI89 at each time point from culture in the presence of oxygen, presented as the fold-change from the starting culture (as presented in **Figure 20**). **(B)** Represents *fimI* expression levels in UTI89Δ*fnr* at each time point from culture in the presence of oxygen, presented as the fold-change from the corresponding WT UTI89 culture and time point. **(C)** Represents *fimI* expression levels in WT UTI89 at each time point from culture in the absence of oxygen, presented as the fold-change from the starting culture. **(D)** Represents *fimI* expression levels in UTI89Δ*fnr* at each time point from culture in the absence of oxygen, presented as the fold-change from the corresponding WT UTI89 culture and time point. Data are representative of one biological replicate.

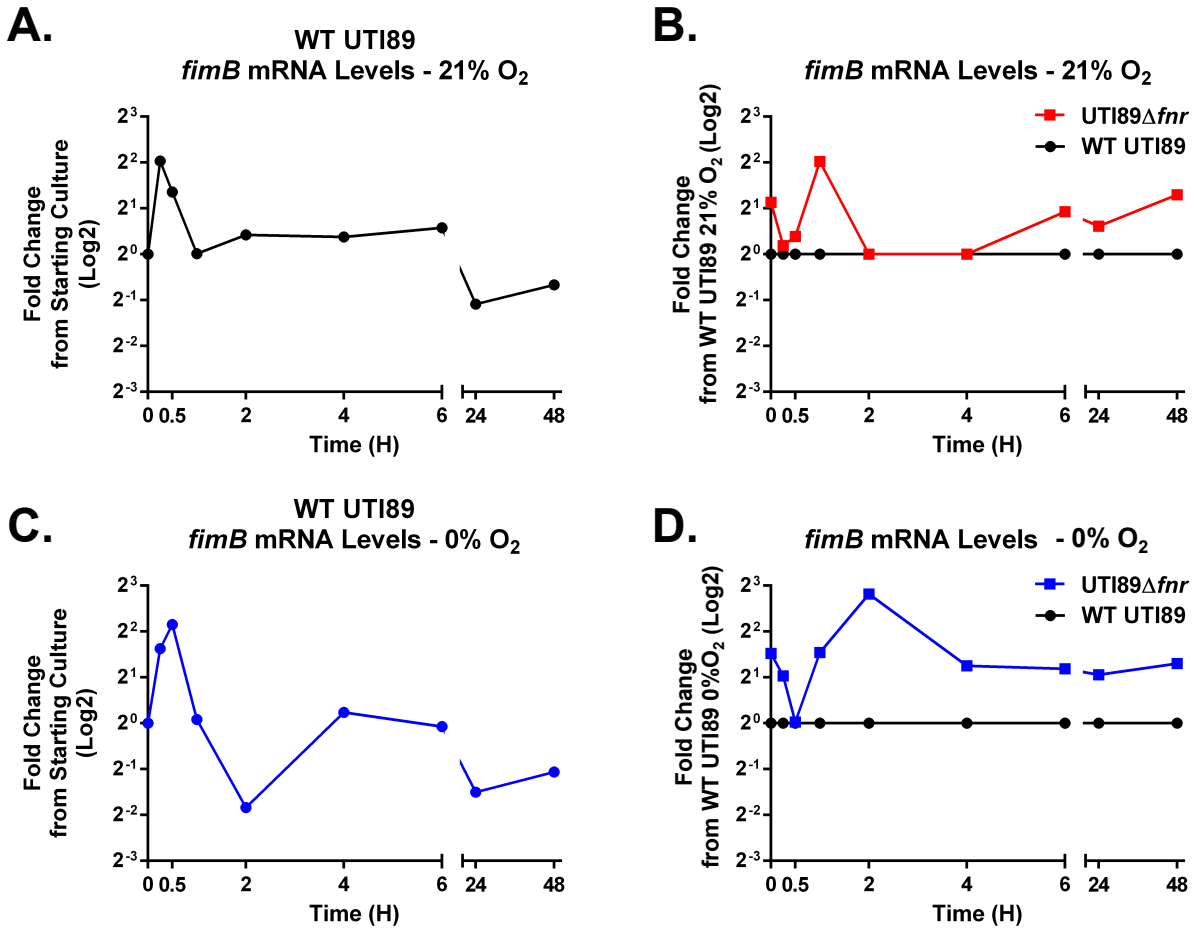

Figure 29. Deletion of *fnr* increases anoxic *fimB* transcript levels. Graphs depict qPCR analysis of recombinase steady-state mRNA transcript levels at 0.25, 0.5, 1, 2, 4, 6, 24, and 48 hours from cultures grown statically at 37°C in either the presence or absence of oxygen. Cultures were seeded at an OD_{600} of 1.0 from overnight cultures grown statically in LB media at 37°C. qPCR analysis was performed using primers and probes specific to the target gene of interest with two concentrations of cDNA (50 ng and 25 ng) in duplicate for each sample, and internal 16s rRNA (*rrsH*) levels were used for normalization. **(A)** Represents *fimB* expression levels in WT UTI89 at each time point from culture in the presence of oxygen, presented as the fold-change from the starting culture (as presented in **Figure 21A**). **(B)** Represents *fimB* expression levels in UTI89Δ*fnr* at each time point from culture in the presence of oxygen, presented as the fold-change from the corresponding WT UTI89 culture and time point. **(C)** Represents *fimB* expression levels in WT UTI89 at each time point from culture in the absence of oxygen, presented as the fold-change from the starting culture. **(D)** Represents *fimB* expression levels in UTI89Δ*fnr* at each time point from culture in the absence of oxygen, presented as the fold-change from the corresponding WT UTI89 culture and time point. Data are representative of one biological replicate.

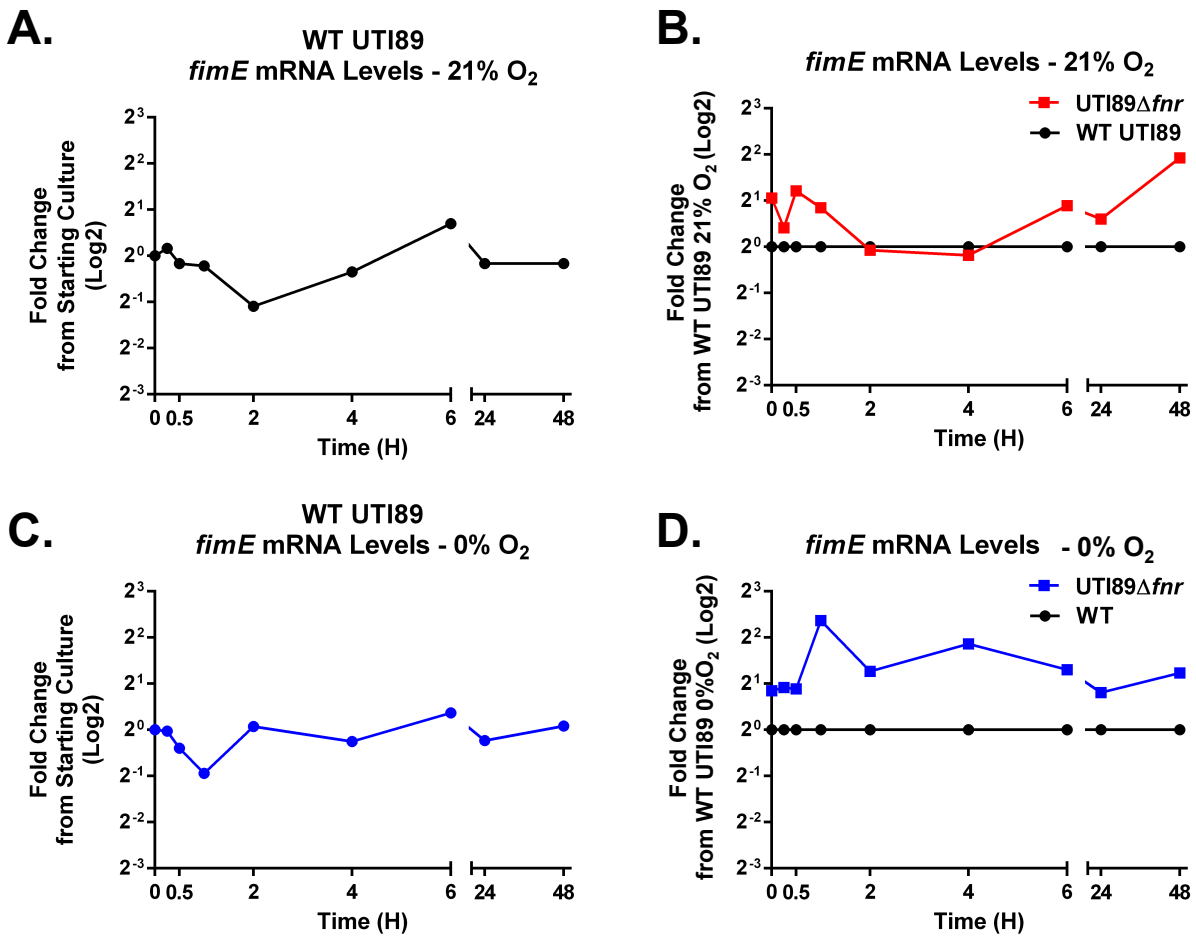

Figure 30. Deletion of *fnr* increases anoxic *fimE* transcript levels. Graphs depict qPCR analysis of recombinase steady-state mRNA transcript levels at 0.25, 0.5, 1, 2, 4, 6, 24, and 48 hours from cultures grown statically at 37°C in either the presence or absence of oxygen. Cultures were seeded at an OD_{600} of 1.0 from overnight cultures grown statically in LB media at 37°C. qPCR analysis was performed using primers and probes specific to the target gene of interest with two concentrations of cDNA (50 ng and 25 ng) in duplicate for each sample, and internal 16s rRNA (*rrsH*) levels were used for normalization. **(A)** Represents *fimE* expression levels in WT UTI89 at each time point from culture in the presence of oxygen, presented as the fold-change from the starting culture (as presented in **Figure 21B**). **(B)** Represents *fimE* expression levels in UTI89Δ*fnr* at each time point from culture in the presence of oxygen, presented as the fold-change from the corresponding WT UTI89 culture and time point. **(C)** Represents *fimE* expression levels in WT UTI89 at each time point from culture in the absence of oxygen, presented as the fold-change from the starting culture. **(D)** Represents *fimE* expression levels in UTI89Δ*fnr* at each time point from culture in the absence of oxygen, presented as the fold-change from the corresponding WT UTI89 culture and time point. Data are representative of one biological replicate.

in the UTI89Δ*fnr* strain under anoxic conditions, also showed increased transcript levels at each time point (between 2- and 4-fold) compared to WT UTI89 (**Figure 30D**). The UTI89Δ*fnr* demonstrated varied effects in *fimB* and *fimE* expression under atmospheric conditions, with increased expression only at distinct time points compared to WT UTI89. These data suggest that FNR impacts the expression of *fimB* and *fimE* under both oxygen conditions, with more pronounced effects exerted under anoxic conditions. However, these data do not explain how FNR could be mediating the *fimB/fimE* imbalance observed in WT UTI89 under anoxic conditions.

FNR interacts with or influences anoxic FimE interactions with the fimS promoter

Given that deletion of *fnr* induced higher *fim* operon transcript levels and both conserved Fim recombinases, we next investigated how FNR could control the *fim* operon on the transcript level. In previous studies, a UPEC strain (UTI89_LON) in which the *fimS* promoter element is genetically locked into the transcription-competent *fim*ON orientation was generated through alteration of left invertible repeat sequence (Kostakioti *et al.*, 2012). We postulated that if oxygen/respiration state only impacts the phase-state of the *fim* promoter, then UTI89_LON would show FimA protein levels equivalent to atmospheric conditions when cultured in the absence of oxygen. UTI89_LON cultured under anoxic conditions exhibited a marked reduction in FimA protein levels, similar to wild-type (WT) UTI89, despite the "locked *fim*ON" position of the promoter (**Figure 25C**). The phase state of the *fimS* promoter in UTI89_LON was verified by phase assays (**Figure 25C**) to exclude the possibility of mutations affecting the phase state under the conditions tested. Interestingly, anaerobic growth in the presence of nitrate maintained *fim* gene expression in UTI89_LON (**Figure 25C**), similar to the *fim*ON populations (**Figure 25B**).

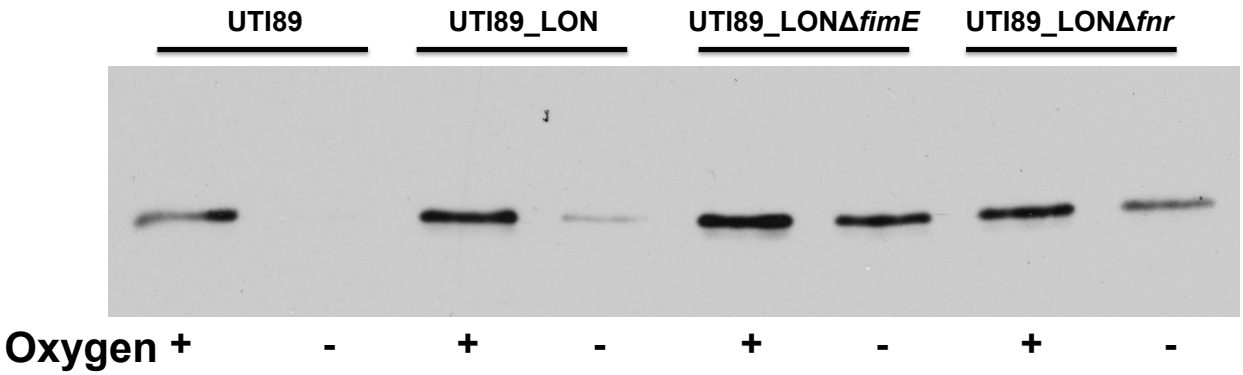

Figure 31. FNR appears to interact directly with or influence FimE interactions with the *fimS* promoter under anoxic conditions. FimA immunoblot comparing WT UTI89, UTI89_LON, UTI89_LONΔ*fimE,* and UTI89_LONΔ*fnr* after 48 hour culture in either the presence or absence of oxygen.

These data indicated the presence of either a transcriptional or post-transcriptional mechanism regulating *fim* expression downstream of *fimS* promoter inversion.

To investigate further how FNR influences *fim* expression, we generated and tested an *fnr* deletion mutant in the UTI89_LON background (UTI89_LONΔ*fnr*). When grown under anoxic conditions UTI89_LON demonstrated a reduction in total FimA protein levels similar to UTI89, matching previous observations (**Figure 31**). Deletion of *fnr* from the UTI89_LON strain, led to a partial restoration of anoxic FimA protein levels compared to the WT UTI89_LON (**Figure 31**). These data suggest a possible role of FNR in mediating *fim* expression directly, through interactions with the *fimS* promoter under anoxic conditions. However, there is also a possibility that FNR could be mediating interactions of FimE and/or FimB with the *fimS* promoter.

To test this possibility, a *fimE* deletion from the UTI89_LON background (UTI89_LONΔ*fimE*) was next generated and tested. Analysis of the UTI89_LONΔ*fimE* mutant demonstrated a full restoration in FimA protein levels under anoxic conditions (**Figure 31**). These data suggest that the decrease in FimA protein levels under anoxic conditions in the UTI89_LON strain (**Figures 25 and 31**) is the result of FimE (or FimE-associated) interactions with the *fimS*-LON promoter under anoxic conditions, leading to lowered transcription of the *fim* operon. These data in turn validate the role of FimE in the anoxic regulation of *fim* expression, as opposed to representing an independent secondary regulatory mechanism in the UTI89_LON strain. The partial restoration in total FimA protein levels observed upon deletion of *fnr*, suggests that FNR may be in fact mediating FimE-*fimS* interactions, or directly interacting with the *fimS* promoter in the UTI89_LON strain under anoxic conditions. However, these data do not provide evidence that FNR promotes this interaction in a WT UTI89 strain. Studies are currently ongoing

to determine if FNR directly engages the *fimS* promoter, or mediates interactions of FimE (and/or FimB) with *fimS* in both WT UTI89 and UTI89_LON strains.

A post-translational mechanism controls piliation and biofilm formation in the absence of oxygen

Deletion of *fimE* or *fnr* from UTI89 restored FimA protein levels under anoxic conditions compared to WT UTI89 (**Figures 23, 26, and 32A**). Subsequent TEM analyses to enumerate pili levels of the cell surface revealed that like WT UTI89 (**Figures 16 and 23**), UTI89Δ*fimE* (**Figure 23**) and UTI89Δ*fnr* (**Figure 32C**) bacteria had fewer pili on the cell surface in the absence of oxygen. These data suggest that despite increased FimA protein levels under anoxic conditions, UTI89Δ*fimE* and UTI89Δ*fnr* are deficient in elaboration of functional pili on the cell surface. Also, in the absence of *fnr* cells demonstrated shed pili and flagella in the extracellular milieu at both atmospheric and anoxic oxygen concentrations (**Figure 32E**), suggesting a possible role for FNR in mediating proper flagellar and pilus anchoring to the membrane. In motility analysis to further investigate the TEM observations, UTI89Δ*fnr* demonstrated significantly reduced flagellar-based motility under atmospheric conditions and completely ablated motility under anoxic conditions compared to WT UTI89 (**Figure 32D**). Deletion of *fimE* from UTI89 had no significant impacts on bacterial motility under either oxygen condition (**Figure 33D**). Future studies will aim to understand the basis of this *fnr*-deletion effect.

We next investigated the biofilm forming abilities of both the *fnr* and *fimE* deletion mutants. We hypothesized that if the UTI89Δ*fimE* and UTI89Δ*fnr* strains produced functional type 1 pili on the cell surface, they would demonstrate anoxic *fim*-dependent biofilm levels similar to WT UTI89 under atmospheric conditions. Analysis of *fim*-dependent biofilm formation by

UTI89Δ*fimE* and UTI89Δ*fnr* at atmospheric oxygen concentrations demonstrated biofilm levels equivalent to WT UTI89, suggesting no defects in functional type 1 pilus production under these conditions (**Figure 32B**). When cultured under anoxic conditions biofilm levels in both UTI89Δ*fimE* and UTI89Δ*fnr* were as low as those obtained for WT UTI89 (**Figure 32B**). These data corroborated the observed decrease in surface pili levels in the mutant strains by TEM, and indicated that in addition to the regulation of the *fimS* promoter switch, there exits a post-translational mechanism that controls pilus elaboration and thereby possibly biofilm formation in response to decreased oxygen levels.

Discussion

Anoxic growth conditions lead to reduced pili production and biofilm formation in UPEC strain UTI89 (**Figures 16, 23, and 32**). Based on work presented in this chapter, and previous chapters, these reductions appear to be mediated by three levels of regulation; 1) at the level of the *fimS* promoter switch, 2) at the level of *fim* operon and Fim recombinase gene expression, and 3) at the post-translational level. We have ruled out regulation by the anaerobic-sensing ArcAB two-component system, and have identified the oxygen-sensing protein FNR as a regulator of *fim* expression. A UTI89 strain lacking *fnr* (UTI89Δ*fnr*) demonstrated a decrease in the *fim*OFF switch, and increased expression of the Fim recombinases and the *fim* operon under both atmospheric and anoxic conditions. Despite demonstrating regulation under both oxygen conditions, UTI89Δ*fnr* showed higher expression of the Fim recombinases and *fim* operon under anoxic conditions. Together these data suggest that FNR is not likely the primary regulator

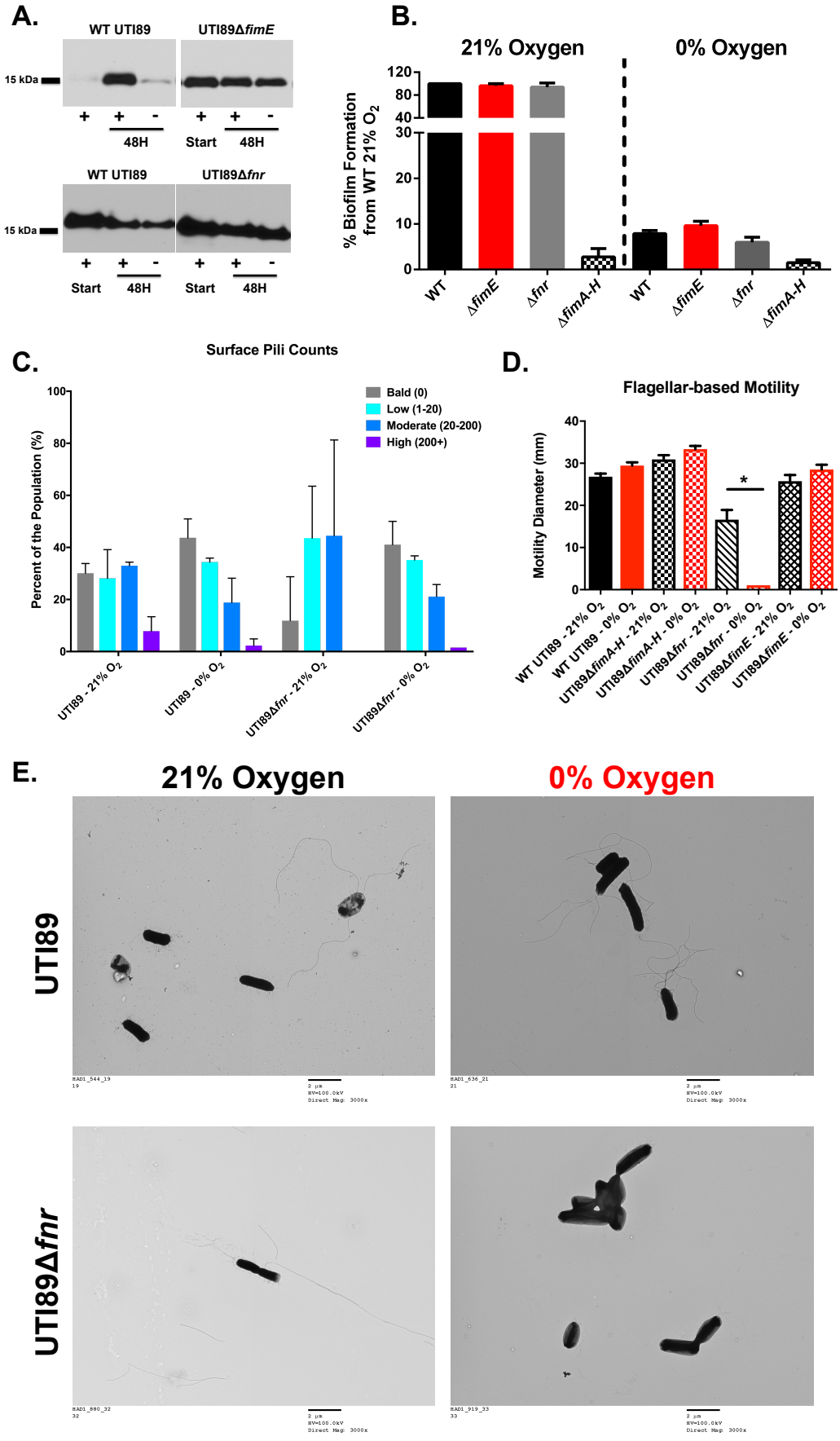
A.
WT UTI89
UTI89ΔfimE
15 kDa
+ + -
48H
Start 48H
WT UTI89
UTI89Δfnr
15 kDa
+ + -
Start 48H
B.
21% Oxygen
0% Oxygen
% Biofilm Formation from WT 21% O2
120
80
40
30
20
10
0
WT
ΔfimE
Δfnr
ΔfimA-H
C.
Surface Pili Counts
Bald (0)
Low (1-20)
Moderate (20-200)
High (200+)
Percent of the Population (%)
100
80
60
40
20
0
UTI89 - 21% O2
UTI89 - 0% O2
UTI89Δfnr - 21% O2
UTI89Δfnr - 0% O2
D.
Flagellar-based Motility
Motility Diameter (mm)
40
30
20
10
0
*
WT UTI89 - 21% O2
WT UTI89 - 0% O2
UTI89ΔfimA-H - 21% O2
UTI89ΔfimA-H - 0% O2
UTI89Δfnr - 21% O2
UTI89Δfnr - 0% O2
UTI89ΔfimE - 21% O2
UTI89ΔfimE - 0% O2
E.
21% Oxygen
0% Oxygen
UTI89
UTI89Δfnr

Figure 32. Deletion of *fimE* or *fnr* fails to restore *fim*-dependent anoxic biofilm formation and surface pili levels, and UTI89Δ*fnr* demonstrates altered flagella production and motility. (A) Representative immunoblots analyzing total FimA protein levels in WT UTI89, UTI89Δ*fimE*, and UTI89Δ*fnr* demonstrate the restoration of anoxic FimA protein levels upon deletion of *fimE* or *fnr*. **(B)** Biofilms were grown at room temperature for 48 hours in PVC 96-well plates, and were started from overnight cultures grown statically at 37°C for initial populations with high levels of type 1 pili expression. Biofilm levels are presented as a percentage of WT UTI89 biofilm formation at atmospheric oxygen levels. Statistical analysis performed by one-way ANOVA with Tukey correction for multiple comparisons ($p < 0.0001$) using GraphPad Prism 7. **(C)** Pili were enumerated from 48 hour static cultures grown in LB media with 20μg/mL chloramphenicol and 0.01% arabinose, in either the presence or absence of oxygen at 37°C, from starting cultures with high levels of type 1 pili expression. All strains carried the pBAD33 plasmid. WT pili numbers are the same as in the graph in **Figure 23.** All pili were enumerated from TEM micrographs by a blinded reviewer. Statistical analysis performed by one-way ANOVA with Tukey correction for multiple comparisons ($p < 0.05$) using GraphPad Prism 7. **(D)** Flagellar-based motility was measured using a soft-agar bacterial swimming assay. Overnight cultures for inoculation to soft agar were grown for ~20 hours in LB media statically at 37°C. Soft agar plates used for analyses at 0% oxygen were incubated in the anaerobic chamber overnight prior to inoculation, to allow for gas equilibration. Anoxic plates were then stabbed in the anaerobic chamber, and incubated at 37°C for ~7-8 hours before swimming motility was measured. Plates cultured under atmospheric oxygen conditions were inoculated under ambient conditions, and then incubated at 37°C for ~7-8 hours. Motility was measured as the diameter of swimming from the site of inoculation. Data presented as the mean with the standard error of the mean (n = 2), and statistical analysis was performed using a Student's *t*-Test with GraphPad Prism 6. **(E)** Representative TEM micrographs from WT UTI89 and UTI89Δ*fnr* grown in the presence and absence of oxygen in LB media with 20μg/mL chloramphenicol and 0.05% (WT) or 0.01% (Δ*fnr*) arabinose, two biological replicates of each strain at each condition were analyzed. Each strain carried empty pBAD33 plasmid. Scale bar = 2μm.

lending to the anoxic repression of *fim* expression, but that FNR might contribute on some level to the regulation.

In 2014, Barbieri *et al.* demonstrated that deletion of *fnr* in UPEC strain CFT073 attenuated adherence to bladder epithelial cells *in vitro*, as well as *in vivo* virulence in a murine model of cystitis (Barbieri *et al.*, 2014). Specifically, they demonstrated that FNR regulates genes associated with CFT073 virulence, including; type 1 and P CUP pili systems, flagellar-based motility, α-ketoglutarate metabolism, and α-hemolysin (Barbieri *et al.*, 2014). When examining impacts on type 1 pili, they observed that deletion of *fnr* resulted in reduction in *fimA* transcription using a β-galactosidase assay with a *fimA-lacZ* fusion. They further demonstrated direct interactions of FNR with the *fimS* promoter via electrophoretic mobility shift assay (EMSA). The reduction in *fimA* expression upon deletion of *fnr* in CFT073, resulted from repression of *fimB* expression and maintenance of the *fimS* promoter in the *fim*OFF orientation (Barbieri *et al.*, 2014). It is important to note that *fimB* and *fimA* expression levels, as well as the *fimS* phase, were determined from samples grown under atmospheric oxygen concentrations.

Similar to the Barbieri *et al.* studies in CFT073, our studies also demonstrated *fnr*-based regulation of *fim* expression and bacterial motility in UTI89. Our studies demonstrated *fnr*-mediated regulation of *fim* expression under both atmospheric and anoxic oxygen conditions, with the UTI89Δ*fnr* mutant showing a reduction in the *fim*OFF switch under both oxygen conditions. Analysis of Fim recombinase and operon transcript levels by qPCR demonstrated that FNR appears to have increased repressive functions under anoxic conditions, yet still shows significant repression under atmospheric conditions. The UTI89Δ*fnr* mutant also demonstrated reduced motility under atmospheric conditions, while motility was completely ablated under anoxic conditions. We further showed this reduction in motility resulted from significantly

higher shedding of pili and flagella under both atmospheric oxygen conditions in UTI89Δ*fnr*, suggesting a function for FNR in mediating proper elaboration of several different macromolecular structures. Combined, this *fnr*-mediated regulation of *fim* and motility under atmospheric oxygen conditions is intriguing given that FNR should be inactive in the presence of oxygen (Unden *et al.*, 2002). Combined, our data and that of Barbieri *et al.*, point towards a possible function for FNR in the non-functional apo state. Studies are currently under way to address this observation.

Other studies in non-UPEC strains, have indicated that mutants with *fnr* deletion have increased levels of the DNA-bending protein Lrp under anaerobic growth conditions, suggestive of FNR down-regulating lrp expression in the absence of oxygen (Salmon *et al.*, 2003). Previous studies have suggested that Lrp facilitates bending the *fimS* promoter into a position that will bring the invertible repeat elements together to allow for Fim recombinase switching (Schwan, 2011). Possible repression of *lrp* expression by FNR, may explain how FNR could impact *fim* expression in the absence of oxygen without direct impacts of Fim recombinase expression or interactions with the *fimS* promoter.

The *fimS* promoter is perhaps the most complexly regulated and controlled promoter found in *E. coli*. To date at least 10 different proteins have been demonstrated to regulate the orientation of the *fimS* promoter (Schwan, 2011). Along with the traditional invertible repeats responsible for alterations in the *fimS* phase orientation, Zhang *et al.* recently reported the identification of an additional invertible repeats in the *fimS* region of UTI89 that also contributes to phase variation and *fim* expression (Zhang *et al.*, 2016). Despite its role in the regulation of type 1 pili, FNR appears to only partially regulate anoxic *fim* expression in UTI89, as bacteria still retain some ability to invert or maintain *fimS* in a *fim*OFF orientation. These data

demonstrate that there are likely other regulators that mediate the repression of type 1 pili under anoxic conditions, which have yet to be characterized.

Along with the sensory systems that respond to decreases in environmental oxygen concentration, *E. coli* also harbor systems that elicit responses to oxidative stresses, including OxyR and SoxRS. Production of reactive oxygen (ROS) and reactive nitrogen (RNS) species formation within bacterial cells can be induced by environmental stresses, as well as be a byproduct of bacterial respiration. In high concentrations ROS and RNS can lead to bacterial cell death, yet in low concentrations and under certain circumstances can promote bacterial growth (Paiva and Bozza, 2014). OxyR is a LysR-family transcriptional regulator that responds to, and protects bacteria from oxidative stresses (Hahn *et al.*, 2002b). In aerobic environments, OxyR typically senses intracellular hydrogen peroxide (H_2O_2) levels (Antelmann and Helmann, 2011). Normal intracellular H_2O_2 levels approach concentrations close to 20 nM, and typically it takes concentrations upwards of 2mM to completely inhibit bacterial growth (Seaver and Imlay, 2001, González-Flecha and Demple, 1997). OxyR becomes active when intracellular H_2O_2 reaches ~ 100 nM, to regulate the expression of genes that confer protection to H_2O_2 stress (González-Flecha and Demple, 1997). Under anaerobic conditions, OxyR can respond to reactive nitrogen species in a manner similar to H_2O_2 responses under aerobic conditions (Seth *et al.*, 2012). OxyR can serve as a transcriptional regulator in both inactive and active states, and targets of its regulation include a small regulatory RNA termed *oxyS* and genes involved with H_2O_2 detoxification, heme biosynthesis, iron-sulfur (Fe-S) center repair, iron binding, manganese import, etc. (Kehres *et al.*, 2002, Liu *et al.*, 2011, Zeller *et al.*, 2007, Zheng *et al.*, 2001, Aslund *et al.*, 1999, Zheng *et al.*, 1999). Deletion of *oxyR* and *oxyS* in a human urinary O1:K1:H7 *E. coli*

isolate, significantly attenuated virulence in a murine model of acute cystitis (Johnson *et al.*, 2006).

Similar to OxyR, the SoxRS system in *E. coli* responds to stresses from both reactive oxygen and reactive nitrogen species. Activation of the SoxR transcriptional regulator leads to activation of the subsequent SoxS transcriptional regulator, which has been shown to up-regulate the expression of genes coding for; manganese superoxide dismutase, ferredoxin/flavodoxin-NADP+ reductase, glucose 6-phosphate dehydrogenase, fumarase C, endonuclease IV, aconitase A, and a small regulatory RNA *micF* (Zheng *et al.*, 1999). The SoxRS system can be activated under anaerobic conditions in which NADPH levels have been highly depleted (Krapp *et al.*, 2011) The OxyR and SoxRS systems represent responses to oxidative insults that are primarily imparted under aerobic conditions, but both can also respond to environmental stresses produced under anoxic conditions. Given that reactive oxygen and nitrogen species can be byproducts of bacterial respiration, and that repression of type 1 pili has been shown to be mediated by the cellular respiration state (Hadjifrangiskou *et al.*, 2011, Alteri *et al.*, 2009), there is a possibility that these oxidative stress response systems could play a role in modulating *fim* expression under the conditions tested here. It is also possible that a byproduct of the mixed-acid fermentation pathway utilized by *E. coli* (e.g. lactate, acetate, formate, succinate, ethanol, carbon dioxide, or hydrogen) could also serve as a signal for the repression of type 1 pili expression (Clark, 1989). Further studies are required, and are currently underway in our laboratory, to identify additional regulators impacting inversion of *fimS* under anoxic conditions.

Despite a restoration of total FimA protein levels under anoxic conditions, UTI89Δ*fimE* and UTI89Δ*fnr* mutants demonstrated diminished levels of *fim*-dependent biofilm formation and fewer pili on the cell surface. These data suggest the presence of a post-translational checkpoint

preventing pilus elaboration and/or anchoring under oxygen-deplete conditions. Post-translational control has been well documented for several types of adhesive macromolecular fibers. Bacteria encoding adhesive type IV pili can assemble and disassemble pilus structures. Bacteria such as the opportunistic urinary pathogen *P. aeruginosa*, utilize type IV pili for motility and surface attachment lending to biofilm formation (van Schaik *et al.*, 2005, Qi *et al.*, 2012, Barken *et al.*, 2008, Klausen *et al.*, 2003). In *P. aeruginosa*, a series of ATPase proteins facilitate assembly (PilB) and disassembly (PilT) on the surface of the bacterial cell (Chiang *et al.*, 2005). The ability to protrude and retract expands the functionality of type IV pili in processes like adherence and motility (Burrows, 2012). Type IV pili are assembled via a Type 2 secretion system (**Figure 4C**), in a process that is starkly different from the chaperone-usher pathway (**Figure 4B**) that drives type 1 pilus assembly (Allen *et al.*, 2012). To date, CUP pili have not been shown to posses the ability to disassemble from the bacterial surface. It is thus possible that pili are prevented from assembling, or are released into the extracellular milieu upon assembly under anoxic conditions. Given that energy production is significantly reduced under anoxic fermentative conditions, and the high-energy costs associated with pilus elaboration, we would postulate that the post-translational control would favor preventing pilus assembly. However, further study is needed to determine if this is true, and we will begin to address the energy impacts on anoxic pilus elaboration in **Chapter V**.

The addition of FNR as a modulator of *fim* expression in UTI89 continues to highlight the complex regulation of the *fim* operon in response to diverse environmental niches. But the question remains as to how oxygen-mediated regulation of fim could contribute to UPEC pathogenesis. **Chapter V** presents work aimed at addressing this particular question.

CHAPTER V

ON THE INSIDE: THE MURINE BLADDER ENVIRONMENT INDUCES AEROBIC BACTERIAL RESPIRATION

Introduction

[5]A range of regulators have been shown to act on the *fim* promoter, or downstream of it, in response to diverse environmental signals such as nutrient availability, temperature, and osmolality (Aberg *et al.*, 2006, Gally *et al.*, 1996, Greene *et al.*, 2015, Hadjifrangiskou *et al.*, 2011, Kuwahara *et al.*, 2010, Schwan, 2011). So far the studies presented in this dissertation suggest that oxygen serves as another environmental cue to regulate the expression of type 1 pili. UPEC-host interactions occur over a range of oxygen gradients beginning in the gastro-intestinal (GI) tract, where UPEC can reside as a reservoir (Chen *et al.*, 2013). Within the gastrointestinal tract, the oxygen tension can vary between 3 – 60 Torr (0.4 – 8.4%) depending on the location (He *et al.*, 1999). Upon exit into the environment, the oxygen tension surges to 21%, but then again drops significantly to around 4 – 7% in the bladder lumen (Wang *et al.*, 2008).

As with other *E. coli* commensal and pathogenic strains, fluctuations in the environmental oxygen concentration and alternative terminal electron acceptors, will dictate the

[5] Portions of this chapter adapted from and published in:

Floyd KA and Mitchell CA *et al.* The UbiI (VisC) aerobic ubiquinone synthase is required for expression of type 1 pili, biofilm formation, and pathogenesis in uropathogenic *Escherichia coli*. ***J. Bact.*** 2016 Oct. 198(19). 2662-2672. (PMID: 27161114).

metabolic energy production pathway used by UPEC. Typically aerobic respiration is active at oxygen concentrations > 5 μM, producing the greatest amounts of energy (Unden *et al.*, 2002, Becker *et al.*, 1997, Becker *et al.*, 1996). Anaerobic respiration is used at O_2 concentrations < 5 μM, with the energy output being dependent upon the type of alternative terminal electron acceptor present. Mixed acid fermentation is employed at oxygen concentrations < 1 μM, and produces the lowest amount of ATP through glycolysis. We have shown that in the absence of oxygen, and other terminal electron acceptors, type 1 pili expression is diminished in UPEC strain UTI89. Addition of nitrate to the growing cultures, did not fully restore *fim* expression under anaerobic conditions.

Previous studies from at least two different groups have demonstrated the importance of the aerobic arm of the TCA cycle in the virulence potential of UPEC during acute UTI (Alteri *et al.*, 2009, Hadjifrangiskou *et al.*, 2011). Stemming from proteomic studies examining pathways that promote the growth of UPEC strain CFT073 in human urine, Alteri *et al.* observed that proteins related to the import and metabolism of sialic acid, gluconate, and xylose sugars; along proteins involved with biosynthetic pathways for arginine and serine were significantly increased in expression during growth in urine (Alteri *et al.*, 2009). Alteri *et al.* went on to delete key components for each of the major central metabolism pathways in strain CFT073, and test the resulting single mutants for fitness in a murine model of UTI. They discovered that while the pentose phosphate and Entner-Doudoroff pathways were not required, gluconeogenesis and the TCA cycle were essential for the establishment of infection (Alteri *et al.*, 2009). Similarly, in studies evaluating the effects of a sensor kinase deletion, Hadjifrangiskou *et al.* demonstrated that disruption of the TCA cycle resulted in drastic reduction of type 1 pili from the surface of UPEC strain UTI89 (Hadjifrangiskou *et al.*, 2011).

Previous reports have also indicated the importance of aerobic respiration for enterohemorragic *E. coli* colonization in the murine intestine (Jones *et al.*, 2007). Energy production by both aerobic and anaerobic respiration in *E. coli,* relies on the production of an electrochemical proton gradient across the bacterial inner membrane (Unden and Bongaerts, 1997). This electrochemical gradient is produced through the oxidation of highly reduced chemical compounds, such as NADH and $FADH_2$, generated through glycolysis or the citric acid (TCA) cycle. The oxidation of these compounds occurs via the electron transport chain, shuttling protons to the outside of the inner membrane (Unden and Bongaerts, 1997). The build up of protons on the outside of the membrane generates a proton motive force (PMF) that drives protons down the electrochemical gradient, and through an ATPsynthase transporter lending to the production of energy in the form of ATP (Kashket, 1985). These studies combined with the work presented here demonstrating that type 1 pili expression requires the presence of oxygen, raises the question of whether repression of type 1 pili in the absence of molecular oxygen is the result of diminished TCA flux, and therefore, reduced ATP levels.

Previously, Hadjifrangiskou *et al.* reported the creation of a transposon mutant library in UPEC strain UTI89, which was screened in multiple *in vitro* biofilm settings to identify mutants with broad biofilm defects (Hadjifrangiskou *et al.*, 2012). Among the factors identified in these studies was the gene *visC*, the disruption of which significantly impaired biofilm formation *in vitro* and *in vivo* (Hadjifrangiskou *et al.*, 2012). The VisC protein was recently described to function as a C5-hydroxylase during aerobic ubiquinone synthesis and was renamed UbiI (Hajj Chehade *et al.*, 2013). In the non-pathogenic *E. coli* strain MG1655, deletion of *ubiI* resulted in reduced production of ubiquinone-8, but only under aerobic conditions (Hajj Chehade *et al.*, 2013). Ubiquinones are central to the electron transport chain and the generation of a PMF (as

described above), as they are reduced by Complexes I and II during oxidation of NADH resulting in proton translocation across the membrane (Brown and Brand, 1988, Galkin *et al.*, 1999, Pozzan *et al.*, 1979). However, under anoxic growth, ubiquinone-8 is replaced by menaquinone-8, the synthesis of which does not require UbiI (Hajj Chehade *et al.*, 2013). Given the requirement of UbiI for aerobic respiration, but not anaerobic respiration or fermentation, we hypothesized that the *ubiI* deletion mutant in UTI89 could serve as a biosensor to determine if the bladder environment *in vivo* is sufficiently oxygenated to drive UPEC to utilize aerobic respiration. This chapter describes experiments aimed at addressing this hypothesis.

Methods

Bacterial Strains and Constructs

All strains used in these studies are listed in **Table 1** in **Appendix A**. Non-polar deletion of the *ubiI* gene in strains UTI89 and UTI89_LON was performed using λ Red Recombinase-mediated recombination as previously described (Murphy and Campellone, 2003) with the primers presented in **Table 2** in **Appendix B.** Verification of *ubiI* deletion was performed using primers flanking the *ubiI* sequence (**Table 2, Appendix B**). The complementation construct UTI89Δ*ubiI*/pUbiI was constructed by cloning the *ubiI* gene into the SmaI – XbaI restriction sites of vector pBAD33 (Hadjifrangiskou *et al.*, 2011, Floyd *et al.*, 2016), using the primers listed in **Table 2** in **Appendix B**, and the resulting construct was verified by sequencing. Clinical urinary *E. coli* isolates (VUTI67 and VUTI73) were obtained from the Vanderbilt University Medical Center Clinical Microbiology Laboratory, with approval from the Vanderbilt Institutional Review Board. Briefly, isolates were obtained from infected urine samples that

tested positive for *E. coli* only infection (monocultures). Strains were streaked for colony isolation, an individual colony was selected and grown overnight in LB shaking at 37°C, and then freezer stocks were made form the overnight culture.

Biofilm Assays

Strains were grown logarithmically in 3 mL LB media and normalized to an OD_{600} of 1. Cultures were then diluted 200-fold in fresh LB and used to seed biofilm plates. Biofilm assays in LB at room temperature were performed in 96-well PVC plates as previously described (Pinkner *et al.*, 2006) and quantitatively measured 48 hours post-seeding, using crystal violet. Colony biofilms were seeded on minimal media supplemented with ferric iron to induce the rugose phenotype, as previously described (DePas *et al.*, 2013) and images were obtained 48 hours post seeding. Biofilm cultures for the analysis of impacts of alternative terminal electron acceptors were set up in the same way, with the addition of either 40mM $NaNO_3$, dimethylsulfoxide (DMSO), trimethylamine N-oxide (TMAO), or fumarate and cultured for 48 hours in the anaerobic chamber.

Growth Curves

Bacterial cultures were seeded in LB media, 0.1% arabinose, 20 μg/mL chloramphenicol, and incubated at 37°C overnight with shaking. Aliquots of overnight cultures were sub-cultured in 15 mL fresh LB, 0.1% arabinose, 20 μg/mL chloramphenicol, and normalized to a starting OD600=0.05. Sub-cultures were incubated at 37°C under shaking conditions. A 100-μL aliquot was removed from each culture hourly and diluted in 900 μL fresh LB and the OD600 was

recorded using a NanoDrop 2000 spectrophotometer (Thermo Scientific). Growth curves were repeated independent 3 times.

Motility Assays

Motility assays were performed as previously described (Nobelmann and Lengeler, 1996). Briefly, strains were stabbed in soft LB agar (0.25%) containing tetrazolium chloride (and 0.1% arabinose for complementation experiments), and incubated at 37°C for 7 hours in the presence of atmospheric oxygen. Motility was recorded as the diameter (in mm) containing bacteria migrating away from the inoculation point. For the assays set up under anoxic conditions (0% O_2, 2-3% H_2), plates were equilibrated overnight in the anaerobic chamber, and bacteria were inoculated and incubated in an anaerobic chamber for the duration of the assay.

Phase Assays and FimA Immunoblot Analyses

Phase assays for *fimS* orientation (**Figure 15**), and FimA immunoblots were performed as described in **Chapters III and IV**.

Flow Cytometry and Proton Motive Force (PMF) Measurements

Membrane potential measurements were performed using the BacLight kit (Invitrogen) with the following modifications to the manufacturer's instructions: Bacterial cells were normalized in PBS to an OD_{600} of 0.01 (~106 CFU/ml) and 0.5 mL of the normalized bacteria were incubated with 10 mM glucose and 30 mM $DiOC_2$ for 30 minutes at 300 rpm, 37°C. For the depolarizing controls, 30 mM of the proton ionophore CCCP was added to abolish the membrane potential. Some reactions contained EDTA at a final concentration of 1 mM, which

was added to every reaction simultaneously with $DiOC_2$. $DiOC_2$ internalization was measured as a fluorescence emission shift from green (membrane-associated) to red (cytosolic), by calculating the ratio of [cells emitting at 543 nm / cells emitting at 488 nm]. A total of 20,000 events were measured in every experiment. Experiment was repeated 3 times.

Metabolic Phenotype Microarrays.

Metabolic profiling was performed according to the Biolog guidelines (http://www.biolog.com) using plate PM1. Bacteria from LB agar plates were resuspended to an 85% transmittance into 10 mL of IF-0a GN/GP Base IF (Biolog Inc.) supplemented with niacin (10 μg/ml). Microplate PM1 was inoculated with 100 μL of the bacterial suspension and incubated at 37ºC for 48 hours (OmniLog Incubator, Biolog). Optical density measurements were obtained at 15-minute intervals (OmniLog PM DC 1.30.01 software). Data analysis and kinetic plots generation were performed using OmniLog PM software. Average plot height was used for data comparisons and a difference >20 was set as the significance threshold.

Transmission Electron Microscopy (TEM)

Samples for TEM were obtained from cultures grown statically for 24 hours in LB at 37°C. Cells were normalized in PBS, as described above for the HA assays and samples were submitted to the Washington University – St. Louis Imaging Facility for fixing and imaging by TEM. Samples from 3 independently grown cultures per strain were sampled. The pilus enumerator was blinded with respect to the identity of the sample.

Antibiotic Susceptibility Assays

Strains were grown to an OD_{600} of 1.0 and were spread to confluence on 150 mm LB agar plates. Gentamycin and streptomycin discs (both at 10 μg potency) were applied onto the agar plates and plates were incubated overnight at 37°C. Zones of clearance were recorded as diameters (in mm). The susceptibility assays were repeated 4 times. Average zones of clearance are reported.

Quantitation of ATP Levels

ATP quantitation was performed using the CellTiter-Glo Luminescent Cell Viability Assay (Promega). Triplicate samples of 50 μL of each culture per time point tested were transferred to a black well/clear bottom, 96-well plate (Costar). An equal volume (50 μL) of CellTiter-Glo substrate/buffer mix was added to each well and mixed thoroughly. The plates were allowed to shake orbitally for 2 minutes to stabilize the signal, and then luminescence values of ATP were measured using a SpectraMax i3 instrument (Molecular Devices). Luminescence was also determined for wells filled only with LB to subtract background luminescence due to the media. A standard curve was determined using ATP disodium salt hydrate (Sigma) to allow for ATP quantification of the unknown samples. Known concentrations of ATP disodium salt hydrate were diluted in LB and the corresponding luminescence value was recorded (after background subtraction of LB). To quantify the amount of ATP in cell cultures at each growth phase, we matched luminescence values from the standard curve created. Experiments were performed with at least 3 biological replicates of 3 technical replicates. Statistical analyses were performed using a One-way ANOVA with $P < 0.05$ (95% confidence interval) considered significant.

qPCR Analyses.

Samples for RNA extraction were obtained from cultures grown statically for 18 hours at 37 °C in LB. RNA extraction was performed using the RNeasy kit (Qiagen); RNA quality was checked via Bioanalyzer and 1 microgram of RNA was DNase-treated using DNase Turbo (Life Technologies-Thermo Fischer). Subsequent cDNA synthesis was performed as previously described (Hadjifrangiskou *et al.*, 2011) using SuperScript II or III, random hexamers and dNTPs (Life Technologies – Thermo Fischer). qPCR analysis of steady-state mRNA transcript levels of *sdhB*, *mdh*, *fliM*, *cydA*, *fimB*, *fimE*, and *rrsH* was performed with SYBR green methodologies using the primers listed in **Table 2** in **Appendix B**. Determination of relative-fold change was calculated according to Pfaffl *et al.* (Pfaffl, 2001), using *rrsH* as the housekeeping gene.

Mouse Infections

Seven-to-nine week old female C3H/HeN mice (Harlan Laboratories) were used in all studies presented here. Bacteria were instilled in mouse bladders using transurethral inoculation as previously described (Hung *et al.*, 2009) using an inoculum size of 107 CFU in 50 μL PBS. Acute and chronic infection experiments were performed three times, and statistical analyses were performed using the Mann-Whitney test (two-tailed). $P<0.05$ was considered significant. Early infection (3 hour) studies with gentamycin protection assays were performed once with at least 5 mice used per bacterial strain. At 3 hours post inoculation, bladders were removed from sacrificed animals, bisected, washed three times with PBS to remove loosely adherent bacteria and treated with 50 μg/mL gentamycin for 90 minutes, as previously described (Hung *et al.*, 2009). At the end of the 90-minute incubation, bladders were washed and homogenized to retrieve intracellular CFUs. For each set of gentamicin-treated bladders, there was an age-

matched set of 5 untreated controls that were used to enumerate total CFUs. Statistical analyses were performed between groups using two-tailed Mann-Whitney, with $P<0.05$ considered significant.

Results

Alternative terminal electron acceptors fail to restore fim-dependent biofilm formation

As a facultative anaerobe, *E. coli* can utilize a series of alternative terminal electron acceptors (ATEAs) for anaerobic respiration. The preferential order of ATEA use is dictated by the amount of energy produced with their utilization, and the hierarchy is; nitrate, dimethylsulfoxide (DMSO), trimethylamine N-oxide (TMAO), and fumarate (Unden and Bongaerts, 1997). TMAO is a breakdown product of L-carnitine, and as such individuals with diets high in intake of red meats and fish have increased levels of TMAO in their urine (Koeth *et al.*, 2013). Therefore particular populations of individuals could have increased levels of ATEA in their urine, which could prime the utilization of anaerobic respiration by invading UPEC.

To determine if anaerobic respiratory conditions could promote the expression of type 1 pili, we had previously evaluated how nitrate influenced *fim* gene expression (**Figure 25**). Those studies indicated that nitrate addition only allowed for *fim* gene expression in populations that already had the *fimS* promoter in the *fim*ON orientation. To determine how ATEAs influence biofilm-formation, we then performed biofilm assays in the absence of oxygen, from cultures starting *fim*ON supplemented with 40mM concentration of each ATEA individually. Compared to culture at atmospheric oxygen concentrations, biofilm formation was drastically reduced under anoxic conditions without any ATEA supplementation (**Figure 33**). Addition of any ATEA

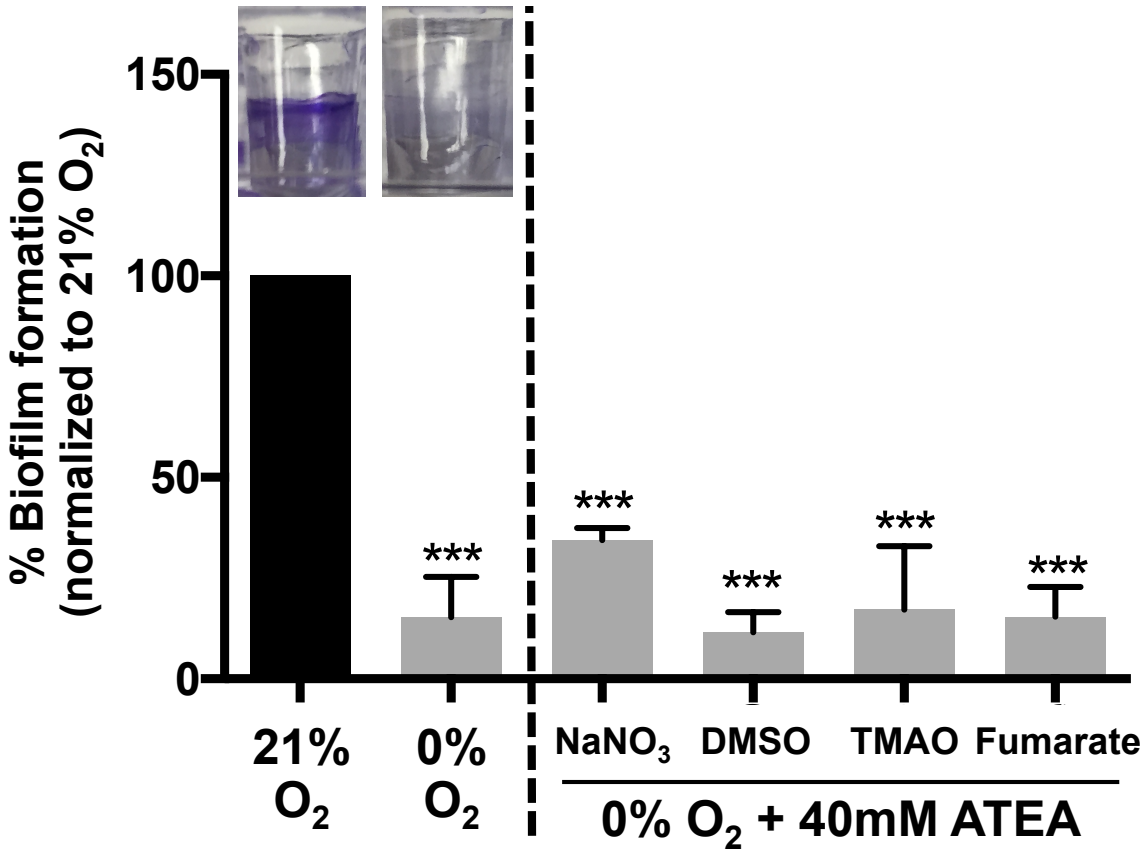

Figure 33. Alternative terminal electron acceptors fail to restore *fim*-dependent biofilm formation under anoxic conditions. Biofilm formation presented as a percentage of biofilm formation at atmospheric (~21%) oxygen conditions, with representative pictures of crystal violet stained biofilms at 21% and 0% oxygen. Alternative terminal electron acceptor cultures were treated with a final concentration of 40mM of the respective compound; sodium nitrate ($NaNO_3$), dimethylsulfoxide (DMSO), trimethylamine N-oxide (TMAO), and sodium fumarate. Biofilm levels are presented as the mean with the standard error of the mean, from at least three biological replicates with at least three technical replicates of each biological replicate. Statistical analysis was performed by one-way ANOVA with Bonferroni correction for multiple comparisons (***$P<0.0001$). The author would like to thank Allison Eberly for the contribution of this graph to this work.

under anaerobic conditions also resulted in a drastic reduction of *fim*-dependent biofilm formation compared to atmospheric growth conditions (**Figure 34**). These observations led to the hypothesis that over the course of infection, the bladder environment is conducive to aerobic bacterial respiration.

Deletion of ubiI lowers the membrane potential of UPEC

UbiI is an aerobic ubiquinone synthase enzyme that is requisite for proper aerobic respiration in *E. coli* (Hajj Chehade *et al.*, 2013). Therefore, a mutant lacking *ubiI* can be used as a biosensor for detecting the presence or absence of oxygen in the bladder. To determine the impacts of UbiI on UPEC pathogenic behavior, our lab previously created a clean *ubiI* deletion mutant in UTI89 (UTI89Δ*ubiI*). The resulting mutant UTI89Δ*ubiI* was attenuated in its ability to form biofilm in LB (**Figure 34A**), exhibited an altered colony biofilm morphotype on solid agar (**Figure 34B**), and exhibited a lag during growth in rich media under aerobic conditions (**Figure 34C**).

Using flow cytometry and the oxocarbocyanine dye, $DiOC_2$, UTI89Δ*ubiI* was determined to have a decrease in overall PMF when grown under aerobic conditions (**Figure 35A**). Membrane-associated $DiOC_2$ emits green fluorescence and it is readily detectable in all bacteria. The presence of membrane potential across the inner membrane facilitates the import of $DiOC_2$ into the cytosol, where fluorescence emission shifts to red. Flow cytometry measurements revealed that $DiOC_2$ internalization by UTI89Δ*ubiI* was consistently lower compared to WT UTI89 (**Figure 35A**). This reduction in PMF correlated with increased resistance to aminoglycoside antibiotics (streptomycin and gentamicin), which require energy to be imported

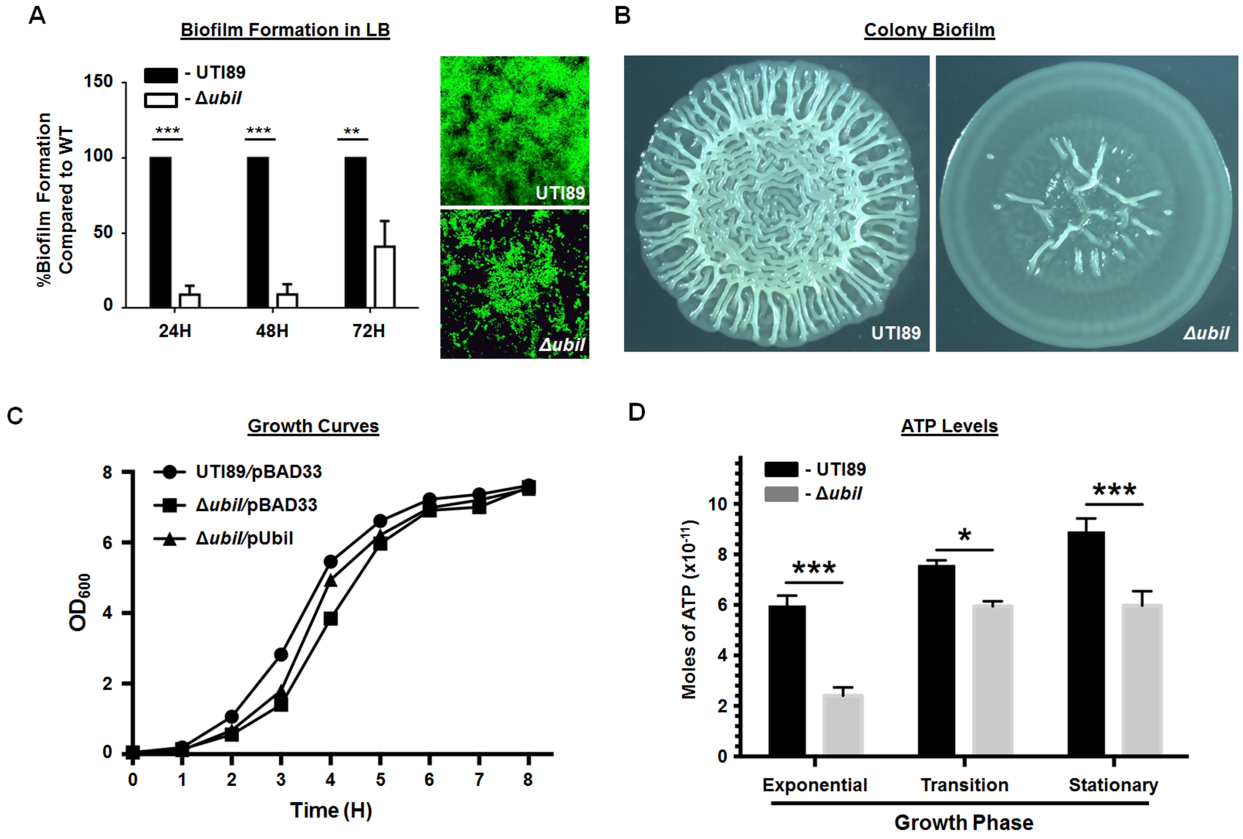

Figure 34. Deletion of *ubiI* leads to reduced biofilm formation, a lag during growth in rich media, and reduced production of ATP under aerobic conditions. (A) Graph depicts percent biofilm formation by UTI89Δ*ubiI* (white bars) compared to WT UTI89 (black bars) on PVC 96-well plates during aerobic growth in LB media. Images on the right are representative 72 hour confocal laser scanning microscopy (CLSM) images of wild-type WT UTI89 and the isogenic *ubiI* deletion mutant. **(B)** Images of representative colony biofilms formed by WT UTI89 and UTI89Δ*ubiI* during growth on minimal media agar supplemented with ferric iron. **(C)** Growth curves of WT UTI89 containing empty pBAD33 plasmid, UTI89Δ*ubiI* containing empty pBAD33 plasmid, and complemented UTI89Δ*ubiI*/pUbiI during aerobic growth in LB media induced with 0.1% arabinose. **(D)** ATP values for WT UTI89 (black bars) and UTI89Δ*ubiI* (gray bars) during different phases of growth, using a standard curve plotted for ATP quantitation using the CellTiter-Glo Luminescent Cell Viability Assay (Promega; see also materials and methods). The standard curve was determined using ATP disodium salt hydrate (Sigma). All experiments were repeated at least three times. Statistical analyses in A and D were performed with One-way ANOVA with $P<0.05$ (95% confidence interval) considered significant.

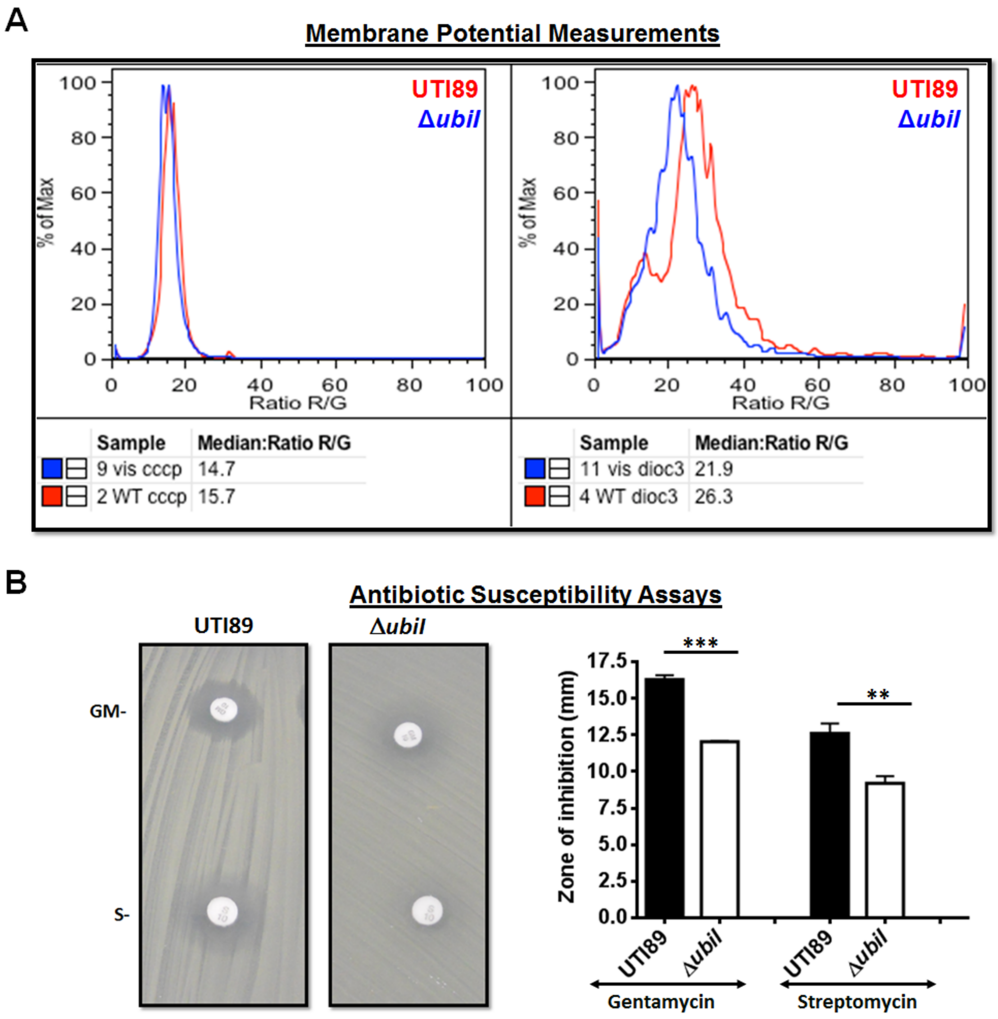

Figure 35. Deletion of *ubiI* leads to reduced PMF across the inner membrane, increasing tolerance to certain antibiotics. (A) Proton motive force (PMF) differences between UTI89 and UTI89Δ*ubiI* were measured using flow cytometry and the oxocarbocyanine dye, $DiOC_2$. The left panel indicates the background dye incorporation of depolarizing controls, in which 30 mM of the proton ionophore carbonyl cyanide *m*-chlorophenylhydrazone (CCCP) was added to abolish the membrane potential prior to addition of $DiOC_2$. Membrane-associated $DiOC_2$ emits green fluorescence and it is readily detectable in all bacteria. The presence of membrane potential across the inner membrane facilitates the import of $DiOC_2$ into the cytosol, where fluorescence emission shifts to red. Panel on the right indicate $DiOC_2$ internalization by WT UTI89 and UTI89Δ*ubiI*. Results shown are representative of three independent experiments. **(B)** Panels on the left indicate growth of WT UTI89 or UTI89Δ*ubiI* in the presence of antibiotics that require energy-dependent transport (gentamycin, GM; streptomycin, S). The graph on the right depicts the quantitation of the zones of clearance determined for WT UTI89 and UTI89Δ*ubiI* from 5 biologically independent experiments with 3 technical replicates each. Statistical analyses were performed using unpaired students t-test, with ***, $p<0.0001$ and **, $p<0.001$

across the inner membrane, in UTI89Δ*ubiI* compared to WT UTI89 (**Figure 35B**). Subsequent quantitation of ATP levels in WT UTI89 and UTI89Δ*ubiI* during exponential, transition and stationary phases of growth indicated consistently lower overall ATP levels in the *ubiI* deletion mutant compared to WT UTI89 (**Figure 35D**). Combined these studies validated that UTI89Δ*ubiI* is deficient in energy production by aerobic respiration, and therefore UbiI is involved in PMF generation as has been proposed for K12 *E. coli*.

Deletion of ubiI leads to reduced production of extracellular fibers during aerobic growth

Intact membrane potential is critical for flagellar rotation, as well as Sec-dependent translocation of periplasmic and membrane proteins, including the subunits that are required for the assembly of curli and chaperone-usher pathway pili that are important components of UPEC biofilms as discussed in **Chapters I and II** (Driessen, 1992, Maurer *et al.*, 2005, Minamino and Namba, 2008, Paul *et al.*, 2008, Sowa *et al.*, 2005). Motility assays revealed that UTI89Δ*ubiI* was consistently significantly less motile than WT UTI89 during aerobic growth (**Figure 36A**). This motility defect was rescued in UTI89Δ*ubiI*/pUbiI, which harbors an extra-chromosomal wild-type copy of *ubiI* (**Figure 36A**). Hemagglutination assays demonstrated a significant reduction in the ability of UTI89Δ*ubiI* to agglutinate red blood cells compared to WT UTI89, suggesting lowered expression of type 1 pili (**Figure 36B**). Subsequent imaging of bacteria by TEM revealed a greater proportion of non-piliated bacteria in the UTI89Δ*ubiI* population (**Figure 37**). Analysis of the *fimS* promoter phase orientation demonstrated that UTI89Δ*ubiI* cultures had a greater proportion of the population in the *fim*OFF orientation, resulting in decreased expression of the *fim* operon as measured by immunoblot for total FimA protein levels (**Figure 38A**). This increase in the *fim*OFF population, and reduction of FimA protein levels,

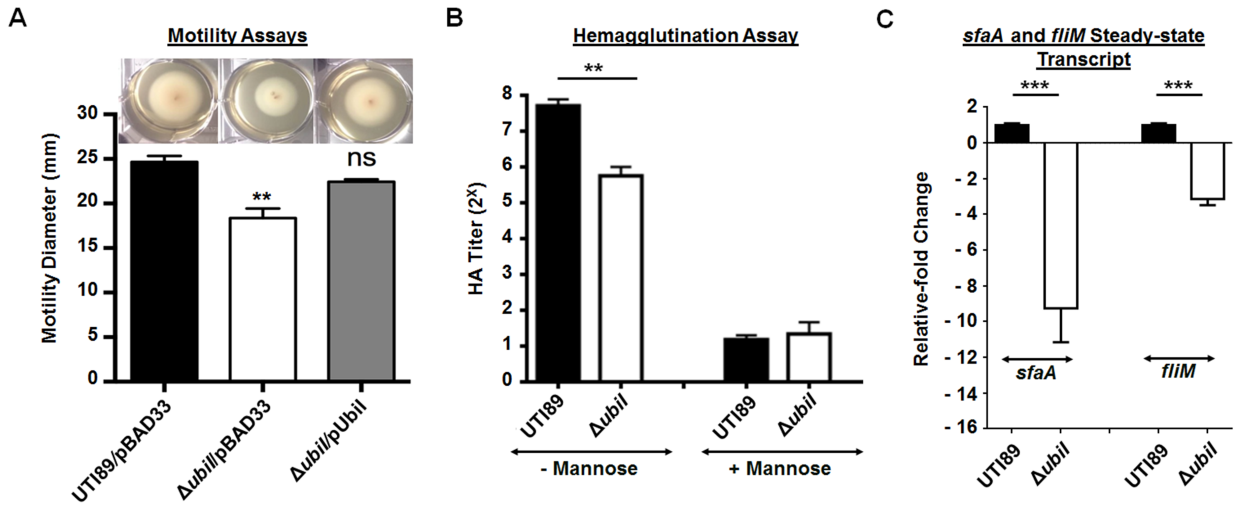

Figure 36. Deletion of *ubiI* decreases motility and production of adhesive chaperone-usher pathway pili under aerobic conditions. (A) Assays comparing swimming motility in WT UTI89 (black bar), UTI89Δ*ubiI* (white bar) and complemented UTI89Δ*ubiI*/pUbiI (gray bar) on plasmid pBAD33 during aerobic growth in LB media induced with 0.1% arabinose in the presence of atmospheric oxygen. Motility was recorded as the diameter (in mm) containing bacteria migrating away from the inoculation point. Experiment was repeated 3 times. Graph depicts average diameters from the 3 experiments. Pictures depict representative motility phenotypes for the 3 strains. **(B)** Bar graph depicting HA titers by UTI89Δ*ubiI* (white bars), compared to WT UTI89 (black bars) in the presence and absence of 4% D-mannose. The small degree of agglutination remaining in the WT strain is attributable to some expression of S-pili. Graph depicts average HA titers from 4 independent experiments. Statistical analyses were performed using unpaired, two-tailed Student's t-test, with ** $P<0.05$ considered significant. **(C)** Expression profiles of the gene encoding for the major subunit of S pili (*sfaA*) and one component of the flagellar switch complex (*fliM*) measured as a relative-fold change normalized to the housekeeping *rrsH* gene and compared to normalized expression in WT UTI89. The average of at least 3 independent biological replicates is shown, each with at least 3 technical replicates per qPCR run. Statistical analysis was performed with One-way ANOVA for A and C, with *, $p<0.05$; **, $p<0.001$, and ***, $p<0.0001$.

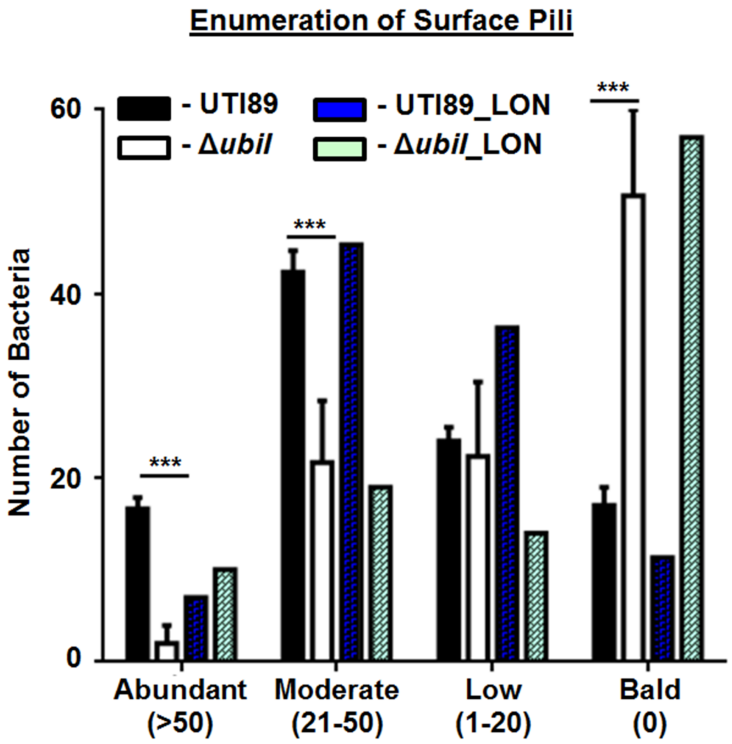

Figure 37. Deletion of *ubiI* reduces bacterial surface pili levels independent of the *fim* promoter orientation under aerobic conditions. Graph depicts the enumeration of bacteria with zero, low (1-20), moderate (21-50), or abundant (>50) numbers of pili in the WT UTI89 (black bars), UTI89Δ*ubiI* (white bars), UTI89_LON (blue bars), and UTI89Δ*ubiI*_LON after aerobic growth for 2 x 24 h in static LB media. Pili images were obtained from TEM. The person enumerating bacteria was blinded to the identity of samples. The graph depicts the average from enumerating bacteria from three independent experiments. Statistical analysis was performed by two-tailed Student's t-test with $P<0.05$ considered significant

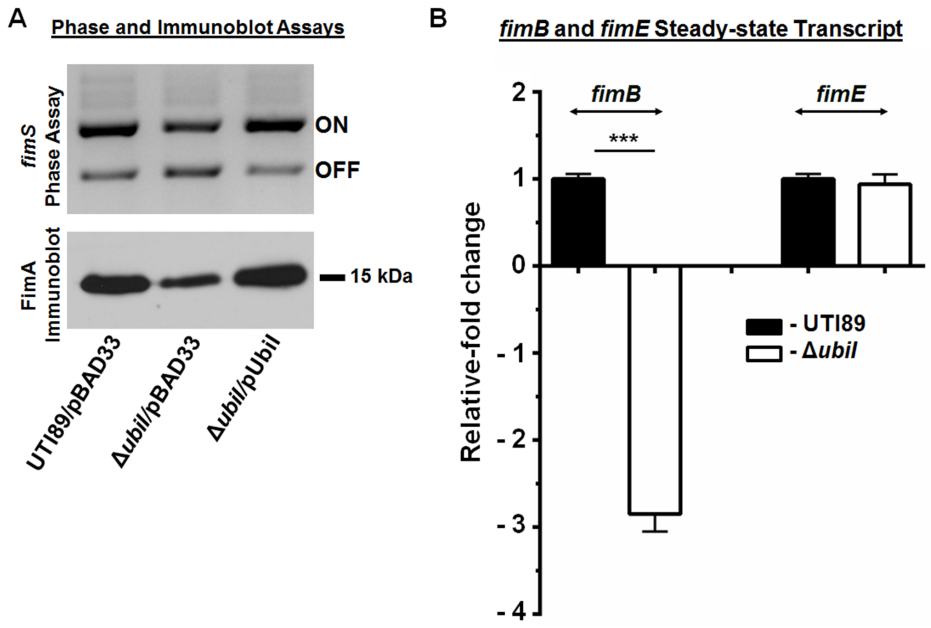

Figure 38. The *fimB* recombinase is down-regulated in the *ubiI* mutant. (A) Analysis of the phase state of the *fimS* promoter region, through PCR amplification and restriction enzyme digest as previously reported (**Figure 15**). Immunoblot analysis, probing for the major pilin subunit FimA in samples corresponding to those shown above in the fimS Phase Assay. **(B)** Expression of genes encoding the two primary Fim site-specific recombinases (*fimB*, *fimE*) measured as a relative-fold change normalized to the housekeeping *rrsH* gene and compared to normalized expression in WT UTI89. The average of at least 3 independent biological replicates is shown, each with at least 3 technical replicates per qPCR run. Statistical analysis was performed with One-way ANOVA, with *, $p<0.05$; **, $p<0.001$, and ***, $p<0.0001$.

was restored in the UTI89Δ*ubiI*/pUbiI strain (**Figure 38A**). Parallel qPCR analyses of aerobically grown cultures incubated under pili-inducing conditions showed no alterations in *fimE* transcript levels, but *fimB* steady-state transcript levels were reduced 4-fold in UTI89Δ*ubiI* compared to WT UTI89 (**Figure 38B**).

Defects in the assembly of type 1 pili have previously been shown to exert negative feedback on the orientation of the *fimS* promoter (Greene *et al.*, 2014, Chen *et al.*, 2009). It is possible that insufficient energy to translocate *fim* subunits across the inner membrane in the *ubiI* mutant could exert a similar effect on *fimS* promoter orientation. To this end, we examined surface pili levels in a *ubiI* mutant with the *fim* promoter genetically locked in a transcription-competent state (UTI89Δ*ubiI*_LON) by deleting *ubiI* from the previously established UTI89_LON strain (Pallesen *et al.*, 1989). TEM analyses revealed that the numbers of surface pili in the UTI89Δ*ubiI*_LON strain were as low as the numbers recorded for UTI89Δ*ubiI* (**Figure 37**). These data indicate that restoring expression of the *fim* operon in the absence of UbiI does not restore surface piliation.

As described in **Chapter III**, the same hemagglutination assays used to probe for type 1 pili expression can also evaluate S pili-mediated adherence. Previous studies have demonstrated that type 1 pili and S pili are inversely regulated; reduction in type 1 pili production leads to up-regulation of S pili (Greene *et al.*, 2014, Hadjifrangiskou *et al.*, 2012). The hemagglutination studies with UTI89Δ*ubiI* indicated no increase in mannose resistant HA (**Figure 36B**); this observation suggests that reduction of type 1 pili from the bacterial cell surface does not induce the typical up-regulation of the S pilus system in the *ubiI* deletion mutant. Subsequent qPCR analyses probing for expression of *sfaA* (the primary S pilus subunit) indicated a marked reduction of *sfaA* transcript in the *ubiI* deletion mutant, compared to WT UTI89 (**Figure 36C**).

Expression of type 1 pili and flagellar motility are also inversely regulated (Lane *et al.*, 2007). Yet, the *ubiI* deletion mutant simultaneously exhibited reduced motility and pili-mediated adherence (**Figure 36A-B**). Previous studies demonstrated that disturbances in proton flux across the membrane exert a negative feedback on the transcription of flagellar genes (Maurer *et al.*, 2005). qPCR analysis probing for *fliM* (one of the flagellar motor subunit genes) steady-state transcript, indicated a 3-fold reduction in UTI89Δ*ubiI* compared to WT UTI89 (**Figure 36C**), consistent with a negative regulatory feedback in response to lower PMF across the membrane. Combined, these data suggested that a reduction in PMF in UTI89Δ*ubiI* impacts the elaboration of adhesive appendages involved in biofilm formation, as well as appendages used for motility.

Loss of UbiI exerts a negative impact on aerobic respiration components

During respiration, ubiquinone reduction is coupled with NADH/FADH oxidation by respiratory complexes I and II (Damper and Epstein, 1981). A drop in ubiquinone/menaquinone levels results in decreased oxidation of FADH/NADH, which down-regulates the FADH/NADH-producing steps of the TCA cycle (Damper and Epstein, 1981). Given the implication of UbiI in aerobic ubiquinone synthesis, we next evaluated the effects of *ubiI* deletion on the expression of the *cydA* gene that encodes subunit 1 of the cytochrome bd-I, the primary terminal oxidase during aerobic growth of *E. coli* (Miller and Gennis, 1983). To evaluate effects on the aerobic arm of the TCA cycle, genes *sdhB* and *mdh* that encode the succinate- and malate dehydrogenase enzymes respectively, were sampled by qPCR. Transcriptional analyses were performed on samples obtained during logarithmic growth with aeration, which are conditions conducive to aerobic respiration. Under these conditions expression of all three genes was significantly reduced in UTI89Δ*ubiI* compared to WT UTI89 (**Figure 39A**). Together, these data

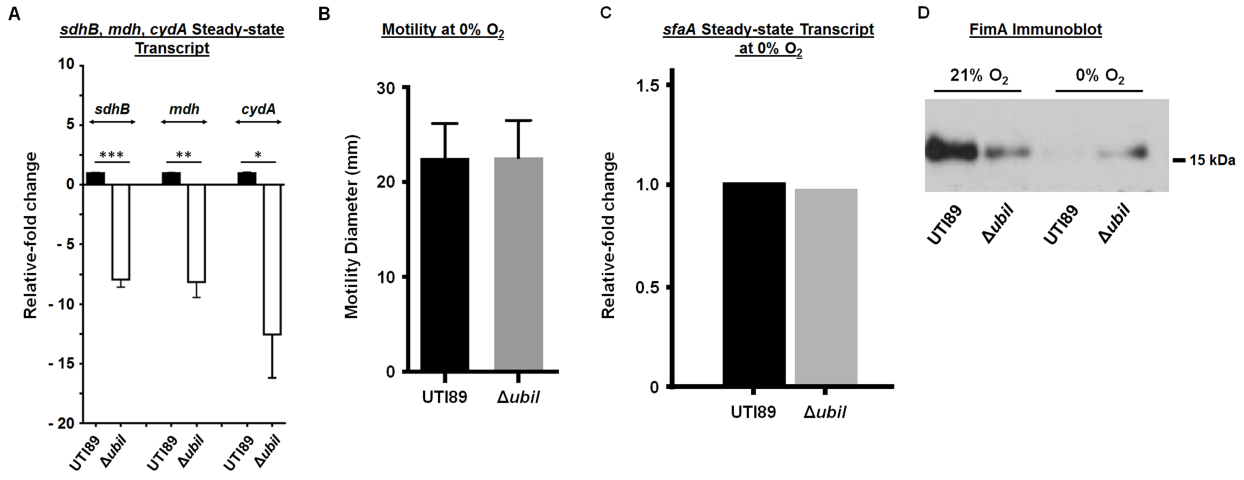

Figure 39. Deletion of *ubiI* exerts a negative effect on components of aerobic respiration, but does not impact anaerobic respiration. (A) Expression profiles of three genes involved in the TCA cycle or aerobic respiration: *sdhB*, *mdh*, *cydA* measured as relative-fold change normalized to the housekeeping *rrsH* gene and compared to normalized expression in WT UTI89. The average of at least 3 independent biological replicates is shown, each with at least 3 technical replicates per qPCR run. Statistical analysis was performed with One-way ANOVA, with *, $p<0.05$; **, $p<0.001$, and ***, $p<0.0001$. **(B)** Motility assay diameters of WT UTI89 and the Δ*ubiI* mutant under anoxic conditions. The graph is a representative of at least two biological replicates, each with at least 3 technical repeats per strain. Statistical analysis was performed with Student's *t*-test. **(C)** Anoxic expression profile of the gene for the major subunit of S pili, *sfaA*, measured as relative-fold change normalized to the housekeeping *rrsH* gene and compared to normalized expression in WT UTI89. Representative experiment shown with at least 3 technical replicates per qPCR run. **(D)** Immunoblot analysis for expression of the major subunit of type 1 pili, FimA in WT UTI89 or UTI89Δ*ubiI* samples, grown under aerobic or anoxic conditions. Immunoblot is a representative of at least three biological repeats.

demonstrated that UTI89Δ*ubiI* was deficient in aerobic respiration components under conditions conducive to their utilization.

Anoxic growth restores UPEC motility and expression of S pili, but does not restore type 1 pili expression

The data presented thus far demonstrated that UbiI is a critical component of PMF generation under aerobic respiration conditions requisite for ubiquinone synthesis, and its deletion significantly impairs the expression of TCA cycle genes and UPEC pathogenic determinants during aerobic growth. Our studies have thus far, also indicated that oxygen is required for optimal expression of type 1 pili. This may be due to differences in the proton motive force produced by anaerobic quinone synthases that replace UbiI during anoxic growth (Hajj Chehade *et al.*, 2013). To determine whether anoxic growth leads to an overall down-regulation of extracellular fibers, we next tested the motility and ability to express S pili under anoxic conditions of WT UTI89 and UTI89Δ*ubiI*. Motility assays indicated that UTI89Δ*ubiI* was able to swim as well as WT UTI89 under anoxic conditions (**Figure 39B**), and qPCR analyses demonstrated equal levels of *sfaA* transcript between WT UTI89 and UTI89Δ*ubiI* (**Figure 39C**). These observations were consistent with the hypothesis that UbiI is dispensable under anoxic conditions, with the proton flux across the inner membrane indirectly drive by other synthases. However, under anoxic conditions both WT UTI89 and UTI89Δ*ubiI* remained defective in their ability to express type 1 pili (**Figure 39D**), in agreement with the previous studies presented here, which demonstrating that complete lack of oxygen exerts a negative impact on the expression of type 1 pili. Combined, these data suggest that the down-regulation of type 1 pili

under oxygen-deplete conditions is not due to reduced energy production during anaerobic respiration, and that UbiI is only active in the presence of oxygen.

Deletion of ubiI impairs UPEC virulence in the hypoxic bladder environment

UPEC colonization of the urinary tract relies heavily on the expression of type 1 pili and biofilm formation. UPEC have also adapted a unique intracellular pathogenic cascade in which they form biofilm-like intracellular bacterial communities (IBCs) inside bladder epithelial cells (Anderson *et al.*, 2003). This unique intracellular lifestyle primarily serves as a strategy for bacteria to evade host immune responses (Anderson *et al.*, 2004), allowing for the replication of bacteria to high numbers to persist in infection. IBC formation begins with the initial adherence of a bacterium to the bladder epithelial cell surface via type 1 pili interactions with manosylated-uroplakin proteins on the surface of the cell. Adherence triggers internalization of the bacteria, which can then escape to the cytoplasm and clonally expand into an IBC in a process that resembles the developmental stages of extracellular biofilm formation (**Figure 3**) (Justice *et al.*, 2004, Anderson *et al.*, 2003). When the size of the IBC becomes large enough to fill the host cell, UPEC respond to a yet uncharacterized signal and assume a filamentous cellular morphology to flux out of the cell and disperse to continue infection within the bladder to ascend to the kidneys (Justice *et al.*, 2006, Justice *et al.*, 2004, Khandige *et al.*, 2016). This pathogenic cascade has been well described in murine models of acute cystitis (Hung *et al.*, 2009, Anderson *et al.*, 2003), but also occurs within the human host (Rosen *et al.*, 2007). Formation of IBCs enhances the colonization and pathogenesis of UPEC within the urinary tract.

So far we have demonstrated that UTI89Δ*ubiI* is deficient in components required for aerobic respiration and the TCA cycle, resulting in decreased PMF and energy production, which

leads to decreased virulence-associated phenotypes (e.g. motility, surface pilus expression, biofilm formation, etc.). Although UPEC is a facultative anaerobe, previous studies demonstrated that TCA cycle mutants displayed a significant fitness disadvantage compared to the isogenic WT strains in murine models of bladder infection (Alteri *et al.*, 2009, Hadjifrangiskou *et al.*, 2011). This would suggest that the bladder contains enough oxygen to induce aerobic respiration in UPEC, yet this has yet to be shown. Given the defects associated with deletion of *ubiI* under aerobic conditions, we hypothesized that UTI89Δ*ubiI* could be utilized as a biosensor to determine if the bladder environment forces aerobic bacterial respiration. If so, since UTI89Δ*ubiI* is deficient in aerobic respiration, it would have a fitness defect during *in vivo* infection compared to WT UTI89.

At both 6 and 16 hours post-infection, in a well-established murine model of acute cystitis, UTI89Δ*ubiI* exhibited a 10-fold reduction in bladder colonization (**Figure 40A**) and formed very few to no IBCs (**Figure 40B**). In the murine model of infection used for these studies, mice either resolve the infection over a period of 48-72 hours, or elicit an exacerbated immune response that suppresses urothelial regeneration and facilitates chronic colonization of the bladder surface by extracellular bacterial communities (Hannan *et al.*, 2012, Hannan *et al.*, 2010). Evaluation of bladder bacterial titers at two weeks post infection revealed that only 4/36 (11.1%) mice infected with UTI89Δ*ubiI* progressed to chronic infection, compared to 27/34 mice (79%) infected with WT UTI89 (**Figure 40C**). Consistent with the persisting piliation defect of UTI89Δ*ubiI*_LON **(Figure 37)**, this strain exhibited the same effects as UTI89Δ*ubiI* demonstrating a defect in the number of both intracellular and luminal bacteria within the bladder compared to WT UTI89 (**Figure 40C**). These data suggest that during acute bladder

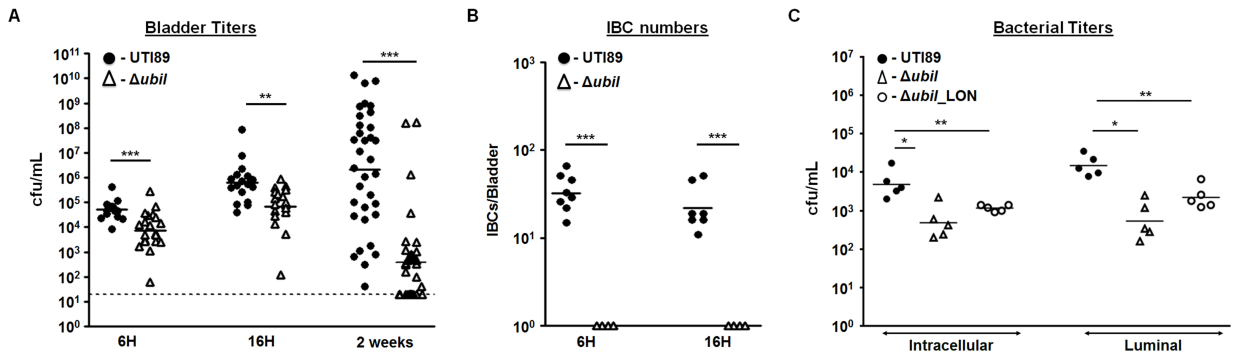

Figure 40. Deletion of *ubiI* attenuates virulence in a murine model of UTI, independent of the *fimS* promoter orientation. (A) Colony-forming units (CFU) recovered from the bladders of 7-8 week old female C3H/HeN mice infected with either WT UTI89 or UTI89Δ*ubiI*, at stages of acute or chronic UTI. Graph depicts numbers from two independent experiments. **(B)** Intracellular bacterial community (IBC) numbers at 6- and 16 hours post infection with WT UTI89 or UTI89Δ*ubiI*. A representative from two experiments is shown. **(C)** Gentamicin protection assay for the analysis of intracellular versus luminal bacteria. Graph indicates CFUs recovered from bladders infected with WT UTI89, UTI89Δ*ubiI*, or UTI89Δ*ubiI*_LON at 3 h post inoculation. On the left hand side are intracellular CFUs recovered after a 90-minute incubation of bisected bladders in gentamycin to eliminate extracellular bacteria. On the right hand side are the luminal CFUs recovered from non-treated bladders. Experiment was performed once, with 5 mice per strain per treatment group. Significance was determined for all experiments using the two-tailed Mann-Whitney with *, $p<0.05$; **, $p<0.001$, and ***, $p<0.0001$.

infection there is enough oxygen to induce aerobic respiration within UPEC, and impairment of aerobic ubiquinone synthesis leads to reduced virulence in a murine model of infection.

Anoxic repression of type 1 pili appears conserved across fim-expressing E. coli strains

The studies mentioned above indicated that the bladder environment contains enough oxygen to require aerobic bacterial respiration, combined with the other data presented in this dissertation, this suggests that the bladder environment is highly conducive to the expression of type 1 pili. Therefore, oxygen-mediated control of *fim* expression could present a new target for the development of anti-adhesive and anti-biofilm strategies to attenuate UTI pathogenesis. However, these studies were limited to UPEC strain UTI89, and to truly understand if this oxygen-mediated control could be a new therapeutic target, we must determine if it is conserved across *fim*-expressing *E. coli* strains. To begin to address this question, we next examined *fim* expression in the absence of oxygen in UPEC strain CFT073 as well as two *fim*-expressing clinical urinary *E. coli* isolates (VUTI strains) obtained from the Vanderbilt University Medical Center (VUMC) Clinical Microbiology Laboratory. UPEC strain CFT073 was isolated from the bloodstream of a patient with pyelonephritis that had become septicemic (Mobley *et al.*, 1990). Based upon amino acid sequence alignment, FimA is 80% identical between UPEC strains UTI89 and CFT073 (UniprotKB). FimA from UPEC strain CFT073 migrates faster by SDS-PAGE, presenting at a slightly lower molecular weight (**Figure 41A**). Upon static culture for 48 hours in anoxic conditions, CFT073 showed a decrease in FimA protein levels similar to that of UTI89 (**Figure 41A**).

Over the course of this dissertation work, our lab has established collaboration with the VUMC Clinical Microbiology Laboratory to establish a database of *E. coli* isolates collected

from patient urines. VUTI strains were collected from urines that tested monoculture positive for the presence of *E. coli*, samples that tested positive for *E. coli* and other bacterial species were discarded. Within the first month of collection, we had accumulated a total of 182 VUTI strains that were monoculture positive for *E. coli*. The original IRB application was written to allow for the collection of VUTI cultures and any matching urine samples, but did not include any patient information. Therefore, there was no data on the disease state of the individual (e.g. ASB vs. cystitis vs. pyelonephritis vs. CAUTI) to match to the corresponding isolate. For this reason, only the first 100 VUTI isolates were stored for future characterization and use.

Fifty of the first 100 VUTI isolates were screened by FimA immunoblot after overnight static incubation at 37°C in LB media, to determine strains that expressed type 1 pili. Approximately 50% of the 50 VUTI strains tested expressed some form of FimA, or high levels of another CUP pilus subunit that cross-reacts with the anti-FimA antibody (data not shown). By SDS-PAGE analysis the strain VUTI67 was observed to express a form of FimA similar to UTI89, while strain VUTI73 expressed a form similar to CFT073 (**Figure 41A**). Both VUTI strains formed biofilm levels similar to UTI89 and CFT073 under atmospheric conditions (**Figure 41B**). Upon anoxic culture, both strains VUTI67 and VUTI73 demonstrated reduced FimA protein levels that corresponded to decreased *fim*-dependent biofilm formation (**Figure 41A-B**). Together these data suggest that the oxygen-dependent regulation of type 1 pili expression is not unique to UPEC strain UTI89, and may be conserved across *fim*-expressing *E. coli* strains associated with the urinary tract. Further studies will aim to elucidate if this regulation occurs in other UPEC, as well as non-extraintestinal pathogenic and commensal *E. coli* strains.

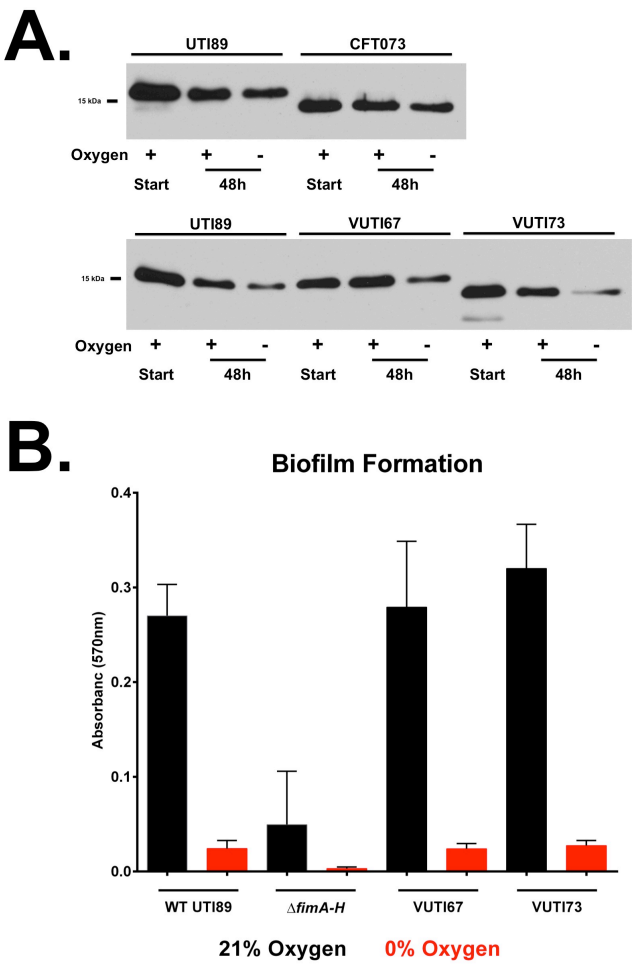

Figure 41. Anoxic repression of type 1 pili appears conserved across *fim*-expressing urinary *E. coli* strains. (A) Representative immunoblot comparing expression of FimA between UPEC strains UTI89 and CFT073, and *fim*-expressing VUMC clinical urinary *E. coli* isolates VUTI67 and VUTI73, after culture in the presence or absence of oxygen for 48 hours. Cultures were started from overnight stocks grown under type 1 pili inducing conditions (static in LB media at 37°C), and cultured statically for 48 hours in LB media at 37°C. **(B)** Biofilm formation at atmospheric and anoxic oxygen conditions for UTI89, UTI89Δ*fimA-H*, VUTI67, and VUTI73. Biofilm levels are presented as the mean with the standard error of the mean, from at least two biological replicates with at least three technical replicates of each biological replicate.

Discussion

This work demonstrates that the ubiquinone 8 synthase UbiI is critical for the appropriate generation of proton motive force in UPEC during aerobic growth, and that its loss impairs the expression of several macromolecular structures that are critical for UPEC biofilm formation and virulence in the urinary tract. Although *E. coli* is a versatile microorganism, able to respire in the presence and absence of oxygen and the presence of different alternative electron acceptors, these data indicate that aerobic conditions are optimal for expression of type 1 pili and interfering with aerobic respiration impairs the ability of UPEC to successfully colonize the murine urinary tract. Using the UTI89Δ*ubiI* strain as a biosensor confirms that the bladder environment contains enough oxygen to promote aerobic bacterial respiration, and induce optimal virulence factor production by UPEC that ascend to this organ. Indeed, studies measuring dissolved oxygen in the urine of human patients place the oxygen concentration at ~4 - 7% (Wang *et al.*, 2008), which is enough to induce aerobic ubiquinone synthesis. This explains both the virulence defects associated with the *ubiI* mutant observed here, and mutants within the TCA cycle previously reported to have severe defects during acute UTI studies (Hadjifrangiskou *et al.*, 2011, Alteri *et al.*, 2009).

Together this supports a model in which deletions in TCA cycle genes or ubiquinone synthesis impairs optimal proton flux, which cannot be transcriptionally bypassed due to the presence of the preferred electron acceptor (oxygen) at high enough concentrations to prevent the exchange of aerobic to anaerobic respiration components. Based on this model, assembly of type 1 pili in UTI89Δ*ubiI* is compromised because of reduced transport of subunits across the inner membrane, and as a result feeds back to repress *fim* operon transcription (**Figure 38 and model Figure 42**). Such feedback has previously been demonstrated for pili assembly mutants such as

UTI89Δ*fimD* and UTI89Δ*fimH* (Greene *et al.*, 2014, Chen *et al.*, 2006). This study and others, suggest that *fim* repression occurs at least in part at the level of the *fimS* promoter switch via imbalanced expression of the Fim recombinases (Greene *et al.*, 2015, Greene *et al.*, 2014). The mechanism by which *fimB/E* transcription and function is controlled in response to changes in proton flux remains unexplored, and is a subject of further study in our lab. This phenomenon appears to be true for other macromolecular structures that rely on Sec-dependent translocation or proton flux for transport or function, since motility and production of S pili is also compromised under reduced proton motive force conditions in the *ubiI* mutant at atmospheric conditions.

Interestingly, under conditions of complete anoxia when UbiI becomes dispensable due to its replacement by anaerobic quinone synthases, or by engagement of the fermentation pathway, most energy-dependent deficits such as motility and production of S pili are restored. This further confirms that anaerobic respiration does not require UbiI in UTI89, and that under such conditions enough energy is being produced to sustain the formation of macromolecular structures. Despite adequate energy generation during anaerobic respiration, production of type 1 pili remains diminished for both wild-type UTI89 and the UTI89Δ*ubiI* mutant. These data corroborate our previous findings that oxygen-deplete conditions specifically repress type 1 pili, but not all other chaperone-usher pathway pili (**Chapter III**). This suggests that the mechanism by which wild-type UPEC respond to anoxic conditions to repress expression of the *fim* operon, is distinct from the proposed mechanism where reduced overall piliation results from compromised proton flux during anaerobic growth in the *ubiI* mutant. **Figure 42** presents a model comparing and contrasting the types of regulation that occur in WT UTI89 and UTI89Δ*ubiI* lending to the repression of type 1 pili.

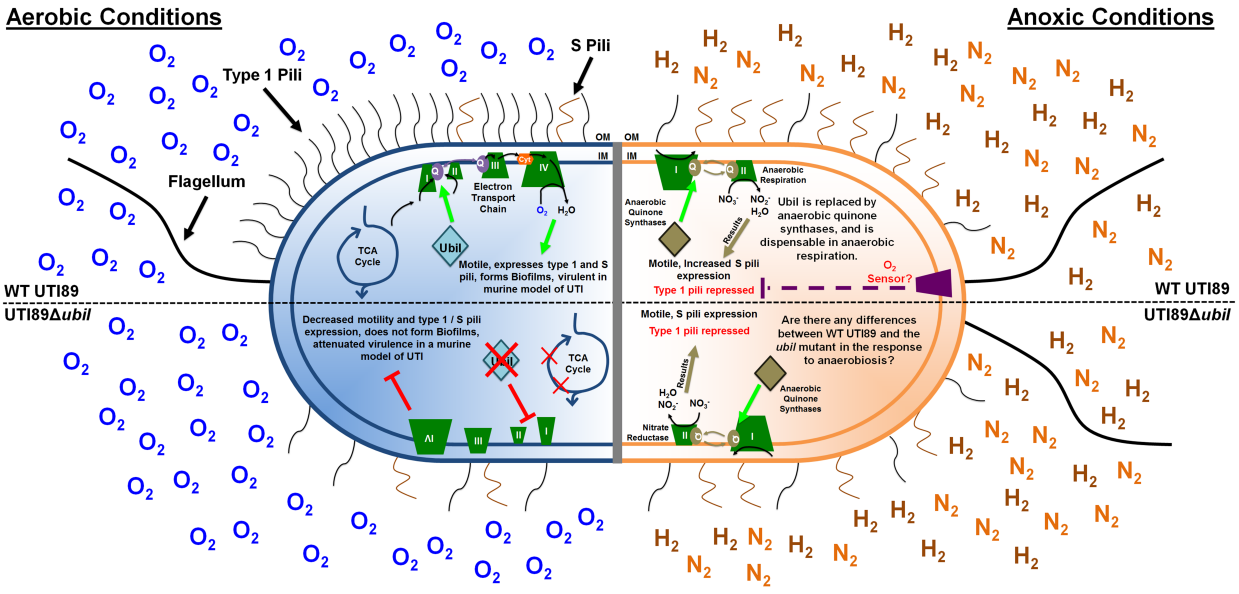

Figure 42. Model depicting potential mechanisms leading to repression of type 1 pili in the wild-type parent and the *ubiI* mutant under aerobic and anoxic conditions. (Left panel) When oxygen is present, aerobic ubiquinone synthesis requires the UbiI enzyme for optimal synthesis of ubiquinones and the generation of appropriate proton motive force to sustain transport across the inner membrane. Deletion of *ubiI* lowers the PMF and compromises ATP-dependent transport. This leads to reduced translocation of Fim components and a negative feedback that turns the *fimS* promoter to the *fim*OFF orientation by the action of the dedicated Fim recombinases that results in lack of fim operon transcription. This mechanism would also explain the reduction in pilus expression in previously published TCA cycle mutants. The mechanism by which reduction in PMF is transduced to the Fim recombinase machinery or genes is still unknown. (Right Panel) Under anoxic conditions, aerobic ubiquinone synthesis by UbiI is dispensable, due to the use of menaquinones for anaerobic respiration or use of the fermentation pathway. Under these conditions, the PMF across the inner membrane is restored, restoring ATP-dependent transport and the elaboration of macromolecular structures on the bacterial surface. However, a yet unidentified mechanism senses the lack of oxygen (or the presence of a fermentation by-product?) and somehow transduces this information to the regulatory network that controls expression of type 1 pili. The result is decreased *fim* expression and thereby pili on the surface of the bacteria, independent of an adequate energy supply typically required for their assembly. Whether this occurs differently in the *ubiI* mutant remains unknown.

Our lab is currently exploring sensing mechanisms that may be directly involved in sensing oxygen fluctuations and transducing them to regulators of FimB and FimE, as well as to pathways ultimately connected to pilus biogenesis. We have ruled out the major respiration two-component system ArcA/B, and determined the regulator FNR is involved in mediating pilus expression (**Chapter IV**). Currently, we are exploring the effects of other potential regulators (OxyR, SoxRS, etc.) in combination with studies aimed at delineating additional factors mediating oxygen-dependent regulation of type 1 pili in multiple UPEC strains. In these studies, the UTI89Δ*ubiI* mutant provides a unique tool to distinguish differences between the oxygen- and PMF-responsive mechanisms that regulate expression of type 1 pili. Analyses presented in **Figure 38D**, which indicate that during anoxic conditions WT UTI89 exhibits a swift repression of type 1 pili, while UTI89Δ*ubiI* appears to have consistently low levels of FimA during both conditions tested, suggest that UTI89Δ*ubiI* may be overall less sensitive to oxygen fluctuations in the surrounding environment.

In summary, emerging research continues to shed light onto the effects of environmental gradients on the expression and function of gene products, especially in the context of pathogenesis. *E. coli,* a traditional commensal of the GI tract, is a facultative anaerobe that has long been thought of to thrive in the near-anoxic environment of the gut. However, recent research indicates that the gut comprises pockets of oxygen and that loss of aerobic respiration compromises *E. coli* fitness in the gut (Jones *et al.*, 2007, Jones *et al.*, 2011). Here, we demonstrate that the same is true for uropathogenic *E. coli* in the bladder environment, building upon previous work demonstrating that aerobic respiration is a critical determinant for fitness in the urinary tract.

CHAPTER VI

TYING IT ALL TOGETHER: FUTURE DIRECTIONS AND BROAD RESEARCH IMPLICATIONS

Bacterial UTIs are among the most common nosocomial infections, accounting for approximately 30% of all hospital-acquired infections (Flores-Mireles *et al.*, 2015). Urinary catheters are the most common indwelling medical device used in hospital settings, with 18-24% of inpatients requiring catheterization (Zarb *et al.*, 2012, Magill *et al.*, 2014). The rates of urinary catheter utilization contribute to the high frequency of hospital-acquired UTI, as highlighted recently by the Centers for Disease Control and Prevention who reported a 6% increase in the incidence rate of CAUTI between 2009 and 2013 (Prevention, Published January 14, 2015.). Bacterial adherence and subsequent biofilm formation on the catheter surface is one of the confounding factors that has thus far prevented the development of effective and reproducible strategies to combat or prevent catheter contamination. The development of distinct subpopulations during biofilm development further enhances resilience of the multicellular community and greatly increases the likelihood of one or more of these subpopulations to survive therapeutic treatment, adding to persistence of biofilm-associated infections (Tolker-Nielsen, 2015). Therefore, delineating the mechanisms that drive the generation of subpopulations could allow for manipulation to synchronize biofilm bacterial populations as a novel method for treatment to combat biofilm-associated infections like CAUTI. Work presented in this dissertation lays the foundation for the development of such future studies.

UPEC account for the vast majority of UTIs and CAUTIs, and with the rise in antibiotic resistance, are becoming increasingly difficult to treat (Flores-Mireles *et al.*, 2015). Prior to the initiation of the herein described studies (summarized in **Figure 43**), knowledge of UPEC biofilm subpopulations was limited to the observation of phenotypic differences in bacterial shape and size induced by varying environmental conditions (Hung *et al.*, 2013a). The IMS studies presented in **Chapter II** of this work demonstrated the ability to decipher bacterial subpopulations within multicellular biofilms based upon the local protein expression profile of the community (**Figure 43A**). As a direct result of developing an approach for the study of biofilm subpopulations, the work presented in **Chapters III – V** uncovered key oxygen-mediated mechanisms that regulate the expression of adhesive type 1 pili in UPEC (**Figure 43C**). Our work determined that anoxic environmental conditions reduced expression of type 1 pili in UPEC strain UTI89, and that this reduction appears to be mediated by three levels of regulation; 1) transcriptionally at the level of the *fimS* promoter switch, 2) at the level of *fim* operon and Fim recombinase gene expression, and 3) at the post-translational level. To further assess these mechanisms and determine their viability to serve as potential therapeutic targets for biofilm-associated infection, future studies will seek to further define their mechanisms of action, as well as identify additional subpopulation-specific targets. To this end, we will:

Further define the mechanism of anoxic transcriptional control of the fimS switch

At the level of the phase-variable promoter, we have shown that anoxic conditions repress type 1 pili expression (**Figure 43D**) partly by promoting an imbalance in Fim recombinase gene expression that favors the *fim*OFF switching machinery to promote inversion of *fimS* to a transcription-incompetent state. Further work is needed to determine if these

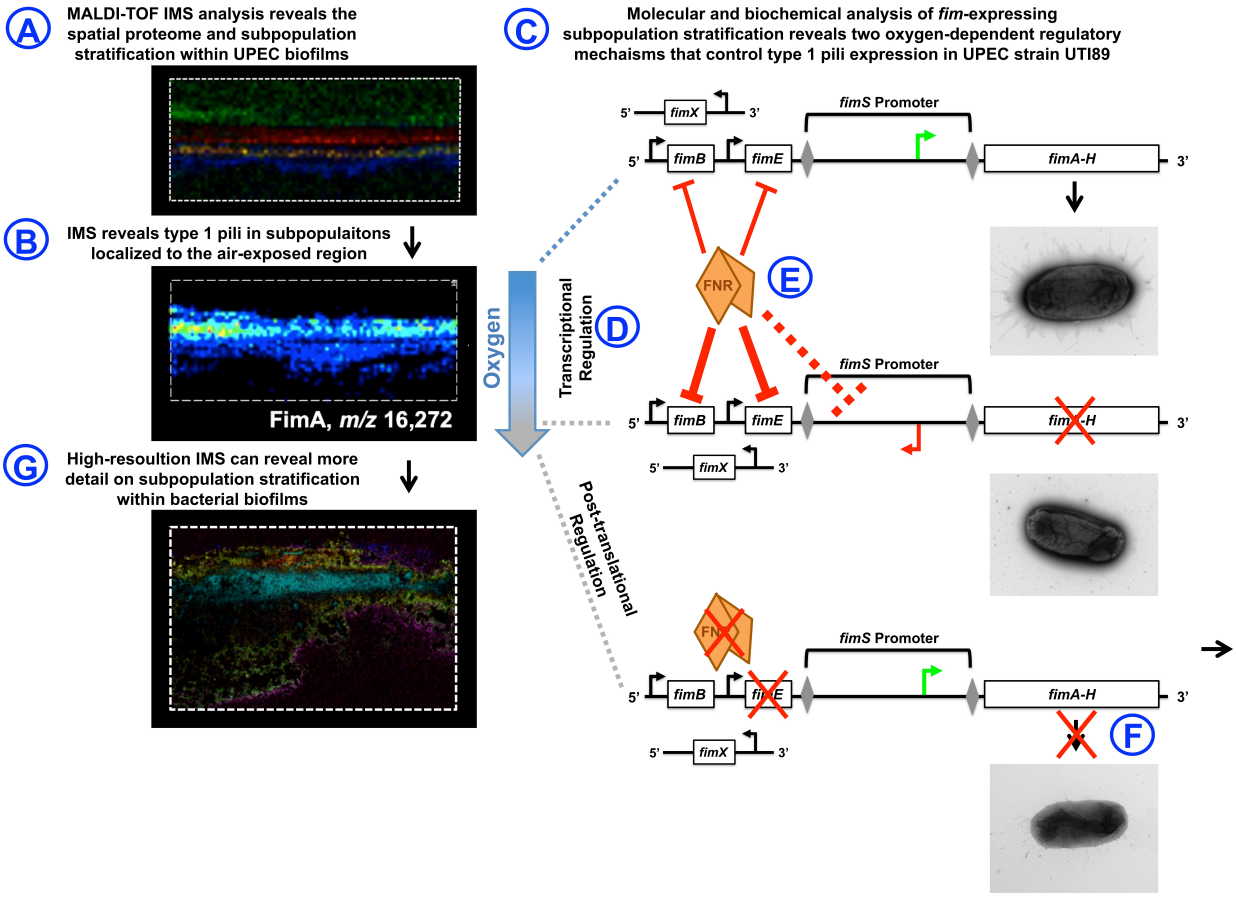

Figure 43. IMS helps to unveil multiple modes of oxygen-dependent regulation of type 1 pili expression in UPEC. (A) MALDI-TOF IMS of the surface-associated UPEC biofilm spatial proteome reveals distinct protein localization within the multicellular community. **(B)** IMS reveled adhesive fiber expression within distinct biofilm subpopulations. Type 1 pili were consistently observed only within subpopulations comprising the air-exposed region of the biofilm. **(C)** Molecular and biochemical characterization of this unique localization, led to the discovery of at least two regulatory mechanisms that control expression of type 1 pili in UPEC in response to the environmental oxygen levels and/or bacterial respiration state. **(D)** One-mechanism functions at the transcriptional level, by promoting the inversion or maintenance of the *fimS* promoter in a transcription-incompetent orientation. **(E)** The regulatory protein FNR functions to promote this transcriptional regulation, through repression of Fim recombinase expression under both atmospheric and anoxic conditions, among other ways. Analysis of recombinase and operon transcript levels, suggest a slight increase in FNR-mediated regulation under anoxic conditions (indicated by bolder red lines). **(F)** Beyond the transcriptional regulation, data suggest the presence of an additional mechanism that functions at the post-translational level to prevent pilus elaboration in the absence of oxygen. Mutants that express type 1 pili subunits under anoxic conditions fail to elaborate functional pili on the bacterial cell surface. This suggests a mechanism that serves as a control point to prevent pilus elaboration even when subunits are expressed, under unfavorable conditions. **(G)** High-resolution IMS provides more detailed information on biofilm subpopulations, and could afford the ability to examine subpopulation stratification directly within catheter-associated biofilms.

alterations in *fim* recombinase gene expression correspond with alterations in protein expression. To date, we do not have antibodies specific for the FimB, FimE, or FimX recombinases. To address this issue, we are generating tagged versions of each recombinase (Myc-tagged FimB, 6x histidine-tagged FimE, and FLAG-tagged FimX), which will be knocked into the UTI89 chromosome (Zhang *et al.*, 2016) and will allow for protein quantification by immunoblot under physiological conditions. In parallel, FimB/FimE/FimX protein will also be purified using the tagged-constructs, and submitted to the Vanderbilt Antibody and Protein Resource core for the production of specific antibodies. These additional tools will help elucidate whether the observed changes in recombinase transcript levels in fact result in alterations in protein abundance, as we hypothesize that they will.

The ability to monitor recombinase expression at the transcript and protein levels, will allow for the identification of factors that mediate the imbalance in Fim recombinase levels under anoxic conditions. To date, we have ruled out the anaerobic-sensing ArcAB two-component system as potential anoxic regulatory factor. We have also examined the oxygen-sensing regulatory protein FNR for potential modulation of anoxic *fim* regulation. Preliminary data suggest that FNR functions to regulate *fim* expression under both atmospheric and anoxic conditions, yet it demonstrates more pronounced regulation under anoxic conditions. To further examine this probable regulation, future studies will seek to:

Determine the impacts of FNR-mediated fim regulation at atmospheric and anoxic conditions

Our studies to date suggest that FNR functions under both atmospheric and anoxic conditions to regulate *fim* expression in UPEC strain UTI89 (**Figure 43E**). Under atmospheric conditions, deletion of *fnr* led to an increase in total FimA protein levels and resulted in

increased numbers of pili on the cell surface compared to the WT UTI89 strain. Further FNR-mediated regulation under atmospheric conditions was observed through a reduction in flagellar-based motility upon deletion of *fnr*. This FNR-mediated regulation under atmospheric conditions is intriguing, because as mentioned in **Chapter IV**, in the presence of oxygen FNR is found in a non-functional or apo state. Previous studies performed by Barbieri *et al.*, demonstrated that in UPEC strain CFT073 FNR functions to control *fim* expression in the presence of oxygen. Together, our data and these previous studies suggest a role for FNR in the non-functional or apo state to regulate *fim* expression. Future studies will aim to determine the mechanisms of both atmospheric and anoxic regulation of *fim* expression by FNR.

As mentioned in **Chapter IV**, protein levels of FNR do not change during growth under aerobic or anoxic conditions (Unden *et al.*, 2002). Deletion of *fnr* from UTI89 decreases both atmospheric and anoxic inversion of the *fimS* promoter to the transcription-incompetent *fim*OFF orientation, a phenomenon that could be the result of FNR repressing *fimB/fimE* expression (**Figures 27-30**). To definitively assess the interactions of active and inactive forms of FNR with the *fimB/fimE/fim* operon promoters, *in vitro* binding assays with active and inactive FNR are needed. Using EMSAs, Barbieri *et al.* demonstrated interactions of purified FNR with the *fimS* promoter region of UPEC strain CFT073 (Barbieri *et al.*, 2014). In these studies, a FNR dimer variant (fnr(D154A)$_2$) was used that has been previously shown to functionally bind DNA in the presence of oxygen (Barbieri *et al.*, 2014, Shan *et al.*, 2012). We received this construct mimicking the "activated" FNR state typically triggered under anoxic conditions (gift of Drs. Ganwu Li and Aixin Yan). [pET28a-(fnr(D154A)$_2$)] will be used to express and purify this oxygen-functional version of FNR, and further evaluate "activated" FNR interactions with the promoters of *fimB/fimE/fimS*. To examine the interactions of "in-active" FNR with theses

promoters, we will generate a 6x-His tagged version of native FNR for protein purification. Once purified this "in-active" form of FNR can be used to probe interactions with the promoters by EMSA, in comparison to the studies with "active" FNR mentioned above. Our data also suggest that if not directly interacting with the *fimS* promoter under anoxic conditions, FNR could be promoting the interactions of the FimE recombinase with the *fimS* promoter. In order to determine if FNR influences FimE interactions with the *fimS* promoter, we have generated an overexpression construct that codes for a 6x-histidine tagged version of FimE (pET28a-FimE) for protein purification. FimE will then be examined for interactions with the *fimS* promoter via EMSA in the presence and absence of active and inactive FNR. These experiments will allow us to delineate if FNR interacts directly with, or promotes interactions of other regulators, with Fim recombinase and *fim* operon promoters in the presence and absence of oxygen.

During the examination of the impacts of FNR on *fim* expression, it was observed that deletion of *fnr* significantly reduced bacterial flagellar-based motility under atmospheric conditions and completely ablated motility under anoxic conditions compared to WT UTI89 (**Figure 32**). Analysis of UTI89Δ*fnr* grown under atmospheric and anoxic conditions by TEM, demonstrated altered flagellar structure and increased shedding of flagella under both conditions (**Figure 32**). Along with alterations in flagellar structure and function, UTI89Δ*fnr* was observed to extrude branched surface appendages not reminiscent of type 1 or other CUP pili (**Figure 32**). Further studies will determine the identity of these structures, utilizing proteomics or NMR-based identification methodologies as required (McCrate *et al.*, 2013). A simultaneous method that can be used to potentially identify these structures, as well as validate FNR regulation of Fim recombinases and help to determine the impacts of *fnr* deletion on motility, would be RNA sequencing (RNA-seq). RNA will be obtained from WT UTI89 and UTI89Δ*fnr* grown under

atmospheric and anoxic conditions, and submitted for RNA-seq. This comparison will determine genes that are either up- or down-regulated under anoxic compared to atmospheric conditions in WT UTI89, and allow for the determination of altered gene expression upon the deletion of *fnr* under both conditions. Complementary RNA-seq studies performed with RNA obtained from bacteria cultured in urine, will allow for a comparison of FNR regulation in a physiologically relevant medium.

Barbieri *et al.* demonstrated that FNR functions in CFT073 to promote expression of *fimB* in the presence of oxygen, with no observable impacts on *fimE* expression (Barbieri *et al.*, 2014). Our preliminary analyses with UPEC strain CFT073, demonstrated a reduction in FimA protein levels under anoxic conditions similar to UTI89 (**Figure 41**). However, our preliminary data in UTI89 suggest that FNR represses *fimB* and *fimE* expression under atmospheric and anoxic conditions. If FNR fails to interact with and promoter the expression of *fimE*, as determined by EMSA studies described above, there must be another explanation for the increase in *fimE* transcript levels observed upon *fnr* deletion. Previous studies have determined that placing the *fimS* promoter in the *fim*OFF orientation, places *fimE* mRNA transcripts in a position to be more prone to 3' to 5' degradation (Sohanpal *et al.*, 2001). Deletion of *fnr* from UTI89 reduced the *fim*OFF switch under both atmospheric and anoxic conditions. Therefore, our observed increase in *fimE* expression upon deletion of *fnr* could be the result of increased *fimE* transcript stability and protection from degradation. One difference between the Barbieri *et al.* studies and our own, was the way in which recombinase and operon expression was measured. Barbieri *et al.* used transcriptional fusions of the individual promoters with *lacZ* to measure expression, while our TaqMan based approach directly measures mRNA transcript levels. Therefore increased stability of *fimE* transcript levels would only be detectable through direct

measurement of transcript as we have performed in these studies, and not through those methods used by *Barbieri et al.* This may help to explain the differences in FNR impacts observed between CFT073 and UTI89. To determine if deletion of *fnr* increases *fimE* transcript stability in UTI89, we will utilize a ribonuclease protection assay comparing *fimE* mRNA obtained from WT UTI89 and UTI89Δ*fnr* cultured under both atmospheric and anoxic conditions. To determine if the same is true for CFT073, we have generated our own *fnr* deletion in UPEC strain CFT073 and will examine recombinase and operon transcript levels by qPCR, as well as stability of *fimE* transcript. Combined with the EMSA analyses, these studies will allow us to determine the mechanism responsible for increased *fimE* transcript levels upon deletion of *fnr*.

Analysis of surface pili levels by TEM in both the WT UTI89 and UTI89Δ*fnr* strains, demonstrated that *fim* expression within a static culture population is heterogeneous in nature. Even during growth under atmospheric conditions, the oxygen concentration will vary within different regions of the culture, as the bacteria utilize the available oxygen and depending upon the proximity to the air-exposed culture surface. Therefore, there is the possibility that the FNR-mediated regulation observed in atmospheric cultures, may be the result of subpopulations that occupy anoxic or semi-anoxic regions of the culture. Therefore, future studies will seek to address the impact of culture subpopulation development on FNR-mediated *fim* regulation. First, establishment of the oxygen gradients within atmospheric cultures will be important. Oxygen-specific probes (such as those used in our collaborative studies with the MSU CBE, mentioned below) can be used to monitor the levels of oxygen within defined regions of the culture over the course of 48 hours. These measurements will also be performed using anoxically grown cultures, to determine the rate of utilization of the initial dissolved oxygen within the culture, and to compare to those measurements obtained from atmospheric cultures.

To determine the impact of FNR-mediated regulation on *fim* expression within culture subpopulations, we would need to develop methods for the isolation of individual subpopulations. One-way to achieve this isolation, would be through the use of fluorescence activated cell sorting (FACS). Using this technique we could isolate out dead vs. alive bacterial populations, and then sort the live populations using an antibody against the type 1 pilus terminal adhesin FimH. Fluorescent intensity of interactions with the antibody, will allow us to sort bacteria based upon the level of type 1 pili on the cell surface (from no to high level expression). Sorting of these subpopulations into a non-replicative medium (such as PBS), will allow us to further dissect the contribution of FNR to *fim* regulation within each subpopulation. Along with FACS another method that could be employed for subpopulation isolation, is laser-based optical tweezer methodologies. Conversely, our studies can also be performed while continually supplying oxygen to atmospherically grown cultures. This would allow for a more consistent oxygen concentration within the culture, and the ability to determine if FNR remains active when oxygen levels remain steady.

Despite demonstrating regulation under both oxygen conditions, FNR did show slightly more pronounced regulation under anoxic conditions. These data suggest that FNR may play a role in mediating the anoxic imbalance of Fim recombinase expression, however FNR is not the major regulator mediating this anoxic transcriptional control. Therefore to fully understand the anoxic regulation of *fim*, future studies will continue to identify modulators or mechanisms modulating the imbalance in Fim recombinase expression resulting in anoxic transcriptional control of *fim* expression. To this end, we will:

Identify additional anoxic regulators of fim expression and biofilm formation

Given that FNR appears to only partially influence anoxic *fimS* inversion in UPEC strain UTI89, it is likely that another regulatory factor(s) are the primary mediators regulating the anoxic transcriptional control of *fim* expression. Therefore, the actual sensor(s) detecting oxygen fluctuations and transducing them eventually to the *fim* expression/biogenesis machines remain to be identified. One way to address this would be through the high-throughput screening of a transposon mutant library constructed from UTI89. Mutants showing decreased biofilm formation under atmospheric conditions, will elucidate factors important for biofilm formation in the presence of oxygen. However, mutants that show increased *fim*-dependent biofilm formation under anoxic conditions could represent factors that play a role in anoxic repression of type 1 pili. Our lab has recently generated a transposon mutagenesis library in UTI89 containing 30,000 mutant strains (representing ~6x coverage of the UTI89 genome). Other studies in the lab are currently testing this mutant library for the ability to form *fim*-dependent biofilm under atmospheric and anoxic conditions. Mutants with increased anoxic biofilm levels will be sequenced to determine the site of transposon insertion, such that clean deletion mutants of the corresponding genes can be generated and validated for their effects. These mutants will then be further characterized to determine their role in anoxic repression of *fim* expression or pilus elaboration.

In addition to screening a library of transposon mutants, *in vivo* experiments to delineate how the *fimS* promoter is regulated under anoxic conditions (EMSA assays described in the section above) can be extended to "bio-panning" analyses, in which the *fimS* promoter is used as bait for the interaction with potential regulatory proteins under anoxic conditions. Identification of novel proteins that interact with *fimS*, can be performed using a DNA pull-down assay. This

assay would function similar to a co-immunoprecipitation assay used to identify protein-protein interactions. Iterations of the *fimS* promoter in the *fim*ON and *fim*OFF orientations will be amplified using primers designed for the EMSA assays mentioned above, and tagged with biotin. Amplified tagged-promoter will then be incubated with atmospheric or anoxic cell lysates, followed by purification of the promoter-protein complexes, and identification of interacting proteins by SDS-PAGE and LC-MS/MS. This assay should demonstrate the presence of known *fimS*-binding proteins, and allow for the identification of any novel interacting protein species. Novel interacting species, specifically those observed to interact under anoxic conditions, will then be examined for their role in regulating *fim* expression. Together, these studies will allow for the identification of additional regulators of *fim* expression, and potentially the regulator(s) responsible for mediating the anoxic transcriptional regulation.

Determine the impacts of bacterial respiration state on type 1 pili expression

As a facultative anaerobe, *E. coli* strains can respire aerobically or anaerobically with the use of alternative terminal electron acceptors. While oxygen is the preferred terminal electron acceptor, in the absence of oxygen nitrate, DMSO, TMAO, and fumarate can be used if present and the appropriate corresponding enzymes are expressed (Unden and Bongaerts, 1997). Lack of a terminal electron acceptors forces the utilization of mixed acid fermentation, which has the lowest energy yield of all respiration modes (Unden and Bongaerts, 1997). While the standing dogma in the field used to be that *E. coli* respire anaerobically in host niches, recent work including what is presented here, argues against this model. The studies presented here demonstrated that UPEC respire aerobically in the bladder, and that aerobic bacterial respiration supports the production of type 1 pili, corroborating previous reports that the aerobic arm of the

TCA cycle and gluconeogenesis are important for the expression of type 1 pili (Hadjifrangiskou *et al.*, 2011, Alteri *et al.*, 2009).

Additionally, even though aerobic respiration is critical for the expression of type 1 pili, oxygen sensing appears to be acting separately but in parallel to regulate *fim* genes. Here we have shown that growth under the least energetically favorable conditions (fermentation), produces enough PMF to energize Sec-dependent translocation of other CUP and flagellar components, and it produces enough proton flux to power the flagellar motor. These observations rule out diminished energy production as a blanket regulator of type 1 pili.

While oxygen appears to serve as an environmental cue for the regulation of *fim* expression mediated by FNR, the impact of bacterial respiration state on *fim* expression suggests that it is not necessarily the only cue. While environmental conditions supportive of aerobic bacterial respiration were observed to be the most conducive to expression of type 1 pili, fermentative conditions actively supported repression. Therefore, it is possible that a byproduct of the mixed acid fermentation pathway (e.g. lactate, acetate, formate, succinate, ethanol, carbon dioxide, or hydrogen) could serve as an additional environmental cue to promote repression (Clark, 1989). To begin to address this hypothesis, we will examine *fim* expression under atmospheric conditions in cultures spiked with concentrations of each fermentative byproduct, or grown under increasing concentrations of carbon dioxide and hydrogen. If the byproduct supports *fim* repression, we would expect to observe decreased total FimA protein levels similar to anoxic growth conditions. If a fermentative byproduct is observed to promote *fim* repression, further studies will be performed to determine the mechanism by which it functions to regulate expression.

Determine the mechanism of anoxic post-translational control of type 1 pili

As the work presented here demonstrates, expression of type 1 pili is subject to multi-factorial control at the transcriptional and post-translational levels in response to several environmental signals, and these studies add oxygen to the roster of cues that are somehow transduced to the pilus gene operon and at stages downstream of transcription. Our analyses examining the oxygen-dependent transcriptional regulation of *fim* in response to FNR, also led to the discovery of a secondary checkpoint that functions downstream of the *fimS* promoter to regulate *fim* expression under anoxic conditions (**Figure 43F**). Deletion of *fimE* or *fnr* restored anoxic total FimA protein levels, yet failed to restore anoxic *fim*-dependent biofilm formation or surface pili levels (**Figure 32**). These data suggest an additional level of regulation that occurs post-translationally to control the elaboration of functional type 1 pili in the absence of oxygen. TEM analysis of WT UTI89 as well as *fimE* and *fnr* deletion mutants, showed a decreased number of pili on the bacterial cell surface under anoxic conditions. Given that the *fimE* and *fnr* mutants make FimA under anoxic conditions, it is likely that the protein subunits are simply not assembled into functional pili on the cell surface. If so, it is likely that unassembled FimA subunits are accumulating within the bacterium. To determine if this is the case, we will examine UTI89Δ*fimE* and UTI89Δ*fnr* cultured under anoxic conditions through cell fractionation to examine for unassembled pilus subunits by immunoblot. Typical immunoblot analysis for FimA requires acidification and heating of the sample prior to SDS-PAGE separation, to break apart assembled pili into detectable monomers of FimA (Floyd *et al.*, 2015b). Therefore, by not acidifying samples prior to SDS-PAGE analysis and comparing to acidified samples, we can determine the amount of assembled FimA compared to total FimA protein levels. Each fraction form the cell lysates will then be examined for unassembled and total FimA protein levels. This

will allow for the determination of buildup of unassembled protein within the bacterial cell. If there is an observed increase in unassembled FimA in the periplasm of the cell, we can also probe for expression levels of the stress-response protease DegP by qPCR (Lipinska *et al.*, 1990). Increased levels of *degP* expression would suggest increased periplasmic stress, validating accumulation of unassembled FimA.

For CUP P pili in UPEC, the PapH protein serves as a terminator to control pilus length, as well as an anchor to hold the pilus structure in the outer membrane (Volkan *et al.*, 2013). However to date, no such terminator/anchor has been identified for type 1 pili. TEM analysis of *fimE* and *fnr* deletion mutants under anoxic conditions appeared to show some increase in pili sheared from the cell surface within the cultures. Therefore, anoxic post-translational regulation of pilus elaboration could result from the inability to anchor assembled pili to the outer bacterial membrane. To determine if there is increased sheering, lending to decreased functional pili on the cell surface, supernatants of atmospheric and anoxic cultures of WT UTI89 and the *fimE*/*fnr* mutants will be obtained. Pili sheared and secreted in the media can be precipitated from the supernatants, and quantified by both FimA immunoblot and TEM analysis (Hahn *et al.*, 2002a). Atmospheric cultures for all strains should show minimal numbers of pili within the supernatant. However, if the anoxic post-translational mechanism results from lack of pilus retention, *fimE* or *fnr* mutant anoxic supernatants would likely show increased pili levels by TEM and FimA immunoblot.

The only gene with a product of unknown function in the *fim* operon is *fimI* (**Figure 15**). If anoxic post-translational regulation occurs through lack of pilus retention, it is likely the result of decreased ability to anchor the structure in the outer membrane. Given that there is no known function of FimI, we will examine its potential to serve as a terminator or anchor for type 1 pili.

Our lab has previously constructed an over expression plasmid construct containing *fimI* (pTRC99a-*fimI*). To determine if FimI serves as a terminator protein for type 1 pilus length, this construct will be placed into UTI89 and pilus length under type 1 pili inducing conditions will be examined by TEM. Over expression of a terminator protein will result in significantly shorter pili compared to the WT UTI89 control. Therefore if FimI functions as a terminator for type 1 pili, overexpression would result in short stubby pili compared to the WT control. If the anoxic post-translational regulation observed in the *fimE* and *fnr* mutant strains results from a lack of pilus retention, we can utilize these strains to determine if FimI functions as an anchor protein for type 1 pili. In this case if FimI serves as an anchor protein, over expression in either deletion mutant should increase the number of pili on the cell surface under anoxic conditions. Coinciding with the *fimI* overexpression studies, we can also generate a functional deletion mutant (in which a premature stop codon is inserted into the *fimI* coding sequence) lacking FimI to test its effects on type 1 pili formation. Impacts of functional deletion of *fimI* can be examined using FimA immunoblot, TEM, *fim*-dependent biofilm assay, and hemagglutination assay to determine the ability of UTI89 to produce and elaborate functional pili in the absence of FimI. These experiments are currently in the process of being initiated in our lab, and have the potential of uncovering new insights into the regulation and biogenesis of type 1 pili.

Develop an in vitro system for the formation of catheter-associated UPEC biofilms

Our studies have identified novel mechanisms for environmental induced regulation of type 1 pili within UPEC strain UTI89. However, so far our studies have largely examined this regulation within planktonic bacterial cultures. In order to determine if this altering this regulation could serve as a potential anti-biofilm strategies, particularly for urinary catheter-

associated biofilms, we need to examine this regulation within a more relevant model system. Catheter-associated biofilms formed within patients may vary significantly in terms of their architecture, total volume, and biomass depending upon the specific UPEC strain. Therefore, in order the analysis of biofilms formed directly on urinary catheters must be performed. To this goal, we have established collaboration with the Center for Biofilm Engineering (CBE) at Montana State University (MSU). The MSU CBE is a world-renowned institute with expertise in all areas of biofilm research, including urinary catheter-associated biofilms.

In collaboration with the CBE, we have established a protocol for the formation of biofilms onto silicone urinary catheters using a flow reactor setup *in vitro*. Bacteria are introduced and allowed to colonize the urinary catheter under conditions that closely simulate the host environment (e.g. low flow rate, artificial urine, 37°C, ~7% oxygen). Using this approach, mature biofilms form by 72 hours of incubation, which can readily be observed on the catheter material using confocal microscopy (**Figure 44**). Currently, the thickest point of these resulting biofilms is only approximately 10μm thick (~10-20 bacteria). Current method development is underway with the MSU CBE, to increase the size of the catheter-associated biofilm in order to better identify and characterize catheter-associated subpopulations.

Though no analyses have been performed yet, owing to the methodology modifications that are still required (as described below), future studies will focus on determining whether *in vitro* modeled catheter-associated biofilms can yield meaningful reproducible data by MALDI-TOF IMS. Imaging of these catheter-associated biofilms can be performed from a top-down approach at the surface level, and/or by imaging biofilm cross-sections (such as those shown in **Figure 44**) across the catheter. The former method has the potential to capture changes based on flow, including how fluctuations in oxygen and nutrients (from high concentrations at the

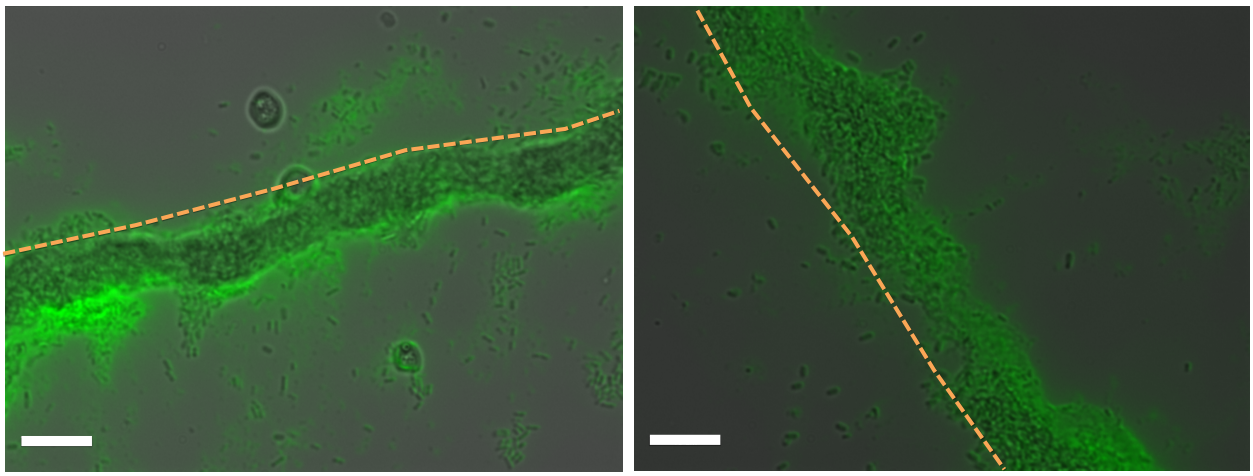

Figure 44. Flow reactor allows for UTI89 biofilm formation onto silicone urinary catheters *in vitro.* These experiments were performed by the Center for Biofilm Engineering at Montana State University, as a part of an active collaboration with our laboratory. Biofilms were grown in artificial urine media (pH 6.7). Prior to inoculation with bacteria, the catheter was equilibrated for 30 minutes with media. The catheter was then seeded with 2mL of UTI89 culture grown under type 1 pili inducing conditions, and bacteria were allowed to adhere with no flow for 2 hours. Flow was then established at 0.75 mL/min and the catheter was incubated at 37°C for 72 hours. Following incubation, the catheter lumen was filled with carboxymethylcellulose for removal of the resulting biofilm. Biofilms were then cryo-sectioned, and images obtained by confocal microscopy using DIC and a live-dead stain. Images are representative of different regions of biofilm obtained from one catheter. Scale bar = 10μm

catheter inflow, to low concentrations at the catheter outflow) alter biofilm physiology along the catheter. The latter method, however, has the potential to provide information on the subpopulations that form within the biofilm in response to alterations in environmental gradients at varying depths within the biomass. Both methods would provide novel information on the underlying mechanism and regulation of biofilm formation on indwelling urinary catheters.

To further enhance the observations made, the flow reactor for *in vitro* catheter-associated biofilm formation has a diverse range of parameters that can be changed for comparative analysis of how varying host environmental conditions will impact biofilm formation on the indwelling catheter. The growth medium used in the *in vitro* setup can be altered, allowing for the use of varying artificial media with different nutrient compositions or concentrations, as well as the use of donated human urine, which could come from patients with different disease state backgrounds (e.g. urine from patients with diabetes or other metabolic disorders). The *in vitro* system also allows for the regulation, and measurement of, oxygen concentration within the media. This would allow for the opportunity to determine the impacts of increased or reduced urine oxygen concentration on the development of biofilm onto the catheter surface. Therefore, the *in vitro* biofilm system has the potential to reveal invaluable insights into the mechanisms underlying catheter-associated biofilm formation.

Refine MALDI-TOF IMS methodologies for high-spatial resolution analysis of UPEC biofilms and catheter-associated biofilms

We have demonstrated how MALDI-TOF IMS is a powerful tool for the identification and visualization of UPEC biofilm subpopulations. However, so far our MALDI-TOF IMS studies have only examined biofilms cultured directly onto electrically conductive glass slides.

Before analysis of more clinically relevant catheter-associated biofilms can be performed, slight adjustments to our current methodologies must be made in order to enhance IMS image resolution, and maximize the information obtained.

The MALDI-TOF IMS studies performed here were executed at an imaging resolution of 150 μm across the biofilm. This step size encompasses ~75-300 bacterial cells per analysis point, given that the UPEC cell size ranges between ~0.5 to 2 μm in length (**Figure 7**). Variations in environmental gradients can occur on very small scale. Therefore, to determine the true extent of subpopulation formation and augment the number and types of subpopulations observed, the imaging resolution needs to be increased to sample fewer bacteria at each point within the array. Using surface-associated biofilms formed by *K. pneumoniae* as a tool for further method development we have begun to increase the resolution at which IMS analyses are performed, beginning by testing analyses with a 50 μm imaging array. When imaged at 150 μm resolution three distinct protein stratification patterns had been observed within surface-associated *K. pneumoniae* biofilms (**Figure 10**), as was the case with UPEC biofilms. Increasing the resolution to 50μm resolved six distinct protein stratification patterns within the *K. pneumoniae* biofilms (**Figure 45**). Continued development of high-resolution biofilm imaging, has the potential to further increase the number of overall subpopulations that can be identified *in situ* and over time, facilitating a thorough molecular "deconstruction" of biofilm composition (**Figure 43G**). The ultimate goal is to increase the resolution of the IMS methodologies to a point where each point in the array encompasses only one to two bacteria (e.g. 1-2 μm). This would allow for the most detailed analysis of biofilm subpopulations, and provide the ability to more closely examine individual bacterial interactions.

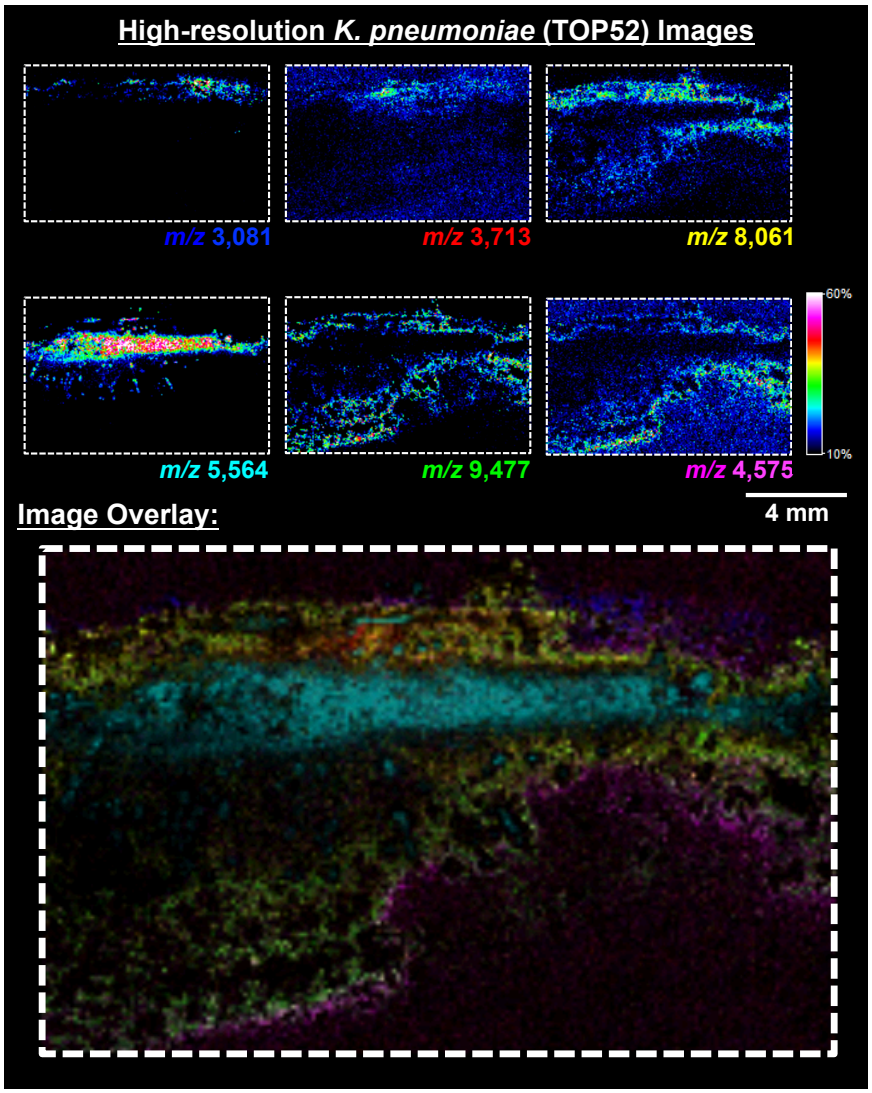

Figure 45. High-resolution MALDI-TOF IMS reveals increased diversity of distinct protein localization patterns within *Klebsiella pneumoniae* biofilms. Representative ion images depicting protein localization patterns observed in *K. pneumoniae* biofilms after 48 hours. Images used were from the same IMS analysis, obtained at a 50 µm spatial resolution. The average spectrum was normalized to the total ion current of the analysis, and the mass-to-charge (*m/z*) ratio of each selected ion is given. Images are shown as ± 5 Da for each *m/z* species. Data are presented as a heat map intensity of relative abundance from 10 (blue) – 100% (Red/White). Overlay images are presented using the same criteria, with single color distribution instead of a heat map from 10 - 100% intensity. Scale bar, 4 mm. Data processed and presented as outlined in Figure 8.

Along with increasing the imaging resolution, altering the matrix used for MALDI ionization will also allow for a more detailed analysis of the biofilm proteome. Our initial studies only identified 6 of 60 proteins observed by IMS. Increasing the range in proteins detected will also allow for more detailed characterization of the types of subpopulations that exist within the biofilm, and the ability to garner a deeper understanding of their role and regulation within the multicellular community. Altering the type of matrix used for IMS analyses will change the profile of proteins that are observed. Our initial studies utilized a mixture of DHB/CHCA that was specialized for low molecular weight protein species. The same analyses can be performed with matrices that allow for ionization of larger molecular weight proteins (e.g. sinipic acid, DHA, etc.) or the creation of multiple charge state species (e.g. 2-NPG). While altering the matrix used for the analysis can increase the range of proteins detected, further work is also needed to identify the protein species being observed. To this end, we will perform LC-MS/MS analysis or MudPIT analysis on enzymatically digested biofilm lysates for each bacterial strain used for IMS analysis. These analyses will provide for the development of a biofilm proteome library for each bacterial strain (or species), and provide a reference to initiate the identification of signals observed by IMS.

Another method for the identification of biofilm proteins would be to use *in situ* enzymatic digestion. For this method, proteolytic enzymes (e.g. trypsin) are applied directly to the biofilm prior to IMS analysis. The enzymatically treated biofilm is then covered with a MALDI matrix suited for peptides, and analyzed by IMS. These techniques allow for the simultaneous localization and identification of proteins within a single analysis. The applicability of *in situ* enzymatic digestion for bacterial biofilm analysis could present some challenges. From our studies to date, we know that we observe both intracellular and extracellular proteins by

IMS. This suggests that during the IMS analysis, bacterial cells are lysed open from laser ablation thus allowing for the detection of intracellular proteins. Therefore prior to IMS analysis the cells largely remain intact, which could prevent access of the proteolytic enzyme to the intracellular compartment. Also, encapsulation of the bacteria by the ECM could hinder penetration of the proteolytic enzymes even to the cell surface. So while *in situ* enzymatic digestion should be considered for the identification of biofilm proteins, it could also present many challenges.

While we began our studies examining UPEC biofilm subpopulations with analyses looking specifically for differences in protein expression patterns, IMS methodologies can also be tailored to examine for differences in small molecule or lipid patterns that can also be indicative of distinct biofilm subpopulations. Analysis of the lipid and small molecule profile of bacterial biofilms by IMS would further enhance the information obtained. The ability to examine small signaling molecules could offer insights into the pathways UPEC use to establish and maintain multicellular community structure. These analyses could offer further insight for the development of potential strategies to prevent biofilm formation or abolish formed structures. These improvements to the IMS methodologies we have used to date, will greatly enhance our ability to examine biofilm subpopulations within intact communities.

Examine the stratification of fim-expressing and other subpopulations within catheter-associated biofilms formed by different urinary E. coli strains

Optimization of our IMS methodologies will afford us the ability to analyze subpopulation stratification within biofilms formed using the *in vitro* catheter-associated biofilm system (described above). First, we will use the system to examine the stratification of *fim*-

expressing subpopulations within catheter-associated biofilm formed by UTI89. These studies will allow us to determine if catheter-associated biofilms demonstrate air-exposed specific localization of *fim* expression, similar to the biofilms cultured onto the electrically conductive slides. This would be the first step in determining if the oxygen-dependent regulation of type 1 pili is important for the development of catheter-associated biofilms. As described above, we can also modulate the oxygen concentration within the *in vitro* biofilm reactor to levels below, at, or above physiological bladder concentrations, to determine how oxygen drives stratification of *fim*-expressing subpopulations on the urinary catheter. Together, these studies would allow us to determine if modulation of the oxygen-dependent regulation of type 1 pili in UPEC, could be a suitable target for strategies to prevent or abolish catheter-associated biofilm.

Along with the analysis of UTI89, our *in vitro* reactor and IMS methodologies will also allow us to examine differences in subpopulations within catheter-associated biofilms between different UPEC strains. To begin these studies we have started collaboration with Drs. Charles Stratton and Jonathan Schmitz, at the VUMC Clinical Microbiology Laboratory, for the establishment of the urinary *E. coli* isolate (VUTI) database as described in **Chapter V**. We will utilize begin by identifying VUTI clinical isolates that have the ability to form biofilms, using the 96-well PVC plate assay. Those isolates that form biofilms can then next be tested for their ability to form biofilms on urinary catheter material, using our *in vitro* reactor system. Those isolates that do form catheter-associated biofilms will be analyzed by IMS. These strains will also be serotyped, and have their genomes sequenced for classification and comparison. These analyses will allow us to compare the types of subpopulations that exist between different urinary *E. coli* strains, and to determine how conserved subpopulations are across different strains. For those strains that express *fim*, these studies offer us the ability to compare the

stratification of type 1 pili between the strains. This will allow us to further access the ability to target the oxygen-dependent regulation of *fim* as a potential therapeutic target.

Examine subpopulation stratification in catheter-associated biofilms obtained from CAUTI patients

The ultimate goal of our studies is to leverage the methods developed from the use of the *in vitro* catheter-associated biofilm system, to be able to use the IMS technology for the analysis of catheters obtained directly from CAUTI patients. These studies will be conducted as a part of our collaboration with Drs. Charles Stratton and Jonathan Schmitz, at the VUMC Clinical Microbiology Laboratory. For the pioneering studies, we will focus on CAUTI patients determined to be mono-infected with *E. coli*. Over a set period of time, all catheters possibly associated with a CAUTI will be collected and correlated with the corresponding urine sample collected from the same patient. Catheters and corresponding urine samples that test positive for an *E. coli* mono-infection will be used for further analysis. *E. coli* strains will be characterized by serotyping and whole genome sequencing. Catheters will be stained with crystal violet to highlight the biofilm region, and will be analyzed by MALDI-TOF IMS. Additionally, a section of the biofilm-containing part of the catheter will be removed, and bacteria removed via sonication for more in-depth proteome analysis by LC-MS/MS. If the catheter-associated biofilm is too small for detailed analysis by IMS, these CAUTI-specific *E. coli* strains can also be tested for more robust biofilm formation in the *in vitro* model with the MSU CBE.

Characterization of CAUTI-specific *E. coli* strains, and analysis by IMS, will allow for the comparison of subpopulation production and stratification across multiple medically relevant *E. coli* strains. These studies will have the potential for identifying common biofilm

subpopulations across CAUTI strains, which could present new targets for the development of novel anti-biofilm strategies. Also, these studies have the potential to identify protein biomarkers for CAUTI that could be used for more accurate diagnosis and even perhaps early detection of CAUTI to aid in rapid treatment to prevent continued or secondary-site infection. Eventually, if successful, similar approached can be leveraged to study the spatial proteome of multi-species catheter-associated biofilms.

Final thoughts and looking forward

Together, the studies presented in this dissertation, have significantly advanced the field examining UPEC biofilm subpopulations. The adaptation of new technologies, such as MALDI-TOF IMS, for the identification and characterization of biofilm subpopulations is crucial to the deeper understanding of the role and regulation of subpopulations within pathogenic multicellular communities. In the work presented here, analysis of a single subpopulation observed with these technologies, has led to significant progression in the understanding of how environmental cues drive infection of UPEC to a specific niche within the urinary tract environment. The observed oxygen-dependent regulation of type 1 pili in UPEC, and the understanding of how this regulation is mediated (via transcriptional and/or post-transcriptional, and post-translational mechanisms), could represent a mechanistic target for the development of novel anti-biofilm strategies. Perhaps this regulation could be targeted to synchronize all biofilm subpopulations to the same level of *fim* expression, for the prevention of bacterial adhesion and the establishment of infection. Such advancement in the understanding of the foundation of UPEC infection within the urinary tract was gained from the analysis of one single-subpopulation observed by IMS. Moving forward, the identification and analysis of additional

subpopulations can only further enhance the understanding of UPEC biofilms, bringing us closer to the ultimate goal of preventing UTIs and CAUTIs.

LIST OF PUBLICATIONS

Shaffer CL, Zhang EW, Dudley AG, Dixon BREA, Guckes KR, Breland EJ, **Floyd KA**, Casella DP, Scott Allgood HM, Clayton DB, Hadjifrangiskou M. Purine biosynthesis metabolically constrains vacuolar escape and intracellular survival of uropathogenic *E. coli*. ***Infection and Immunity.*** 2016 Dec 29; 85 (1). (PMID: 27795353)

Floyd KA, Eberly AR, Hadjifrangiskou M. Chapter 3. Adhesion of Bacteria to Surfaces and Biofilm Formation on Medical Devices. ***Biofilms and implantable medical devices: infection and control (Textbook).*** Woodhead Publishing Series in Biomaterials. 2016.

Floyd KA*, Mitchell CA*, Eberly AR, Colling SJ, Zhang EW, DePas W, Chapman MR, Conover M, Rogers BR, Hultgren SJ, Hadjifrangiskou M. The UbiI (VisC) aerobic ubiquinone synthase is required for expression of type 1 pili, biofilm formation, and pathogenesis in uropathogenic *Escherichia coli*. ***J. Bact.*** 2016 Sep 9;198(19):2662-72. (PMID: 27161114)

Floyd KA, Meyer AE, Nelson G, Hadjifrangiskou M. The yin-yang driving urinary tract infection and how proteomics can enhance research, diagnostics and treatment. ***Proteomics Clin. Appl***. 2015 Dec; 9 (11-12). (PMID: 26255866)

Floyd KA, Moore JL, Eberly AR, Good JA, Shaffer CL, Zaver H, Almqvist F, Skaar EP, Caprioli RM, Hadjifrangiskou M. Adhesive Fiber Stratification in Uropathogenic *Escherichia coli* Biofilms Unveils Oxygen-Mediated Control of Type 1 Pili. ***PLoS Pathog.*** 2015 Mar 4;11(3):e1004697. (PMID: 25738819)

APPENDIX A

Bacterial Strains Described in this Work

Strain	Description	Source / Reference
UTI89	UPEC isolate collected from a female patient with symptomatic cystitis	Mulvey *et al.*, 2001*
UTI89/pBAD33	UTI89 with empty pBAD33 as control for complementation studies	Floyd and Mitchel *et al.*, 2016
UTI89Δ*fimA-H*	UTI89 lacking all genes of the *fim* operon	Greene *et al.*, 2014*
UTI89_LON	*fimS* promoter genetically locked *fim*ON through disruption of the left invertible repeat	Kostakioti *et al*., 2012*
UTI89_LONΔ*fimE*	Gene deletion of *fimE* in the UTI89_LON strain	This study
UTI89_LONΔ*fnr*	Gene deletion of *fnr* in the UTI89_LON strain	This study
UTI89Δ*hupA*	Gene deltion of *hupA* in UTI89	Floyd *et al*., 2015
UTI89Δ*yahO*	Gene deltion of *yahO* in UTI89	Floyd *et al*., 2015
UTI89Δ*fimE*	Gene deltion of *fimE* in UTI89	This study
UTI89Δ*fimE*/pFimE	UTI89 carrying pBAD33 with *fimE* cloned into XbaI - HindIII sites for arabinose-inducible complementation	This study
UTI89Δ*arcA*	Gene deltion of *arcA* in UTI89	Gift of Dr. Matthew Chapman
UTI89Δ*fnr*	Gene deltion of *fnr* in UTI89	This study
UTI89Δ*ubiI*	Gene deltion of *ubiI* in UTI89	Floyd and Mitchel *et al.*, 2016
UTI89Δ*ubiI*/pUbiI	UTI89 carrying pBAD33 with *ubiI* cloned into SmaI – XbaI sites for arabinose-inducible complementation	Floyd and Mitchel *et al.*, 2016
UTI89_LONΔ*ubiI*	Gene deletion of *ubiI* in the UTI89_LON strain	Floyd and Mitchel *et al.*, 2016
CFT073	UPEC isolate collected from blood stream of a female patient with pyelonephritis	Mobley *et al.*, 1990*
VUTI67	Clinical urinary *E. coli* strain collected from VUMC	This study
VUTI73	Clinical urinary *E. coli* strain collected from VUMC	This study
TOP52	Cystitis strain of *Klebsiella pneumoniae*	(Rosen *et al.*, 2008)*

*Strain courtesy of Dr. Scott Hultgren

Table 1. List of all bacterial strains used in these studies. The name of each strain is presented, along with a brief description of the strain, and the source or a reference to the source of each strain.

APPENDIX B

A. Primers for Phase Assay

Phase_L	GAGAAGAAGCTTGATTTAACTAATTG	Amplification of *fimS* for phase assay
Phase_R	AGAGCCGCTGTAGAACTCAGG	Amplification of *fimS* for phase assay

B. Primers for Gene Deletion

Primer Name	Sequence 5' - 3'	Purpose
Chapter II		
*hupA*_Fwd	TTACTTAACTGCGTCTTTCAGTGCCTTGCCAGAAACAAATGCCGGTACGTGTGTAGGCTGGAGCTGCTT	Amplification of KO DNA for *hupA* deletion
*hupA*_REV	ATGAACAAGACTCAACTGATTGATGTAATTGCAGAGAAAGCAGAACTGTCCATATGAATATCCTCCTTAG	Amplification of KO DNA for *hupA* deletion
*hupA*_KO_Test_Fwd	GTGGCTATCGGTGCGTGTATG	Validaiton of *hupA* deletion
*hupA*_KO_Test_REV	GCCCTGGTCTTCAGCAAATCC	Validaiton of *hupA* deletion
*yahO*_Fwd	ATGAAAATAATCTCTAAAATGTTAGTCGGTGCGTTAGCGTTTGCCGTTACGTGTAGGCTGGAGCTGCTTC	Amplification of KO DNA for *yahO* deletion
*yahO*_REV	TTACTTCTTCTTATAAATATTTGCCGTGCCGTGAATCTTATTGTCAGTTTCATATGAATATCCTCCTTAG	Amplification of KO DNA for *yahO* deletion
*yahO*_KO_Test_Fwd	ATAATCGGGTGCGAGAGAGA	Validaiton of *yahO* deletion
*yahO*_KO_Test_REV	CGATAAAACAGCAGCGGCGA	Validaiton of *yahO* deletion
Chapter III		
*fimE*_KO_Fwd	ATATCTCAGTCAGGAGTACTACTATTGTGAGTAAACGTCGTTATCTTACCGGTAGTGTAGGCTGGAGCTGCTTC	Amplification of KO DNA for *fimE* deletion
*fimE*_KO_Rev	CCGGCAAAACGAGCAGCATTACTGGCGGTATAACGCACAGTATGGCGAATATCATATGAATATCCTCCTTAG	Amplification of KO DNA for *fimE* deletion
*fimE*_Test_Fwd	GACCGATTGAGGTTTCCTATAG	Validaiton of *fimE* deletion
*fimE*_Test_Rev	CAATTAGTTAAATCAAGCTTCTTCTC	Validaiton of *fimE* deletion
fimE_pBAD33_XbaI_Fwd	CATTCTAGAGTGAGTAAACGTCGTTATCT	Amplification of *fimE* for cloning into pBAD33
fimE_pBAD33_HindIII_Rev	CATAAGCTTTCAAGCTTCTTCTCTTTTTA	Amplification of *fimE* for cloning into pBAD33
Chapter IV		
*fnr*_KO_L	CAGAAGGATAGTGAGTTATGCGGAAGAATCAGGCAACGTTACGCGTGTGTAGGCTGGAGCTGCTTC	Amplification of KO DNA for *fnr* deletion
*fnr*_KO_R	AATTATACGGCGCATTCAGTCTGGCGGTTGTGCTATCCATTGCCAGGCATATGAATATCCTCCTTAG	Amplification of KO DNA for *fnr* deletion
*fnr*_Test_L	CAGTGATGAACCTTCTGTCAGA	Validaiton of *fnr* deletion
*fnr*_Test_R	ATATCAATTACGGCTTGAGCAGAC	Validaiton of *fnr* deletion
Chpater V		
ubiI (*visC*)_KO_L	TTAACGCAGCC-ATTCAGGCAAATCGTTTAATCCCATTGCCTGACGAATAAGTGTAGGCTGGAGCTGCTTC	Amplification of KO DNA for *ubiI* deletion
ubiI (visC)_KO_R	ATGCAAAGTGTTGATGTAGCCATTGTTGGTG-GCGGCATGGTGGGGCTGGCCATATGAATATCCTCCTTAG	Amplification of KO DNA for *ubiI* deletion
ubiI (visC)_KO_test_L	GGAAAATCTCCCGGCGAAAA	Validaiton of *ubiI* deletion
ubiI (visC)_KO_test_R	GCGTCACGGACAGCCTTGTA	Validaiton of *ubiI* deletion
pBAD_*ubiI(visC)*_Fwd_SmaI	TCCCCCGGGATGCAAAGTGTTGATGTAGCCATT	Amplification of *ubiI* for plasmid insertion and complementation
pBAD_*ubiI(visC)*_Rev_XbaI	GCTCTAATTAACGCAGCCATTCAGGCAAATCG	Amplification of *ubiI* for plasmid insertion and complementation

C. Primers and Probes for quantitative PCR

Primer Name	Sequence 5' - 3'	Purpose
Primers		
Chapters III and IV		
*fimB*_qPCR_Fwd	GCATGCTGAGAGCGAGTCGGTA	Primers for qPCR amplification *of fimB* using TaqMan-based Methods
*fimB*_qPCR_Rev	GGCGGTATACCAGACAGTATGACG	Primers for qPCR amplification of *fimB* using TaqMan-based Methods
*fimE*_qPCR_Fwd	ATGAGCGTGAAGCCGTGGAACG	Primers for qPCR amplification of *fimE* using TaqMan-based Methods
*fimE*_qPCR_Rev	TATCTGCACCACGCTCAGCCAG	Primers for qPCR amplification of *fimE* using TaqMan-based Methods
*fimX*_qPCR_Fwd	GAAGTCTACAGGCTGATGGATGCA	Primers for qPCR amplification of *fimX* using TaqMan-based Methods
*fimX*_qPCR_Rev	TCAAGAAGTTCACTGGCCCTAAAACC	Primers for qPCR amplification of *fimX* using TaqMan-based Methods
*fimI*_qPCR_Fwd	GCGGAAGCTTGCCGGATTGAAG	Primers for qPCR amplification of *fimI* using TaqMan-based Methods
*fimI*_qPCR_Rev	AAGGCACCGGTGAGCTATCTTCC	Primers for qPCR amplification of *fimI* using TaqMan-based Methods
*rrsH*_483_qPCR_Fwd	CGTTACCCGCAGAAGAAGCAC	Primers for qPCR amplification of *rrsH* using TaqMan-based Methods
*rrsH*_637_qPCR_Rev	GATGCAGTTCCCAGGTTGAGC	Primers for qPCR amplification of *rrsH* using TaqMan-based Methods
Chapter V		
*sdhB*_Forw_SYBR	AGCCGGGCAAGAAGATTG	Primers for qPCR amplification of *sdhB* using SYBR Green Methods
*sdhB*_Rev_SYBR	ACCCGTCGAGTTTTTCGCGC	Primers for qPCR amplification of *sdhB* using SYBR Green Methods
*mdh*_Forw_SYBR	CCACCGGCTTTCGCTTCAAC	Primers for qPCR amplification of *mdh* using SYBR Green Methods
*mdh*_Rev_SYBR	CATTCGTTCCAACACCTTTGTTGC	Primers for qPCR amplification of *mdh* using SYBR Green Methods
*fliM*_Forw_SYBR	GTCGGGGCCATCCGCATTCA	Primers for qPCR amplification of *fliM* using SYBR Green Methods
*fliM*_Rev_SYBR	GGGTAAACTCGCGGCCTTCC	Primers for qPCR amplification of *fliM* using SYBR Green Methods
*cydA*_Forw_SYBR	CTATGCGTATGGAGATGGTGAGC	Primers for qPCR amplification of *cydA* using SYBR Green Methods
*cydA*_Rev_SYBR	CGGCAGCCATACCGAAGCTG	Primers for qPCR amplification of *cydA* using SYBR Green Methods
*fimB*_ Fwd_SYBR	GCATGCTGAGAGCGAGTGGGTA	Primers for qPCR amplification of *fimB* using SYBR Green Methods
*fimB*_ Rev_SYBR	CTCCAGTGACAACCCGGCATTAC	Primers for qPCR amplification of *fimB* using SYBR Green Methods
*fimE*_ Fwd_SYBR	GAGCGTGAAGCCGTGGAACG	Primers for qPCR amplification of *fimE* using SYBR Green Methods
*fimE*_ Rev_SYBR	GGCGAGAAAGCCGACTCCCA	Primers for qPCR amplification of *fimE* using SYBR Green Methods
*rrsH*_Forw_SYBR	CGTTACCCGCAGAAGAAGCAC	Primers for qPCR amplification of *rrsH* using SYBR Green Methods
*rrsH*_Rev_SYBR	GATGCAGTTCCCAGGTTGAGC	Primers for qPCR amplification of *rrsH* using TaqMan-based Methods
Probes (with flurophore and quencher denoted)		
Chapters III and IV		
fimB	6FAM-TCATCCGCACATGTTAC-MGBNFQ	Probe for quatitation of *fimB*
fimE	NED-CGGACCGACGCTATAT-MGBNFQ	Probe for quatitation of *fimE*
fimX	NED-TCGCTGTCTGATTATGATG-MGBNFQ	Probe for quatitation of *fimX*
fimI	FAM-CAGCAGTAACCGGTT-MGBNFQ	Probe for quatitation of *fimI*
rrsH	VIC-CGTTAATCGGAATTACTG-MGBNFQ	Probe for quatitation of *rrsH*

Table 2. Sequences of primers and probes used throughout this work. Sequences are presented in the 5' to 3' orientation by name, with a description of their purpose. Sequences are broken down by type, and by the Chapters in which they are used. Probes for quantitative PCR are presented with the 5' flurophore and 3' quencher molecule used for each.

APPENDIX C

UPEC Ions observed by IMS

Ion Observed (*m/z*)	Localization within Biofilm	Ion Observed (*m/z*)	Localization within Biofilm
2,528	Throughout, to Liquid	7,500	Throughout, higher in Air
2,577	Liquid	7,718 - **YahO**	Throughout, higher at Interface
2,591	Throughout, to Liquid	8,141	Air
2,904	Throughout, to Liquid	8,200	Air
3,463	Throughout, higher at Interface	8,356	Interface to Liquid
3,479	Throughout, higher at Interface	8,397	Interface to Liquid
3,491	Interface to Air	8,889	Interface to Air
3,652	Throughout	9,064 - **HdeB**	Interface to Liquid
3,687	Air	9,192	Interface
3,718	Throughout, higher in Air	9,226 - **HupB**	Throughout, higher in Air
4,405	Interface to air	9,282	Interface
4,573	Interface	9,535 - **HupA**	Throughout, higher in Air
4,652	Throughout, higher at Interface	9,710	Interface to Liquid
4,808	Interface to Air	9,961	Throughout, higher in Liquid
4,894	Interface to Liquid	10,133	Throughout, higher at Interface
5,131	Interface to Air	10,293	Air
5,151	Interface to Air	10,732	Throughout, higher in Air
5,412	Interface to Air	10,912	Interface
5,595	Interface	11,205	Throughout, higher in Air
5,638	Throughout	11,716	Interface
6,277	Interface to Air	12,218	Interface to Air
6,338	Interface to Air	12,643	Interface
6,432	Interface to Air	12,754	Throughout, higher in Air
6,873	Throughout	13,036 - **CsgA**	Interface
7,189	Interface	13,349	Throughout
7,215	Interface	15,398	Throughout, higher at Interface
7,285	Interface to Air	16,269 - **FimA**	Air
7,346	Interface to Air	16,374	Air
7,414	Throughout, higher in Air	17,573	Interface to Air
7,481	Air	20,866	Interface

*Ions listed were taken from the internally calibrated average spectrum described in Figure 8

Table 3. List of Reproducible *m/z* Ions Observed by MALDI-TOF IMS from 48-hour UPEC Biofilms

APPENDIX D

K. pneumoniae Ions observed by IMS			
Ion Observed (*m/z*)	**Localization within Biofilm**	**Ion Observed (*m/z*)**	**Localization within Biofilm**
2,292	Liquid	7,712	Interface to Air
2,391	Liquid	7,754	Throughout, higher at Interface
2,594	Liquid	8,064	Air
2,819	Liquid	8,318	Air
2,933	Liquid	8,439	Interface to Air
3,008	Liquid	8,902	Interface to Air
3,080	Liquid	9,147	Interface
3,105	Liquid	9,263	Interface to Liquid
3,416	Air	9,487	Interface to Liquid
3,443	Air	9,858	Air
3,602	Throughout, higher at Interface	10,255	Interface
3,858	Interface to Air	10,591	Interface to air
4,578	Interface to Air	10,764	Interface
4,747	Air	10,902	Throughout, higher at Interface
5,387	Interface to Air	11,228	Throughout
5,570	Interface to Air	12,285	Interface to Liquid
6,300	Interface	16,115	Interface
6,393	Interface to Air	17,472	Interface to Air
6,865	Interface	18,035	Interface
7,177	Interface	18,515	Interface
7,201	Interface	21,508	Interface
7,278	Interface		
7,328	Interface to Air		
7,436	Interface to Air		

Table 4. List of Reproducible *m/z* Ions Observed by MALDI-TOF IMS from 48-hour *K. pneumoniae* Biofilms

APPENDIX E

Protein Name	UniProtKB Acession #	Ther. Avg. Mass (Da)	Predicted Signal Peptide*	Ther. Mass Minus Signal Peptide (Da)	Observed Avg. Mass (Da)#
Adhesion					
Type 1 pili major subunit FimA	Q1R2K0	18,553	aa1-23 / 2,302 Da	16,269	16,269
Major Curlin Subunit CsgA	Q1RDB7	14,992	aa1-20 / 1,974 Da	13,036	13,036
DNA Binding / Transcriptional Regulator					
DNA-binding Protein HU-α	Q1R5W6	9,534	n/a	9,534	9,535
DNA-binding Protein HU-β	Q1RF95	9,226	n/a	9,226	9,226
Stress-Response					
Acid stress-response protein hdeB	Q1R595	12,522	aa1-33 / 3,475 Da	9,065	9,064
Uncharacterized					
Putative Uncharacterized Protein yahO	Q1RFK1	9,929	aa1-21 / 2,240 Da	7,707	7,718

Table 5. Identified proteins observed by IMS within 48-hour UPEC biofilms. Observed proteins were identified by LC-MS/MS, as outlined in the Methods section. *The predicted signal peptides obtained using the SignalP Server. # The observed average mass obtained from IMS analysis of one representative 48 hour UPEC biofilm. Internal calibration was performed with mMass Software using the theoretical mass minus the signal peptide for proteins identified by tandem mass spectrometry analyses to obtain the best mass accuracy from the data, as previously described (Anderson *et al.*, 2013).

REFERENCES

ABERG, A., SHINGLER, V. & BALSALOBRE, C. 2006. (p)ppGpp regulates type 1 fimbriation of *Escherichia coli* by modulating the expression of the site-specific recombinase FimB. *Mol Microbiol,* 60**,** 1520-33.

ABRAHAM, J. M., FREITAG, C. S., CLEMENTS, J. R. & EISENSTEIN, B. I. 1985. An invertible element of DNA controls phase variation of type 1 fimbriae of *Escherichia coli. Proc Natl Acad Sci U S A,* 82**,** 5724-7.

ABSOLOM, D. R., LAMBERTI, F. V., POLICOVA, Z., ZINGG, W., VAN OSS, C. J. & NEUMANN, A. W. 1983. Surface thermodynamics of bacterial adhesion. *Applied and Environmental Microbiology,* 46**,** 90-97.

ALEXEEVA, S., DE KORT, B., SAWERS, G., HELLINGWERF, K. J. & DE MATTOS, M. J. T. 2000. Effects of Limited Aeration and of the ArcAB System on Intermediary Pyruvate Catabolism in *Escherichia coli*. *Journal of Bacteriology,* 182**,** 4934-4940.

ALEXEEVA, S., HELLINGWERF, K. J. & TEIXEIRA DE MATTOS, M. J. 2003. Requirement of ArcA for Redox Regulation in *Escherichia coli* under Microaerobic but Not Anaerobic or Aerobic Conditions. *Journal of Bacteriology,* 185**,** 204-209.

ALLEN, W. J., PHAN, G. & WAKSMAN, G. 2012. Pilus biogenesis at the outer membrane of Gram-negative bacterial pathogens. *Curr Opin Struct Biol,* 22**,** 500-6.

ALTERI, C. J., SMITH, S. N. & MOBLEY, H. L. 2009. Fitness of *Escherichia coli* during urinary tract infection requires gluconeogenesis and the TCA cycle. *PLoS Pathog,* 5**,** e1000448.

ANDERSON, D. M., MILLS, D., SPRAGGINS, J., LAMBERT, W. S., CALKINS, D. J. & SCHEY, K. L. 2013. High-resolution matrix-assisted laser desorption ionization-imaging mass spectrometry of lipids in rodent optic nerve tissue. *Mol Vis,* 19**,** 581-92.

ANDERSON, G. G., MARTIN, S. M. & HULTGREN, S. J. 2004. Host subversion by formation of intracellular bacterial communities in the urinary tract. *Microbes Infect,* 6**,** 1094-101.

ANDERSON, G. G., PALERMO, J. J., SCHILLING, J. D., ROTH, R., HEUSER, J. & HULTGREN, S. J. 2003. Intracellular bacterial biofilm-like pods in urinary tract infections. *Science,* 301**,** 105-7.

ANDES, D., NETT, J., OSCHEL, P., ALBRECHT, R., MARCHILLO, K. & PITULA, A. 2004. Development and Characterization of an *In Vivo* Central Venous Catheter *Candida albicans* Biofilm Model. *Infection and Immunity,* 72**,** 6023-6031.

ANTELMANN, H. & HELMANN, J. D. 2011. Thiol-based redox switches and gene regulation. *Antioxid Redox Signal,* 14**,** 1049-63.

ARINZON, Z., SHABAT, S., PEISAKH, A. & BERNER, Y. 2012. Clinical presentation of urinary tract infection (UTI) differs with aging in women. *Arch Gerontol Geriatr,* 55**,** 145-7.

ARNOLD, J. W. & BAILEY, G. W. 2000. Surface finishes on stainless steel reduce bacterial attachment and early biofilm formation: scanning electron and atomic force microscopy study. *Poult Sci,* 79**,** 1839-45.

ASLUND, F., ZHENG, M., BECKWITH, J. & STORZ, G. 1999. Regulation of the OxyR transcription factor by hydrogen peroxide and the cellular thiol-disulfide status. *Proc Natl Acad Sci U S A,* 96**,** 6161-5.

BALABAN, N. Q., MERRIN, J., CHAIT, R., KOWALIK, L. & LEIBLER, S. 2004. Bacterial persistence as a phenotypic switch. *Science,* 305**,** 1622-5.

BARBER, A. E., NORTON, J. P., SPIVAK, A. M. & MULVEY, M. A. 2013. Urinary Tract Infections: Current and Emerging Management Strategies. *Clinical Infectious Diseases,* 57**,** 719-724.

BARBIERI, N. L., NICHOLSON, B., HUSSEIN, A., CAI, W., WANNEMUEHLER, Y. M., DELL'ANNA, G., LOGUE, C. M., HORN, F., NOLAN, L. K. & LI, G. 2014. FNR Regulates Expression of Important Virulence Factors Contributing to Pathogenicity of Uropathogenic *Escherichia coli*. *Infect Immun,* 82**,** 5086-98.

BARKEN, K. B., PAMP, S. J., YANG, L., GJERMANSEN, M., BERTRAND, J. J., KLAUSEN, M., GIVSKOV, M., WHITCHURCH, C. B., ENGEL, J. N. & TOLKER-NIELSEN, T. 2008. Roles of type IV pili, flagellum-mediated motility and extracellular DNA in the formation of mature multicellular structures in *Pseudomonas aeruginosa* biofilms. *Environ Microbiol,* 10**,** 2331-43.

BARNHART, M. M. & CHAPMAN, M. R. 2006. Curli biogenesis and function. *Annu Rev Microbiol,* 60**,** 131-47.

BARRAUD, N., HASSETT, D. J., HWANG, S.-H., RICE, S. A., KJELLEBERG, S. & WEBB, J. S. 2006. Involvement of Nitric Oxide in Biofilm Dispersal of *Pseudomonas aeruginosa*. *Journal of Bacteriology,* 188**,** 7344-7353.

BARRAUD, N., KELSO, M. J., RICE, S. A. & KJELLEBERG, S. 2015. Nitric oxide: a key mediator of biofilm dispersal with applications in infectious diseases. *Curr Pharm Des,* 21**,** 31-42.

BATEMAN, S. L., STAPLETON, A. E., STAMM, W. E., HOOTON, T. M. & SEED, P. C. 2013. The type 1 pili regulator gene fimX and pathogenicity island PAI-X as molecular markers of uropathogenic *Escherichia coli*. *Microbiology,* 159**,** 1606-17.

BECKER, S., HOLIGHAUS, G., GABRIELCZYK, T. & UNDEN, G. 1996. O2 as the regulatory signal for FNR-dependent gene regulation in *Escherichia coli. J Bacteriol,* 178**,** 4515-21.

BECKER, S., VLAD, D., SCHUSTER, S., PFEIFFER, P. & UNDEN, G. 1997. Regulatory O2 tensions for the synthesis of fermentation products in *Escherichia coli* and relation to aerobic respiration. *Arch Microbiol,* 168**,** 290-6.

BOUCKAERT, J., BERGLUND, J., SCHEMBRI, M., DE GENST, E., COOLS, L., WUHRER, M., HUNG, C. S., PINKNER, J., SLATTEGARD, R., ZAVIALOV, A., CHOUDHURY, D., LANGERMANN, S., HULTGREN, S. J., WYNS, L., KLEMM, P., OSCARSON, S., KNIGHT, S. D. & DE GREVE, H. 2005. Receptor binding studies disclose a novel class of high-affinity inhibitors of the *Escherichia coli* FimH adhesin. *Mol Microbiol,* 55**,** 441-55.

BRANDA, S. S., VIK, S., FRIEDMAN, L. & KOLTER, R. 2005. Biofilms: the matrix revisited. *Trends Microbiol,* 13**,** 20-6.

BROWN, G. C. & BRAND, M. D. 1988. Proton/electron stoichiometry of mitochondrial complex I estimated from the equilibrium thermodynamic force ratio. *Biochem J,* 252**,** 473-9.

BRYAN, A., ROESCH, P., DAVIS, L., MORITZ, R., PELLETT, S. & WELCH, R. A. 2006. Regulation of type 1 fimbriae by unlinked FimB- and FimE-like recombinases in uropathogenic *Escherichia coli* strain CFT073. *Infect Immun,* 74**,** 1072-83.

BURNS, L. S., SMITH, S. G. & DORMAN, C. J. 2000. Interaction of the FimB integrase with the *fimS* invertible DNA element in Escherichia coli *in vivo* and *in vitro*. *J Bacteriol,* 182**,** 2953-9.

BURROWS, L. L. 2012. *Pseudomonas aeruginosa* twitching motility: type IV pili in action. *Annu Rev Microbiol,* 66**,** 493-520.

BUSCH, A. & WAKSMAN, G. 2012. Chaperone-usher pathways: diversity and pilus assembly mechanism. *Philos Trans R Soc Lond B Biol Sci,* 367**,** 1112-22.

CANTEY, J. R., LUSHBAUGH, W. B. & INMAN, L. R. 1981. Attachment of Bacteria to Intestinal Epithelial Cells in Diarrhea Caused by *Escherichia coli* Strain RDEC-1 in the Rabbit: Stages and Role of Capsule. *Journal of Infectious Diseases,* 143**,** 219-230.

CAPRIOLI, R. M., FARMER, T. B. & GILE, J. 1997. Molecular imaging of biological samples: localization of peptides and proteins using MALDI-TOF MS. *Anal Chem,* 69**,** 4751-60.

CHEN, S. L., HUNG, C. S., PINKNER, J. S., WALKER, J. N., CUSUMANO, C. K., LI, Z., BOUCKAERT, J., GORDON, J. I. & HULTGREN, S. J. 2009. Positive selection identifies an *in vivo* role for FimH during urinary tract infection in addition to mannose binding. *Proc Natl Acad Sci U S A,* 106**,** 22439-44.

CHEN, S. L., HUNG, C. S., XU, J., REIGSTAD, C. S., MAGRINI, V., SABO, A., BLASIAR, D., BIERI, T., MEYER, R. R., OZERSKY, P., ARMSTRONG, J. R., FULTON, R. S., LATREILLE, J. P., SPIETH, J., HOOTON, T. M., MARDIS, E. R., HULTGREN, S. J. & GORDON, J. I. 2006. Identification of genes subject to positive selection in

uropathogenic strains of *Escherichia coli*: a comparative genomics approach. *Proc Natl Acad Sci U S A,* 103**,** 5977-82.

CHEN, S. L., WU, M., HENDERSON, J. P., HOOTON, T. M., HIBBING, M. E., HULTGREN, S. J. & GORDON, J. I. 2013. Genomic Diversity and Fitness of *E. coli* Strains Recovered from the Intestinal and Urinary Tracts of Women with Recurrent Urinary Tract Infection. *Sci Transl Med,* 5**,** 184ra60.

CHIANG, P., HABASH, M. & BURROWS, L. L. 2005. Disparate Subcellular Localization Patterns of *Pseudomonas aeruginosa* Type IV Pilus ATPases Involved in Twitching Motility. *Journal of Bacteriology,* 187**,** 829-839.

CLARK, D. P. 1989. The fermentation pathways of *Escherichia coli*. *FEMS Microbiol Rev,* 5**,** 223-34.

COLLINSON, S. K., DOIG, P. C., DORAN, J. L., CLOUTHIER, S., TRUST, T. J. & KAY, W. W. 1993. Thin, aggregative fimbriae mediate binding of *Salmonella enteritidis* to fibronectin. *J Bacteriol,* 175**,** 12-8.

CONNELL, I., AGACE, W., KLEMM, P., SCHEMBRI, M., MARILD, S. & SVANBORG, C. 1996. Type 1 fimbrial expression enhances *Escherichia coli* virulence for the urinary tract. *Proc Natl Acad Sci U S A,* 93**,** 9827-32.

CONSTANTINIDOU, C., HOBMAN, J. L., GRIFFITHS, L., PATEL, M. D., PENN, C. W., COLE, J. A. & OVERTON, T. W. 2006. A reassessment of the FNR regulon and transcriptomic analysis of the effects of nitrate, nitrite, NarXL, and NarQP as *Escherichia coli* K12 adapts from aerobic to anaerobic growth. *J Biol Chem,* 281**,** 4802-15.

COQUE, T. M., NOVAIS, A., CARATTOLI, A., POIREL, L., PITOUT, J., PEIXE, L., BAQUERO, F., CANTÓN, R. & NORDMANN, P. 2008. Dissemination of clonally related *Escherichia coli* strains expressing extended-spectrum beta-lactamase CTX-M-15. *Emerg Infect Dis,* 14**,** 195-200.

CORCORAN, C. P. & DORMAN, C. J. 2009. DNA relaxation-dependent phase biasing of the *fim* genetic switch in *Escherichia coli* depends on the interplay of H-NS, IHF and LRP. *Mol Microbiol,* 74**,** 1071-82.

CORNETT, D. S., REYZER, M. L., CHAURAND, P. & CAPRIOLI, R. M. 2007. MALDI imaging mass spectrometry: molecular snapshots of biochemical systems. *Nat Methods,* 4**,** 828-33.

CRAIG, L., TAYLOR, R. K., PIQUE, M. E., ADAIR, B. D., ARVAI, A. S., SINGH, M., LLOYD, S. J., SHIN, D. S., GETZOFF, E. D., YEAGER, M., FOREST, K. T. & TAINER, J. A. 2003. Type IV pilin structure and assembly: X-ray and EM analyses of *Vibrio cholerae* toxin-coregulated pilus and *Pseudomonas aeruginosa* PAK pilin. *Mol Cell,* 11**,** 1139-50.

DAMPER, P. D. & EPSTEIN, W. 1981. Role of the membrane potential in bacterial resistance to aminoglycoside antibiotics. *Antimicrob Agents Chemother,* 20**,** 803-8.

DANIELS, K. R., LEE, G. C. & FREI, C. R. 2014. Trends in catheter-associated urinary tract infections among a national cohort of hospitalized adults, 2001-2010. *Am J Infect Control,* 42**,** 17-22.

DAS, T., SHARMA, P. K., KROM, B. P., VAN DER MEI, H. C. & BUSSCHER, H. J. 2011. Role of eDNA on the adhesion forces between *Streptococcus mutans* and substratum surfaces: influence of ionic strength and substratum hydrophobicity. *Langmuir,* 27**,** 10113-8.

DE BEER, D., STOODLEY, P., ROE, F. & LEWANDOWSKI, Z. 1994. Effects of biofilm structures on oxygen distribution and mass transport. *Biotechnol Bioeng,* 43**,** 1131-8.

DEBOIS, D., HAMZE, K., GUERINEAU, V., LE CAER, J. P., HOLLAND, I. B., LOPES, P., OUAZZANI, J., SEROR, S. J., BRUNELLE, A. & LAPREVOTE, O. 2008. In situ localisation and quantification of surfactins in a *Bacillus subtilis* swarming community by imaging mass spectrometry. *Proteomics,* 8**,** 3682-91.

DEPAS, W. H., HUFNAGEL, D. A., LEE, J. S., BLANCO, L. P., BERNSTEIN, H. C., FISHER, S. T., JAMES, G. A., STEWART, P. S. & CHAPMAN, M. R. 2013. Iron induces bimodal population development by *Escherichia coli*. *Proc Natl Acad Sci U S A,* 110**,** 2629-34.

DI MARTINO, P., CAFFERINI, N., JOLY, B. & DARFEUILLE-MICHAUD, A. 2003. *Klebsiella pneumoniae* type 3 pili facilitate adherence and biofilm formation on abiotic surfaces. *Res Microbiol,* 154**,** 9-16.

DICKSON, J. S. & KOOHMARAIE, M. 1989. Cell surface charge characteristics and their relationship to bacterial attachment to meat surfaces. *Applied and Environmental Microbiology,* 55**,** 832-836.

DIELUBANZA, E. J., MAZUR, D. J. & SCHAEFFER, A. J. 2014. Management of non-catheter-associated complicated urinary tract infection. *Infect Dis Clin North Am,* 28**,** 121-34.

DODSON, K. W., PINKNER, J. S., ROSE, T., MAGNUSSON, G., HULTGREN, S. J. & WAKSMAN, G. 2001. Structural basis of the interaction of the pyelonephritic *E. coli* adhesin to its human kidney receptor. *Cell,* 105**,** 733-43.

DONLAN, R. M. 2002. Biofilms: microbial life on surfaces. *Emerg Infect Dis,* 8**,** 881-90.

DRIESSEN, A. J. 1992. Precursor protein translocation by the *Escherichia coli* translocase is directed by the protonmotive force. *EMBO J,* 11**,** 847-53.

EDIRISINGHE, P. D., MOORE, J. F., SKINNER-NEMEC, K. A., LINDBERG, C., GIOMETTI, C. S., VERYOVKIN, I. V., HUNT, J. E., PELLIN, M. J. & HANLEY, L.

2007. Detection of *in situ* derivatized peptides in microbial biofilms by laser desorption 7.87 eV postionizaton mass spectrometry. *Anal Chem,* 79**,** 508-14.

ETO, D. S., JONES, T. A., SUNDSBAK, J. L. & MULVEY, M. A. 2007. Integrin-mediated host cell invasion by type 1-piliated uropathogenic *Escherichia coli*. *PLoS Pathog,* 3**,** e100.

EVANS, M. L. & CHAPMAN, M. R. 2014. Curli biogenesis: order out of disorder. *Biochim Biophys Acta,* 1843**,** 1551-8.

EVANS, M. L., CHORELL, E., TAYLOR, J. D., ÅDEN, J., GÖTHESON, A., LI, F., KOCH, M., SEFER, L., MATTHEWS, S. J., WITTUNG-STAFSHEDE, P., ALMQVIST, F. & CHAPMAN, M. R. 2015. The bacterial curli system possesses a potent and selective inhibitor of amyloid formation. *Mol Cell,* 57**,** 445-55.

FLEMMING, H. C. & WINGENDER, J. 2010. The biofilm matrix. *Nat Rev Microbiol,* 8**,** 623-33.

FLORES-MIRELES, A. L., WALKER, J. N., CAPARON, M. & HULTGREN, S. J. 2015. Urinary tract infections: epidemiology, mechanisms of infection and treatment options. *Nat Rev Microbiol,* 13**,** 269-84.

FLOYD, K. A., MEYER, A. E., NELSON, G. & HADJIFRANGISKOU, M. 2015a. The yin-yang driving urinary tract infection and how proteomics can enhance research, diagnostics, and treatment. *Proteomics Clin Appl,* 9**,** 990-1002.

FLOYD, K. A., MITCHELL, C. A., EBERLY, A. R., COLLING, S. J., ZHANG, E. W., DEPAS, W., CHAPMAN, M. R., CONOVER, M., ROGERS, B. R., HULTGREN, S. J. & HADJIFRANGISKOU, M. 2016. The UbiI (VisC) Aerobic Ubiquinone Synthase Is Required for Expression of Type 1 Pili, Biofilm Formation, and Pathogenesis in Uropathogenic *Escherichia coli. J Bacteriol,* 198**,** 2662-72.

FLOYD, K. A., MOORE, J. L., EBERLY, A. R., GOOD, J. A., SHAFFER, C. L., ZAVER, H., ALMQVIST, F., SKAAR, E. P., CAPRIOLI, R. M. & HADJIFRANGISKOU, M. 2015b. Adhesive Fiber Stratification in Uropathogenic *Escherichia coli* Biofilms Unveils Oxygen-Mediated Control of Type 1 Pili. *PLoS Pathog,* 11**,** e1004697.

FOXMAN, B. 2010. The epidemiology of urinary tract infection. *Nat Rev Urol,* 7**,** 653-60.

FOXMAN, B. 2014. Urinary tract infection syndromes: occurrence, recurrence, bacteriology, risk factors, and disease burden. *Infect Dis Clin North Am,* 28**,** 1-13.

FOXMAN, B. & BUXTON, M. 2013. Alternative approaches to conventional treatment of acute uncomplicated urinary tract infection in women. *Curr Infect Dis Rep,* 15**,** 124-9.

FRIEDMAN, L. & KOLTER, R. 2004. Genes involved in matrix formation in *Pseudomonas aeruginosa* PA14 biofilms. *Mol Microbiol,* 51**,** 675-90.

FRONZES, R., REMAUT, H. & WAKSMAN, G. 2008. Architectures and biogenesis of non-flagellar protein appendages in Gram-negative bacteria. *EMBO J,* 27**,** 2271-80.

GADDY, J. A., TOMARAS, A. P. & ACTIS, L. A. 2009. The *Acinetobacter baumannii* 19606 OmpA protein plays a role in biofilm formation on abiotic surfaces and in the interaction of this pathogen with eukaryotic cells. *Infect Immun,* 77**,** 3150-60.

GALKIN, A. S., GRIVENNIKOVA, V. G. & VINOGRADOV, A. D. 1999. -->H+/2e- stoichiometry in NADH-quinone reductase reactions catalyzed by bovine heart submitochondrial particles. *FEBS Lett,* 451**,** 157-61.

GALLO, P. M., RAPSINSKI, G. J., WILSON, R. P., OPPONG, G. O., SRIRAM, U., GOULIAN, M., BUTTARO, B., CARICCHIO, R., GALLUCCI, S. & TÜKEL, Ç. 2015. Amyloid-DNA Composites of Bacterial Biofilms Stimulate Autoimmunity. *Immunity,* 42**,** 1171-84.

GALLY, D. L., LEATHART, J. & BLOMFIELD, I. C. 1996. Interaction of FimB and FimE with the *fim* switch that controls the phase variation of type 1 fimbriae in *Escherichia coli* K-12. *Mol Microbiol,* 21**,** 725-38.

GEIBEL, S. & WAKSMAN, G. 2014. The molecular dissection of the chaperone-usher pathway. *Biochim Biophys Acta,* 1843**,** 1559-67.

GEORGELLIS, D., KWON, O. & LIN, E. C. 2001. Quinones as the redox signal for the arc two-component system of bacteria. *Science,* 292**,** 2314-6.

GONZALEZ, C. M. & SCHAEFFER, A. J. 1999. Treatment of urinary tract infection: what's old, what's new, and what works. *World J Urol,* 17**,** 372-82.

GONZÁLEZ-FLECHA, B. & DEMPLE, B. 1997. Homeostatic regulation of intracellular hydrogen peroxide concentration in aerobically growing *Escherichia coli*. *J Bacteriol,* 179**,** 382-8.

GREENE, S. E., HIBBING, M. E., JANETKA, J., CHEN, S. L. & HULTGREN, S. J. 2015. Human Urine Decreases Function and Expression of Type 1 Pili in Uropathogenic *Escherichia coli*. *MBio,* 6**,** e00820.

GREENE, S. E., PINKNER, J. S., CHORELL, E., DODSON, K. W., SHAFFER, C. L., CONOVER, M. S., LIVNY, J., HADJIFRANGISKOU, M., ALMQVIST, F. & HULTGREN, S. J. 2014. Pilicide ec240 disrupts virulence circuits in uropathogenic *Escherichia coli*. *MBio,* 5**,** e02038.

GUCKES, K. R., KOSTAKIOTI, M., BRELAND, E. J., GU, A. P., SHAFFER, C. L., MARTINEZ, C. R., 3RD, HULTGREN, S. J. & HADJIFRANGISKOU, M. 2013. Strong cross-system interactions drive the activation of the QseB response regulator in the absence of its cognate sensor. *Proc Natl Acad Sci U S A*.

GUNSALUS, R. P. 1992. Control of electron flow in *Escherichia coli*: coordinated transcription of respiratory pathway genes. *J Bacteriol,* 174**,** 7069-74.

GUNSALUS, R. P. & PARK, S. J. 1994. Aerobic-anaerobic gene regulation in *Escherichia coli:* control by the ArcAB and Fnr regulons. *Res Microbiol,* 145**,** 437-50.

HADJIFRANGISKOU, M., GU, A. P., PINKNER, J. S., KOSTAKIOTI, M., ZHANG, E. W., GREENE, S. E. & HULTGREN, S. J. 2012. Transposon mutagenesis identifies uropathogenic *Escherichia coli* biofilm factors. *J Bacteriol,* 194**,** 6195-205.

HADJIFRANGISKOU, M., KOSTAKIOTI, M., CHEN, S. L., HENDERSON, J. P., GREENE, S. E. & HULTGREN, S. J. 2011. A central metabolic circuit controlled by QseC in pathogenic *Escherichia coli. Mol Microbiol,* 80**,** 1516-29.

HAHN, E., WILD, P., HERMANNS, U., SEBBEL, P., GLOCKSHUBER, R., HÄNER, M., TASCHNER, N., BURKHARD, P., AEBI, U. & MÜLLER, S. A. 2002a. Exploring the 3D molecular architecture of *Escherichia coli* type 1 pili. *J Mol Biol,* 323**,** 845-57.

HAHN, J. S., OH, S. Y. & ROE, J. H. 2002b. Role of OxyR as a peroxide-sensing positive regulator in *Streptomyces coelicolor* A3(2). *J Bacteriol,* 184**,** 5214-22.

HAJJ CHEHADE, M., LOISEAU, L., LOMBARD, M., PECQUEUR, L., ISMAIL, A., SMADJA, M., GOLINELLI-PIMPANEAU, B., MELLOT-DRAZNIEKS, C., HAMELIN, O., AUSSEL, L., KIEFFER-JAQUINOD, S., LABESSAN, N., BARRAS, F., FONTECAVE, M. & PIERREL, F. 2013. *ubiI*, a new gene in *Escherichia coli* coenzyme Q biosynthesis, is involved in aerobic C5-hydroxylation. *J Biol Chem,* 288**,** 20085-92.

HALEY, R. W., HOOTON, T. M., CULVER, D. H., STANLEY, R. C., EMORI, T. G., HARDISON, C. D., QUADE, D., SHACHTMAN, R. H., SCHABERG, D. R., SHAH, B. V. & SCHATZ, G. D. 1981. Nosocomial infections in U.S. hospitals, 1975-1976: estimated frequency by selected characteristics of patients. *Am J Med,* 70**,** 947-59.

HALL-STOODLEY, L. & STOODLEY, P. 2002. Developmental regulation of microbial biofilms. *Curr Opin Biotechnol,* 13**,** 228-33.

HALL-STOODLEY, L. & STOODLEY, P. 2005. Biofilm formation and dispersal and the transmission of human pathogens. *Trends Microbiol,* 13**,** 7-10.

HAMMER, N. D., CASSAT, J. E., NOTO, M. J., LOJEK, L. J., CHADHA, A. D., SCHMITZ, J. E., CREECH, C. B. & SKAAR, E. P. 2014. Inter- and intraspecies metabolite exchange promotes virulence of antibiotic-resistant *Staphylococcus aureus*. *Cell Host Microbe,* 16**,** 531-7.

HANNAN, T. J., MYSOREKAR, I. U., CHEN, S. L., WALKER, J. N., JONES, J. M., PINKNER, J. S., HULTGREN, S. J. & SEED, P. C. 2008. LeuX tRNA-dependent and -independent mechanisms of *Escherichia coli* pathogenesis in acute cystitis. *Mol Microbiol,* 67**,** 116-28.

HANNAN, T. J., MYSOREKAR, I. U., HUNG, C. S., ISAACSON-SCHMID, M. L. & HULTGREN, S. J. 2010. Early severe inflammatory responses to uropathogenic *E. coli* predispose to chronic and recurrent urinary tract infection. *PLoS Pathog,* 6**,** e1001042.

HANNAN, T. J., TOTSIKA, M., MANSFIELD, K. J., MOORE, K. H., SCHEMBRI, M. A. & HULTGREN, S. J. 2012. Host-pathogen checkpoints and population bottlenecks in persistent and intracellular uropathogenic *Escherichia coli* bladder infection. *FEMS Microbiol Rev,* 36**,** 616-48.

HARRISON, J. J., TURNER, R. J. & CERI, H. 2005. Persister cells, the biofilm matrix and tolerance to metal cations in biofilm and planktonic *Pseudomonas aeruginosa*. *Environ Microbiol,* 7**,** 981-94.

HE, G., SHANKAR, R. A., CHZHAN, M., SAMOUILOV, A., KUPPUSAMY, P. & ZWEIER, J. L. 1999. Noninvasive measurement of anatomic structure and intraluminal oxygenation in the gastrointestinal tract of living mice with spatial and spectral EPR imaging. *Proc Natl Acad Sci U S A,* 96**,** 4586-91.

HICKS, L. A., BARTOCES, M. G., ROBERTS, R. M., SUDA, K. J., HUNKLER, R. J., TAYLOR, T. H. & SCHRAG, S. J. 2015. US Outpatient Antibiotic Prescribing Variation According to Geography, Patient Population, and Provider Specialty in 2011. *Clinical Infectious Diseases*.

HOBLEY, L., OSTROWSKI, A., RAO, F. V., BROMLEY, K. M., PORTER, M., PRESCOTT, A. R., MACPHEE, C. E., VAN AALTEN, D. M. & STANLEY-WALL, N. R. 2013. BslA is a self-assembling bacterial hydrophobin that coats the *Bacillus subtilis* biofilm. *Proc Natl Acad Sci U S A,* 110**,** 13600-5.

HOLDEN, N., BLOMFIELD, I. C., UHLIN, B.-E., TOTSIKA, M., KULASEKARA, D. H. & GALLY, D. L. 2007. Comparative analysis of FimB and FimE recombinase activity. *Microbiology,* 153**,** 4138-4149.

HOOTON, T. M. 2001. Recurrent urinary tract infection in women. *Int J Antimicrob Agents,* 17**,** 259-68.

HOOTON, T. M., BRADLEY, S. F., CARDENAS, D. D., COLGAN, R., GEERLINGS, S. E., RICE, J. C., SAINT, S., SCHAEFFER, A. J., TAMBAYH, P. A., TENKE, P. & NICOLLE, L. E. 2010. Diagnosis, prevention, and treatment of catheter-associated urinary tract infection in adults: 2009 International Clinical Practice Guidelines from the Infectious Diseases Society of America. *Clin Infect Dis,* 50**,** 625-63.

HUEBNER, J. & GOLDMANN, D. A. 1999. Coagulase-negative staphylococci: role as pathogens. *Annu Rev Med,* 50**,** 223-36.

HULTGREN, S. J., LINDBERG, F., MAGNUSSON, G., KIHLBERG, J., TENNENT, J. M. & NORMARK, S. 1989. The PapG adhesin of uropathogenic *Escherichia coli* contains separate regions for receptor binding and for the incorporation into the pilus. *Proc Natl Acad Sci U S A,* 86**,** 4357-61.

HULTGREN, S. J., SCHWAN, W. R., SCHAEFFER, A. J. & DUNCAN, J. L. 1986. Regulation of production of type 1 pili among urinary tract isolates of *Escherichia coli. Infection and Immunity,* 54**,** 613-620.

HUNG, C., ZHOU, Y., PINKNER, J. S., DODSON, K. W., CROWLEY, J. R., HEUSER, J., CHAPMAN, M. R., HADJIFRANGISKOU, M., HENDERSON, J. P. & HULTGREN, S. J. 2013a. *Escherichia coli* biofilms have an organized and complex extracellular matrix structure. *MBio,* 4**,** e00645-13.

HUNG, C., ZHOU, Y., PINKNER, J. S., DODSON, K. W., CROWLEY, J. R., HEUSER, J., CHAPMAN, M. R., HADJIFRANGISKOU, M., HENDERSON, J. P. & HULTGREN, S. J. 2013b. *Escherichia coli* Biofilms Have an Organized and Complex Extracellular Matrix Structure. *MBio,* 4.

HUNG, C. S., BOUCKAERT, J., HUNG, D., PINKNER, J., WIDBERG, C., DEFUSCO, A., AUGUSTE, C. G., STROUSE, R., LANGERMANN, S., WAKSMAN, G. & HULTGREN, S. J. 2002. Structural basis of tropism of *Escherichia coli* to the bladder during urinary tract infection. *Mol Microbiol,* 44**,** 903-15.

HUNG, C. S., DODSON, K. W. & HULTGREN, S. J. 2009. A murine model of urinary tract infection. *Nat Protoc,* 4**,** 1230-43.

IZANO, E. A., AMARANTE, M. A., KHER, W. B. & KAPLAN, J. B. 2008. Differential roles of poly-N-acetylglucosamine surface polysaccharide and extracellular DNA in *Staphylococcus aureus* and *Staphylococcus epidermidis* biofilms. *Appl Environ Microbiol,* 74**,** 470-6.

JACOBSEN, S. M. & SHIRTLIFF, M. E. 2011. Proteus mirabilis biofilms and catheter-associated urinary tract infections. *Virulence,* 2**,** 460-5.

JIANG, F., AN, C., BAO, Y., ZHAO, X., JERNIGAN, R. L., LITHIO, A., NETTLETON, D., LI, L., WURTELE, E. S., NOLAN, L. K., LU, C. & LI, G. 2015. ArcA Controls Metabolism, Chemotaxis, and Motility Contributing to the Pathogenicity of Avian Pathogenic *Escherichia coli. Infection and Immunity,* 83**,** 3545-3554.

JOHNSON, J. R., CLABOTS, C. & ROSEN, H. 2006. Effect of Inactivation of the Global Oxidative Stress Regulator *oxyR* on the Colonization Ability of *Escherichia coli* O1:K1:H7 in a Mouse Model of Ascending Urinary Tract Infection. *Infection and Immunity,* 74**,** 461-468.

JOHNSON, J. R., JOHNSTON, B., CLABOTS, C., KUSKOWSKI, M. A. & CASTANHEIRA, M. 2010. *Escherichia coli* sequence type ST131 as the major cause of serious multidrug-resistant *E. coli* infections in the United States. *Clin Infect Dis,* 51**,** 286-94.

JOHNSON, J. R., NICOLAS-CHANOINE, M. H., DEBROY, C., CASTANHEIRA, M., ROBICSEK, A., HANSEN, G., WEISSMAN, S., URBAN, C., PLATELL, J., TROTT, D., ZHANEL, G., CLABOTS, C., JOHNSTON, B. D. & KUSKOWSKI, M. A. 2012.

Comparison of *Escherichia coli* ST131 pulsotypes, by epidemiologic traits, 1967-2009. *Emerg Infect Dis,* 18**,** 598-607.

JONES, S. A., CHOWDHURY, F. Z., FABICH, A. J., ANDERSON, A., SCHREINER, D. M., HOUSE, A. L., AUTIERI, S. M., LEATHAM, M. P., LINS, J. J., JORGENSEN, M., COHEN, P. S. & CONWAY, T. 2007. Respiration of *Escherichia coli* in the mouse intestine. *Infect Immun,* 75**,** 4891-9.

JONES, S. A., GIBSON, T., MALTBY, R. C., CHOWDHURY, F. Z., STEWART, V., COHEN, P. S. & CONWAY, T. 2011. Anaerobic respiration of *Escherichia coli* in the mouse intestine. *Infect Immun,* 79**,** 4218-26.

JUSTICE, S. S., HUNG, C., THERIOT, J. A., FLETCHER, D. A., ANDERSON, G. G., FOOTER, M. J. & HULTGREN, S. J. 2004. Differentiation and developmental pathways of uropathogenic *Escherichia coli* in urinary tract pathogenesis. *Proc Natl Acad Sci U S A,* 101**,** 1333-8.

JUSTICE, S. S., HUNSTAD, D. A., SEED, P. C. & HULTGREN, S. J. 2006. Filamentation by *Escherichia coli* subverts innate defenses during urinary tract infection. *Proc Natl Acad Sci U S A,* 103**,** 19884-9.

KAPLAN, J. B. 2010. Biofilm dispersal: mechanisms, clinical implications, and potential therapeutic uses. *J Dent Res,* 89**,** 205-18.

KASHKET, E. R. 1985. The proton motive force in bacteria: a critical assessment of methods. *Annu Rev Microbiol,* 39**,** 219-42.

KASPER, D. L. 1986. Bacterial capsule--old dogmas and new tricks. *J Infect Dis,* 153**,** 407-15.

KEHRES, D. G., JANAKIRAMAN, A., SLAUCH, J. M. & MAGUIRE, M. E. 2002. Regulation of *Salmonella enterica* serovar Typhimurium mntH transcription by H(2)O(2), Fe(2+), and Mn(2+). *J Bacteriol,* 184**,** 3151-8.

KEREN, I., SHAH, D., SPOERING, A., KALDALU, N. & LEWIS, K. 2004. Specialized persister cells and the mechanism of multidrug tolerance in *Escherichia coli. J Bacteriol,* 186**,** 8172-80.

KHANDELWAL, P., ABRAHAM, S. N. & APODACA, G. 2009. Cell biology and physiology of the uroepithelium. *Am J Physiol Renal Physiol,* 297**,** F1477-501.

KHANDIGE, S., ASFERG, C. A., RASMUSSEN, K. J., LARSEN, M. J., OVERGAARD, M., ANDERSEN, T. E. & MØLLER-JENSEN, J. 2016. DamX Controls Reversible Cell Morphology Switching in Uropathogenic *Escherichia coli*. *mBio,* 7.

KIKUCHI, T., MIZUNOE, Y., TAKADE, A., NAITO, S. & YOSHIDA, S. 2005. Curli fibers are required for development of biofilm architecture in *Escherichia coli* K-12 and enhance bacterial adherence to human uroepithelial cells. *Microbiol Immunol,* 49**,** 875-84.

KLAUSEN, M., HEYDORN, A., RAGAS, P., LAMBERTSEN, L., AAES-JORGENSEN, A., MOLIN, S. & TOLKER-NIELSEN, T. 2003. Biofilm formation by *Pseudomonas aeruginosa* wild type, flagella and type IV pili mutants. *Mol Microbiol,* 48**,** 1511-24.

KLEVENS, R. M., EDWARDS, J. R., RICHARDS, C. L., HORAN, T. C., GAYNES, R. P., POLLOCK, D. A. & CARDO, D. M. 2007. Estimating health care-associated infections and deaths in U.S. hospitals, 2002. *Public Health Rep,* 122**,** 160-6.

KOETH, R. A., WANG, Z., LEVISON, B. S., BUFFA, J. A., ORG, E., SHEEHY, B. T., BRITT, E. B., FU, X., WU, Y., LI, L., SMITH, J. D., DIDONATO, J. A., CHEN, J., LI, H., WU, G. D., LEWIS, J. D., WARRIER, M., BROWN, J. M., KRAUSS, R. M., TANG, W. H., BUSHMAN, F. D., LUSIS, A. J. & HAZEN, S. L. 2013. Intestinal microbiota metabolism of L-carnitine, a nutrient in red meat, promotes atherosclerosis. *Nat Med,* 19**,** 576-85.

KOO, H., XIAO, J., KLEIN, M. I. & JEON, J. G. 2010. Exopolysaccharides produced by *Streptococcus mutans* glucosyltransferases modulate the establishment of microcolonies within multispecies biofilms. *J Bacteriol,* 192**,** 3024-32.

KORHONEN, T. K., VAISANEN-RHEN, V., RHEN, M., PERE, A., PARKKINEN, J. & FINNE, J. 1984. *Escherichia coli* fimbriae recognizing sialyl galactosides. *J Bacteriol,* 159**,** 762-6.

KOSTAKIOTI, M., HADJIFRANGISKOU, M., CUSUMANO, C. K., HANNAN, T. J., JANETKA, J. W. & HULTGREN, S. J. 2012. Distinguishing the contribution of type 1 pili from that of other QseB-misregulated factors when QseC is absent during urinary tract infection. *Infect Immun,* 80**,** 2826-34.

KOSTAKIOTI, M., HADJIFRANGISKOU, M. & HULTGREN, S. J. 2013. Bacterial biofilms: development, dispersal, and therapeutic strategies in the dawn of the postantibiotic era. *Cold Spring Harb Perspect Med,* 3**,** a010306.

KOSTAKIOTI, M., HADJIFRANGISKOU, M., PINKNER, J. S. & HULTGREN, S. J. 2009. QseC-mediated dephosphorylation of QseB is required for expression of genes associated with virulence in uropathogenic *Escherichia coli*. *Mol Microbiol,* 73**,** 1020-31.

KRAPP, A. R., HUMBERT, M. V. & CARRILLO, N. 2011. The soxRS response of *Escherichia coli* can be induced in the absence of oxidative stress and oxygen by modulation of NADPH content. *Microbiology,* 157**,** 957-65.

KUEHN, M. J., HEUSER, J., NORMARK, S. & HULTGREN, S. J. 1992. P pili in uropathogenic *E. coli* are composite fibres with distinct fibrillar adhesive tips. *Nature,* 356**,** 252-5.

KUWAHARA, H., MYERS, C. J. & SAMOILOV, M. S. 2010. Temperature control of fimbriation circuit switch in uropathogenic *Escherichia coli*: quantitative analysis via automated model abstraction. *PLoS Comput Biol,* 6**,** e1000723.

LANE, M. C., ALTERI, C. J., SMITH, S. N. & MOBLEY, H. L. 2007. Expression of flagella is coincident with uropathogenic *Escherichia coli* ascension to the upper urinary tract. *Proc Natl Acad Sci U S A,* 104**,** 16669-74.

LAU, S. H., KAUFMANN, M. E., LIVERMORE, D. M., WOODFORD, N., WILLSHAW, G. A., CHEASTY, T., STAMPER, K., REDDY, S., CHEESBROUGH, J., BOLTON, F. J., FOX, A. J. & UPTON, M. 2008a. UK epidemic *Escherichia coli* strains A-E, with CTX-M-15 beta-lactamase, all belong to the international O25:H4-ST131 clone. *J Antimicrob Chemother,* 62**,** 1241-4.

LAU, S. H., REDDY, S., CHEESBROUGH, J., BOLTON, F. J., WILLSHAW, G., CHEASTY, T., FOX, A. J. & UPTON, M. 2008b. Major uropathogenic *Escherichia coli* strain isolated in the northwest of England identified by multilocus sequence typing. *J Clin Microbiol,* 46**,** 1076-80.

LAZAZZERA, B. A., BEINERT, H., KHOROSHILOVA, N., KENNEDY, M. C. & KILEY, P. J. 1996. DNA binding and dimerization of the Fe-S-containing FNR protein from *Escherichia coli* are regulated by oxygen. *J Biol Chem,* 271**,** 2762-8.

LEWIS, K. 2005. Persister cells and the riddle of biofilm survival. *Biochemistry (Mosc),* 70**,** 267-74.

LEWIS, K. 2007. Persister cells, dormancy and infectious disease. *Nat Rev Microbiol,* 5**,** 48-56.

LEWIS, K. 2008. Multidrug tolerance of biofilms and persister cells. *Curr Top Microbiol Immunol,* 322**,** 107-31.

LEWIS, K. 2010. Persister cells. *Annu Rev Microbiol,* 64**,** 357-72.

LIPINSKA, B., ZYLICZ, M. & GEORGOPOULOS, C. 1990. The HtrA (DegP) protein, essential for *Escherichia coli* survival at high temperatures, is an endopeptidase. *Journal of Bacteriology,* 172**,** 1791-1797.

LIPSKY, B. A. 1989. Urinary tract infections in men. Epidemiology, pathophysiology, diagnosis, and treatment. *Ann Intern Med,* 110**,** 138-50.

LIU, Y., BAUER, S. C. & IMLAY, J. A. 2011. The YaaA protein of the *Escherichia coli* OxyR regulon lessens hydrogen peroxide toxicity by diminishing the amount of intracellular unincorporated iron. *J Bacteriol,* 193**,** 2186-96.

LOPEZ, D., VLAMAKIS, H. & KOLTER, R. 2010. Biofilms. *Cold Spring Harb Perspect Biol,* 2**,** a000398.

LÓPEZ, D., VLAMAKIS, H. & KOLTER, R. 2010. Biofilms. *Cold Spring Harb Perspect Biol,* 2**,** a000398.

M T, M. B., AYDIN, B., CARLSON, R. P. & HANLEY, L. 2012. Identification and imaging of peptides and proteins on *Enterococcus faecalis* biofilms by matrix assisted laser desorption ionization mass spectrometry. *Analyst,* 137**,** 5018-25.

MAGILL, S. S., EDWARDS, J. R., BAMBERG, W., BELDAVS, Z. G., DUMYATI, G., KAINER, M. A., LYNFIELD, R., MALONEY, M., MCALLISTER-HOLLOD, L., NADLE, J., RAY, S. M., THOMPSON, D. L., WILSON, L. E., FRIDKIN, S. K. & TEAM, E. I. P. H.-A. I. A. A. U. P. S. 2014. Multistate point-prevalence survey of health care-associated infections. *N Engl J Med,* 370**,** 1198-208.

MALPICA, R., SANDOVAL, G. R., RODRÍGUEZ, C., FRANCO, B. & GEORGELLIS, D. 2006. Signaling by the arc two-component system provides a link between the redox state of the quinone pool and gene expression. *Antioxid Redox Signal,* 8**,** 781-95.

MARTINEZ, J. J., MULVEY, M. A., SCHILLING, J. D., PINKNER, J. S. & HULTGREN, S. J. 2000. Type 1 pilus-mediated bacterial invasion of bladder epithelial cells. *EMBO J,* 19**,** 2803-12.

MATZ, C. & KJELLEBERG, S. 2005. Off the hook--how bacteria survive protozoan grazing. *Trends Microbiol,* 13**,** 302-7.

MATZ, C., MCDOUGALD, D., MORENO, A. M., YUNG, P. Y., YILDIZ, F. H. & KJELLEBERG, S. 2005. Biofilm formation and phenotypic variation enhance predation-driven persistence of *Vibrio cholerae*. *Proc Natl Acad Sci U S A,* 102**,** 16819-24.

MAURER, L. M., YOHANNES, E., BONDURANT, S. S., RADMACHER, M. & SLONCZEWSKI, J. L. 2005. pH regulates genes for flagellar motility, catabolism, and oxidative stress in *Escherichia coli* K-12. *J Bacteriol,* 187**,** 304-19.

MAY, L., MULLINS, P. & PINES, J. 2014. Demographic and treatment patterns for infections in ambulatory settings in the United States, 2006-2010. *Acad Emerg Med,* 21**,** 17-24.

MCCRATE, O. A., ZHOU, X., REICHHARDT, C. & CEGELSKI, L. 2013. Sum of the parts: composition and architecture of the bacterial extracellular matrix. *J Mol Biol,* 425**,** 4286-94.

MCGANN, P., SNESRUD, E., MAYBANK, R., COREY, B., ONG, A. C., CLIFFORD, R., HINKLE, M., WHITMAN, T., LESHO, E. & SCHAECHER, K. E. 2016. *Escherichia coli* Harboring *mcr-1* and *blaCTX-M* on a Novel IncF Plasmid: First Report of *mcr-1* in the United States. *Antimicrobial Agents and Chemotherapy,* 60**,** 4420-4421.

MERZ, A. J., SO, M. & SHEETZ, M. P. 2000. Pilus retraction powers bacterial twitching motility. *Nature,* 407**,** 98-102.

MILLER, M. J. & GENNIS, R. B. 1983. The purification and characterization of the cytochrome d terminal oxidase complex of the *Escherichia coli* aerobic respiratory chain. *J Biol Chem,* 258**,** 9159-65.

MINAMINO, T. & NAMBA, K. 2008. Distinct roles of the FliI ATPase and proton motive force in bacterial flagellar protein export. *Nature,* 451**,** 485-8.

MOBLEY, H. L., GREEN, D. M., TRIFILLIS, A. L., JOHNSON, D. E., CHIPPENDALE, G. R., LOCKATELL, C. V., JONES, B. D. & WARREN, J. W. 1990. Pyelonephritogenic *Escherichia coli* and killing of cultured human renal proximal tubular epithelial cells: role of hemolysin in some strains. *Infection and Immunity,* 58**,** 1281-1289.

MORRIS, D., MCGARRY, E., COTTER, M., PASSET, V., LYNCH, M., LUDDEN, C., HANNAN, M. M., BRISSE, S. & CORMICAN, M. 2012. Detection of OXA-48 carbapenemase in the pandemic clone *Escherichia coli* O25b:H4-ST131 in the course of investigation of an outbreak of OXA-48-producing Klebsiella pneumoniae. *Antimicrob Agents Chemother,* 56**,** 4030-1.

MULCAHY, L. R., BURNS, J. L., LORY, S. & LEWIS, K. 2010. Emergence of *Pseudomonas aeruginosa* Strains Producing High Levels of Persister Cells in Patients with Cystic Fibrosis. *Journal of Bacteriology,* 192**,** 6191-6199.

MULLER, C. M., ABERG, A., STRASEVICIENE, J., EMODY, L., UHLIN, B. E. & BALSALOBRE, C. 2009. Type 1 fimbriae, a colonization factor of uropathogenic *Escherichia coli*, are controlled by the metabolic sensor CRP-cAMP. *PLoS Pathog,* 5**,** e1000303.

MULVEY, M. A., LOPEZ-BOADO, Y. S., WILSON, C. L., ROTH, R., PARKS, W. C., HEUSER, J. & HULTGREN, S. J. 1998. Induction and evasion of host defenses by type 1-piliated uropathogenic *Escherichia coli*. *Science,* 282**,** 1494-7.

MURPHY, C. N., MORTENSEN, M. S., KROGFELT, K. A. & CLEGG, S. 2013. Role of *Klebsiella pneumoniae* type 1 and type 3 fimbriae in colonizing silicone tubes implanted into the bladders of mice as a model of catheter-associated urinary tract infections. *Infect Immun,* 81**,** 3009-17.

MURPHY, K. C. & CAMPELLONE, K. G. 2003. Lambda Red-mediated recombinogenic engineering of enterohemorrhagic and enteropathogenic *E. coli*. *BMC Mol Biol,* 4**,** 11.

MÖKER, N., DEAN, C. R. & TAO, J. 2010. *Pseudomonas aeruginosa* Increases Formation of Multidrug-Tolerant Persister Cells in Response to Quorum-Sensing Signaling Molecules. *Journal of Bacteriology,* 192**,** 1946-1955.

NEAL, D. E. 2008. Complicated urinary tract infections. *Urol Clin North Am,* 35**,** 13-22; v.

NGUYEN, D. D., WU, C. H., MOREE, W. J., LAMSA, A., MEDEMA, M. H., ZHAO, X., GAVILAN, R. G., APARICIO, M., ATENCIO, L., JACKSON, C., BALLESTEROS, J., SANCHEZ, J., WATROUS, J. D., PHELAN, V. V., VAN DE WIEL, C., KERSTEN, R. D., MEHNAZ, S., DE MOT, R., SHANK, E. A., CHARUSANTI, P., NAGARAJAN, H., DUGGAN, B. M., MOORE, B. S., BANDEIRA, N., PALSSON, B. O., POGLIANO, K., GUTIERREZ, M. & DORRESTEIN, P. C. 2013. MS/MS networking guided analysis of molecule and gene cluster families. *Proc Natl Acad Sci U S A,* 110**,** E2611-20.

NICOLLE, L. E. 2008. Short-term therapy for urinary tract infection: success and failure. *Int J Antimicrob Agents,* 31 Suppl 1**,** S40-5.

NICOLLE, L. E. 2014a. Asymptomatic bacteriuria. *Curr Opin Infect Dis,* 27**,** 90-6.

NICOLLE, L. E. 2014b. Catheter associated urinary tract infections. *Antimicrob Resist Infect Control,* 3**,** 23.

NIELSEN, H. V., FLORES-MIRELES, A. L., KAU, A. L., KLINE, K. A., PINKNER, J. S., NEIERS, F., NORMARK, S., HENRIQUES-NORMARK, B., CAPARON, M. G. & HULTGREN, S. J. 2013. Pilin and sortase residues critical for endocarditis- and biofilm-associated pilus biogenesis in *Enterococcus faecalis*. *J Bacteriol,* 195**,** 4484-95.

NIVEDITHA, S., PRAMODHINI, S., UMADEVI, S., KUMAR, S. & STEPHEN, S. 2012. The Isolation and the Biofilm Formation of Uropathogens in the Patients with Catheter Associated Urinary Tract Infections (UTIs). *J Clin Diagn Res,* 6**,** 1478-82.

NOBELMANN, B. & LENGELER, J. W. 1996. Molecular analysis of the gat genes from *Escherichia coli* and of their roles in galactitol transport and metabolism. *J Bacteriol,* 178**,** 6790-5.

NORRIS, J. L. & CAPRIOLI, R. M. 2013. Imaging mass spectrometry: a new tool for pathology in a molecular age. *Proteomics Clin Appl,* 7**,** 733-8.

O'TOOLE, G. A., PRATT, L. A., WATNICK, P. I., NEWMAN, D. K., WEAVER, V. B. & KOLTER, R. 1999. Genetic approaches to study of biofilms. *Methods Enzymol,* 310**,** 91-109.

OKSHEVSKY, M. & MEYER, R. L. 2015. The role of extracellular DNA in the establishment, maintenance and perpetuation of bacterial biofilms. *Crit Rev Microbiol,* 41**,** 341-52.

PAIVA, C. N. & BOZZA, M. T. 2014. Are reactive oxygen species always detrimental to pathogens? *Antioxid Redox Signal,* 20**,** 1000-37.

PALLESEN, L., MADSEN, O. & KLEMM, P. 1989. Regulation of the phase switch controlling expression of type 1 fimbriae in *Escherichia coli. Mol Microbiol,* 3**,** 925-31.

PARSEK, M. R. & GREENBERG, E. P. 2005. Sociomicrobiology: the connections between quorum sensing and biofilms. *Trends Microbiol,* 13**,** 27-33.

PATTERSON, J. E. & ANDRIOLE, V. T. 1995. Bacterial urinary tract infections in diabetes. *Infect Dis Clin North Am,* 9**,** 25-51.

PAUL, K., ERHARDT, M., HIRANO, T., BLAIR, D. F. & HUGHES, K. T. 2008. Energy source of flagellar type III secretion. *Nature,* 451**,** 489-92.

PAUL, S., LINARDOPOULOU, E. V., BILLIG, M., TCHESNOKOVA, V., PRICE, L. B., JOHNSON, J. R., CHATTOPADHYAY, S. & SOKURENKO, E. V. 2013. Role of

homologous recombination in adaptive diversification of extraintestinal *Escherichia coli*. *J Bacteriol,* 195**,** 231-42.

PEIRANO, G., SCHRECKENBERGER, P. C. & PITOUT, J. D. 2011. Characteristics of NDM-1-producing *Escherichia coli* isolates that belong to the successful and virulent clone ST131. *Antimicrob Agents Chemother,* 55**,** 2986-8.

PETROVA, O. E. & SAUER, K. 2012. Sticky Situations: Key Components That Control Bacterial Surface Attachment. *Journal of Bacteriology,* 194**,** 2413-2425.

PETTY, N. K., BEN ZAKOUR, N. L., STANTON-COOK, M., SKIPPINGTON, E., TOTSIKA, M., FORDE, B. M., PHAN, M.-D., GOMES MORIEL, D., PETERS, K. M., DAVIES, M., ROGERS, B. A., DOUGAN, G., RODRIGUEZ-BAÑO, J., PASCUAL, A., PITOUT, J. D. D., UPTON, M., PATERSON, D. L., WALSH, T. R., SCHEMBRI, M. A. & BEATSON, S. A. 2014. Global dissemination of a multidrug resistant *Escherichia coli* clone. *Proceedings of the National Academy of Sciences,* 111**,** 5694-5699.

PFAFFL, M. W. 2001. A new mathematical model for relative quantification in real-time RT-PCR. *Nucleic Acids Res,* 29**,** e45.

PINKNER, J. S., REMAUT, H., BUELENS, F., MILLER, E., ABERG, V., PEMBERTON, N., HEDENSTROM, M., LARSSON, A., SEED, P., WAKSMAN, G., HULTGREN, S. J. & ALMQVIST, F. 2006. Rationally designed small compounds inhibit pilus biogenesis in uropathogenic bacteria. *Proc Natl Acad Sci U S A,* 103**,** 17897-902.

PLATE, L. & MARLETTA, M. A. 2012. Nitric oxide modulates bacterial biofilm formation through a multicomponent cyclic-di-GMP signaling network. *Mol Cell,* 46**,** 449-60.

PLATT, R., POLK, B. F., MURDOCK, B. & ROSNER, B. 1982. Mortality associated with nosocomial urinary-tract infection. *N Engl J Med,* 307**,** 637-42.

POZZAN, T., MICONI, V., DI VIRGILIO, F. & AZZONE, G. F. 1979. H+/site, charge/site, and ATP/site ratios at coupling sites I and II in mitochondrial e- transport. *J Biol Chem,* 254**,** 12000-5.

PREVENTION, C. F. D. C. A. 2013. Antibiotic resistance threats in the United States,. http://www.cdc.gov/drugresistance/threat-report-2013/ . .

PREVENTION, C. F. D. C. A. Published January 14, 2015. 2013 National and State Healthcare-Associated Infections Progress Report. Available at http://www.cdc.gov/hai/progress-report/index.html.

PÓL, J., STROHALM, M., HAVLÍČEK, V. & VOLNÝ, M. 2010. Molecular mass spectrometry imaging in biomedical and life science research. *Histochem Cell Biol,* 134**,** 423-43.

QI, Y., XU, L., DONG, X., YAU, Y. H., HO, C. L., KOH, S. L., SHOCHAT, S. G., CHOU, S. H., TANG, K. & LIANG, Z. X. 2012. Functional divergence of FimX in PilZ binding and type IV pilus regulation. *J Bacteriol,* 194**,** 5922-31.

RANI, S. A., PITTS, B., BEYENAL, H., VELUCHAMY, R. A., LEWANDOWSKI, Z., DAVISON, W. M., BUCKINGHAM-MEYER, K. & STEWART, P. S. 2007. Spatial patterns of DNA replication, protein synthesis, and oxygen concentration within bacterial biofilms reveal diverse physiological states. *J Bacteriol,* 189**,** 4223-33.

RAPSINSKI, G. J., NEWMAN, T. N., OPPONG, G. O., VAN PUTTEN, J. P. & TÜKEL, Ç. 2013. CD14 protein acts as an adaptor molecule for the immune recognition of *Salmonella* curli fibers. *J Biol Chem,* 288**,** 14178-88.

REISNER, A., HAAGENSEN, J. A., SCHEMBRI, M. A., ZECHNER, E. L. & MOLIN, S. 2003. Development and maturation of *Escherichia coli* K-12 biofilms. *Mol Microbiol,* 48**,** 933-46.

RENTSCHLER, A. E., LOVRICH, S. D., FITTON, R., ENOS-BERLAGE, J. & SCHWAN, W. R. 2013. OmpR regulation of the uropathogenic *Escherichia coli fimB* gene in an acidic/high osmolality environment. *Microbiology,* 159**,** 316-27.

ROLFE, M. D., TER BEEK, A., GRAHAM, A. I., TROTTER, E. W., ASIF, H. M., SANGUINETTI, G., DE MATTOS, J. T., POOLE, R. K. & GREEN, J. 2011. Transcript profiling and inference of *Escherichia coli* K-12 ArcA activity across the range of physiologically relevant oxygen concentrations. *J Biol Chem,* 286**,** 10147-54.

ROSEN, D. A., HOOTON, T. M., STAMM, W. E., HUMPHREY, P. A. & HULTGREN, S. J. 2007. Detection of intracellular bacterial communities in human urinary tract infection. *PLoS Med,* 4**,** e329.

SALMON, K., HUNG, S. P., MEKJIAN, K., BALDI, P., HATFIELD, G. W. & GUNSALUS, R. P. 2003. Global gene expression profiling in *Escherichia coli* K12. The effects of oxygen availability and FNR. *J Biol Chem,* 278**,** 29837-55.

SARKAR, S., ROBERTS, L. W., PHAN, M. D., TAN, L., LO, A. W., PETERS, K. M., PATERSON, D. L., UPTON, M., ULETT, G. C., BEATSON, S. A., TOTSIKA, M. & SCHEMBRI, M. A. 2016. Comprehensive analysis of type 1 fimbriae regulation in *fimB*-null strains from the multidrug resistant *Escherichia coli* ST131 clone. *Mol Microbiol,* 101**,** 1069-87.

SAUER, K., CULLEN, M. C., RICKARD, A. H., ZEEF, L. A. H., DAVIES, D. G. & GILBERT, P. 2004. Characterization of Nutrient-Induced Dispersion in *Pseudomonas aeruginosa* PAO1 Biofilm. *Journal of Bacteriology,* 186**,** 7312-7326.

SAVAGE, V. J., CHOPRA, I. & O'NEILL, A. J. 2013. Population diversification in *Staphylococcus aureus* biofilms may promote dissemination and persistence. *PLoS One,* 8**,** e62513.

SCHILLING, J. D., MULVEY, M. A. & HULTGREN, S. J. 2001. Structure and function of *Escherichia coli* type 1 pili: new insight into the pathogenesis of urinary tract infections. *J Infect Dis,* 183 Suppl 1**,** S36-40.

SCHNEIDER, C. A., RASBAND, W. S. & ELICEIRI, K. W. 2012. NIH Image to ImageJ: 25 years of image analysis. *Nat Methods,* 9**,** 671-5.

SCHRAGER, H. M., ALBERTÍ, S., CYWES, C., DOUGHERTY, G. J. & WESSELS, M. R. 1998. Hyaluronic acid capsule modulates M protein-mediated adherence and acts as a ligand for attachment of group A *Streptococcus* to CD44 on human keratinocytes. *J Clin Invest,* 101**,** 1708-16.

SCHWAN, W. R. 2011. Regulation of *fim* genes in uropathogenic *Escherichia coli*. *World J Clin Infect Dis,* 1**,** 17-25.

SCHWARTZ, S. A., REYZER, M. L. & CAPRIOLI, R. M. 2003. Direct tissue analysis using matrix-assisted laser desorption/ionization mass spectrometry: practical aspects of sample preparation. *J Mass Spectrom,* 38**,** 699-708.

SEAVER, L. C. & IMLAY, J. A. 2001. Hydrogen peroxide fluxes and compartmentalization inside growing *Escherichia coli*. *J Bacteriol,* 183**,** 7182-9.

SEELEY, E. H. & CAPRIOLI, R. M. 2008. Molecular imaging of proteins in tissues by mass spectrometry. *Proc Natl Acad Sci U S A,* 105**,** 18126-31.

SEELEY, E. H., OPPENHEIMER, S. R., MI, D., CHAURAND, P. & CAPRIOLI, R. M. 2008. Enhancement of protein sensitivity for MALDI imaging mass spectrometry after chemical treatment of tissue sections. *J Am Soc Mass Spectrom,* 19**,** 1069-77.

SETH, D., HAUSLADEN, A., WANG, Y. J. & STAMLER, J. S. 2012. Endogenous protein S-Nitrosylation in *E. coli*: regulation by OxyR. *Science,* 336**,** 470-3.

SHAN, Y., PAN, Q., LIU, J., HUANG, F., SUN, H., NISHINO, K. & YAN, A. 2012. Covalently linking the *Escherichia coli* global anaerobic regulator FNR in tandem allows it to function as an oxygen stable dimer. *Biochem Biophys Res Commun,* 419**,** 43-8.

SHARIFF V A, A. R., SHENOY M, S., YADAV, T. & M, R. 2013. The antibiotic susceptibility patterns of uropathogenic *Escherichia coli*, with special reference to the fluoroquinolones. *J Clin Diagn Res,* 7**,** 1027-30.

SINGH, K. V., NALLAPAREDDY, S. R. & MURRAY, B. E. 2007. Importance of the *ebp* (endocarditis- and biofilm-associated pilus) locus in the pathogenesis of *Enterococcus faecalis* ascending urinary tract infection. *J Infect Dis,* 195**,** 1671-7.

SINGH, R., RAY, P., DAS, A. & SHARMA, M. 2009. Role of persisters and small-colony variants in antibiotic resistance of planktonic and biofilm-associated *Staphylococcus aureus*: an in vitro study. *J Med Microbiol,* 58**,** 1067-73.

SOHANPAL, B. K., KULASEKARA, H. D., BONNEN, A. & BLOMFIELD, I. C. 2001. Orientational control of *fimE* expression in *Escherichia coli*. *Mol Microbiol,* 42**,** 483-94.

SOWA, Y., ROWE, A. D., LEAKE, M. C., YAKUSHI, T., HOMMA, M., ISHIJIMA, A. & BERRY, R. M. 2005. Direct observation of steps in rotation of the bacterial flagellar motor. *Nature,* 437**,** 916-9.

SPIRO, S. & GUEST, J. R. 1990. FNR and its role in oxygen-regulated gene expression in *Escherichia coli. FEMS Microbiol Rev,* 6**,** 399-428.

STAMM, W. E. & HOOTON, T. M. 1993. Management of urinary tract infections in adults. *N Engl J Med,* 329**,** 1328-34.

STEINBERG, N. & KOLODKIN-GAL, I. 2015. The Matrix Reloaded: How Sensing the Extracellular Matrix Synchronizes Bacterial Communities. *Journal of Bacteriology,* 197**,** 2092-2103.

STEWART, P. S. 2003. Diffusion in Biofilms. *Journal of Bacteriology,* 185**,** 1485-1491.

STOODLEY, P., SAUER, K., DAVIES, D. G. & COSTERTON, J. W. 2002. Biofilms as complex differentiated communities. *Annu Rev Microbiol,* 56**,** 187-209.

STROHALM, M., HASSMAN, M., KOŠATA, B. & KODÍČEK, M. 2008. mMass data miner: an open source alternative for mass spectrometric data analysis. *Rapid Communications in Mass Spectrometry,* 22**,** 905-908.

STRUVE, C., BOJER, M. & KROGFELT, K. A. 2008. Characterization of *Klebsiella pneumoniae* type 1 fimbriae by detection of phase variation during colonization and infection and impact on virulence. *Infect Immun,* 76**,** 4055-65.

STRUVE, C., BOJER, M. & KROGFELT, K. A. 2009. Identification of a conserved chromosomal region encoding *Klebsiella pneumoniae* type 1 and type 3 fimbriae and assessment of the role of fimbriae in pathogenicity. *Infect Immun,* 77**,** 5016-24.

STRUVE, C. & KROGFELT, K. A. 1999. *In vivo* detection of *Escherichia coli* type 1 fimbrial expression and phase variation during experimental urinary tract infection. *Microbiology,* 145 (Pt 10)**,** 2683-90.

SUTHERLAND, I. W. 2001. The biofilm matrix--an immobilized but dynamic microbial environment. *Trends Microbiol,* 9**,** 222-7.

SYSTEM, N. N. I. S. 2004. National Nosocomial Infections Surveillance (NNIS) System Report, data summary from January 1992 through June 2004, issued October 2004. *Am J Infect Control,* 32**,** 470-85.

TETZ, G. V., ARTEMENKO, N. K. & TETZ, V. V. 2009. Effect of DNase and antibiotics on biofilm characteristics. *Antimicrob Agents Chemother,* 53**,** 1204-9.

THANKAVEL, K., MADISON, B., IKEDA, T., MALAVIYA, R., SHAH, A. H., ARUMUGAM, P. M. & ABRAHAM, S. N. 1997. Localization of a domain in the FimH adhesin of *Escherichia coli* type 1 fimbriae capable of receptor recognition and use of a

domain-specific antibody to confer protection against experimental urinary tract infection. *J Clin Invest,* 100**,** 1123-36.

THOMAS, V. C., HIROMASA, Y., HARMS, N., THURLOW, L., TOMICH, J. & HANCOCK, L. E. 2009. A fratricidal mechanism is responsible for eDNA release and contributes to biofilm development of *Enterococcus faecalis*. *Mol Microbiol,* 72**,** 1022-36.

THUMBIKAT, P., BERRY, R. E., ZHOU, G., BILLIPS, B. K., YAGGIE, R. E., ZAICHUK, T., SUN, T. T., SCHAEFFER, A. J. & KLUMPP, D. J. 2009. Bacteria-induced uroplakin signaling mediates bladder response to infection. *PLoS Pathog,* 5**,** e1000415.

TOLKER-NIELSEN, T. 2015. Biofilm Development. *Microbiol Spectr,* 3**,** MB-0001-2014.

TRAN, Q. H., ARRAS, T., BECKER, S., HOLIGHAUS, G., OHLBERGER, G. & UNDEN, G. 2000. Role of glutathione in the formation of the active form of the oxygen sensor FNR ([4Fe-4S].FNR) and in the control of FNR function. *Eur J Biochem,* 267**,** 4817-24.

TRAXLER, M. F., WATROUS, J. D., ALEXANDROV, T., DORRESTEIN, P. C. & KOLTER, R. 2013. Interspecies Interactions Stimulate Diversification of the *Streptomyces coelicolor* Secreted Metabolome. *MBio,* 4.

TÜKEL, C., WILSON, R. P., NISHIMORI, J. H., PEZESHKI, M., CHROMY, B. A. & BÄUMLER, A. J. 2009. Responses to amyloids of microbial and host origin are mediated through toll-like receptor 2. *Cell Host Microbe,* 6**,** 45-53.

UCHIDA, Y., MOCHIMARU, T., MOROKUMA, Y., KIYOSUKE, M., FUJISE, M., ETO, F., ERIGUCHI, Y., NAGASAKI, Y., SHIMONO, N. & KANG, D. 2010. Clonal spread in Eastern Asia of ciprofloxacin-resistant *Escherichia coli* serogroup O25 strains, and associated virulence factors. *Int J Antimicrob Agents,* 35**,** 444-50.

ULETT, G. C., VALLE, J., BELOIN, C., SHERLOCK, O., GHIGO, J. M. & SCHEMBRI, M. A. 2007. Functional analysis of antigen 43 in uropathogenic *Escherichia coli* reveals a role in long-term persistence in the urinary tract. *Infect Immun,* 75**,** 3233-44.

UNDEN, G., ACHEBACH, S., HOLIGHAUS, G., TRAN, H. G., WACKWITZ, B. & ZEUNER, Y. 2002. Control of FNR function of *Escherichia coli* by O2 and reducing conditions. *J Mol Microbiol Biotechnol,* 4**,** 263-8.

UNDEN, G., BECKER, S., BONGAERTS, J., HOLIGHAUS, G., SCHIRAWSKI, J. & SIX, S. 1995. O2-sensing and O2-dependent gene regulation in facultatively anaerobic bacteria. *Arch Microbiol,* 164**,** 81-90.

UNDEN, G. & BONGAERTS, J. 1997. Alternative respiratory pathways of *Escherichia coli*: energetics and transcriptional regulation in response to electron acceptors. *Biochim Biophys Acta,* 1320**,** 217-34.

VALM, A. M., MARK WELCH, J. L., RIEKEN, C. W., HASEGAWA, Y., SOGIN, M. L., OLDENBOURG, R., DEWHIRST, F. E. & BORISY, G. G. 2011. Systems-level analysis

of microbial community organization through combinatorial labeling and spectral imaging. *Proc Natl Acad Sci U S A,* 108**,** 4152-7.

VAN LOOSDRECHT, M. C., LYKLEMA, J., NORDE, W., SCHRAA, G. & ZEHNDER, A. J. 1987. Electrophoretic mobility and hydrophobicity as a measured to predict the initial steps of bacterial adhesion. *Applied and Environmental Microbiology,* 53**,** 1898-1901.

VAN SCHAIK, E. J., GILTNER, C. L., AUDETTE, G. F., KEIZER, D. W., BAUTISTA, D. L., SLUPSKY, C. M., SYKES, B. D. & IRVIN, R. T. 2005. DNA Binding: a Novel Function of *Pseudomonas aeruginosa* Type IV Pili. *Journal of Bacteriology,* 187**,** 1455-1464.

VERMEULEN, S. H., HANUM, N., GROTENHUIS, A. J., CASTAÑO-VINYALS, G., VAN DER HEIJDEN, A. G., ABEN, K. K., MYSOREKAR, I. U. & KIEMENEY, L. A. 2015. Recurrent urinary tract infection and risk of bladder cancer in the Nijmegen bladder cancer study. *Br J Cancer,* 112**,** 594-600.

VIANA, R., BATOURINA, E., HUANG, H., DRESSLER, G. R., KOBAYASHI, A., BEHRINGER, R. R., SHAPIRO, E., HENSLE, T., LAMBERT, S. & MENDELSOHN, C. 2007. The development of the bladder trigone, the center of the anti-reflux mechanism. *Development,* 134**,** 3763-9.

VILAIN, S., PRETORIUS, J. M., THERON, J. & BROZEL, V. S. 2009. DNA as an adhesin: *Bacillus cereus* requires extracellular DNA to form biofilms. *Appl Environ Microbiol,* 75**,** 2861-8.

VLAMAKIS, H., AGUILAR, C., LOSICK, R. & KOLTER, R. 2008. Control of cell fate by the formation of an architecturally complex bacterial community. *Genes Dev,* 22**,** 945-53.

VOLKAN, E., KALAS, V., PINKNER, J. S., DODSON, K. W., HENDERSON, N. S., PHAM, T., WAKSMAN, G., DELCOUR, A. H., THANASSI, D. G. & HULTGREN, S. J. 2013. Molecular basis of usher pore gating in *Escherichia coli* pilus biogenesis. *Proc Natl Acad Sci U S A,* 110**,** 20741-6.

WAGENLEHNER, F. M., HOYME, U., KAASE, M., FÜNFSTÜCK, R., NABER, K. G. & SCHMIEMANN, G. 2011a. Uncomplicated urinary tract infections. *Dtsch Arztebl Int,* 108**,** 415-23.

WAGENLEHNER, F. M., PILATZ, A. & WEIDNER, W. 2011b. Urosepsis--from the view of the urologist. *Int J Antimicrob Agents,* 38 Suppl**,** 51-7.

WAKSMAN, G. & HULTGREN, S. J. 2009. Structural biology of the chaperone-usher pathway of pilus biogenesis. *Nat Rev Microbiol,* 7**,** 765-74.

WANG, Z. J., JOE, B. N., COAKLEY, F. V., ZAHARCHUK, G., BUSSE, R. & YEH, B. M. 2008. Urinary oxygen tension measurement in humans using magnetic resonance imaging. *Acad Radiol,* 15**,** 1467-73.

WATROUS, J., ROACH, P., ALEXANDROV, T., HEATH, B. S., YANG, J. Y., KERSTEN, R. D., VAN DER VOORT, M., POGLIANO, K., GROSS, H., RAAIJMAKERS, J. M., MOORE, B. S., LASKIN, J., BANDEIRA, N. & DORRESTEIN, P. C. 2012. Mass spectral molecular networking of living microbial colonies. *Proc Natl Acad Sci U S A,* 109**,** E1743-52.

WATROUS, J., ROACH, P., HEATH, B., ALEXANDROV, T., LASKIN, J. & DORRESTEIN, P. C. 2013a. Metabolic profiling directly from the Petri dish using nanospray desorption electrospray ionization imaging mass spectrometry. *Anal Chem,* 85**,** 10385-91.

WATROUS, J. D. & DORRESTEIN, P. C. 2011. Imaging mass spectrometry in microbiology. *Nat Rev Microbiol,* 9**,** 683-94.

WATROUS, J. D., PHELAN, V. V., HSU, C. C., MOREE, W. J., DUGGAN, B. M., ALEXANDROV, T. & DORRESTEIN, P. C. 2013b. Microbial metabolic exchange in 3D. *ISME J,* 7**,** 770-80.

WELCH, R. A., BURLAND, V., PLUNKETT, G., 3RD, REDFORD, P., ROESCH, P., RASKO, D., BUCKLES, E. L., LIOU, S. R., BOUTIN, A., HACKETT, J., STROUD, D., MAYHEW, G. F., ROSE, D. J., ZHOU, S., SCHWARTZ, D. C., PERNA, N. T., MOBLEY, H. L., DONNENBERG, M. S. & BLATTNER, F. R. 2002. Extensive mosaic structure revealed by the complete genome sequence of uropathogenic *Escherichia coli. Proc Natl Acad Sci U S A,* 99**,** 17020-4.

WHITCHURCH, C. B., TOLKER-NIELSEN, T., RAGAS, P. C. & MATTICK, J. S. 2002. Extracellular DNA required for bacterial biofilm formation. *Science,* 295**,** 1487.

WILLIAMSON, K. S., RICHARDS, L. A., PEREZ-OSORIO, A. C., PITTS, B., MCINNERNEY, K., STEWART, P. S. & FRANKLIN, M. J. 2012. Heterogeneity in *Pseudomonas aeruginosa* biofilms includes expression of ribosome hibernation factors in the antibiotic tolerant subpopulation and hypoxia induced stress response in the metabolically active population. *Journal of Bacteriology*.

WRIGHT, K. J., SEED, P. C. & HULTGREN, S. J. 2007. Development of intracellular bacterial communities of uropathogenic *Escherichia coli* depends on type 1 pili. *Cell Microbiol,* 9**,** 2230-41.

YANG, J. Y., PHELAN, V. V., SIMKOVSKY, R., WATROUS, J. D., TRIAL, R. M., FLEMING, T. C., WENTER, R., MOORE, B. S., GOLDEN, S. S., POGLIANO, K. & DORRESTEIN, P. C. 2012. Primer on agar-based microbial imaging mass spectrometry. *J Bacteriol,* 194**,** 6023-8.

ZARB, P., COIGNARD, B., GRISKEVICIENE, J., MULLER, A., VANKERCKHOVEN, V., WEIST, K., GOOSSENS, M., VAERENBERG, S., HOPKINS, S., CATRY, B., MONNET, D., GOOSSENS, H., SUETENS, C., SURVEY, N. C. P. F. T. E. P. P. P. & SURVEY, H. C. P. F. T. E. P. P. P. 2012. The European Centre for Disease Prevention and Control (ECDC) pilot point prevalence survey of healthcare-associated infections and antimicrobial use. *Euro Surveill,* 17.

ZELLER, T., MRAHEIL, M. A., MOSKVIN, O. V., LI, K., GOMELSKY, M. & KLUG, G. 2007. Regulation of hydrogen peroxide-dependent gene expression in *Rhodobacter sphaeroides*: regulatory functions of OxyR. *J Bacteriol,* 189**,** 3784-92.

ZHANEL, G. G., HISANAGA, T. L., LAING, N. M., DECORBY, M. R., NICHOL, K. A., PALATNIK, L. P., JOHNSON, J., NOREDDIN, A., HARDING, G. K., NICOLLE, L. E., HOBAN, D. J. & GROUP, N. 2005. Antibiotic resistance in outpatient urinary isolates: final results from the North American Urinary Tract Infection Collaborative Alliance (NAUTICA). *Int J Antimicrob Agents,* 26**,** 380-8.

ZHANG, H., SUSANTO, T. T., WAN, Y. & CHEN, S. L. 2016. Comprehensive mutagenesis of the *fimS* promoter regulatory switch reveals novel regulation of type 1 pili in uropathogenic *Escherichia coli*. *Proceedings of the National Academy of Sciences,* 113**,** 4182-4187.

ZHENG, M., DOAN, B., SCHNEIDER, T. D. & STORZ, G. 1999. OxyR and SoxRS regulation of *fur*. *J Bacteriol,* 181**,** 4639-43.

ZHENG, M., WANG, X., TEMPLETON, L. J., SMULSKI, D. R., LAROSSA, R. A. & STORZ, G. 2001. DNA microarray-mediated transcriptional profiling of the *Escherichia coli* response to hydrogen peroxide. *J Bacteriol,* 183**,** 4562-70.

ZHOU, G., MO, W. J., SEBBEL, P., MIN, G., NEUBERT, T. A., GLOCKSHUBER, R., WU, X. R., SUN, T. T. & KONG, X. P. 2001. Uroplakin Ia is the urothelial receptor for uropathogenic *Escherichia coli*: evidence from in vitro FimH binding. *J Cell Sci,* 114**,** 4095-103.

ZOGAJ, X., NIMTZ, M., ROHDE, M., BOKRANZ, W. & ROMLING, U. 2001. The multicellular morphotypes of *Salmonella typhimurium* and *Escherichia coli* produce cellulose as the second component of the extracellular matrix. *Mol Microbiol,* 39**,** 1452-63.